

Microvascular Exchange in Human Tissue

By

Ian Gates

B.Sc. (Chemical Engineering) University of Calgary, Canada.

A THESIS SUBMITTED IN PARTIAL FULFILLMENT OF
THE REQUIREMENTS FOR THE DEGREE OF
MASTER OF APPLIED SCIENCE

in

THE FACULTY OF APPLIED SCIENCE
CHEMICAL ENGINEERING

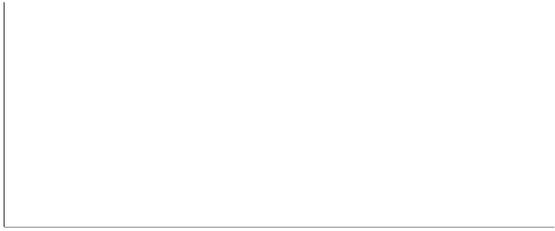
We accept this as conforming
to the required standard

THE UNIVERSITY OF BRITISH COLUMBIA

September 1992

© Ian Gates, 1992

In presenting this thesis in partial fulfillment of the requirements for an advanced degree at the University of British Columbia, I agree that the Library shall make it freely available for reference and study. I further agree that permission for extensive copying of this thesis for scholarly purposes may be granted by the head of my department or by his or her representatives. It is understood that copying or publication of this thesis for financial gain shall not be allowed without my written permission.



Department of Chemical Engineering
The University of British Columbia
Vancouver, British Columbia
September 1992

Abstract

A transient, spatially distributed mathematical model is developed describing the exchange of materials (fluid and solute) across the capillary membrane into the interstitial space. The formulation includes a lymphatic sink which drains both fluid and solute from the tissue. This can be located anywhere within the tissue. The model is constructed in cylindrical coordinates and consist of the capillary lying along the z axis and the tissue envelope surrounding the capillary.

The driving force for fluid motion is the fluid chemical potential. This is equal to the difference between the local fluid hydrostatic pressure and the local colloid osmotic pressure. Starling's hypothesis governs fluid flow across the capillary wall. This states that the amount of fluid that crosses the capillary membrane is due to the transmembrane potential difference. The fact that solute may leak across the membrane promotes the use of a capillary membrane reflection coefficient. In the tissue, the fluid motion is found from a modified Darcy's law which makes use of the gradient in the fluid potential rather than the hydrostatic pressure. In addition, a tissue reflection coefficient is used.

The study consists of an evaluation of the effect the physiological parameters have on the system. This is presented in the form of a sensitivity analysis for steady state results only. It is shown that the strength of the lymphatic sink is important in promoting fluid reabsorption back into the capillary and negative hydrostatic pressures (subatmospheric) throughout the tissue.

Transient test are performed to evaluate the regulating mechanisms for capillary-tissue fluid balance. The capillary membrane, the colloid osmotic pressure, and the lymphatic sink are examined for their roles in maintaining fluid balance. It is found that the colloid osmotic pressure acts as a negative feedback signal regulating the cycle of solute concentrations and fluid hydrostatic pressures throughout the tissue. The lymphatic sink is

important as it provides a mechanism for lowering tissue pressures and removing solute from the interstitial space, thus lowering the tissue colloid osmotic pressure. The trends indicated in the results compare well with results from Manning *et al.* (1983) and Taylor *et al.* (1973).

Table of Contents

Abstract	ii
List of Figures	viii
List of Tables	xv
Acknowledgement	xvi
1 Introduction	1
2 Microvascular Exchange Physiology	4
2.1 Body Fluid Compartments and the Circulation System	5
2.1.1 The Blood and Plasma Proteins.....	7
2.2 The Blood and Lymphatic Flow and Microvascular Exchange.....	8
2.2.1 Blood Vessel Classification.....	9
2.2.2 The Lymphatics	10
2.2.3 Microvascular Exchange	12
<i>The Capillary Wall and Basement Membrane</i>	12
<i>Transcapillary Transport</i>	15
2.3 The Interstitial Space	18
2.3.1 Volume Exclusion.....	22
2.3.2 Geometry of Tissue.....	23
3 Model Development and Formulation	24
3.1 Literature Review	24

3.2	The Interstitium as a Continuum.....	28
3.3	Model Formulation	29
3.3.1	Model Geometry	29
3.3.2	Fluid Transport in the Fiber Matrix Porous Media.....	31
3.3.3	Solute Transport in the Fiber Matrix Porous Medium.....	35
3.3.4	The Lymphatic Sink.....	40
3.3.5	Volume Exclusion and Surface Depletion	43
	<i>Volume Exclusion (Inaccessible Volume)</i>	43
	<i>Surface Depletion</i>	47
3.4	Boundary Conditions	49
3.5	Fluid and Solute Exchange in the Capillary	51
3.6	Numerical Procedure and Solution Algorithm.....	54
3.7	Summary of Equations in Dimensionless Form.....	56
4	Effects of System Parameters on Steady State Microvascular Exchange : A	
	Sensitivity Analysis.....	59
4.1	Introduction	59
4.2	Problem Statement.....	60
4.3	Parameter Values.....	60
4.4	Case Studies	62
4.5	Discussion of Results and Sensitivity Analysis.....	66
4.5.1	The Base Case.....	66
4.5.2	Sensitivity Analysis.....	73
	<i>Retardation Factor, ξ</i>	73
	<i>Capillary Reflection Coefficient, σ</i>	76
	<i>Tissue Reflection Coefficient, σ_t</i>	80

	<i>Solute Diffusion Coefficient, D_{diff}</i>	82
	<i>Tissue Hydraulin Conductivity, K</i>	84
	<i>Capillary Membrane Diffusive Permeability, PS</i>	88
	<i>Lymphatic Sink Strength, LS</i>	90
	<i>Lymphatic Sink Pressure, P_L</i>	92
	<i>Lymphatic Sink Radial Position</i>	94
	<i>Capillary Membrane Filtration Coefficient, L_p</i>	97
	<i>Mechanical Dispersion</i>	101
4.5.3	Variable Capillary Membrane Filtration Coefficient, $L_p(z)$	103
4.5.4	High Flow Channels.....	108
4.6	Conclusions	113
5	Capillary - Tissue Fluid Balance and the Effects of Perturbations on Material Exchange	116
5.1	Introduction	116
5.2	Transcapillary Fluid Flow.....	117
5.3	Capillary - Tissue Fluid Balance : Mechanisms of Regulation.....	122
5.3.1	Perturbed Tissue Solute Concentration	122
5.3.2	Perturbed Venous Hydrostatic Pressure	127
5.3.3	Perturbed Capillary Solute Concentration.....	134
5.3.4	Transient Analysis of the Effects of Osmotic Pressure.....	146
5.4	Discussion and Conclusions.....	153
6	Conclusions and Recommendations	157
	Nomenclature.....	160

References	165
Appendices	171
A The Petrov-Galerkin Finite Element Method.....	171
A.1 The Galerkin Finite Element Method	171
<i>Discretization</i>	173
<i>Interpolation</i>	175
<i>Weak formulation</i>	176
<i>Formation of elemental matrices</i>	178
<i>Solution of the resulting algebraic equations</i>	182
<i>Cylindrical geometry and variable properties</i>	183
A.2 The Petrov-Galerkin Upwinding Method.....	183
B The Solution Algorithm and Under-relaxation Scheme.....	186
B.1 The Solution Algorithm	186
B.2 The Under-relaxation Scheme	188
C Program Listing	190

List of Figures

2.1	Distribution of body fluid compartments.	5
2.2	Structure of lymphatics in cat mesentery (taken from Schmid-Schonbein, 1990).	11
2.3	Structure of and transport mechanisms through capillary walls.	14
2.4	Starling forces.	15
2.5	The interstitial space (taken from Bert and Pearce, 1984).	19
2.6	Microvascular network of the frog sartorius muscle (taken from Dietrich and Tyml, 1992).	23
3.1	Model geometry.	30
3.2	Lymph flow versus average tissue hydrostatic pressure (taken from Taylor <i>et al.</i> , 1973).	41
3.3	Conceptual picture of the lymphatic sink.	42
3.4	Volume exclusion of solute.	44
3.5	Partitioning of a representative elementary volume into the various volume fractions.	45
3.6	Schematic diagram of (a) surface depletion of spherical and rod-like molecules from fiber and (b) steric exclusion of sphere in random network of fibers.	48
3.7	Fluid and solute flow in capillary.	52
4.1	Dimensionless tissue solute concentration, hydrostatic pressure, Peclet number, potential and velocity vector distributions for the base case at steady-state (<i>base</i>).	67

4.2	Dimensionless tissue solute concentration, hydrostatic pressure, Peclet number, potential and velocity vector distributions for the case without osmotic pressure effects but with the lymphatic sink at steady-state (<i>nows</i>). ..	72
4.3	Dimensionless tissue solute concentration, hydrostatic pressure, Peclet number, potential and velocity vector distributions for the case with the retardation factor, ξ , equal to 0.1 at steady-state.	75
4.4	Dimensionless tissue solute concentration, hydrostatic pressure, Peclet number, potential and velocity vector distributions for the case with the capillary reflection coefficient, σ , equal to 0.1 at steady-state.	77
4.5	Dimensionless tissue solute concentration, hydrostatic pressure, Peclet number, potential and velocity vector distributions for the case with the capillary reflection coefficient, σ , equal to 0.99 at steady-state.	79
4.6	Dimensionless tissue solute concentration, hydrostatic pressure, Peclet number, potential and velocity vector distributions for the case with the tissue reflection coefficient, σ_t , equal to 0.0 at steady-state.	81
4.7	Dimensionless tissue solute concentration, hydrostatic pressure, Peclet number, potential and velocity vector distributions for the case with the solute molecular diffusion coefficient, D_{diff} , increased by an order of magnitude from the base value at steady-state.	83
4.8	Dimensionless tissue solute concentration, hydrostatic pressure, Peclet number, potential and velocity vector distributions for the case with the hydraulic conductivity, K , decreased by an order of magnitude from the base value at steady-state.	85
4.9	Dimensionless tissue solute concentration, hydrostatic pressure, Peclet number, potential and velocity vector distributions for the case with the	

hydraulic conductivity, K , increased by an order of magnitude from the base value at steady-state.	86
4.10 Dimensionless tissue solute concentration, hydrostatic pressure, Peclet number, potential and velocity vector distributions for the case with the capillary membrane diffusive permeability, PS , increased by a large amount (x10000) from the base value at steady-state.	89
4.11 Dimensionless tissue solute concentration, hydrostatic pressure, Peclet number, potential and velocity vector distributions for the case with the lymphatic sink strength, LS , decreased by a factor of five from the base value at steady-state.	91
4.12 Dimensionless tissue solute concentration, hydrostatic pressure, Peclet number, potential and velocity vector distributions for the case with the lymphatic sink pressure, P_L^* , lowered to -0.4 (-12 mmHg) at steady-state. ...	93
4.13 Dimensionless tissue solute concentration, hydrostatic pressure, Peclet number, potential and velocity vector distributions for the case with the lymphatic sink repositioned at $r^* = 0.025$ at steady-state.	95
4.14 Dimensionless tissue solute concentration, hydrostatic pressure, Peclet number, potential and velocity vector distributions for the case with the capillary membrane filtration coefficient, L_p , increased by a factor of two from the base value at steady-state.	99
4.15 Dimensionless tissue solute concentration, hydrostatic pressure, Peclet number, potential and velocity vector distributions for the case with the capillary membrane filtration coefficient, L_p , decreased by a factor of two from the base value at steady-state.	100

4.16	Dimensionless tissue solute concentration, hydrostatic pressure, Peclet number, potential and velocity vector distributions for the case with the inclusion of mechanical dispersion at steady-state.	102
4.17	Dimensionless tissue solute concentration, hydrostatic pressure, Peclet number, potential and velocity vector distributions for the case with the capillary membrane filtration coefficient, L_p , varied linearly from the base value at the arteriolar end to twice the base value at the venular end of the capillary at steady-state.	104
4.18	Step function for variable capillary membrane filtration coefficient.	106
4.19	Dimensionless tissue solute concentration, hydrostatic pressure, Peclet number, potential and velocity vector distributions for the case with a step change in the capillary membrane filtration coefficient, L_p , at $z^* = 0.50$ from the base value at the arteriolar end to twice the base value at the venular end of the capillary at steady-state.	107
4.20	Dimensionless tissue solute concentration, hydrostatic pressure, Peclet number, potential and velocity vector distributions for the case with a single high flow channel centred at $z^* = 0.50$ at steady-state.	110
4.21	Dimensionless tissue solute concentration, hydrostatic pressure, Peclet number, potential and velocity vector distributions for the case with the double high flow channels centred at $z^* = 0.30$ and 0.70 at steady-state.	112
5.1	Starling forces across capillary wall. Taken from Taylor and Townsley (1987).	120
5.2	Transcapillary fluid motion : Driving forces for base case.	120
5.3	Transcapillary fluid motion : Driving forces for LS reduced by a factor of five.	121

5.4	Dimensionless tissue solute concentration, hydrostatic pressure, Peclet number, potential and velocity vector distributions for the case with lowered tissue solute concentration at $t = 1800$ s.	124
5.5	Dimensionless tissue solute concentration, hydrostatic pressure, Peclet number, potential and velocity vector distributions for the case with lowered tissue solute concentration at $t = 3600$ s.	125
5.6	Dimensionless tissue solute concentration, hydrostatic pressure, Peclet number, potential and velocity vector distributions for the case with lowered tissue solute concentration at new steady-state.	126
5.7	Dimensionless tissue solute concentration, hydrostatic pressure, Peclet number, potential and velocity vector distributions for the case with elevated venous hydrostatic pressure ($P_{ven}^* = 0.6667$) at $t = 120$ s.	129
5.8	Dimensionless tissue solute concentration, hydrostatic pressure, Peclet number, potential and velocity vector distributions for the case with elevated venous hydrostatic pressure ($P_{ven}^* = 0.6667$) at $t = 240$ s.	130
5.9	Dimensionless tissue solute concentration, hydrostatic pressure, Peclet number, potential and velocity vector distributions for the case with elevated venous hydrostatic pressure ($P_{ven}^* = 0.6667$) at $t = 600$ s.	131
5.10	Dimensionless tissue solute concentration, hydrostatic pressure, Peclet number, potential and velocity vector distributions for the case with elevated venous hydrostatic pressure ($P_{ven}^* = 0.6667$) at new steady-state.	132
5.11	Dimensionless tissue solute concentration, hydrostatic pressure, Peclet number, potential and velocity vector distributions for the case with lowered capillary solute concentration ($c_{art}^* = 0.1000$) at $t = 300$ s.	135
5.12	Dimensionless tissue solute concentration, hydrostatic pressure, Peclet number, potential and velocity vector distributions for the case with lowered capillary solute concentration ($c_{art}^* = 0.1000$) at $t = 600$ s.	136

5.13	Dimensionless tissue solute concentration, hydrostatic pressure, Peclet number, potential and velocity vector distributions for the case with lowered capillary solute concentration ($c_{art}^* = 0.1000$) at $t = 1800$ s.	137
5.14	Dimensionless tissue solute concentration, hydrostatic pressure, Peclet number, potential and velocity vector distributions for the case with lowered capillary solute concentration ($c_{art}^* = 0.1000$) at new steady-state.	138
5.15	Dimensionless tissue solute concentration, hydrostatic pressure, Peclet number, potential and velocity vector distributions for the case with enlarged capillary solute concentration ($c_{art}^* = 1.2000$) at $t = 300$ s.	141
5.16	Dimensionless tissue solute concentration, hydrostatic pressure, Peclet number, potential and velocity vector distributions for the case with enlarged capillary solute concentration ($c_{art}^* = 1.2000$) at $t = 600$ s.	142
5.17	Dimensionless tissue solute concentration, hydrostatic pressure, Peclet number, potential and velocity vector distributions for the case with enlarged capillary solute concentration ($c_{art}^* = 1.2000$) at $t = 1800$ s.	143
5.18	Dimensionless tissue solute concentration, hydrostatic pressure, Peclet number, potential and velocity vector distributions for the case with enlarged capillary solute concentration ($c_{art}^* = 1.2000$) at new steady-state.	144
5.19	Average tissue and lymphatic fluid solute concentrations through time.	147
5.20	Dimensionless tissue solute concentration, hydrostatic pressure, Peclet number, potential and velocity vector distributions for the case with colloid osmotic pressure effects throughout the system and zero arteriolar capillary solute concentration ($c_{art}^* = 0.0000$) at $t = 600$ s.	148
5.21	Dimensionless tissue solute concentration, hydrostatic pressure, Peclet number, potential and velocity vector distributions for the case with colloid osmotic pressure effects throughout the system and zero arteriolar capillary solute concentration ($c_{art}^* = 0.0000$) at $t = 1200$ s.	149

5.22	Dimensionless tissue solute concentration, hydrostatic pressure, Peclet number, potential and velocity vector distributions for the case with colloid osmotic pressure effects throughout the system and zero arteriolar capillary solute concentration ($c_{art}^* = 0.0000$) at $t = 1800$ s.	150
5.23	Dimensionless tissue solute concentration, hydrostatic pressure, Peclet number, potential and velocity vector distributions for the case with colloid osmotic pressure effects throughout the system and zero arteriolar capillary solute concentration ($c_{art}^* = 0.0000$) at $t = 3600$ s.	151
5.24	Dimensionless tissue solute concentration, hydrostatic pressure, Peclet number, potential and velocity vector distributions for the case with colloid osmotic pressure effects throughout the system and zero arteriolar capillary solute concentration ($c_{art}^* = 0.0000$) at new steady-state.	152
A.1	General description of elliptic boundary value problem.	173
A.2	Discretized geometry using linearly interpolated rectangular elements.	174
A.3	Rectangular element with linear interpolation.	175
A.4	Node communication.	181

List of Tables

2.1	Electrolyte compositions of human body fluids (in meq/l water) (taken from Ganong, 1989).	6
2.2	Plasma proteins and their approximate molecular weights (taken from Ganong, 1989).	8
2.3	Types of blood vessels in humans (taken from Ganong, 1989).	9
3.1	General model assumptions.....	32
4.1	Parameter values.	63
4.2	List of cases.	65
4.3	Results from various cases.	115
5.1	Results summary for transient cases performed at new steady-state.	153
B.1	Overall solution algorithm.	186
B.2	Capillary hydrostatic pressure solution algorithm.	187

Acknowledgement

I would like to express my thanks to N.S.E.R.C. for funding me during my stay at the University of British Columbia.

I would also like to thank the following individuals:

- Drs. J.L. Bert and B.D. Bowen for their help and guidance during the past two years,
- Dr. Clive Brereton for free beer and some lively conversations,
- Linda Hou and Katrina Gaarder (yes negative time) for the great chats,
- Mike 'MTSman' Choi, Ian 'Spud' Wilson, and Rory 'Sheep' Todd for their friendship,
- my parents for all their support and love over the years,
- and Raksha, I thank you the most for the love and caring that makes you the most important person in my life - LILLYANDIVY forever my love.

Chapter 1 : Introduction

The circulating blood contains various solutes which are distributed via the cardiovascular system to the tissues within the human body. These solutes are transported into the space between the tissue cells (the interstitium). Nearly all of this material exchange between the circulatory system and interstitial space occurs in capillaries. This is termed microvascular exchange and involves specifically the transport of fluid and solutes (proteins and electrolytes) across the capillary membrane, within the interstitial space, and out the lymphatics. The lymphatics drain fluid from the interstitium back into the circulation. The regulation of the microvascular exchange system is very complex and depends largely on the properties of the capillary membrane, the interstitium, and the lymphatics. The regulatory mechanisms of microvascular exchange protect against edema formation (excess accumulation of fluid) or dehydration. The objective is to identify controlling features of microvascular exchange system and their influence on the system dynamics for the prevention of edema or dehydration.

The dominant forces driving fluid motion across the capillary wall and within the interstitium are the hydrostatic and colloid osmotic pressures. The colloid osmotic pressure lowers the driving potential for fluid motion and is a non-linear function of the protein concentration. In this way, it acts to dilute protein. The driving potential is the difference between the hydrostatic pressure and the colloid osmotic pressure. This exists across the capillary wall and within the tissue. Proteins are driven across the capillary membrane by

two main mechanisms. The concentration difference across the capillary membrane and the fluid motion induce both diffusion and convection respectively.

The potential drop along the capillary causes fluid and solutes to be filtered into the interstitial space at the arteriolar end of the capillary. Depending on the strength of the lymphatic sink, material may be reabsorbed back into the capillary at the venular end of the capillary. An increase in the lymphatic sink strength enlarges the lymph drainage from the system. The filtration, reabsorption, and lymphatic drainage create recirculation patterns within the tissue space.

The amount of fluid which leaves via the lymphatic sink is a function of the local tissue hydrostatic pressure. Similarly, the rate at which solute that drains out through the lymphatic sink is both a function of the local tissue pressure and solute concentration. The microvascular exchange system obviously permits complex behaviours which are the result of the fluid-solute-tissue matrix interactions in the presence of the pressure and concentration fields.

Experimental investigations of the microvascular exchange system are difficult due to the scale of the system. Typical dimensions are in the range of tens to hundreds of micrometers. An alternative and complementary approach is the development of complex mathematical models describing microvascular exchange. These models can be used to examine system dynamics and sensitivity and suggest directions for further experimental research. Several mathematical models of microvascular exchange have appeared in the past few years (Baxter and Jain, 1989, 1990, 1991a, 1991b; Taylor *et al.*, 1990b; Chapple, 1990). The two types of models in common use are compartmental and spatially distributed models. Compartmental models assume well-mixed, homogeneous compartments between which material exchange occurs. The equations governing transport between the compartments are functions of time only. In spatially distributed models, the material spatially distributes itself throughout the system space nonhomogeneously. The equations are functions of position in addition to time.

In this work, a transient, spatially distributed model is developed in cylindrical coordinates to describe microvascular exchange of fluid and a single solute. The distributions of fluid velocity and solute concentration are determined. In this manner, the effects of capillary membrane properties, osmotic pressure, the lymphatic sink, and high fluid conductivity channels can be examined. It also permits the use of the model to suggest key features of the system that modulate and control hydrostatic pressure, fluid motion, and solute field behaviour, possibly by some feedback mechanism. One of the primary uses of such models is use as a tool to suggest possible further experimental work. Also, assumptions about the system may be tested and validated.

In Chapter 2 the pertinent microvascular physiology is briefly outlined. Chapter 3 presents the governing equations of microvascular exchange and model assumptions. The appropriate boundary conditions are also presented. In Chapter 4, a sensitivity analysis is presented detailing the influence of various physiological parameters on the microvascular exchange system. The effects of variable capillary membrane permeability and tissue hydraulic conductivity are also examined in this chapter. The latter allows us to investigate the impact of high flow channels on the system. The controlling features of the capillary membrane, the osmotic pressure, and the lymphatic sink are investigated in Chapter 5. The transient simulations performed here permit the identification of the roles of the capillary membrane, the osmotic pressure, and the lymphatic sink within the system from the fluid balance point of view. The results suggest that the osmotic pressure acts as a negative feedback signal regulating capillary-tissue fluid balance. The final chapter, Chapter 6, lists some general conclusions and recommendations for further research work.

Chapter 2 : Microvascular Exchange Physiology

This chapter discusses the underlying physiology of the microvascular exchange system. The circulation system is a closed loop through which blood flows. The heart pumps blood into the arteriolar circulation first via the aorta, then arteries, arterioles, and eventually capillaries. Microvascular exchange occurs between the capillaries and the surrounding tissue. The blood returns to the heart by venules and then veins.

The discussion of physiology is divided into five sections. The first section will outline broadly the physiology of the circulatory system and body fluids. The second section details the flow of blood and lymph through the circulatory system and lymphatics and the major microvascular mass exchangers, the capillaries. The third section presents the interstitium, its constituent materials, and properties. In the fourth section, the flow properties of membranes and the nature of capillary walls will be summarized. The remaining section, section five, will briefly describe the structure and function of some tissues. The focus in that section will be on the geometrical configuration of capillaries within tissues.

2.1 Body Fluid Compartments and the Circulation System

The basic unit of machinery in all living creatures is the cell. Cells exist in multicellular organisms in a sea of extracellular fluid. This fluid supplies cells with nutrients and accumulates metabolic wastes. The extracellular fluid is divided into two compartments, the interstitial fluid and the blood circulation. In an average adult male human, the intracellular water (fluid within cells) constitutes about 40% of the total body weight (Ganong, 1989). The extracellular component, meanwhile, makes up about 20%. About one-quarter of the extracellular fluid is the circulating blood plasma and the remaining three-quarters is the interstitial fluid (Ganong, 1989). This means the blood plasma and interstitial fluid comprise about 5% and 15% of the total body weight respectively. The distribution of the body fluid compartments are shown in Figure (2.1).

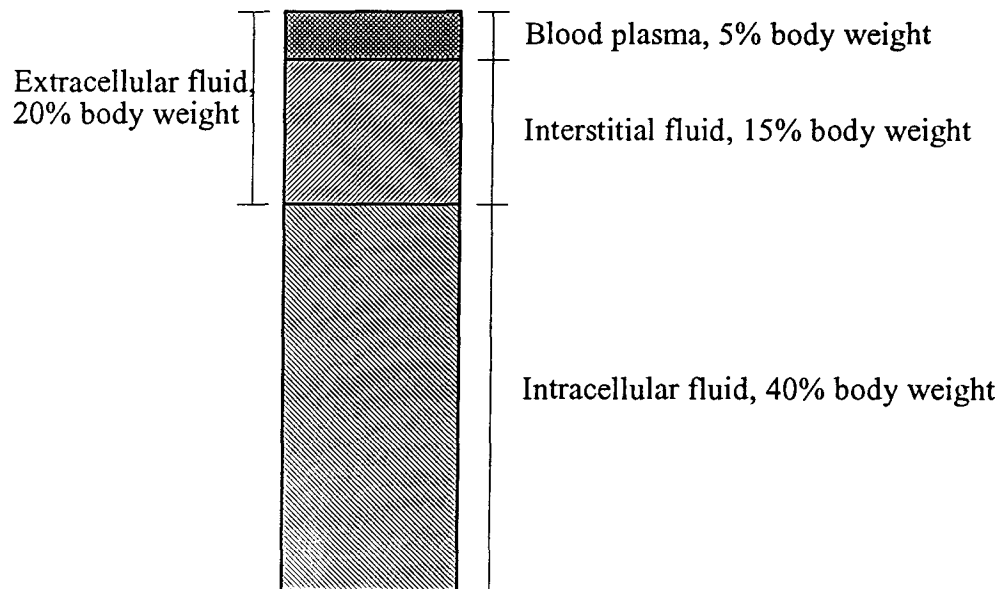


Figure 2.1: Distribution of body fluid compartments.

The composition of solutes (proteins and electrolytes) is considerably different in each of the body fluid compartments. These differences in composition are largely due to the character of the barriers between the fluid compartments. As seen from Table (2.1), the concentration of protein anions in the interstitial fluid is significantly lower than that in the intracellular fluid and the blood plasma. Also the electrolytes Na^+ and Cl^- are predominantly found in the extracellular fluid whereas K^+ is largely intracellular (Ganong, 1989).

Table 2.1: Electrolyte compositions of human body fluids (in meq/L water) (Ganong, 1989).

Solute	Blood Plasma	Interstitial Fluid	Intracellular Fluid
Na^+	152	143	14
Cl^-	113	117	small
K^+	5	4	157
Mg^{2+}	3	3	26
Protein anions	16	2	74
HCO_3^-	27	27	10

Besides supplying nutrients to cells and accumulating wastes, another function of the body fluids is to provide buffering capacity. Buffering allows the intracellular and extracellular fluids to maintain a constant pH. For instance, the pH of the extracellular fluid is maintained at 7.40 ± 0.05 (Ganong, 1989).

The particular fluid compartments of interest in this work are the blood circulation (in the capillaries) and the interstitial space. The blood circulation system removes wastes (for example carbon dioxide) from and supplies nutrients (for example oxygen) to body tissues. This is achieved via the cardiovascular system. The latter consists of the heart (a pump) and a complex system of branching elastic tubes that distribute the blood throughout the body. The left ventricle of the heart pumps blood first through arteries, then arterioles,

and ultimately capillaries. After mass exchange within the capillaries, the blood drains through venules and then veins back to the right atrium of the heart. This closed circuit is the systemic (major) circulation. In the pulmonary (lesser) circulation, the right ventricle pumps blood into the vessels of the lungs. This is the site of gas exchange.

An additional circulatory system is the lymphatic circulation. Fluid and solutes exchange across the capillary wall into the tissue. Some of this exchanged material that is derived from the interstitium flows into the lymphatic vessels that drain via the thoracic duct into the venous system. This fluid is known as lymph. More details about the lymphatics and capillary exchange will be discussed later.

2.1.1 The Blood and Plasma Proteins

The blood is essentially a suspension of several cellular components - red and white blood cells and platelets - in plasma. Red blood cells carry oxygen bound to hemoglobin. The white blood cells are instrumental in the immune system for body defenses to viral and bacterial infections. Dissolved within the blood plasma are many ions, proteins, organic and inorganic molecules. These may serve several functions, for example, as nutrients, hormones, or aid in the transport of other compounds.

Table (2.2) lists some plasma proteins found in blood. The most abundant proteins are albumin, globulin, and fibrinogen. At the normal plasma pH of 7.40, these proteins are in their anionic forms. The proteins cannot easily traverse the capillary walls and thus exert a colloid osmotic pressure difference across the capillary wall. A reduction in the tissue-side colloid osmotic pressure tends to draw water back into the blood circulation from the interstitial space (this effect actually manifests itself as a reduction in the local transmembrane potential). The most abundant and osmotically active protein is albumin. Normally, over 50% of the plasma protein is albumin. Previous work (Taylor, 1990) on

microvascular exchange indicates that colloid osmotic pressure and its gradients have significant effects on fluid flows and solute distributions within the interstitium. When plasma protein levels are low (prolonged starvation or liver disease), this is known as hypoproteinemia. The decrease in protein osmotic activity leads to edema formation, i.e., excess fluid in tissues.

Table 2.2: Plasma proteins and their approximate molecular weights (Ganong, 1989).

Plasma Protein	Molecular Weight (Daltons)
Albumin	69000
Hemoglobin	64450
Fibrinogen	340000
β_1 - Globulin	90000
γ - Globulin	156000

2.2 The Blood and Lymphatic Flow and Microvascular Exchange

Blood flows throughout the systemic circulation via different blood vessels. The driving force for flow is mainly the hydrostatic pressure gradient set up by the pumping action of the heart. To a lesser degree, diastolic recoil of the arterial walls, vein compression during exercise, and negative pressure generated in the thorax during inspiration also contribute to blood flow. The blood vessels are organized into various types based on their size.

2.2.1 Blood Vessel Classification

Table (2.3) categorizes the various types of blood vessels. Upon leaving the heart, the blood enters immediately the aorta and then the arteries. These vessels are thick-walled and of large diameter. The walls of the aorta and arteries contain copious amounts of elastic material and offer some pumping action as they recoil during diastole (Ganong, 1989).

Table 2.3: Types of Blood Vessels in Humans (Ganong, 1989).

Vessel	Lumen Diameter	Wall Thickness	Approximate Total Cross Sectional Area (cm ²)	Blood Volume Fraction (systemic)
Aorta	2.5 cm	2 mm	5	0.02
Artery	0.4 cm	1 mm	20	0.08
Arteriole	30 μm	20 μm	400	0.10
Capillary	5 μm	1 μm	4500	0.05
Venule	20 μm	2 μm	4000	0.54
Vein	0.5 cm	0.5 mm	40	
Vena cava	3.0 cm	1.5 mm	18	

The blood then flows into smaller diameter vessels called arterioles. These contain less elastic tissue than arteries but contain more smooth muscle. This muscular action provides the main source for resistance to blood flow in the circulation. The arterioles subdivide further into smaller vessels called metarterioles which then empty into the capillary beds. The capillary bed is arranged as a complex random network of relatively highly permeable tubes within the tissue. This is the main site of material exchange between

the blood circulation and the interstitium. Capillaries have a wall thickness and diameter of about 1 μm and 5 μm respectively. The total available area for material exchange exceeds 6300 m^2 in a normal human adult (Ganong, 1989). Section (2.2.3) presents the structure of the capillary wall and describes its functions in detail.

The blood drains from the capillary beds into venules and eventually into veins. The walls of venules and veins are thin and distend easily, but, however, do contain some smooth muscle. This permits them to function as a variable volume blood reservoir (Ganong, 1989).

2.2.2 The Lymphatics

Some of the fluid from the interstitial space flows into the lymphatic circulation. Figure (2.2) illustrates the form and structure of a typical lymphatic terminal. Interstitial fluid enters the lymphatic system through a readily deformable lymphatic bulb into the initial lymphatics that have no smooth muscle and are not contractile. These vessels join to form collecting lymphatics that may or may not contain smooth muscle and valves. A tree structure then follows as the lymphatic vessels converge to form bigger vessels. Lymphatic vessels are not necessarily paired with any blood vessel but are randomly distributed throughout the interstitium (Schmid-Schonbein, 1990).

It is not clearly understood how fluid and solutes are transported into the lymphatics and how lymph is propelled within the lymphatic system. On average, about 50% of the total circulating protein recirculates via the lymphatics and 2-20 liters of fluid pass through the lymphatics daily (Ganong, 1989; Guyton *et al.*, 1987). Material transport requires some form of potential difference. Two different forms of lymph pump are thought to exist corresponding to the two different observed lymphatic anatomies (Schmid-Schonbein, 1990). They are the intrinsic and extrinsic lymph pumps.

The periodic compression of the microlymphatics by its own smooth muscle is the mechanism proposed for the intrinsic lymph pump. Bat wing is the only known mammalian example where this type of mechanism exists. The smooth muscle activity acts to fill the lymphatics by expanding the lymphatic ending. Lymph then empties into the collecting lymphatics. A requirement for this to work is that the membrane of the initial lymphatic bulb be permeable to material in one direction only. This is achieved through the use of endothelial microvalves which prevent fluid from flowing out of the lymphatics (Schmid-Schonbein, 1990).

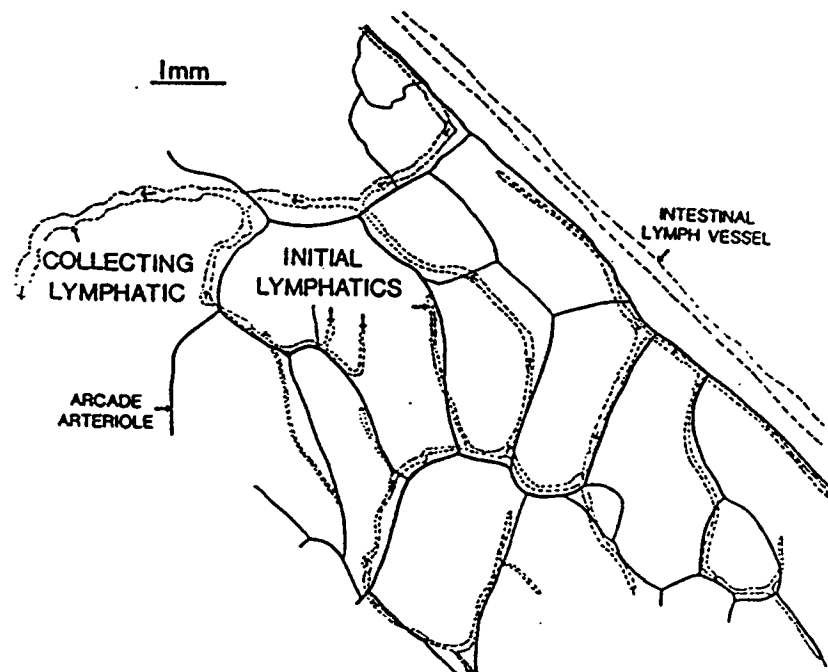


Figure 2.2: Structure of lymphatics in cat mesentery (taken from Schmid-Schonbein, 1990).

The extrinsic pump mechanism does not make use of smooth muscle to drive material into the initial lymphatics. The only way to achieve lymph flow in this case is via a pressure drop from the interstitial space to the initial lymphatics or an active lymphatic membrane

pump operated by some cellular transport mechanism. Such a transport mechanism has not been conclusively identified as yet. Further, a pressure drop from the interstitium to the initial lymphatics has not been firmly established. Pressure drops found experimentally tend to be small and periodic (Schmid-Schonbein, 1990).

The second approach is the one adopted for this work. The lymph drainage rate is assumed to be a function of the local tissue hydrostatic pressure and lymphatic sink pressure.

Tissues subjected to increased pressure drops between the interstitium and the initial lymphatics have enhanced lymph flows. For this reason, passive limb movement and skin massage increase lymph flow. At present, the formation of lymph and dynamics related to its flow are not well understood (Schmid-Schonbein, 1990).

2.2.3 Microvascular Exchange

The basic functional unit of the microvascular exchange system is the capillary and its associated envelope of tissue. Also associated with this system unit are any lymphatics that may drain interstitial fluid. The lymph fluid eventually returns back to the circulation via the right and left subclavian veins.

Material (fluid and solute) exchange between the capillary and interstitium encounter two main resistances, namely the capillary wall/basement membrane, and the interstitium itself. Each of these resistances will be discussed in some detail in the following subsections.

The Capillary Wall and Basement Membrane

The capillary wall consists of a single layer of endothelial cells. Figure (2.3) illustrates the structure of the capillary wall. The basement membrane (or *basal lamina*) is a thin structure consisting primarily of a different specialised form of collagen than that found

in the interstitial space. It surrounds and supports the blood vessels of the microvasculature in an extracellular matrix envelope. In addition to its mechanical functions, the basement membrane may also serve as a resistance to or conductance for material exchange (Bert and Pearce, 1984).

The capillary wall consists of a monolayer of epithelial cells. In general, capillary walls are similar from tissue to tissue. Clear differences arise, however, when considering the relative molecular sizes of substances that may cross the capillary wall in different tissues. In most tissues, water and relatively small solutes are the only materials that may cross the capillary walls with ease. The tissue fiber matrix restricts high molecular weight species such as plasma proteins due to their size. However, these molecules may transfer into the interstitial space by a variety of means.

There is an assortment of different transport pathways across capillary walls that have been proposed. These are outlined in the following :

- vesicular transport

Plasma and substances in solution are taken up by endocytosis on the capillary luminal side, transported across the endothelial cell interior, and then released into the interstitium by exocytosis (Ganong, 1989). These vesicles may fuse to form aqueous channels permitting passage of plasma (Bassingthwaite *et al.*, 1989).

- interendothelial cell clefts

Material transport may go through the endothelial cells or through the clefts between adjacent cells. These junctions usually vary in size from tissue to tissue but average between 10-20 μm except in the brain microvasculature where the junctions are nearly completely closed (the relatively impermeable blood-brain barrier). The structure of these *pores* is not well understood (Silberberg, 1988).

- fenestrations

The walls of some capillaries contain fenestrations. These are areas of the endothelial cell membrane that are stretched to form gaps typically between 20-100 nm in diameter.

These fenestrations allow passage of relatively large molecules. In the liver, these gaps may be of the order of 3000 nm diameter making the capillary wall very porous (Ganong, 1989).

- passive diffusion

The capillary wall is very permeable to water and other small non-polar solutes. Lipid soluble molecules also pass through the capillary wall but are hindered by the aqueous intracellular environment and thus can only pass through the capillary wall by travelling within the endothelial cell membrane of vesicles. These substances simply diffuse down their chemical potential gradient.

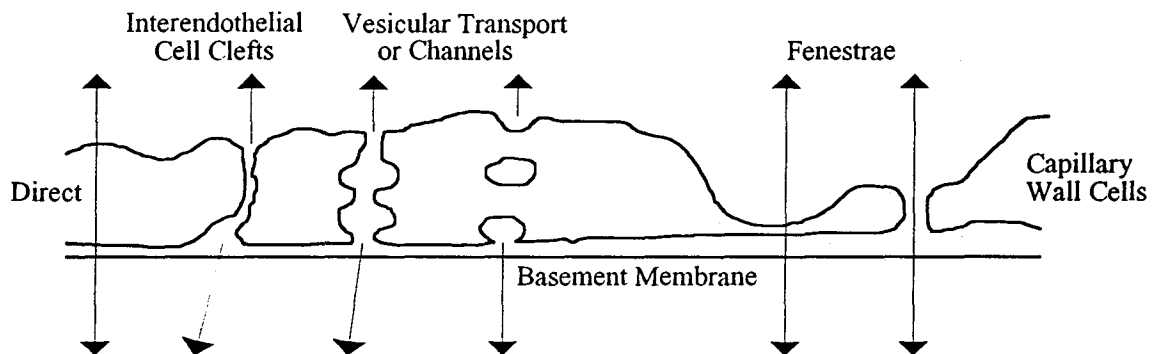


Figure 2.3: Structure of and transport mechanisms through capillary walls

The mechanisms for transport across the capillary wall are summarized in Figure (2.3). There are other factors that affect transcapillary transport of solutes such as electric charge, solute concentration, and pressure differences. The effect of albumin concentration and hydrostatic pressure on capillary wall hydraulic conductivity has been studied extensively (Dull *et al.*, 1991; Iida, 1990; and Parker *et al.*, 1984).

Transcapillary Transport

The capillary wall exhibits sieving characteristics allowing it to be treated simply as a membrane. The various forms of transport across the capillary wall are not all fully understood and so it is often treated mathematically as a porous membrane (Ogston and Michel, 1978; Curry, 1984; Taylor, 1990a). Here material exchange rates are expressed as the product of a driving force, usually the potential gradient, and a conductivity constant (inverse resistance). The mathematical complexity of treating the membrane is simplified via the use of the lumped resistance term.

There are two main driving forces for fluid exchange across the capillary wall. These are the hydrostatic pressure and osmotic pressure gradients. The latter arises because of solute (protein) concentration difference across the capillary membrane. These two forces for fluid flow have been termed the Starling forces. The colloid osmotic pressure is usually a non-linear function of the solute concentration and reduces the local fluid chemical potential. Figure (2.4) illustrates the roles of the Starling forces.

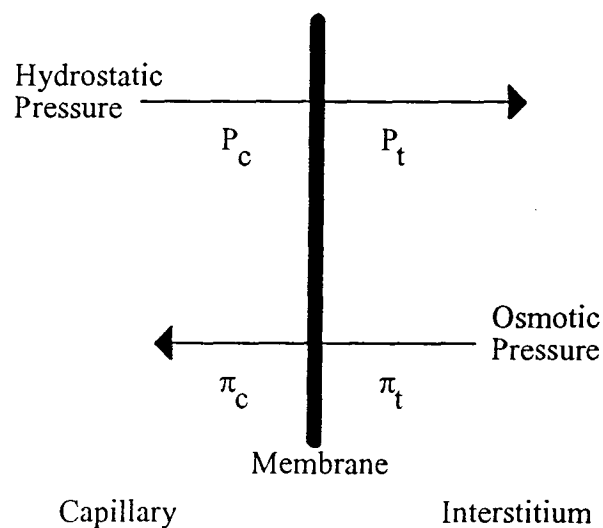


Figure 2.4: Starling Forces

The Starling forces give rise to the Starling hypothesis (Taylor and Townsley, 1987) :

$$v_{f,n} = L_p [P_t - P_c - \sigma(\pi_t - \pi_c)] \quad (2.1)$$

where $v_{f,n}$ is the transmembrane fluid velocity, L_p is the capillary wall filtration coefficient (also known as the capillary wall hydraulic conductivity coefficient), and σ is the particular solute's osmotic reflection coefficient. P_c and P_t are the capillary and interstitial hydrostatic pressures while π_c and π_t are the capillary and interstitial colloid osmotic pressures, respectively. Note that the interstitial hydrostatic and colloid osmotic pressures used in equation (3.1) are evaluated immediately adjacent to the capillary membrane.

The solute osmotic reflection coefficient, σ , accounts for the difference between the effective osmotic pressure difference which actually operates across the membrane and the calculated osmotic pressure difference. If the reflection coefficient is equal to 1.0, the solute is totally reflected from the membrane, i.e., the membrane is impermeable to the solute. A reflection coefficient of 0.0 means the solute has the same permeability as that of water through the membrane, i.e., the only driving force for material exchange is the hydrostatic pressure gradient. Capillaries in the brain display a reflection coefficient of nearly 1.0 (impermeable), while the liver sinusoids have a reflection coefficient of nearly 0.0 (totally permeable) (Taylor and Townsley, 1987).

In most capillary membranes, the protein reflection coefficient is somewhere between 0.5 and 0.95 (Renkin, 1986). This is interpreted as meaning that the solutes are transferred into the interstitium but that the effective colloid osmotic pressure driving force is a fraction (σ) of the actual (measured) colloid osmotic pressure driving force.

If there are two different means of transcapillary exchange, for example two different pore sizes 1 and 2 (small and large pore sizes), this may be treated by an areal weighting between the two flow terms, i.e.,

$$v_{f,n} = \omega L_{p1} [P_t - P_c - \sigma_1 (\pi_t - \pi_c)] + (1 - \omega) L_{p2} [P_t - P_c - \sigma_2 (\pi_t - \pi_c)] \quad (2.2)$$

where ω ($0 < \omega < 1$) is the fractional area of pores having size 1.

The Patlak equation (Patlak *et al.*, 1963; Curry, 1987; Renkin, 1986) links solute flux across the capillary wall to the Starling hypothesis. For a membrane separating a capillary having concentration c_1 and an interstitial solution having concentration c_2 , the solute flux, j_s , is given by :

$$j_s = v_{f,n} (1 - \sigma) c_1 + \frac{PS(c_1 - c_2) Pe_m}{e^{Pe_m} - 1} \quad (2.3)$$

where Pe_m is the modified capillary membrane Peclet number given by :

$$Pe_m = \frac{v_{f,n} (1 - \sigma)}{PS} \quad (2.4)$$

and PS is the diffusive component of the capillary permeability. When the convective transport contribution is zero or the capillary membrane completely reflects the solute, equation (2.3) reduces to the simple form :

$$j_s = PS(c_1 - c_2) \quad (2.5)$$

The Patlak equation, (2.3), is a non-linear flux equation. Two assumptions to bear in mind about its use are that, first, it is only applicable to a single solute species and second, the transport pathways are all the same for both transport mechanisms (convection and diffusion).

The capillary wall Peclet number is important for indicating the relative roles of convection and diffusion in solute transport across the capillary membrane. For convection-dominated flows, Pe_m is greater than unity.

In summary, Starling's hypothesis and Patlak's equation give expressions for the fluid and solute flux across the capillary wall respectively.

2.3 The Interstitial Space

The interstitium is a three-dimensional network of fibrous connective tissue molecules embedded in a gel-like matrix consisting of various polymers dissolved in the intercellular fluid. It includes all of the tissue space outside the capillaries, the lymphatics, and the cells themselves. The fluid and solutes flow around and through the cells and the molecular meshwork occupying the extracellular space. In this respect, the interstitial space is really a porous medium. The fibers impart mechanical strength and elasticity to the interstitium. This allows for deformation and fluid accumulation within the interstitium. The resulting complicated nature and behaviour of tissue is evident. Figure (2.5) provides a visual depiction of the interstitial space.

In the following, each of the various components in the interstitium will be briefly discussed.

- interstitial fluid

The largest component of the interstitial space is water. Some of the fluid is bound to the fibrous elements in the interstitium. In addition, the effective viscosity of the fluid is

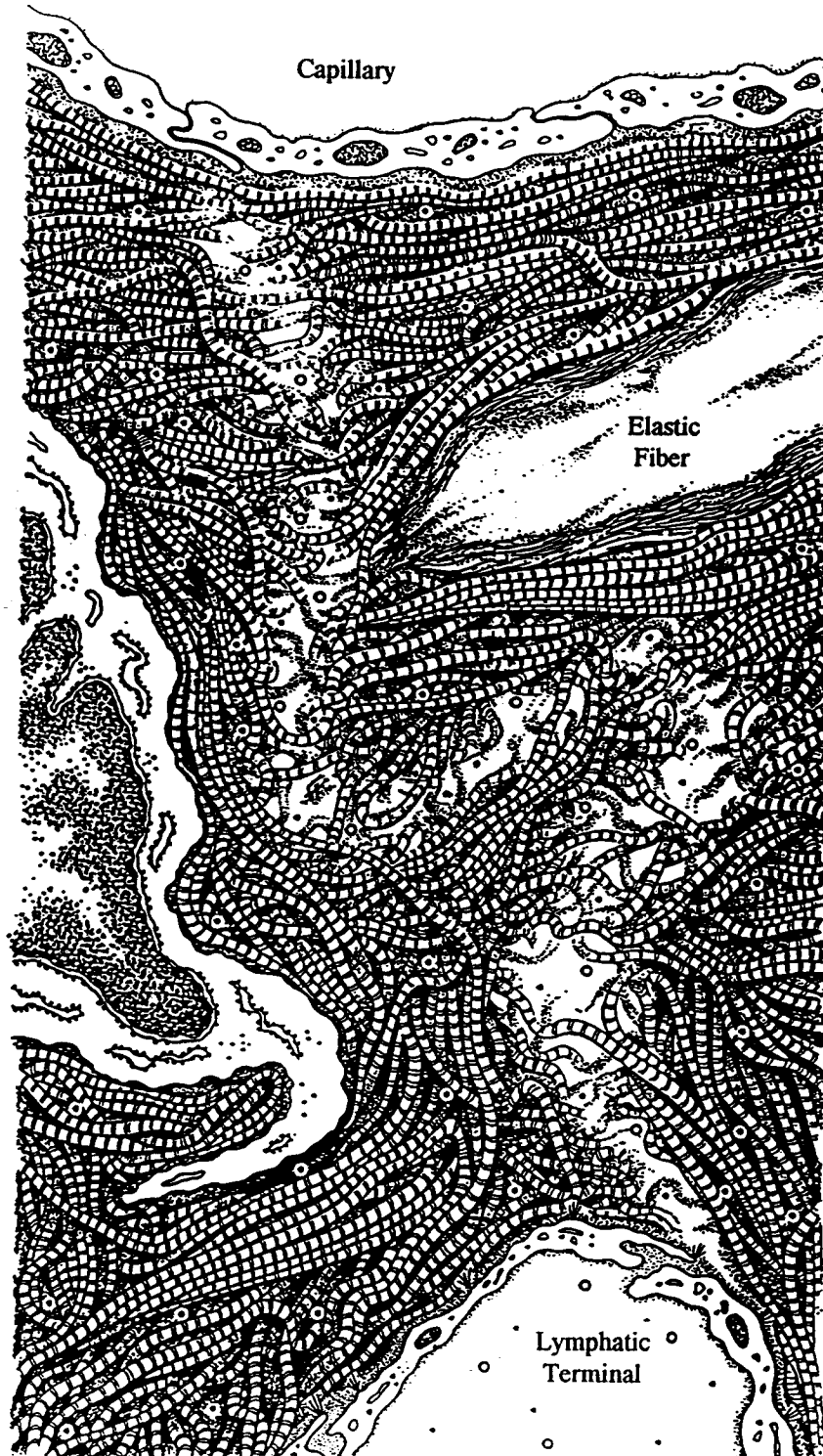


Figure 2.5: The interstitial space (taken from Bert and Pearce, 1984).

increased by the presence of mobile hyaluronan (formerly known as hyaluronate). This means that even under very high pressures, a significant portion of the fluid is retained in the tissue (Lanir, 1983). The interstitial fluid originates from the capillary and either is reabsorbed back into the capillary or drains into the lymphatics. Like many porous media, the interstitial matrix is virtually impossible to describe rigorously from a microscopic point of view. It is expected as fluid and solute traverse the interstitium that some channeling occurs. This phenomena is not well understood and has not been conclusively proven (Bert and Pearce, 1984).

- collagenous fibers

Collagenous fibers impart structure and mechanical strength (in the form of tensile strength) to the interstitium. These are long fiber bundles consisting of collagen molecules (tropocollagen). A collagen fiber consists of an organized array of collagen molecules. All of the molecules are arranged in parallel with many stable covalent cross-linkages between the molecules providing the high tensile strength (Bert and Pearce, 1984; Laurent, 1987).

- elastic fibers

Elastic fibers provide tissues with elasticity, conferring a rubber-like texture to tissues. The aorta and larger arteries are particularly rich in elastic fibers (Laurent, 1987). The main elastic fiber found in tissues is elastin, which is constructed from the tropoelastin molecule. Elastin is a three dimensional network of highly hydrophobic coiled molecules jointed at many cross-links. When unstressed, elastin assumes a random configuration, and contains about 0.56 ml water per ml elastin. This water is most likely accessible to smaller solutes (for example, glucose, urea, and sodium). However, larger molecules like colloid proteins are excluded from this space (Bert and Pearce, 1984).

- glycosaminoglycans and proteoglycans

The properties these substances contribute to the interstitium are physicochemical in nature. Glycosaminoglycans are hydrophilic charged polysaccharide chains containing

an amino sugar. An example of a glycosaminoglycan is hyaluronan (molecular weight usually between 10^6 and 10^7 Daltons) (Laurent, 1987). Glycosaminoglycans are usually covalently bound in tissue to polypeptides known as proteoglycans. Hyaluronan is an unbranched polysaccharide which forms an extended random coil when solubilized. Water is bound by hydrogen bonds to the hyaluronan molecule. The coil is further expanded by the mutual repulsion of the negative charges throughout the hyaluronan molecule. The volume occupied by the random coil is often greater than 1000 times the polymer molecular volume. The effective viscosity of interstitial fluid is increased considerably in the presence of hyaluronan. This is ascribed to entanglement that occurs between different hyaluronan coils. At low hyaluronan concentrations, solutions may gel (Bert and Pearce, 1984). Proteoglycans form aggregates in the presence of and may bind to hyaluronan. These polymer chains are hydrophilic and have a high charge density. They also can bind to collagen fibers providing a stabilizing effect. These fibers tend to bind water due to their hydrophilic nature and restrict movement of the interstitial fluid and matrix (Bert and Pearce, 1984).

- interstitial plasma proteins

There are over 100 different plasma proteins (Bert and Pearce, 1984). The most abundant plasma protein is albumin. About 60% of the total body albumin (approximate molecular diameter is 7.5 nm) is contained in the extravascular space. This means that the interstitium provides a considerable reservoir for plasma proteins. At the physiological pH of roughly 7.40, most of the plasma proteins are negatively charged. All of the plasma proteins exert a colloid osmotic pressure, but most of this is contributed by albumin. This work examines the concentration distributions of protein (albumin) within the interstitium.

The response of the interstitium to any changes is the sum total of the effects of the perturbations on all of the components interacting with each other within the interstitial

space. Thus, the system behaviour is in general, very complex. In this work, several assumptions are made, simplifying the system enormously. These are described in detail in Chapter 3.

The mechanical properties of the interstitial space are predominantly determined by collagen and elastin fibers. The degree of hydration of tissue is largely determined by glycoaminoglycons and proteoglycans. As mentioned earlier, the resistance of tissue to deformation is due to the mechanical properties of the fiber matrix, the binding of the fluid to matrix elements, and the increased fluid viscosity due to hyaluronan. As a tissue deforms, the fibers rotate, stretch, and compress in the tissue volume. This movement exerts stress on the fluid forcing it to be expelled from the matrix.

2.3.1 Volume Exclusion

Volume exclusion is the term applied to the phenomenon occurring when the meshwork flow domain limits solutes of larger dimensions than the matrix voids. The interstitial space consists of collagen, elastin, hyaluronan, and proteoglycans producing a dense fibrous network of molecular dimensions. This means that larger solutes will be restricted from entering some regions of the interstitium because of steric exclusion. The result is a larger effective solute concentration due to the smaller possible occupation volume. It is this effective solute concentration which will determine the osmotic driving force for fluid flow.

An example illustrating the effect of volume exclusion is that of albumin exclusion by hyaluronan. Hyaluronan solutions of 0.5% and 1.5% by weight exclude albumin from 25% and 75% of the solution volume respectively (Bert and Pearce, 1984).

It is necessary to include solute exclusion in any mathematical description of the interstitium due to its effects on solute concentration.

2.3.2 Geometry of Tissue

This section briefly describes the arrangement of capillaries in tissues. This will serve as the basis for defining the functional unit used in the next chapter to formulate the microvascular exchange model.

Figure (2.6) presents a capillary network geometry from the frog sartorius muscle (Dietrich and Tyml, 1992). As can be seen, the capillaries are largely arranged in parallel to each other. Single unbranched capillary lengths appear to average between 200-800 μm . Klitzman and Johnson (1982) determined that the average capillary length in the hamster cremaster muscle was 262 μm . The functional unit described in the next Chapter is based on the single unbranched capillary length. This is assumed in Chapter 4 to be 300 μm . Intercapillary spacing has been experimentally found to be of the order of 40-60 μm (Intaglietta and Zweifach, 1971; Ganong, 1989). This is assumed to be 60 μm in Chapter 4.

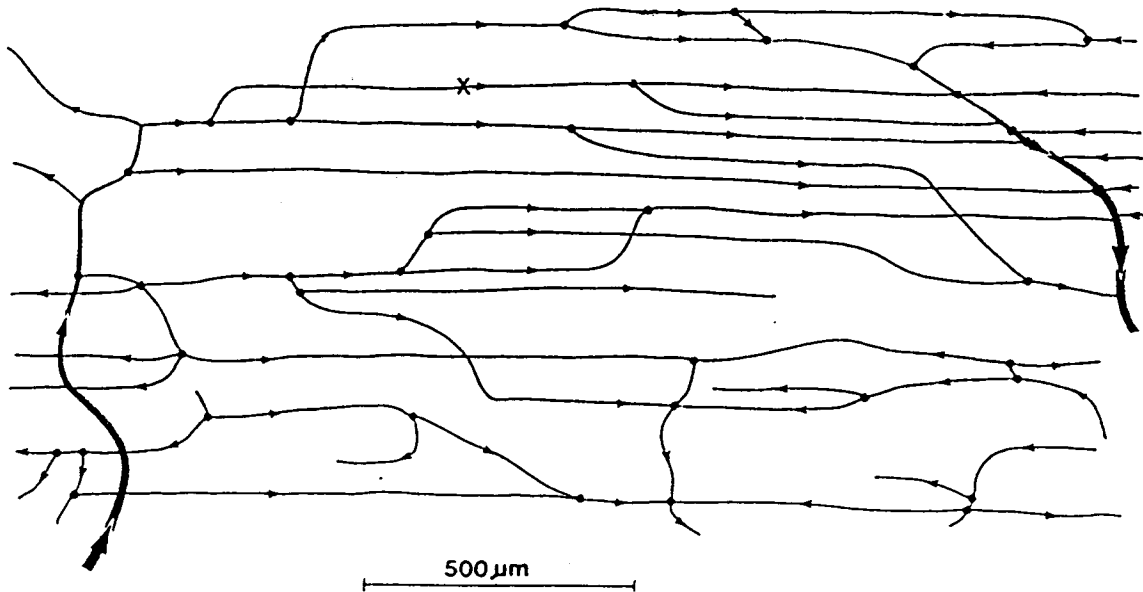


Figure 2.6: Microvascular network of the frog sartorius muscle (taken from Dietrich and Tyml, 1992).

Chapter 3 : Model Development and Formulation

This chapter presents the model development and formulation. The first section reviews microvascular models found in the literature. The second section discusses the continuum approach for fluid and solute transport. The third section presents the governing equations of microvascular exchange. The associated boundary conditions are given in the fourth section. The fifth section briefly outlines the mathematical treatment of fluid and solute exchange in the capillary. The numerical procedure is outlined in the sixth section. The final section summarizes the governing equations and boundary conditions.

3.1 Literature Review

A wide variety of mathematical models have been developed for different physiological systems. These models aid in our understanding of the fundamentals of transport and material exchange in the human body. The expectation is that mathematical models provide a framework for experimentation, especially with respect to determining physiological parameters for predictive behaviour and governing mechanisms of transport and regulation.

Microvascular exchange has been receiving much attention during the last couple of decades. Mathematical models have been developed to investigate the underlying mechanisms of pressure and flow regulation and transcapillary material exchange. The models are becoming increasingly complicated. They include such factors as property heterogeneity, colloid osmotic pressure, and lymphatic sinks, thus serving as more effective research tools.

Early attempts at modeling microvascular exchange (Apelblat *et al.*, 1974; Intaglietta and de Plomb, 1973; Salathe and An, 1976; An and Salathe, 1976) generally investigated fluid exchange. These models did not include solute transport and thus assumed colloid osmotic effects were constant in the region of interest. Salathe and Venkataraman (1978) presented a capillary-tissue fluid exchange model taking variations in plasma and interstitial osmotic pressure into account due to protein convection and diffusion. Their model, however, neglects transcapillary protein exchange. They obtained analytical solutions using perturbation methods. Weiderhielm (1979) performed a non-linear simulation of capillary fluid exchange including the effects of volume exclusion due to glycoaminoglycans and proteoglycans. Plasma protein transfers into the interstitium via convection and diffusion through large pores at the venous end of the capillary. An analog computer model was used to generate the simulations. This analysis is similar conceptually to a compartmental model since tissue and capillary variables were functions of time only (spatially invariant).

Blake and Gross (1980, 1981) presented a series of papers outlining a model for fluid exchange in and between capillaries. The model assumes the capillaries are parallel cylinders of finite length. They assumed that there is Poiseuille flow in the capillaries and transcapillary fluid exchange obeys Starling's hypothesis. Constant protein concentrations throughout the solution domain were assumed and analytical solutions were found for single and multiple capillaries in parallel.

Benoit *et al.* (1984) proposed a compartmental model for fluid and protein exchange in the rat intestine. They consider three compartments: the capillary, interstitium, and lumen. They used the Patlak equation to evaluate the protein flux across the capillary membrane. Flessner *et al.* (1984, 1985a, 1985b) presented a series of papers discussing a distributed model of peritoneal-plasma transport. They use a combined compartmental approach in conjunction with a one-dimensional spatially distributed model for solute transport within the peritoneal tissue. They assumed the colloid osmotic pressure is constant within each compartment. They also included lymphatic drainage of material via the use of

an uptake rate expression. Their analysis treated volume exclusion and tortuosity effects by lumping them into an effective diffusivity. A retardation factor was also included to account for convective transport hindrance due to the intercellular matrix-solute interactions.

Fry (1985) derived a one-dimensional finite element model (and an analytical one) to describe transport of chemically reactive macromolecules across arterial tissues. He found estimates for the tissue diffusivity and convective velocities by fitting the model to experimental data.

Bert *et al.* (1988) presented a dynamic mathematical model describing the distribution and transport of fluid and proteins among the three compartments: circulation, skin, and muscle interstitial spaces. Fluid also drained from the tissues forming lymph that returned to the circulation. They examined two mechanisms of transcapillary exchange: a homoporous 'Starling' model and a heteroporous plasma leak model. The Starling model proposes that fluid filters across a membrane from the circulation to the interstitium. Solutes may cross the membrane by diffusion or by convection due to fluid filtration. The plasma leak model proposes that fluid filters across the membrane through small completely-sieving pores. Solutes cross the membrane via large non-sieving pores at the venular end of the capillary only or by diffusion along the length of the capillary. They concluded that the plasma leak model provides a better description of transcapillary exchange. Bert *et al.* (1989), Bowen *et al.*, (1989), and Lund *et al.*, (1989) presented a series of papers describing a dynamic compartmental model of microvascular exchange after burn injuries. This model contains four compartments: circulation, muscle, injured and non-injured skin.

Recently, microvascular exchange models have shifted from compartmental approaches to spatially distributed formulations. In compartmental modeling, the material exchange occurs between well-mixed homogeneous compartments. Rate constants govern material transfer between compartments. This means that properties in each compartment are constant throughout the compartment, i.e., they represent an average value for the compartment properties. The spatially distributed models do not assume that the

compartments are well mixed and homogeneous. This means that material transport within a compartment affects the systemwide behavior. These models thus approximate the real system more closely. This added benefit is offset by the increasingly more detailed information required about the structure and transport characteristics of each compartment. The mathematical complexity of spatially distributed models also increases. The lack of data in the literature forces the use of estimates for required parameters in mathematical microvascular models. This is especially so for transport characteristics of the interstitium and lymphatics. These models are used primarily for identifying general trends; they are not expected to predict verifiable quantitative results.

Baxter and Jain (1987) presented a transient, two-dimensional model for macromolecular transport in tissues. Their model only accounts for diffusive transport of solute and neglects convection. In a later paper, Jain and Baxter (1988) investigated mechanisms of macromolecular transport in tumors. Their development is transient and included both convective and diffusive solute transport mechanisms within spherical tumors. This model was one-dimensional (radial) for both fluid and solute transport and assumed that the transport parameters and osmotic pressure are constant throughout the tumor. They extended their work (Baxter and Jain, 1989, 1990) by including a lymphatic drainage term and non-uniform heterogeneous perfusion of the tumor. They accomplished this by incorporating a necrotic core in the center of the tumor. They again assume that interstitial transport parameters and osmotic pressure are constant within the solution domain. Baxter and Jain (1991a) further extended their model by introducing extravascular binding of macromolecules and metabolism within the tumor. All of their tumor models so far consider fluid and solute transport in spherical tumors in the radial direction only. They therefore assumed that the lymphatic sinks and capillary sources exist continuously throughout the tumor. These models do not really address microvascular exchange at the capillary level as their material balances are based on differential volumes which include many capillaries.

In their most recent paper, Baxter and Jain (1991b) address microscopic macromolecular transport from capillaries by examining a single capillary in the plane perpendicular to the axis of the capillary. They assumed constant membrane transport parameters, vascular pressure, and osmotic pressures in the solution domain. The models described by Baxter and Jain above are increasingly complex but fail to account for the effects of variations in the osmotic pressure throughout the geometry on fluid movement (and thus the solute concentration distribution).

Taylor *et al.* (1990a, 1990b, 1990c) described a complex transient model of microvascular exchange that potentially includes the combined effects of interstitial swelling and protein exclusion. Local osmotic pressure gradients also determine fluid velocities within the interstitial space, i.e., fluid movement is a function of the protein concentration distribution. Transport of solute occurs by diffusion, dispersion, and convection. This model, however, does not include the effects of lymphatic drainage. The model was applied to both steady-state and transient transport in mesentery (Taylor *et al.*, 1990a, 1990c). However, it neglected the effects of capillary pressure variations as well as swelling, dispersion, and property heterogeneity in the tissue and capillary membranes.

This work extends the model proposed by Taylor *et al.* to include axial pressure and solute concentration variations in the capillary, lymphatics, and property heterogeneity within the interstitial space and the capillary membrane. The tissue is assumed as rigid with constant volume and, hence, swelling effects are assumed to be negligible.

3.2 The Interstitium as a Continuum

As described in Chapter 2, the interstitium is a complex structure consisting of a fiber matrix swollen with fluid. The hydrophilic proteoglycans and collagen form a meshwork that permits fluid to percolate throughout the organic porous medium. Dissolved within the

interstitial fluid are various electrolytes and proteins. At the molecular scale, fluid and solutes traverse the interstitial space through tortuous passages. The solutes may interact with the passage walls throughout their journey and may be hindered by electrostatic forces and the fiber matrix structure (volume exclusion). Any attempt to model the interstitium at the molecular level is impractical since it is both impossible to adequately define the geometry and measure variables (such as the pressure and concentration) at microscopic scales.

The alternative approach moves to the macroscopic scale and considers the interstitium as a continuum. The fluid and solid phases are not dealt with on an individual basis, but considered, rather, as one continuous composite phase exhibiting average properties. This means that the properties of the fluid and solid phases are spatially averaged at some local scale and continuously distributed throughout the interstitial region. Examples of averaged properties are the fluid hydraulic conductivity, the effective protein diffusivities, and the excluded volume fractions.

3.3 Model Formulation

This section presents the geometry of the problem and the governing equations for fluid and solute transport in the interstitium, their associated boundary conditions, and model assumptions. It also includes the mathematical treatment of volume exclusion and its effects on the colloid osmotic pressure and convective velocities.

3.3.1 Model Geometry

For this work, a single capillary is assumed to be the fundamental unit of microvascular exchange. The use of a single capillary model was first introduced by Krogh (1919). Here, the microvascular exchange unit is approximated as a rigid capillary of fixed

length and radius surrounded by an annular tissue space (the Krogh cylinder). Krogh (1919) used this geometry to investigate diffusive exchange of solutes. The Krogh cylinder was used by Apelblat *et al.* (1974) to describe fluid and solute exchange across the capillary. The use of the Krogh cylinder approach implies that there is no intercapillary fluid or solute communication. This means that material can enter the system but may only exit via reabsorption or lymphatic drainage.

For this work, the Krogh cylinder approach is adopted. Tissue swelling is ignored, that is, the tissue is assumed to be rigid. This implies that there is no accumulation of fluid in the system. Blood flows through the capillary due to a drop in the capillary pressure from P_{art} at $z = 0$ to P_{ven} at $z = L$. Fluid flows through the membrane based on Starling's hypothesis. Solute may be transported across the capillary membrane (based on Patlak's equation) and then distribute itself freely throughout the tissue as a consequence of the diffusive, dispersive, and convective mechanisms. The fluid and solute can be withdrawn from the tissue via a lymphatic sink. This may be confined to a specific region or may be distributed throughout the tissue space. The model geometry is presented schematically in Figure (3.1).

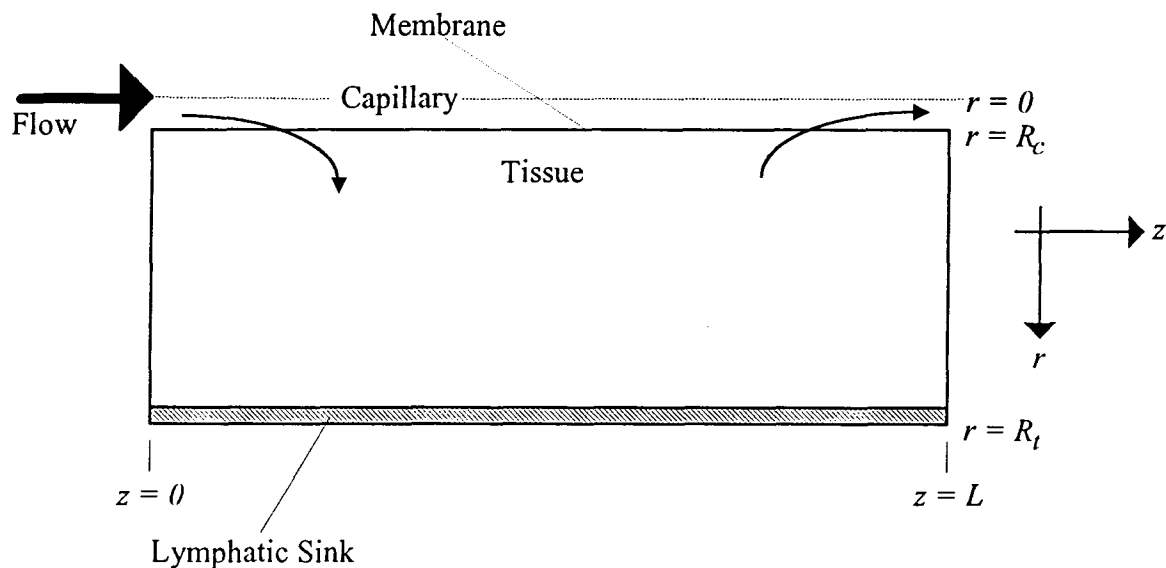


Figure 3.1: Model Geometry.

The cylindrical coordinate system is the natural system to use due to the model geometry. All governing equations are derived in this system of coordinates with axisymmetry. This means that the lymphatic sink as shown in Figure (3.1) is a concentric shell surrounding the tissue space. The outer tissue boundaries (at the $z = 0$ and $z = L$ planes and the concentric shell at $r = R_t$) are assumed to be impermeable, i.e., there is no fluid or solute transport across these boundaries. Material may only enter through the capillary wall and then exit either through reabsorption back into the capillary or through the lymphatic sink. Capillary flow enters at $z = 0$ and exits at $z = L$. The lymphatic sink can be placed at any arbitrary location within the sink and is shown at the edge of the tissue envelope in Figure (3.1). The volume of the lymphatic sink may also be varied.

The general model assumptions are listed in Table (3.1). These assumptions are used in formulating the model and are thus an intrinsic part of the model.

3.3.2 Fluid Transport in the Fiber Matrix Porous Medium

Within a differential element, the fluid mass balance equation has to be satisfied. For cylindrical coordinates in the r and z directions only, this is given by (Bird *et al.*, 1960) :

$$\frac{\partial \rho_f}{\partial t} + \frac{1}{r} \frac{\partial (\rho_f v_r)}{\partial r} + \frac{\partial (\rho_f v_z)}{\partial z} - \rho_f Q = 0 \quad (3.1)$$

where Q is a source term and ρ_f is the fluid density. Equation (3.1) simply states that the amount of fluid entering into the differential element by flow and from the source is equal to that leaving the element by flow. The source term is used to implement the lymphatic sink. In this model, the tissue is assumed to be rigid and non-deformable. The fluid density is assumed constant and as a consequence, the mass balance equation simplifies to :

Table 3.1 : General Model Assumptions.

Model Assumption Summary

Continuum model formulation.

Rigid capillary (not distensible).

Fluid density is constant.

Rigid interstitial space (not deformable).

Fluid motion in tissue can be described by Darcy's law.

Chemical potential driving fluid flow is given by $(P - \sigma\pi)$.

Effective solute drag velocity is some fraction of the fluid velocity (the retardation factor, ξ).

Interstitial space reflection coefficient assumed to be equal to 1.0. The effect of this parameter on the system is examined in Chapter 4.

Lymphatic drainage is treated simply as a sink. Solute is convected with the fluid out the lymphatic sink.

Starling's hypothesis governs fluid flow through capillary membrane.

Patlak's equation governs solute flow through the capillary membrane.

Thin film of fluid between capillary membrane and tissue porous medium (for continuity of pressure and solute concentration).

Capillary pressure only a function of distance down capillary. Capillary pressure may be assumed a linear function from the arterial to the venular pressures (Poiseuille's law).

Capillary solute concentration only a function of distance down capillary. May be assumed as constant along the length of the capillary.

Single aggregate protein represents all distinct protein species.

Dispersion of solute is described by two parameters, the longitudinal and transverse dispersivities.

Lymphatic sink material removal rate is simply given by a linear equation in the local tissue hydrostatic pressure.

$$\frac{\partial v_r}{\partial r} + \frac{v_r}{r} + \frac{\partial v_z}{\partial z} - Q = 0 \quad (3.2)$$

A general macroscopic equation that describes the flow of a fluid through an anisotropic porous medium is Darcy's law (Smith, 1990) given by :

$$v_f - v_s = -\frac{k}{\theta\mu_f} \nabla(P_t + \rho_f g z) \quad (3.3)$$

where k , θ , and μ_f are the anisotropic permeability and porosity of the porous medium, and fluid viscosity respectively. The constant g is the acceleration due to gravity. This empirical law expresses the fluid velocity, v_f , relative to the solid matrix velocity, v_s , due to an imposed fluid pressure drop, P_t , and height difference, z , across the porous matrix. Neglecting the effects of height differences and with zero solid phase velocity, this may be rewritten :

$$v_f = -K \nabla P_t \quad (3.4)$$

where K is the fluid hydraulic conductivity. Substituting Darcy's law, equation (3.4), into the mass balance equation (3.2) yields :

$$-\frac{\partial}{\partial r} \left(K_r \frac{\partial P_t}{\partial r} \right) - \frac{K_r}{r} \frac{\partial P_t}{\partial r} - \frac{\partial}{\partial z} \left(K_z \frac{\partial P_t}{\partial z} \right) - Q(P_t) = 0 \quad (3.5)$$

where P_t is the local tissue pressure. The lymphatic term, $Q(P_t)$, is a function of the local tissue hydrostatic pressure. Equation (3.5) does not include the effects of the colloid osmotic pressure and therefore has to be modified.

The driving force for fluid movement is the chemical potential gradient. In the absence of osmotically active solute, the only driving force for fluid motion is then the hydrostatic pressure. Colloid osmotic pressure serves to reduce the local driving pressure for fluid flow across a membrane. The tissue may be considered as a stack of membranes thus allowing local osmotic pressure gradients throughout the tissue. Equation (3.5) is modified to include the effect of the colloid osmotic pressure as follows :

$$\frac{\partial}{\partial r} \left(K_{rr} \frac{\partial(P_t - \sigma_t \pi_t)}{\partial r} \right) + \frac{K_{rr}}{r} \frac{\partial(P_t - \sigma_t \pi_t)}{\partial r} + \frac{\partial}{\partial z} \left(K_{zz} \frac{\partial(P_t - \sigma_t \pi_t)}{\partial z} \right) + Q(P_t) = 0 \quad (3.6)$$

where π_t is the local osmotic pressure and σ_t is the tissue reflection coefficient. If the reflection coefficient equals 0.0 then the driving force is simply the local hydrostatic pressure gradient. Solving equation (3.6) yields the tissue pressure which equals the fluid pressure since equilibrium exists locally within the porous medium. The local fluid velocities in the r and z directions may then be determined from :

$$v_{f,r} = -K_{rr} \frac{\partial(P_t - \sigma_t \pi_t)}{\partial r} \quad (3.7)$$

and

$$v_{f,z} = -K_{zz} \frac{\partial(P_t - \sigma_t \pi_t)}{\partial z} \quad (3.8)$$

Equations (3.6), (3.7), and (3.8) describe fluid transport in the interstitial space porous medium. They are not complete, however, since they do not include the effects of volume exclusion. The mathematical treatment of volume exclusion and its effects on the above equations will be presented in a later section.

3.3.3 Solute Transport in the Fiber Matrix Porous Medium

Solute transport occurs by three mechanisms in the tissue fiber matrix. These are diffusion, dispersion, and convection. All three modes of solute transport have to be included since at high convective velocities, convection and dispersion may become significant.

Fick's law gives the local diffusive flux of solute through the interstitial space :

$$j_{diff,s} = -D_{diff} \nabla c_s \quad (3.9)$$

where $j_{diff,s}$ and c_s are the diffusive solute flux and solute concentrations respectively and D_{diff} is the anisotropic diffusivity tensor for the solute through the porous medium. These diffusion coefficients are usually less than the solute's free diffusion coefficients because of the impeding effects of the solid matrix. These hindering effects are due to both steric hindrance and electrostatic interactions between the solute and the solid matrix components. For albumin, the diffusion coefficients tend to be about 1.0×10^{-12} m²/s in human tissue (Gerlowski and Jain, 1988). The effects of volume exclusion on solute diffusion is presented in a later section.

Convection is an important mechanism of solute transport in tissue. The mass flux of solute transported by convection, $j_{conv,s}$, is given by :

$$j_{conv,s} = v_{s,eff} c_s \quad (3.10)$$

where $v_{s,eff}$ is the effective solute transport velocity. The local effective solute convective velocity (solvent drag velocity) is expected to be less than the local effective fluid velocity. This is because of several factors. First, the hydrodynamic interactions between the solute and the solid matrix will retard solute flow. Second, the shape and size of the solute

molecule will result in volume exclusion effects. This effect actually promotes increased mean solute flow rates and will be explained later in more depth. The third and final effect is that of electrostatic charge. Repulsion or attraction of the solute to the solid matrix components may increase or decrease the overall solute convective flow rate and relates closely to surface depletion effects. The first factor will be briefly discussed here while the others will be discussed further in the section on volume exclusion.

The hydrodynamic effects on solute convective transport result from the viscous fluid interaction between the convected solute particles and stationary randomly arranged fibers of the solid matrix. This will hinder the movement of the solute front since the particles will be required to travel a tortuous path within the fiber matrix from one location to another and will travel at a slower speed than the transporting fluid due to viscous interaction with the solid components. Brenner and Gaydos (1976) theoretically analyzed transport of neutrally buoyant spherical particles in a Poiseuille flow in narrow capillaries. Their analysis considers specifically solute particles of radius of similar order of magnitude as the channel radius. They predict that two opposing effects will exist. First, the ratio of the particle velocity to the fluid velocity at the particle center decreases as the particle size increases. This is expected since as the particle radius increases, more solute-solid matrix interactions will occur. Second, as the size of the particles increases, they tend to remain in the central region of the fluid flow. This is the surface depletion effect which will be discussed in detail in the volume exclusion section. This effect may cause the mean solute velocities to be greater than the mean fluid velocities.

It is required to define the local effective solute convective velocity. As mentioned above, it is known to be somewhat less than the local fluid velocity. It is useful to define a retardation factor, ξ , which relates the effective solute convective velocity and the effective fluid velocity by :

$$v_s = \xi v_f \quad (3.11)$$

The transport of solute by convection is now given as :

$$j_{conv.s} = \xi v_f c_s = \xi v_s c_s \quad (3.12)$$

The retardation factor is a function of the apparent accessible pore space fraction. It should be also noted that the retardation factor is a function of the tissue hydration since the apparent accessible pore space volume varies with the tissue hydration.

The third and final solute transport mechanism is mechanical dispersion. The dispersive flux originates from microscale fluid velocity variations from the mean fluid velocity and solute flowing into microscale pathways different from the direction of the bulk convective flow. Mechanical dispersion spreads the solute front in a manner similar to molecular diffusion. For this reason, it is assumed that dispersion can be expressed as a Fickian process :

$$j_{disp.s} = -D_{disp} \nabla c_s \quad (3.13)$$

where D_{disp} is the mechanical dispersion tensor. This means that the dispersion term of solute transport can be coupled with the diffusion term as :

$$j_{dd.s} = -D \nabla c_s \quad (3.14)$$

where D is the sum of the molecular diffusion and mechanical dispersion coefficients.

The dispersion coefficients are functions of the effective convective velocities and average pore size in the porous medium (Smith, 1990). The relationship between the dispersion coefficients and the fluid velocities and porous medium structure is given by (Bear, 1972) :

$$D_{disp,ij} = \alpha_{ijkl} \frac{v_{k,s} v_{l,s}}{|v_s|} \quad (3.15)$$

where α_{ijkl} is the anisotropic dispersivity (a fourth rank tensor) and is a function of the porous medium structure and $v_{k,s}$ and $v_{l,s}$ are the fluid velocities in the k and l directions. The product of the dispersivity tensor and the fluid velocities gives the dispersion coefficients in each direction. The absolute magnitude of the velocity, $|v_s|$, is given by :

$$|v_s| = \sqrt{v_{r,s}^2 + v_{z,s}^2} \quad (3.16)$$

For an isotropic porous medium, equation (3.15) may be simplified to a function of two parameters, α_{long} and α_{tran} , the longitudinal and transverse dispersivities respectively (Bear, 1972), i.e.,

$$D_{disp,ij} = \alpha_{tran} |v_s| \delta_{ij} + (\alpha_{long} - \alpha_{tran}) \frac{v_{i,s} v_{j,s}}{|v_s|} \quad (3.17)$$

where δ_{ij} is the Dirac delta function. Typically the value of α_{long} is usually taken to be of the order of magnitude of the grain size of the porous medium (Smith, 1990). Both parameters are usually statistically estimated from experimental data to gain the best fit with model predictions. Such data is not available for human tissue so rules of thumb are used. For human tissue, the typical grain size of the solid matrix can be assumed to be the tissue cell diameter. This results in a longitudinal dispersivity of the scale 10 μm . The transverse dispersivity is usually estimated roughly as being ten percent of the longitudinal dispersivity (Smith, 1990).

In some porous media, for instance in petroleum reservoirs, dispersion exceeds diffusion by about two orders of magnitude due to the highly convective flows. Since fluid velocities tend to be less than 1.0×10^{-7} m/s in humans (Baxter and Jain, 1989), using a longitudinal dispersivity of $10 \mu\text{m}$ for human tissue suggests that dispersion is a secondary transport effect which may be safely neglected for low convective velocities.

The three modes of solute transport have been described mathematically above. Now the solute convective-dispersion equation will be presented describing the transient behaviour of solute within the interstitial space. The derivation of the solute transport equation begins with a mass balance on a differential element. This is stated as follows : the rate of accumulation of solute within a differential volume is equal to the net diffusive, dispersive, and convective transport of solute into the differential volume and the solute influx due to the source. This can be expressed as follows :

$$\begin{array}{l} \text{Rate of} \\ \text{accumulation} \end{array} = \begin{array}{l} \text{diffusive /} \\ \text{dispersive flux} \end{array} + \begin{array}{l} \text{convective} \\ \text{flux} \end{array} + \begin{array}{l} \text{source} \\ \text{term} \end{array} \quad (3.18)$$

$$(j_{dd,s}) \quad (j_{conv,s}) \quad (Q)$$

This is expressed mathematically as :

$$\frac{\partial c_s}{\partial t} = \left(D_{rr} \frac{\partial^2 c_s}{\partial r^2} + \frac{D_{rr}}{r} \frac{\partial c_s}{\partial r} + D_{zz} \frac{\partial^2 c_s}{\partial z^2} \right) - \frac{\partial(v_{r,s} c_s)}{\partial r} - \frac{\partial(v_{z,s} c_s)}{\partial z} + Q_s(c_{s,eff}, P_t) \quad (3.19)$$

where D_{rr} and D_{zz} are the diffusive-dispersive coefficients in the r and z directions respectively. The source term, $Q_s(c_{s,eff}, P_t)$, is a function of the effective solute concentration and local tissue hydrostatic pressure. This term is used to model a lymphatic sink in the tissue space. The left hand side of equation (3.19) is the rate of accumulation of solute term. The first three terms on the right hand side are the diffusive-dispersive terms in the r and z

directions. The fourth and fifth terms represent the convective transport components in the r and z direction respectively. The final term represents the lymphatic drainage of fluid and solute which is treated as a sink in this formulation.

The convective terms contain the effective solute convective velocities. These terms are calculated from the equations (3.7) and (3.8). The potential, $(P_t - \sigma_t \pi_t)$, is obtained from the fluid conservation equation (3.6). This equation, however, is a function of the local colloid osmotic pressure which is also a function of the effective solute concentration. This means that the fluid pressure equation and the solute transport equation are coupled and must be solved simultaneously. The colloid osmotic pressure is a non-linear function of the solute concentration, i.e.,

$$\pi_t = \pi_t(c_{s,eff}) \quad (3.20)$$

and this complicates the solution of the governing equations. The effective solute concentration, $c_{s,eff}$, is evaluated from the actual fluid volume the solute may occupy.

The equations governing fluid and solute movement in the interstitial have been presented. In the following sections, the implementation of the lymphatic sink will be discussed and the mathematical treatment of volume exclusion and its inclusion in the above equations will be presented.

3.3.4 The Lymphatic Sink

The fluid drainage out through the lymphatics is treated as a volumetric sink. The function governing the removal of material by the lymphatic sink is unknown. Taylor *et al.* (1973) report data for the lymph flow rate as a function of the average tissue hydrostatic pressure in a dog's thigh. The function is shown in Figure (3.2). As can be seen, it is nearly

linear below -2 mmHg and levels off when tissue hydrostatic pressures become sufficiently positive.

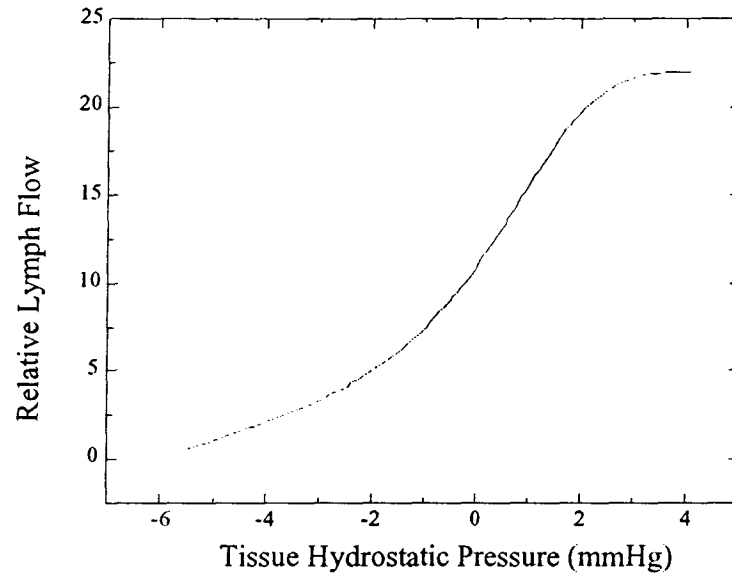


Figure 3.2: Lymph flow versus average tissue hydrostatic pressure (taken from Taylor *et al.*, (1973).

Baxter and Jain (1990) treated the lymphatic sink drainage as a linear function in the tissue hydrostatic pressure. Since there is no data for humans, for this work, as a first approximation, the lymphatic fluid depletion rate is assumed to be a simple linear function of the tissue hydrostatic pressure given by :

$$Q(P_t) = -LS(P_t - P_L) \quad (3.21)$$

This means that the lymphatic drainage is proportional to the difference between the local tissue pressure and the lymphatic sink pressure, P_L . The lymphatic drainage function is negative since the governing equations (3.6) and (3.19) are presented as having a source. The local amount of solute being drained by the lymphatic sink is then given by :

$$Q_s(c_{s,eff}, P_t) = Q(P_t)c_{s,eff} \quad (3.22)$$

This gives the mass of solute leaving the system per unit time.

The sink is implemented as a term where fluid and solute are simply removed from the system at that point. This is analogous to a binding term. This allows the fluid and solute to communicate with the rest of the tissue above and beyond the sink. The tissue fluid flow velocities at the sink are not then necessarily equal to the lymphatic convective velocity since the fluid does not all necessarily exit the system via the sink but rather flows through the local volume associated with the sink.

The conceptual picture of the lymphatic sink is displayed in Figure (3.3). In this representation, the sink is located roughly in the middle of the tissue parallel to the capillary. It is important to bear in mind that the model developed here is in cylindrical coordinates although Figure (3.3) does not reflect this.

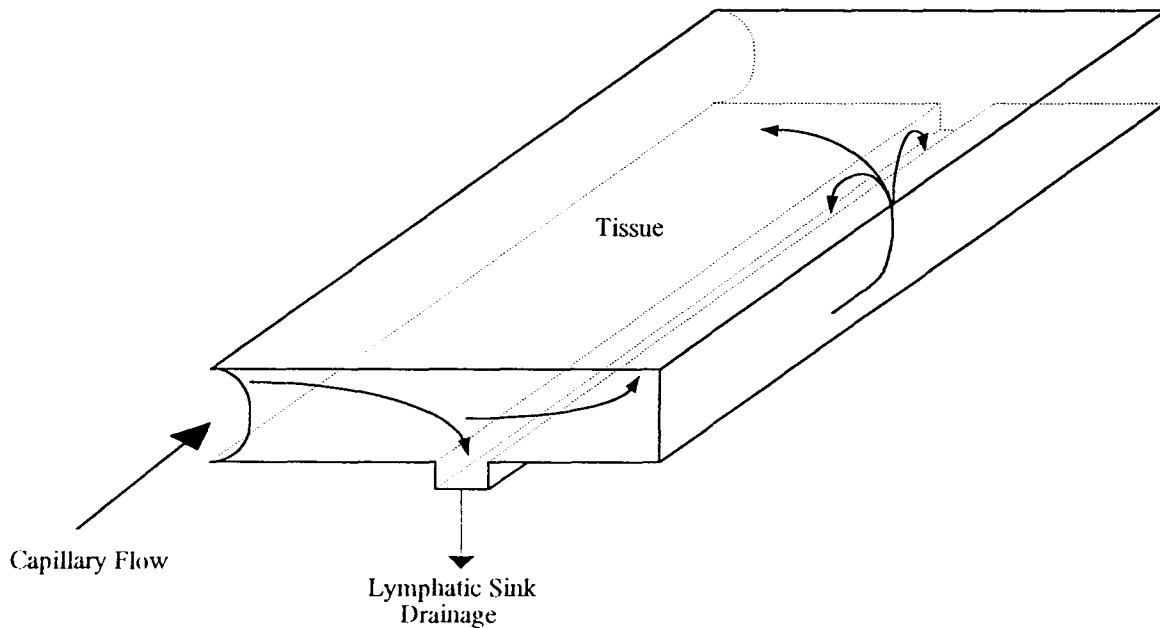


Figure 3.3: Conceptual picture of the lymphatic sink.

3.3.5 Volume Exclusion and Surface Depletion

This section presents : 1) definitions of volume exclusion and surface depletion, 2) their effect on material transport, and 3) their implementation into the governing equations presented above.

Volume Exclusion (Inaccessible Volume)

Volume exclusion refers to the phenomenon that occurs when the macromolecules are restricted from certain regions of the porous medium because the opening sizes connecting these regions are smaller than the size of the macromolecule. This excludes macromolecules from a fraction of the pore space - both in these small pores and any larger pores they give access to. There are two effects of volume exclusion. The first is a relative advancement of the solute front with respect to the fluid front. This is because the fluid front has to pass through all porous regions whereas the solute may bypass certain regions due to volume exclusion. This results in the fluid taking effectively longer flow paths than the solute. The second is that the effective solute concentration in the fiber matrix is greater than the concentration expected if the solute were distributed throughout the entire volume. In tissues, this effect cannot be ignored; for example, albumin is excluded from 60% of the total interstitial space (dermis) due to volume exclusion (Bert and Pearce, 1984).

Figure (3.4) illustrates volume exclusion through a two-dimensional porous medium. As can be seen, the solute particles are excluded from some regions of the space due to the small pore sizes. The implementation of volume exclusion mathematically is facilitated through the use of an representative elementary volume. This is displayed for a single solute in Figure (3.5) The available fraction of space 'seen' by the fluid is f_{av} . The accessible volume fraction available to the solute (space the solute can 'see') is f_{st} . The excluded volume fraction is thus given by :

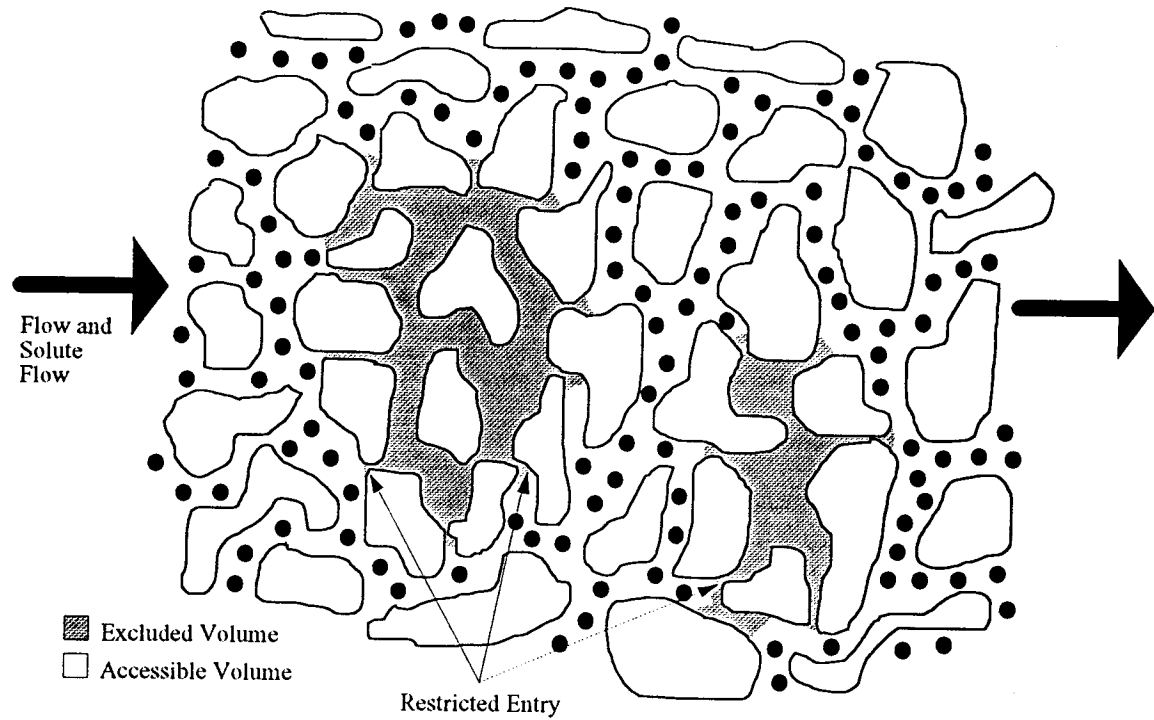


Figure 3.4: Volume Exclusion of Solute.

$$f_{ex} = f_{av} - f_{st} \quad (3.23)$$

The volume fractions must sum to unity, that is :

$$f_{st} + f_{ex} + f_{im} + f_{so} = 1 \quad (3.24)$$

where f_{so} and f_{im} are the fractions of the volume occupied by the solid matrix and the immobile fluid bound to the solid matrix respectively.

The solid phase consists mainly of the large polymers mentioned in Chapter 2, that is collagen, glycosaminoglycans, proteoglycans, and elastin. The dominant glycosaminoglycan, hyaluronan, is hydrophilic and readily binds the interstitial fluid. A more extensive

description of partitioning the representative elementary volume for multiple solutes is provided in Taylor (1990a).

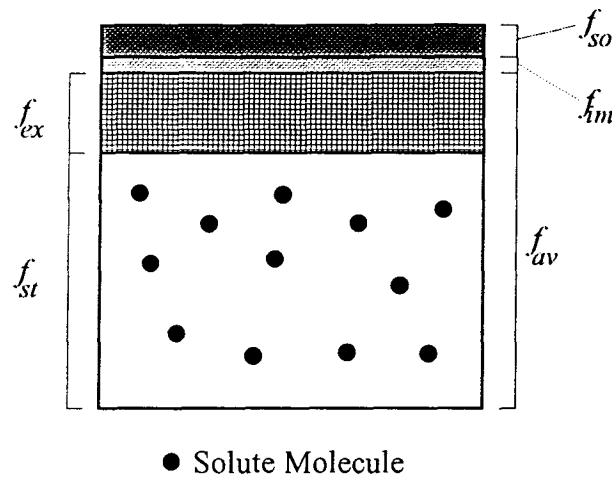


Figure 3.5: Partitioning of a representative elementary volume into the various volume fractions.

The various volume fractions will in general be both functions of the tissue hydration and the fiber matrix properties. Now it remains to be seen how volume exclusion is incorporated into the governing equations of fluid and solute transport mathematically.

The fiber matrix, through volume exclusion, restricts the accessible fluid volume available to solutes. This means that the effective solute concentration within the elementary volume is somewhat greater because it occupies a smaller fluid space. The solute can access only the f_{st} fraction of the elementary volume. This means the effective solute concentration in the elementary volume is given by :

$$c_{s,eff} = \frac{c_s}{f_{st}} \quad (3.23)$$

The osmotic pressure is determined by the effective solute concentration. This is then given by :

$$\pi_t = F(c_{s,eff}) \quad (3.24)$$

where F is typically a low order polynomial in $c_{s,eff}$:

The mechanisms of solute transport will be affected as follows. The diffusive-dispersive flux of solute can only transport material through the volume fraction available to the solute. This gives a diffusive-dispersive flux as follows :

$$j_{d,s} = -f_{st} D \nabla c_{s,eff} \quad (3.25)$$

The convective terms are also affected because volume exclusion has an influence on the fluid velocities. The fluid can only flow through the fraction of pore space available to it, that is f_{av} . The effective fluid velocities through the fiber matrix porous medium will then be given by :

$$v_{f,eff} = \frac{v_f}{f_{av}} \quad (3.26)$$

This, however, is not incorporated into the fluid pressure equation. This is because the experimentally determined hydraulic conductivities are assumed to have the volume exclusion effects lumped into them. Volume exclusion, however, does affect the solute drag velocity since it cannot 'see' all of the fluid flow due to the excluded fluid volume f_{ex} . Therefore, the effective solute convective velocity has to be modified as follows :

$$v_{s,eff} = f_{st} \xi v_{f,eff} \quad (3.27)$$

The final form of the solute transport equation including volume exclusion effects is then given by :

$$\begin{aligned} \frac{\partial c_{s,eff}}{\partial t} + \frac{\partial(v_{r,s,eff} c_{s,eff})}{\partial r} + \frac{\partial(v_{z,s,eff} c_{s,eff})}{\partial z} = \\ f_{st} \left(D_{rr} \frac{\partial^2 c_{s,eff}}{\partial r^2} + \frac{D_{rr}}{r} \frac{\partial c_{s,eff}}{\partial r} + D_{zz} \frac{\partial^2 c_{s,eff}}{\partial z^2} \right) + Q_s(c_{s,eff}, P_i) \end{aligned} \quad (3.28)$$

This equation is solved to obtain the effective solute concentrations. The solute convective velocities are obtained indirectly from the fluid conservation equation which is a function of the solute concentrations via the colloid osmotic pressure. The colloid osmotic, in turn, is a function of the effective solute concentration. The coupled equations (3.6) and (3.28) must be solved simultaneously.

Surface Depletion

To some extent, surface depletion is very similar to volume exclusion in that some portion of the elementary volume is not available to the solute. While volume exclusion refers to an inaccessible pore space due to the sizes of the macromolecules and the pores in the fiber matrix, surface depletion refers to the steric exclusion of macromolecules from the pore wall (Sorbie *et al.*, 1991). Volume exclusion is more likely to occur in low permeability porous media whereas surface depletion is more dependent on the shape and orientation of the molecule. It is expected that surface depletion will be less for spherical globular molecules than long rod-like molecules of equivalent molecular mass.

Figure (3.6a) illustrates surface depletion using two molecules: a rod and sphere and a sphere in a random network of rods. Rod-like molecules will not be allowed to freely rotate within a layer having the same thickness as the length of the rod-like molecule. This layer is referred to as the depleted layer (Sorbie, 1990). Thus the excluded volume is the layer of fluid surrounding the rod having an annular radius equal to the length of the rod. This is dependent on the angle that the rod-like molecule makes with the fiber. Figure (3.6b) displays the available space for a spherical molecule in a random network of fibers. The space the molecule can move freely within is enclosed by the dotted line.

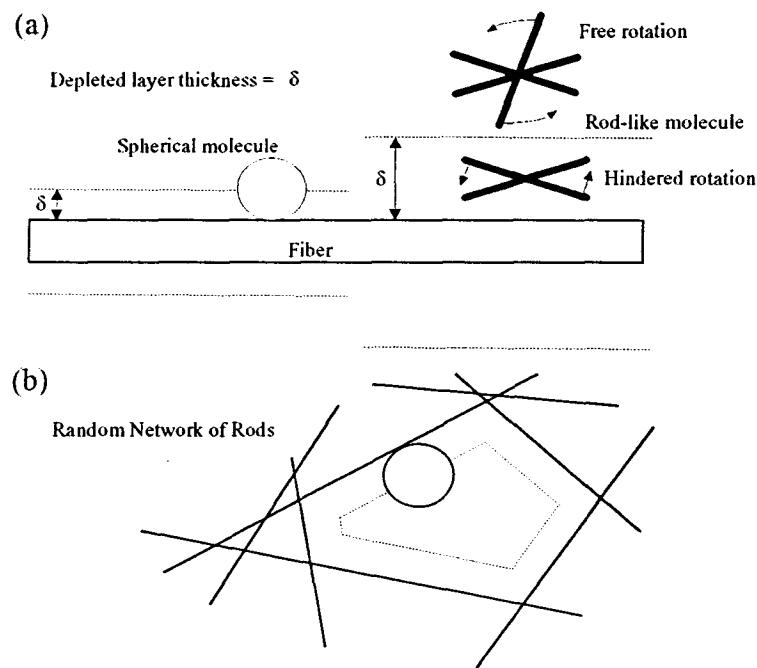


Figure 3.6: Schematic diagram of (a) surface depletion of spherical and rod-like molecules from fiber and (b) steric exclusion of sphere in random network of fibers.

Similar to volume exclusion, surface depletion will lead to an advancement of the macromolecular solute front relative to a low molecular mass tracer. Also, the lower concentrations of the solute at the pore wall will lead to a lower solution apparent viscosity adjacent to the wall.

In this model, the volume exclusion (inaccessible pore space) and surface depletion effects are assumed to be lumped together into the volume fractions presented in Figure 3.5. First, this simplifies the analysis, and second, there is no data available to differentiate between the two phenomena in the human interstitium.

3.4 Boundary Conditions

To solve the above governing equations, the behaviour of the fluid and solute at the boundary has to be specified. As outlined above, the problem is posed in the cylindrical coordinate system.

At an impermeable boundary, the fluid boundary condition is given by :

$$\frac{\partial(P_t - \sigma_t \pi_t)}{\partial n} = 0 \quad (3.29)$$

where n signifies the coordinate normal to the boundary. For the solute, an impermeable boundary is represented by :

$$-D_{nn} \frac{\partial c_{s,eff}}{\partial n} + v_{n,eff} c_{s,eff} = 0 \quad (3.30)$$

This implies that there is no movement of solute across the boundary by any of the various forms of transport: diffusion, dispersion, and convection.

The mathematical treatment of the capillary membrane boundary conditions requires the assumption of an infinitesimally thin layer of fluid between the capillary membrane and the tissue porous medium. In this thin layer, the pressure and solute concentration are in equilibrium with the pressure and solute concentration in the accessible pore space. This is

merely a mathematical convenience but it is required for continuity from the capillary membrane to the tissue space.

At the capillary membrane, fluid continuity is required across the membrane. This means the amount of fluid flowing across the membrane according to Starling's hypothesis (Renkin, 1986) :

$$v_{fn}^{St} = L_p [P_c - P_t - \sigma(\pi_c - \pi_t)] \quad (3.31)$$

must be the same as that indicated from Darcy's law for flow into the tissue, i.e.,

$$v_{fn}^{Da} = -K_{nn} \left. \frac{\partial(P_t - \sigma_t \pi_t)}{\partial n} \right|_{\text{membrane}} \quad (3.32)$$

Equations (3.31) and (3.32) are coupled to provide the following boundary condition :

$$-K_{nn} \left. \frac{\partial(P_t - \sigma_t \pi_t)}{\partial n} \right|_{\text{membrane}} = L_p [P_c - P_t - \sigma(\pi_c - \pi_t)] \quad (3.33)$$

This boundary condition is complicated by the fact that the capillary pressure, P_c , the tissue pressure, P_t , the tissue osmotic pressure, π_t , the capillary membrane hydraulic conductivity L_p , and the capillary membrane reflection coefficient, σ_t , may all be functions of the location down the membrane. This means an iterative procedure has to be used to satisfy the fluid capillary boundary condition. The solution algorithm is presented in the Section 3.6.

The capillary membrane solute boundary condition states that the amount of solute passing through the membrane is given by Patlak's equation (2.3) (see Section 2.2.3). This is given by (Curry, 1984) :

$$J_s = -D_{nn} \frac{\partial c_{s,eff}}{\partial n} + v_{n,eff} c_{s,eff} = v_{n,eff} (1-s)c_c + \frac{PS(c_c - c_{s,eff})Pe_m}{e^{Pe_m} - 1} \quad (3.34)$$

where c_c is the local capillary solute concentration and the membrane Peclet number, Pe_m , is given by :

$$Pe_m = \frac{v_{fn}(1-\sigma)}{PS} \quad (3.35)$$

This states that the diffusive, dispersive, and convective flux of solute into the tissue is equal to the amount passing through the capillary membrane given by Patlak's equation.

3.5 Fluid and Solute Exchange in the Capillary

At the arteriolar end of the capillary, as fluid and solute pass through the membrane into the tissue, the flow rate and concentration of solute decrease with downstream distance. If fluid and solute are reabsorbed back into the capillary at the venular end, the capillary fluid flow rate and solute concentration will increase with z . This section describes how the fluid and solute change in the capillary are treated mathematically.

Figure (3.7) illustrates a differential length of the capillary for the change in a general variable W .

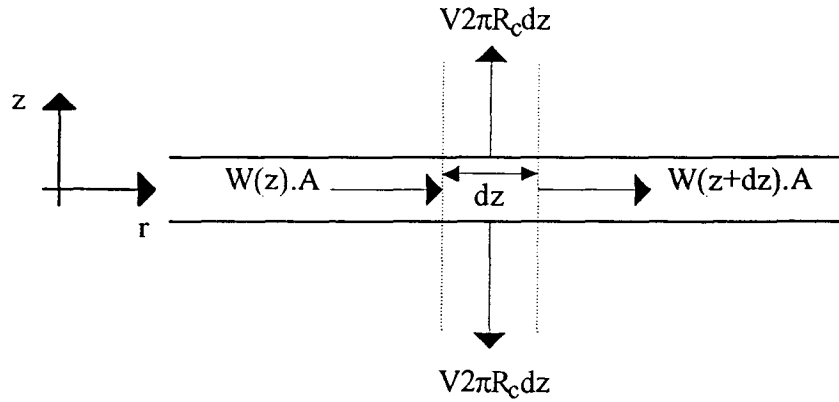


Figure 3.7: Fluid and solute flow in capillary.

Realistically, the pressure and solute concentration are functions of both the radial, r , and longitudinal, z , distances within the capillary. Also, red blood cells moving down the capillary will cause pressure fluctuations along the capillary length. In this model, it is assumed that the pressure and solute concentration are functions of z only and the pressure fluctuations caused by the passage of red blood cells produce, in an average sense, a linear pressure profile down the capillary (Apelblat *et al.*, 1974). The latter assumption is quite drastic but simplifies the analysis substantially. The small amount of fluid leaking into the tissue determined from simulations presented in Chapter 4 (less than 0.1%) indicates that the pressure drop down the capillary is very nearly linear and suggests that the flow is Poiseuille-like. This implies that radial pressure gradients are negligible.

Assuming that on average, flow obeys Poiseuille's law in the capillary yields the normal capillary fluid flow rate at the capillary membrane, $v_{n,c}|_{membrane}$, as :

$$v_{n,c}|_{membrane} = \frac{R_c^3}{16\mu} \frac{d^2 P_c}{dz^2} \quad (3.36)$$

For fluid continuity, this can be set equal to the fluid flow rate across the capillary membrane according to Starling's hypothesis yielding a second order ordinary differential equation given by :

$$\frac{d^2 P_c}{dz^2} = \alpha^2 [P_c - P_t - \sigma_t (\pi_c - \pi_t)] \quad (3.37)$$

where $\alpha^2 = 16L_p\mu/R_c^3$. For these simulations, the pressures at the arteriolar and venular ends (P_{art} and P_{ven}) of the capillary are specified. This means that solution of the pressure in the capillary requires the solution of a second order boundary value problem. It is also noted that the solution of equation (3.37) requires the tissue hydrostatic and osmotic pressures, the membrane filtration coefficient, and the fluid reflection coefficient as functions of the length down the capillary. This forces an iterative solution for the capillary and tissue pressure profiles at the membrane-tissue interface.

It is noted that α^2 is very small (typically about 10^{-4}). This implies that the capillary pressure profile is very nearly linear from the value at the arteriolar end, P_{art} , to the value at the venular end, P_{ven} . Assuming that the capillary pressure is linear from the inlet to the outlet end removes the requirement for iterative solution, reducing computational costs considerably. This has been shown to be a good assumption since the amount of fluid leaking into the tissue is small relative to the flow of fluid (typically $< 0.1\%$) through the capillary wall.

A solute mass balance on the differential length in Figure (3.7) yields :

$$\frac{d(c_c Q_c)}{dz} = -J_s(z) 2\pi R_c \quad (3.38)$$

where Q_c is the volumetric fluid flow down the capillary and the amount of solute passing through the membrane, $J_s(z)$, is given by Patlak's equation (3.34). This is a first order differential equation describing the solute concentration down the capillary as a function on the amount that transfers across the membrane, $J_s(z)$, and the capillary radius. The initial condition for this boundary condition is the arteriolar inlet solute concentration, c_{art} . It was found from simulations performed that the solute concentration changes by less than 0.01% along the length of the capillary. The capillary solute concentration was thereafter assumed as constant along the capillary.

The mathematical model is now complete. It shall be now applied for several cases presented in the following chapters.

3.6 Numerical Procedure and Solution Algorithm

The coupled equations (3.6) and (3.28) are solved using the Petrov-Galerkin finite element method (Hughes, 1978; Brooks and Hughes, 1982; Yu and Heinrich, 1986, 1987, 1988). In the finite element method, the system geometry is divided into elements of varying dimensions. The regions expected to have the highest gradients are subdivided into fine elements while those expected to have relatively lower gradients are subdivided with relatively coarse elements. The method spatially discretizes the problem by specifying nodes within each element at which the dependent variables (P_t and $c_{s,eff}$) are evaluated. The dependent variables are approximated within each element by interpolating or shape functions. In this work, rectangular elements with simple linear basis functions were used. The weighted residual analysis of the weak form of the partial differential equations (see Appendix A for further details about the weak formulation) yields a set of algebraic equations for the dependent variables at each node. These equations can be solved using any standard system of equations solver (Press *et al.*, 1986).

The numerical solution is complicated because there is convective domination within the interstitial space for the solute transport equation (3.28). This changes the nature of the partial differential equation (3.28) from elliptic to hyperbolic-like. The Petrov-Galerkin streamline upwinding method was adopted to deal with the dominance of convection. In this method, artificial diffusion is added to the basis functions. This can be viewed as a modification of the weighting functions for the convective terms. The Petrov-Galerkin method seeks to add the optimal amount of artificial diffusion such that the accuracy is maximized. A more detailed description of the Petrov-Galerkin finite element method is presented in Appendix A.

The fluid conservation and solute transport equations are coupled. This means that the tissue hydrostatic pressure and solute concentrations have to be solved iteratively. At a particular time step, the solute concentrations are assumed within the interstitial space. Usually this is estimated from the values at the past two time steps. The colloid osmotic pressure is then calculated and the tissue hydrostatic pressure is subsequently obtained from equation (3.6) subject to the appropriate boundary conditions. If the capillary hydrostatic pressure is not assumed as linear down the capillary length, then a separate iterative procedure occurs for the solution of the hydrostatic pressures in the capillary, equation (3.37), and within the tissue, equation (3.6). The fluid velocities are then evaluated within the tissue and the solute transport equation is solved using the Petrov-Galerkin method subject to the imposed boundary conditions. The procedure is repeated until the relative change in the solute concentrations and hydrostatic pressures are less than a specified tolerance, typically 10^{-6} , or when the iterations exceeded a specified limit (100).

A modified version of the dominant eigenvalue under-relaxation technique suggested by Orbach and Crowe (1971) is employed. This is discussed in further detail in Appendix B. As a check on the numerical solution accuracy, material balances were performed about the system boundaries. The relative material balance errors for fluid and solute were always less than 0.5%. The number of elements was also tested to ensure accuracy of the numerical

solution. Increasing the number of nodes from 1020 (50x21) to 2000 (80x25) produced less than 0.01% difference in the results. All cases performed in Chapters 4 and 5 were produced using 1020 nodes.

The program listing may be found in Appendix C.

3.7 Summary of Governing Equations in Dimensionless Form

Reference Values

Pressure	P_{art}	Arteriolar hydrostatic pressure
Concentration	c_{art}	Arteriolar solute concentration
Length	L	Capillary length
Diffusion coefficient	D_{diff}	Molecular diffusion coefficient
Tissue hydraulic conductivity	K_{ref}	Base tissue hydraulic conductivity value.

Dimensionless Variables

$$r^* = \frac{r}{L}$$

$$z^* = \frac{z}{L}$$

$$c^* = \frac{c}{c_{art}}$$

$$P^* = \frac{P}{P_{art}}$$

$$\pi^* = \frac{\pi}{P_{art}}$$

$$D_{ii}^* = \frac{D_{ddii}}{D_{diff}}$$

$$K_{ii}^* = \frac{K_{ii}}{K_{ref}}$$

$$Pe_m = \frac{v_{fn}(1-\sigma)}{PS}$$

$$v_i^* = \frac{v_i L}{K_{ref} P_{art}}$$

$$\tau = \frac{t D_{diff}}{L^2}$$

Fluid Flow in Tissue

$$\frac{\partial}{\partial r^*} \left(K_{rr}^* \frac{\partial (P_i^* - \sigma_i \pi_i^*)}{\partial r^*} \right) + \frac{K_{rr}^*}{r^*} \frac{\partial (P_i^* - \sigma_i \pi_i^*)}{\partial r^*} + \frac{\partial}{\partial z^*} \left(K_{zz}^* \frac{\partial (P_i^* - \sigma_i \pi_i^*)}{\partial z^*} \right) + \frac{L^2}{K_{ref} P_{art}} Q(P_i^*) = 0$$

$$Q(P_i^*) = -P_{art} L S(P_i^* - P_l^*)$$

$$v_{f,r} = -\frac{K_{rr}^* K_{ref} P_{art}}{L} \frac{\partial (P_i^* - \sigma_i \pi_i^*)}{\partial r^*}$$

$$v_{f,z} = -\frac{K_{zz}^* K_{ref} P_{art}}{L} \frac{\partial (P_i^* - \sigma_i \pi_i^*)}{\partial z^*}$$

Solute Transport in Tissue

$$\frac{\partial \dot{c}_{s,eff}^*}{\partial \tau} + \frac{P_{art} K_{ref}}{D_{diff}} \frac{\partial (v_{r,s,eff}^* \dot{c}_{s,eff}^*)}{\partial r^*} + \frac{P_{art} K_{ref}}{D_{diff}} \frac{\partial (v_{z,s,eff}^* \dot{c}_{s,eff}^*)}{\partial z^*} =$$

$$f_{st} \left(D_{rr}^* \frac{\partial^2 \dot{c}_{s,eff}^*}{\partial r^{*2}} + D_{rr}^* \frac{1}{r^*} \frac{\partial \dot{c}_{s,eff}^*}{\partial r^*} + D_{zz}^* \frac{\partial^2 \dot{c}_{s,eff}^*}{\partial z^{*2}} \right) + \frac{L^2}{D_{diff} c_{art}} Q_s(\dot{c}_{s,eff}^*, P_i^*)$$

Fluid Flow Boundary Condition at Membrane

$$-K_{nn}^* \frac{\partial (P_i^* - \sigma_i \pi_i^*)}{\partial n^*} \Big|_{membrane} = \frac{LL_p}{K_{ref}} [P_c^* - P_i^* - \sigma(\pi_c^* - \pi_i^*)]$$

Fluid Flow Boundary Condition at Impermeable Boundary

$$\frac{\partial(P_i^* - \sigma_i \pi_i^*)}{\partial n^*} = 0$$

Solute Transport Boundary Condition at Membrane

$$-D_{nn}^* \frac{\partial c_{s,eff}^*}{\partial n^*} + \frac{P_{art} K_{ref} v_{n,eff}^*}{D_{diff}} c_{s,eff}^* = \frac{P_{art} K_{ref} v_{n,eff}^*}{D_{diff}} (1 - \sigma) c_c^* + \frac{L}{D_{diff}} \frac{PS(c_c^* - c_{s,eff}^*) Pe_m}{e^{Pe_m} - 1}$$

Solute Transport Boundary Condition at Impermeable Boundary

$$-D_{nn}^* \frac{\partial c_{s,eff}^*}{\partial n^*} + \frac{P_{art} K_{ref} v_{n,eff}^*}{D_{diff}} c_{s,eff}^* = 0$$

Osmotic Pressure relationship

$$\pi_i^* = \frac{k_1 c_{art}(c_{s,eff}^*) + k_2 c_{art}^2 (c_{s,eff}^*)^2 + k_3 c_{art}^3 (c_{s,eff}^*)^3}{P_{art}}$$

where k_1 , k_2 , and k_3 are fitted parameters dependent on the particular solute species.

Chapter 4 : Effects of System Parameters on Steady State Microvascular Exchange : A Sensitivity Analysis

4.1 Introduction

Chapter 3 presents the formulation of the model equations governing the microvascular exchange system. Using this model we will first evaluate the effects of the various system parameters on the system. In the tissue, these include parameters that affect the lymphatic sink (LS and P_L), tissue fluid motion via the osmotic pressure (σ_t), hydraulic conductivity (K), and solute transport via diffusion (D_{diff}), dispersion (D_{disp}), and convection (ξ). In addition, fluid motion and solute transport across the capillary wall are altered with adjustments in the diffusive permeability (PS), capillary membrane filtration coefficient (L_p), and the capillary reflection coefficient (σ). The position of the lymphatic sink will also be investigated.

The effects of a variable capillary membrane filtration coefficient, L_p , and reflection coefficient, σ , along the capillary membrane and spatially variant tissue hydraulic conductivity, $K(r,z)$, will also be examined briefly. The capillary membrane filtration coefficient and reflection coefficient are assumed to be a known functions which are specified along the length of the capillary wall. The high flow channels are implemented as a locally increased tissue hydraulic conductivity.

In this chapter, the problem will be first summarized. The parameter values are then discussed and then the case studies performed listed. The results are then presented

and discussed in detail for the base case values (the base case). The results from the sensitivity analysis are then presented to evaluate the influence of the physiological parameters. The results obtained by using a variable capillary membrane filtration coefficient and tissue hydraulic conductivity are reported.

4.2 Problem Statement

The system under investigation is displayed schematically in Figure (3.1). The blood plasma flows through the capillary leaking fluid and solute into the tissue through the capillary membrane. As a first approximation, the capillary radius is assumed constant along its length. The tissue envelope surrounding the capillary is also assumed to be of constant outer radius. Fluid and solute may be reabsorbed at the venular end of the capillary but may also leave the system via the lymphatic sink which can be placed anywhere within the tissue space. The tissue is assumed to be perfectly rigid. This means there are no deformations due to swelling.

The problem is stated as follows: given the arteriolar and venular capillary hydrostatic pressures and the arteriolar solute concentration, find the solute concentration and hydrostatic pressure distributions throughout the tissue subject to Starling's hypothesis and Patlak's equation governing fluid and solute transport across the capillary membrane. The other boundaries are impermeable to both fluid and solute. The behaviour will depend on the physiological parameters chosen for the simulation.

4.3 Parameter Values

Table (4.1) lists the parameter values used in the numerical simulations. These values are typical for tissues found in the literature. Many values (e.g., L_p , PS , σ , σ_t , f_{im} ,

and f_{st}) were taken from estimates presented by Taylor (1990a). The value of the capillary permeability, PS , was assumed to be 2.4×10^{-10} m²/s. The capillary wall protein reflection coefficient, σ , was assigned the value 0.85. This value is typical for albumin in capillaries (Ballard and Perl, 1978). The tissue protein reflection coefficient, σ_t , is assumed for most cases to be equal to 1.0. To test the effect this parameter has on the system, it was varied between 0.0 and 1.0 in three cases. There are no data available indicating a better estimate for this parameter. The immobile and accessible fluid volumes, f_{im} and f_{st} , were obtained by assuming that the main component of the immobile fluid volume is the intrafibrillar water associated with the collagen (Taylor, 1990a).

The tissue hydraulic conductivity, K , is estimated to be 3.1×10^{-16} m² /Pa s. This value is typical for subcutaneous tissue (Levick, 1987). The value of the solute diffusivity was taken to be that of albumin in normal tissue. This was assumed to be 1.0×10^{-12} m²/s (Gerlowski and Jain, 1988).

The geometry of the system is shown in Figure (3.1). The length of the capillary, L , is taken to be 300 μ m. This is based on the average capillary length determined by Klitzman and Johnson, (1982). The radius of the capillary, R_c , is set as 3 μ m. This is typical for capillaries (Ganong, 1989). The radius of the tissue envelope, R_t , was assumed to be 30 μ m. This is comparable to the capillary spacing data reported by Intaglietta and Zweifach (1971). The pressure drop from the arterial inlet to the venular outlet of the capillary is taken to be 25 mmHg. The inlet arteriolar hydrostatic pressure is assumed to be 30 mmHg. These values are typical for arterial regions in capillaries (Brace and Guyton, 1977; Ganong, 1989). The concentration of the solute at the arteriolar end of the capillary is taken to be 35.9 mg/ml (Bert and Pearce, 1984).

The lymphatic sink drains fluid and solute according to the simple linear form given by equation (3.20). Using data in Chapple (1990), the value of LS is estimated to be 1.24×10^{-8} m³ fluid/m³ tissue Pa·s. The value of the lymphatic pressure is still under investigation. It is assumed to be near the limit of the most negative hydrostatic pressures

found in tissue where the lymph flow approaches zero. Using various techniques the tissue hydrostatic pressures have been reported to be as low as -9 mmHg (Guyton *et al.*, 1987). The negative value implies that the lymphatics are below atmospheric pressure. Results from Taylor *et al.* (1973) (see Figure (3.2)) suggest that the no flow lymphatic sink pressure is near -6 mmHg. Therefore, the base case value for the lymphatic sink pressure for this work is chosen as -6 mmHg. The value is assumed to be temporally invariant and constant throughout the lymphatic sink. The effect of the lymphatic sink pressure is investigated by lowering its value to -9 mmHg and -12 mmHg. The location of the lymphatic sink was assumed to be at the peripheral edge of the tissue envelope.

The osmotic pressure is assumed to be a simple polynomial function of the protein concentration :

$$\pi_i(c_{s,eff}) = 57.182c_{s,eff} - 1.2388c_{s,eff}^2 + 0.050849c_{s,eff}^3 \quad (4.1)$$

This gives the colloid osmotic pressure (in Pascals) as a function of the effective solute concentration (kg/m^3). This was taken from Bert *et al.* (1988) for albumin in skin.

4.4 Case Studies

A sensitivity analysis was performed to investigate the effects of various system parameters on the microvascular exchange system. These comparisons were for steady-state cases only. These results also illustrate the effect the parameters have on the capillary-tissue fluid balance. The fluid balance and its regulation will be examined further in Chapter 5.

The influence of the lymphatic sink can be investigated from two perspectives. The first is to simply vary the strength of the sink, that is vary LS and/or P_L . The second is to actually move the sink within the tissue domain. In general, the sink may be placed

anywhere in any orientation within the tissue space. For simplicity, we shall assume the lymphatics always run parallel to the capillary. This means only the radial position of the sink is varied. As the sink is moved radially, the lymphatic sink volume reduces because the system is in cylindrical coordinates. There are two methods to maintain the strength of the sink: either by enlarging the sink volume or by simply increasing the value of LS . In this work, the value of LS is increased to reflect the reduction in the lymphatic sink volume as it is moved radially. To examine the effects of the sink position on the system, the sink is placed at various dimensionless radial distances. The baseline position for the sink is against the outer edge of the tissue envelope.

Table 4.1 Parameter Values.

Parameter	Value	Reference
c_{art}	35.9 mg/ml	Bert and Pierce (1984)
P_{art}	30.0 mmHg	Brace and Guyton (1977)
P_{ven}	5.0 mmHg	Ganong (1989)
f_{im}	0.128	Taylor (1990a)
f_{st}	0.680	Taylor (1990a)
ξ	0.0-1.0	See text
σ	0.85	Taylor (1990a)
σ_t	0.0-1.0	See text
PS	2.4×10^{-10} m/s	Taylor (1990a)
L_p	1.35×10^{-10} m/Pa s	Taylor (1990a)
D_{diff}	1.0×10^{-12} m ² /s	Gerlowski and Jain (1988)
K	3.1×10^{-16} m ² /Pa s	Levick (1987)
LS	1.24×10^{-8} m ³ /m ³ Pa s	Chapple (1990)
P_L	-6.0 mmHg	Taylor <i>et al.</i> (1973)
R_c	3 μ m	Ganong (1989)
R_t	30 μ m	Intaglietta and Zweifach (1971)
L	300 μ m	Klitzman and Johnson (1982)
α_{long}	1.0×10^{-5} m	See text
α_{tran}	1.0×10^{-6} m	See text

The effects of mechanical dispersion are also examined. The longitudinal and transverse dispersivities are estimated from the size of the average grain size in the tissue porous medium. At the scale of the present simulations, the longitudinal dispersivity is estimated to be roughly 1×10^{-5} m. This is based loosely on the size of the typical human tissue cell in the interstitium. The hydrodynamics and transport of solute occur around the cell bodies. The framework of cells forms the porous medium through which flow occurs. The scale of the continuum model (of the order of micrometers) suggests that an average cell dimension be used rather than the diameter of the collagen molecule (of the order of nanometers) for instance. As a first approximation, the transverse dispersivity is estimated as ten percent of the longitudinal dispersivity, that is 1×10^{-6} m.

The cases performed are listed in Table (4.2). These are all steady-state cases. Steady-state was determined when the tissue solute concentrations and hydrostatic pressures changed by less than a specified tolerance between consecutive time steps. The results from these cases will be used to investigate the effects of the various parameters on the system. The first case is the base case. This case uses the parameters listed in Table (4.1). The other 28 cases use the same parameters except one is varied to evaluate the influence of that parameter on microvascular exchange. For example, the case $LS \times 0.2$ indicates that this case used a value of the lymphatic sink strength, LS , equal to 2.48×10^{-9} $\text{m}^3/\text{m}^3\text{Pa s}$ instead of the base value 1.24×10^{-8} $\text{m}^3/\text{m}^3\text{Pa s}$. The case in which dispersion is included is case 17, called disp. The two cases L_p to $2L_p$ (linear) and L_p to $2L_p$ (step) denote linear and step variations in the capillary filtration coefficient along the length of the capillary respectively. The functions vary from the base value of L_p in Table (4.1) at the arteriolar end of the capillary to twice this value at the venular end of the capillary. The cases ms3 and ms6 each denote the repositioned sink at $r^* = 0.025$ and $r^* = 0.055$. For the base case, the sink is placed at the outer edge of the tissue envelope, i.e., at $r^* = 0.10$. Each case and its results are discussed in detail in the following section.

Table 4.2 List of Cases

No.	Case	Explanation
1	base	Base Case.
2	nows	No osmotic pressure effects, with lymphatic sink.
3	$LS \times 0.2$	Lymphatic sink permeability reduced by a factor of five.
4	$LS \times 5$	Lymphatic sink permeability increased by a factor of five.
5	$\sigma = 0.1$	Capillary reflection coefficient equal to 0.10.
6	$\sigma = 0.5$	Capillary reflection coefficient equal to 0.50.
7	$\sigma = 0.99$	Capillary reflection coefficient equal to 0.99.
8	$\xi = 0.1$	Retardation factor equal to 0.10.
9	$\xi = 0.5$	Retardation factor equal to 0.50.
10	$PS = 0.0$	Capillary diffusive permeability equal to zero.
11	$PS \times 100$	Capillary diffusive permeability increased by a factor of one hundred.
12	$PS \times 10000$	Capillary diffusive permeability increased by a factor of ten thousand.
13	$\sigma_t = 0.0$	Tissue reflection coefficient equal to zero.
14	$\sigma_t = 0.5$	Tissue reflection coefficient equal to 0.50.
15	$D_{diff} \times 0.1$	Solute diffusion coefficient reduced by a factor of ten.
16	$D_{diff} \times 10$	Solute diffusion coefficient enlarged by a factor of ten.
17	disp	Dispersion included as transport mechanism.
18	$K \times 0.1$	Tissue hydraulic conductivity reduced by a factor of ten.
19	$K \times 10$	Tissue hydraulic conductivity enlarged by a factor of ten.
20	$P_L = -0.40$	Lymphatic sink pressure set equal to -12 mmHg.
21	$P_L = -0.30$	Lymphatic sink pressure set equal to -9 mmHg.
22	$L_n \times 0.5$	Capillary filtration coefficient reduced by a factor of two.
23	$L_n \times 2$	Capillary filtration coefficient enlarged by a factor of two.
24	L_n to $2L_n$ (linear)	Linear capillary filtration coefficient variation from arteriolar to venular end. From base value to twice the base value.
25	L_n to $2L_n$ (step)	Step capillary filtration coefficient variation from arteriolar to venular end. From base value to twice the base value.
26	K1	Single high flow channel at $z^* = 0.5$.
27	K2	Two high flow channels at $z^* = 0.3$ and 0.7 .
28	ms3	Lymphatic sink radial position equal to $r^* = 0.025$.
29	ms6	Lymphatic sink radial position equal to $r^* = 0.055$.

4.5 Discussion of Results and Sensitivity Analysis

In this section, the results for the base case will first be discussed in detail. Figure (4.1) present the results from the base case. This forms the basis for comparison with all other cases and provides insights into the influences of osmotic pressure and the lymphatic sink.

In the first section, the results for the base case will be presented. This will be compared to a case where the osmotic pressure contributions are switched off through the system. The effects of other physiological parameters on the system will next be presented, in the form of a sensitivity analysis, in the second section. Here the effect of a physiological parameter is studied by varying the parameter and observing the change in the results from the base case. The third section presents effects of a variable capillary membrane filtration coefficient (L_p) and the fourth section examines the influence of high flow channels on the hydrodynamics and solute transport in the interstitium.

4.5.1 The Base Case

Figure (4.1) displays the results from the base case. This case uses all the base values specified in Table (4.1) and includes the colloid osmotic pressure effects and the lymphatic sink. The capillary is located at the upper edge of each plot. The inlet arteriolar end of the capillary is at the left end and the outlet venular end is at the right end of the plot. The distance into the tissue increases in the downwards direction. The arrangement is displayed in Figure (3.1). The lymphatic sink is located at the lower edge of the plots. It is important to note that the distance into the tissue scale has been exaggerated (the tissue outer radius is actually one-tenth of the length of the capillary). The first contour plot contains the dimensionless solute concentration given by :

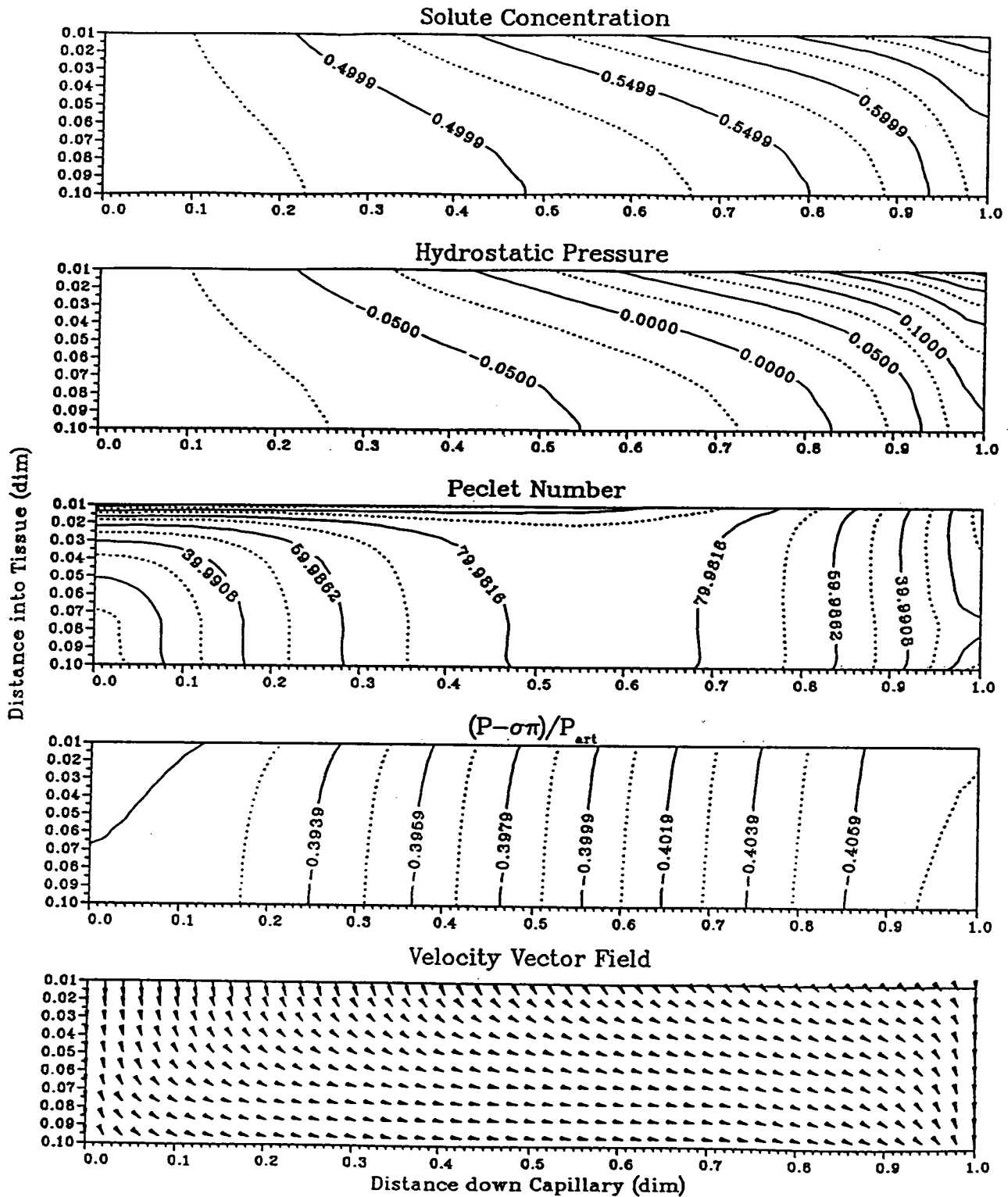


Figure 4.1: Dimensionless tissue solute concentrations, hydrostatic pressure, Peclet number, potential, and velocity vector distributions for the base case at steady-state.

$$c_s^* = \frac{c_s}{c_{art}} \quad (4.2)$$

where c_{art} is the inlet arteriolar capillary solute concentration. The dimensionless tissue hydrostatic pressure is displayed in the second plot. The dimensionless hydrostatic pressure is given by :

$$P_t^* = \frac{P_t}{P_{art}} \quad (4.3)$$

The third plot displays the Peclet number distribution which is calculated as follows :

$$Pe = \frac{|v_{s,eff}|L}{D} \quad (4.4)$$

where

$$|v_{s,eff}| = \sqrt{v_{r,s,eff}^2 + v_{z,s,eff}^2} \quad (4.5)$$

and D is the total diffusion coefficient including molecular and dispersive contributions. The Peclet number distribution is directionless but reflects the importance of convection relative to the total diffusive and dispersive transport. Near the impermeable boundaries, the Peclet numbers attain their lowest values indicating that there is less convective transport near these boundaries. The Peclet numbers are not equal to zero at the impermeable boundaries because there is fluid motion tangential to the boundary.

The fourth plot displays the dimensionless potential :

$$T_i^* = \frac{(P_t - \sigma_t \pi_t)}{P_{art}} \quad (4.6)$$

within the tissue. The potential drives fluid motion. Finally, the velocity vector field is displayed in the fifth plot. The length of the velocity vectors indicates the fluid velocity magnitude (approximately $1 \text{ mm} = 3 \times 10^{-7} \text{ m/s}$).

From the solute concentration contour plot, it is seen that the c_s^* increases from the end of the tissue adjacent to the capillary inlet to the end nearest the capillary outlet (range is from about 0.45 to just greater than 0.72). The solute is washed out to a higher degree at the arteriolar end of the tissue than the venular end due to the higher transmembrane fluid velocities at the arteriolar end of the tissue. This leads to higher solute concentration gradients towards the venular end of the tissue than in the central and arteriolar portions of the tissue. The solute is removed from the system by the lymphatic sink. The average dimensionless solute concentration within the tissue is 0.5258. This corresponds to a dimensional solute concentration of 18.88 mg/ml. This is similar to the average interstitial space protein concentrations (21 mg/ml) estimated by Landis and Pappenheimer (1963). The dimensionless solute concentration in the lymph drainage is lower than the tissue-wide average at 0.5134 (18.43 mg/ml).

The tissue hydrostatic pressure distribution is very similar to the solute concentration distribution. The hydrostatic pressure is lowest at the arteriolar end of the tissue and increases towards the venular end of the tissue. The gradients in the hydrostatic pressure are greatest near the capillary and drop off as the sink is approached. This is especially so at the venular end of the tissue near the capillary. This is explained by the relatively large solute concentration gradients at the venular end of the tissue near the capillary. The hydrostatic pressure responds to the solute concentration via the colloid osmotic pressure. Near the sink, the hydrostatic pressures fall to negative values. This

means that in this region, the tissue is subatmospheric. The dimensionless average tissue hydrostatic pressure is equal to -0.0255 (-0.7650 mmHg). This falls in the range of tissue hydrostatic pressures for tissues (Guyton *et al.*, 1987). The dimensionless lymphatic sink pressure is -0.20 . The relatively more positive hydrostatic pressures in the region of the lymphatic sink cause the removal of fluid. The lymph drainage rate is equal to 5.47 l/day. This is in the range of lymph drainage rates observed experimentally. Mortillaro and Taylor (1976) report lymph flows between 5.53 and 8.64 l/day for similar hydrostatic pressure drops down the capillary as that used in this work.

The Peclet number distribution indicates that solute transport is largely convectively dominated. This is especially so near the capillary and within the central portions of the tissue. The Peclet number distribution passes through a maximum in the central portion of the tissue at approximately $z^* = 0.60$. The range in the Peclet numbers for the base case are roughly between just above 0 and 120 . The Peclet number distribution also indirectly reflects the relative magnitudes of the fluid velocities (see equation (4.4)).

The potential is entirely negative within the tissue. The range in the dimensionless potential is very small (approximately 0.015). Most of the loss of potential occurs across the capillary membrane whereas potential gradients in the tissue are relatively small. This suggests that the capillary membrane resistance to fluid flow is much greater than the tissue flow resistance. The potential drops from the arteriolar end of the tissue near the capillary to the venular end of the tissue near the lymphatic sink. This results in the fluid flow pattern displayed in the velocity vector plot. Fluid filters across the capillary wall into the tissue along the entire length of the capillary and is removed from the system by the lymphatic sink. From the velocity field plot, the fluid velocities are clearly seen to be greater at the arteriolar end of the tissue and drop along the length of the capillary.

The results from the base case illustrate that lower solute concentrations and hydrostatic pressures are at the arteriolar end of the capillary. It is important to bear in mind that the potential and not the hydrostatic pressure drives the fluid motion. The

hydrostatic pressure shifts in response to the solute concentration distribution. The greater amounts of solute at the venular end of the tissue lead to increased colloid osmotic pressure activity in this region. From the results, the importance of the osmotic pressure in determining fluid motion is apparent. In the absence of the colloid osmotic pressure, the hydrostatic pressure distribution is identical to the potential distribution.

For comparison purposes, a case without the effects of the colloid osmotic pressure throughout the system (including the capillary) was performed. This case was termed *nows*. Here, the solute concentration via the colloid osmotic has no effect on fluid motion. The results from this case are presented in Figure (4.2).

From the results, it is clear that the solute concentration distribution becomes more one-dimensional in the radial direction. The solute concentrations change little within the tissue with the highest values at the arteriolar end of the tissue near the capillary. The lowest values occur at the venular end of the tissue near the lymphatic sink. The dimensionless average tissue solute concentration is 0.7462. The tissue hydrostatic pressure and potential distributions are identical. This is because there are no colloid osmotic pressure gradients within the tissue. The tissue hydrostatic pressures are lowered within the tissue (average dimensionless hydrostatic pressure equals -0.1014) when compared with the base case average pressure (-0.0255). This results in lowered lymph drainage rates (3.37 l/day) from the system than the base case (5.47 l/day).

It is interesting to note that the fluid velocities across the capillary membrane are slightly greater for this case than the base case up to $z \cong 0.40$ and beyond $z \cong 0.90$. In the central portion of the capillary length ($0.40 < z < 0.90$), the transcapillary fluid velocities are lower than the base case. This is reflected in the Peclet number distribution. The values are higher at the extreme arteriolar and venular ends and lower in the central portion of the capillary than the base case values. The fluid velocities within the tissue are lower than the base case fluid velocities. As a consequence, the convective transport of solute is lowered and therefore the more uniform solute concentration distribution results. Also the velocity

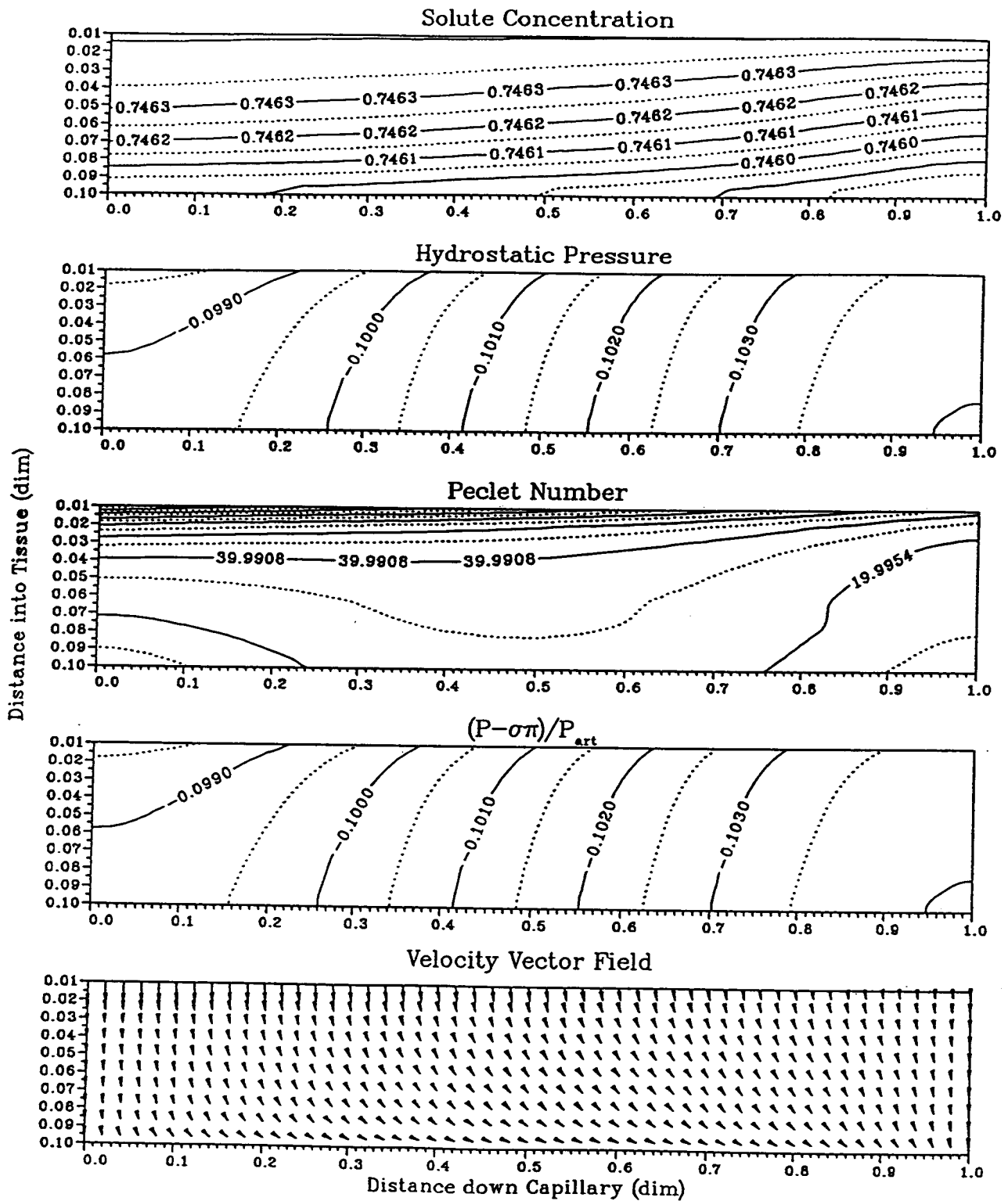


Figure 4.2: Dimensionless tissue solute concentrations, hydrostatic pressure, Peclet number, potential, and velocity vector distributions for the case without colloid osmotic pressure effects but with the lymphatic sink at steady-state.

magnitudes change less along the capillary length than for the base case. This results in less dramatic solute washout from the capillary.

The influence of the colloid osmotic pressure is clearly illustrated by comparing the two above cases. The presence of the colloid osmotic pressure causes the tissue hydrostatic pressure to respond to the solute concentration distribution. This means that the tissue hydrostatic pressures becomes more positive and as a result, increases the lymphatic drainage. The amount of solute removed from the tissue through the lymphatic sink rises leading to lowered solute concentrations within the tissue.

4.5.2 Sensitivity Analysis

The following summarizes the effects physiological parameters had on the system. These simulations indicate the parameters most influential on the system.

Retardation Factor, ξ

The impact of the retardation factor on the system behaviour was evaluated via three cases. First the base case where ξ is set equal to 1.0. The second and third cases were performed with ξ equal to 0.1 and 0.5 respectively.

As the retardation factor is reduced, the amount of convective transport of solute decreases relative to the diffusive transport. If the diffusion coefficient is sufficiently large, diffusive transport begins to dominate the solute behaviour and solute concentration gradients throughout the region are reduced. This can be seen in Figure (4.3) for a retardation factor equal to 0.10. For the base case, the solute dimensionless concentration range is from roughly 0.47 to 0.70 (the range is thus 0.23). This range drops to about 0.13 and 0.03 for retardation factor values of 0.5 and 0.1 respectively. Also at reduced values of

the retardation factor, the solute concentration gradient profile is more uniform within the central portion of the tissue. The highest gradients and solute concentration values are along the capillary wall, especially towards the venular end of the tissue. The dimensionless average tissue concentration of solute increases as the retardation factor decreases to 0.7132 for $\xi = 0.1$.

The pressure distribution displays similar characteristics as the solute concentration distribution. As the retardation factor is reduced, the hydrostatic pressure range is reduced and the solute distribution is more uniform. The average pressure in the tissue increases as the solute hindrance increases. The lower pressure range and more uniform distribution are the results of the increased solute concentration throughout the tissue space. The colloid osmotic pressure values and gradients throughout the tissue are functions of the local solute concentration. In response to the increased colloid osmotic pressure created by elevated solute concentrations, the hydrostatic pressure distribution increases. The dimensionless hydrostatic pressure rises to 0.0406 (1.2180 mmHg) for $\xi = 0.10$. The increase in pressure and solute concentrations leads to a slight increase in the range of the potential distribution. The potential distribution is shifted, at lower retardation factor values, in the negative direction.

The amount of lymph drainage increases as the retardation factor is reduced. For $\xi = 0.10$, the lymph drainage rate is equal to 8.19 l/day. This is due to an increased hydrostatic pressure throughout the tissue. The rise in the solute concentrations result in increased osmotic pressure activity and thus higher hydrostatic pressures. Using the base values for the sink strength (LS and P_L), there is no reabsorption of fluid back into the capillary for all of these cases ($\xi = 0.1, 0.5, \text{ and } 1.0$). The enlarged lymph flow causes an increase in fluid filtration across the capillary membrane. The transcapillary flow velocities are roughly one-third greater than the base case values. Since the solute convective velocities are directly affected by the retardation factor, the Peclet number

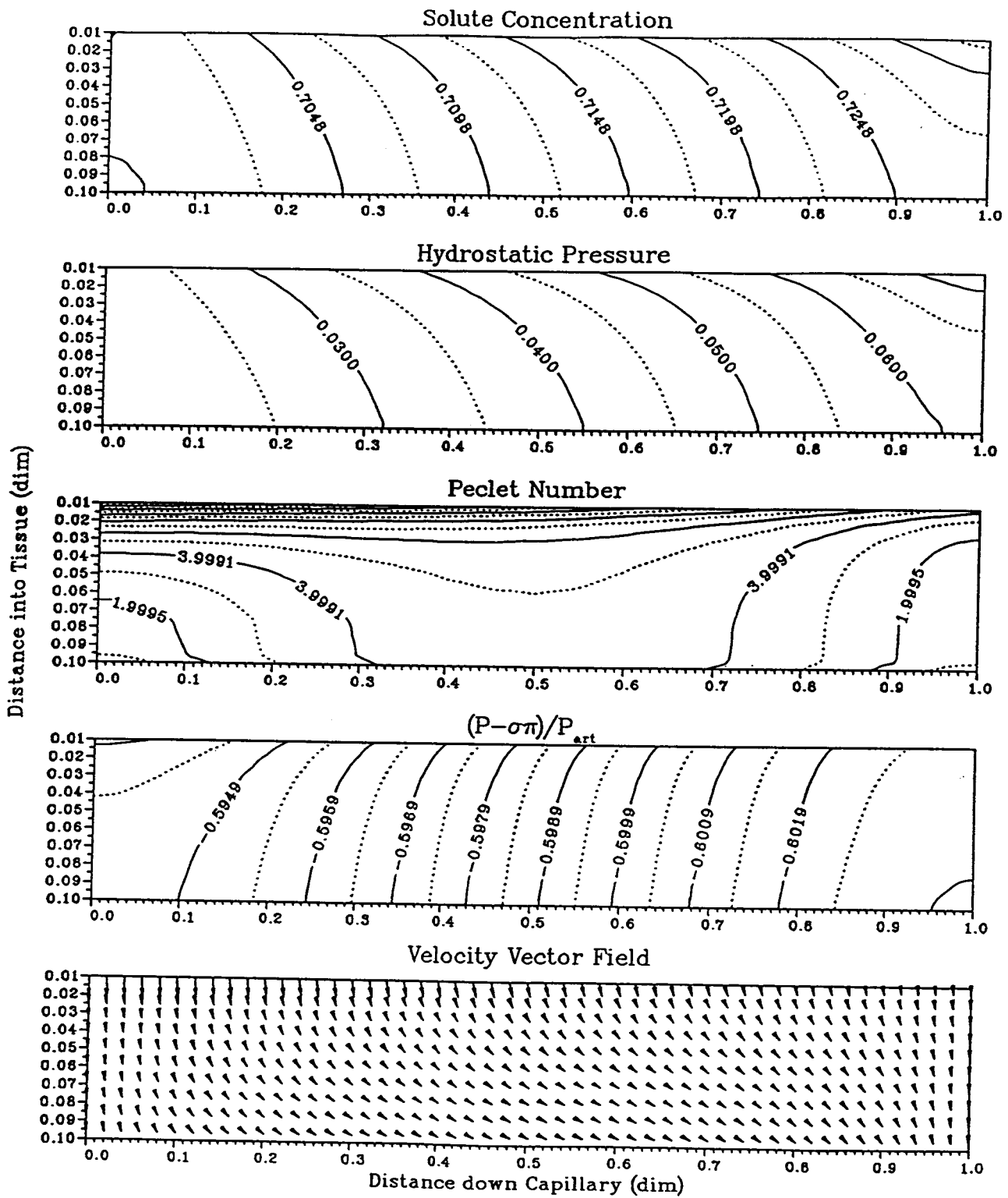


Figure 4.3: Dimensionless tissue solute concentrations, hydrostatic pressure, Peclet number, potential, and velocity vector distributions for the case with the retardation factor, ξ , equal to 0.1 at steady-state.

distribution is decreased and has a much smaller range. This means that for lower values of the retardation factor, as expected, greater portions of the tissue are undergoing greater diffusive transport. It is important to bear in mind that the Peclet numbers indicate the amount of convective solute transport relative to diffusive-dispersive transport. The convective term makes use of the solute convective velocity and not the absolute fluid velocity.

Capillary Reflection Coefficient, σ

The effect of the capillary reflection coefficient is evaluated using the base case and three other cases ($\sigma = 0.10, 0.50, \text{ and } 0.99$).

Figure (4.4) presents the results for the capillary membrane reflection coefficient equal to 0.1. As can be seen from the results, the tissue-side capillary membrane solute concentration and pressure profiles are considerably different from the base case (base, $\sigma = 0.85$). The solute concentration range and gradients are reduced within the tissue space. The dimensionless average tissue solute concentration, however, increases to 0.7150. The gradients tend to become increasingly one-dimensional (in the longitudinal z direction) as the capillary reflection coefficient is reduced.

Similarly, the pressure range and associated gradients also decrease as the reflection coefficient is decreased and the distribution becomes more one-dimensional in the longitudinal direction. The hydrostatic pressure distribution for the lowered reflection coefficients looks very similar to the solute concentration distribution. The hydrostatic pressure distribution is shifted in the positive direction. This is due to the increased osmotic activity in the tissue because of the greater solute concentrations. The dimensionless average tissue hydrostatic pressure rises to 0.04282 (1.2846 mmHg). This results in an increase in the lymph drainage rate to 8.25 l/day. The potential distribution is shifted in the negative direction but has a very similar range as σ is reduced. Radial

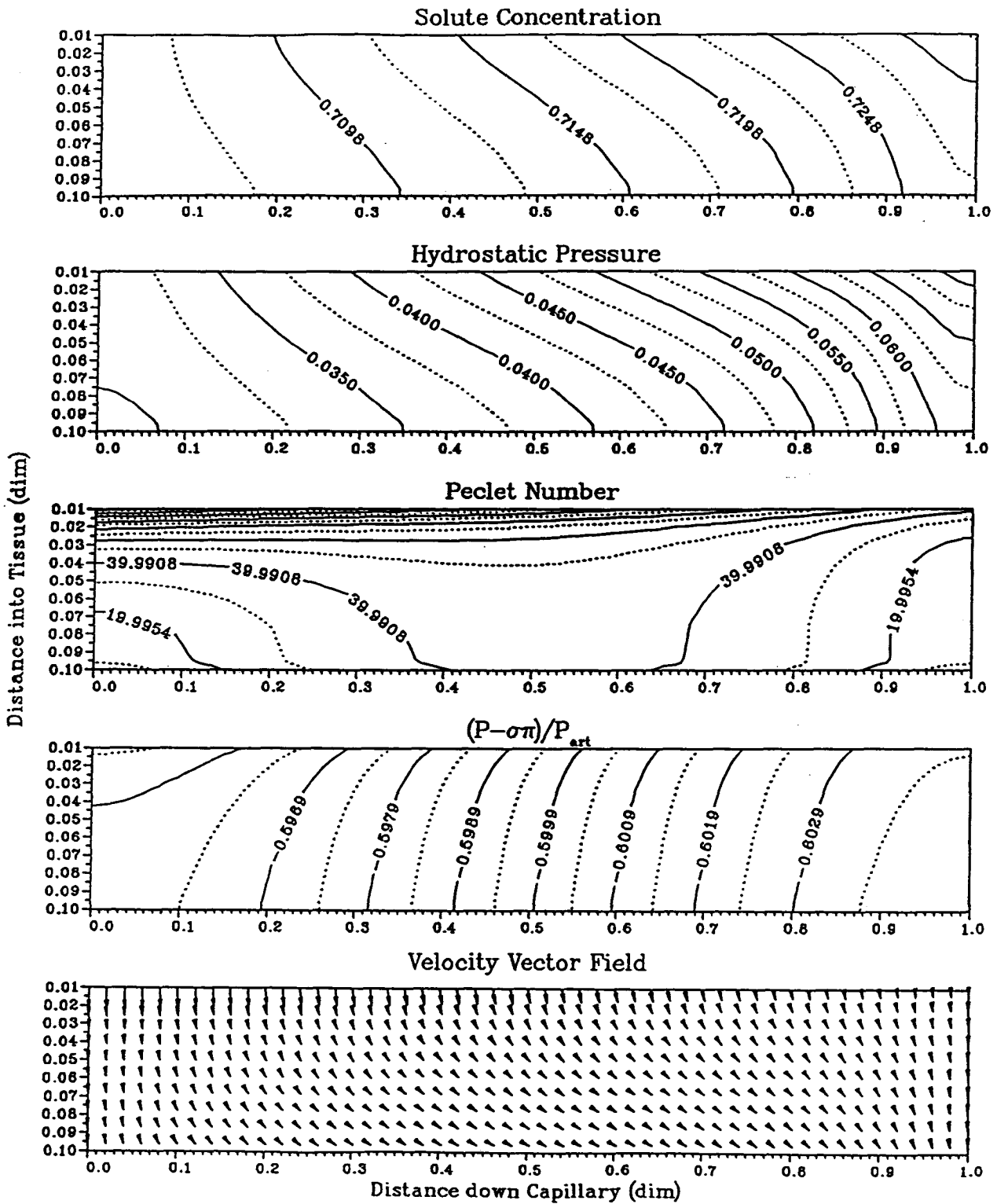


Figure 4.4: Dimensionless tissue solute concentrations, hydrostatic pressure, Peclet number, potential, and velocity vector distributions for the case with the capillary reflection coefficient, σ , equal to 0.1 at steady-state.

gradients are greater especially at the arteriolar and venular ends of the tissue near the capillary wall.

These results are expected since a reduction in the capillary reflection coefficient lowers the osmotic pressure driving force acting against the hydrostatic pressure difference across the membrane. This means the transcapillary fluid velocities are increased. Also from equation (3.34) it is seen that less solute is reflected at the capillary membrane as σ is reduced, thus more solute is convected through the capillary wall. For $\sigma = 0.10$, of the solute that would otherwise have freely convected across the capillary membrane, only 10 percent is reflected back into the capillary flow. The increased transcapillary fluid flow velocities and reduced solute reflection combine to convect more solute into the tissue space resulting in the higher average tissue solute concentration. This, in turn leads to elevated tissue hydrostatic pressures and the increased lymph flow rate.

The increase in the capillary reflection coefficient to 0.99 leads to increased solute concentration gradients within the tissue. The results for this case are displayed in Figure (4.5). The solute concentrations especially at the arteriolar end of the tissue are lower than those found in the base case (the dimensionless average tissue solute concentration is 0.5056). The range in the solute concentrations is increased. The hydrostatic pressure distribution is similarly increased in range and has a slightly lower average tissue hydrostatic pressure equal to -0.0328 (-0.984 mmHg). The potential distribution is relatively unchanged but is shifted in the positive direction and consequently the velocity field and magnitudes are very similar to the base case. This is expected since the base case reflection coefficient is equal to 0.85.

With a reflection coefficient equal to 0.99, this means that 99% of the solute that would be transported convectively across the capillary membrane is reflected. The reduction in the solute crossing the membrane can be seen in the results since the solute concentrations at the arteriolar end of the tissue are reduced. This is the region of highest

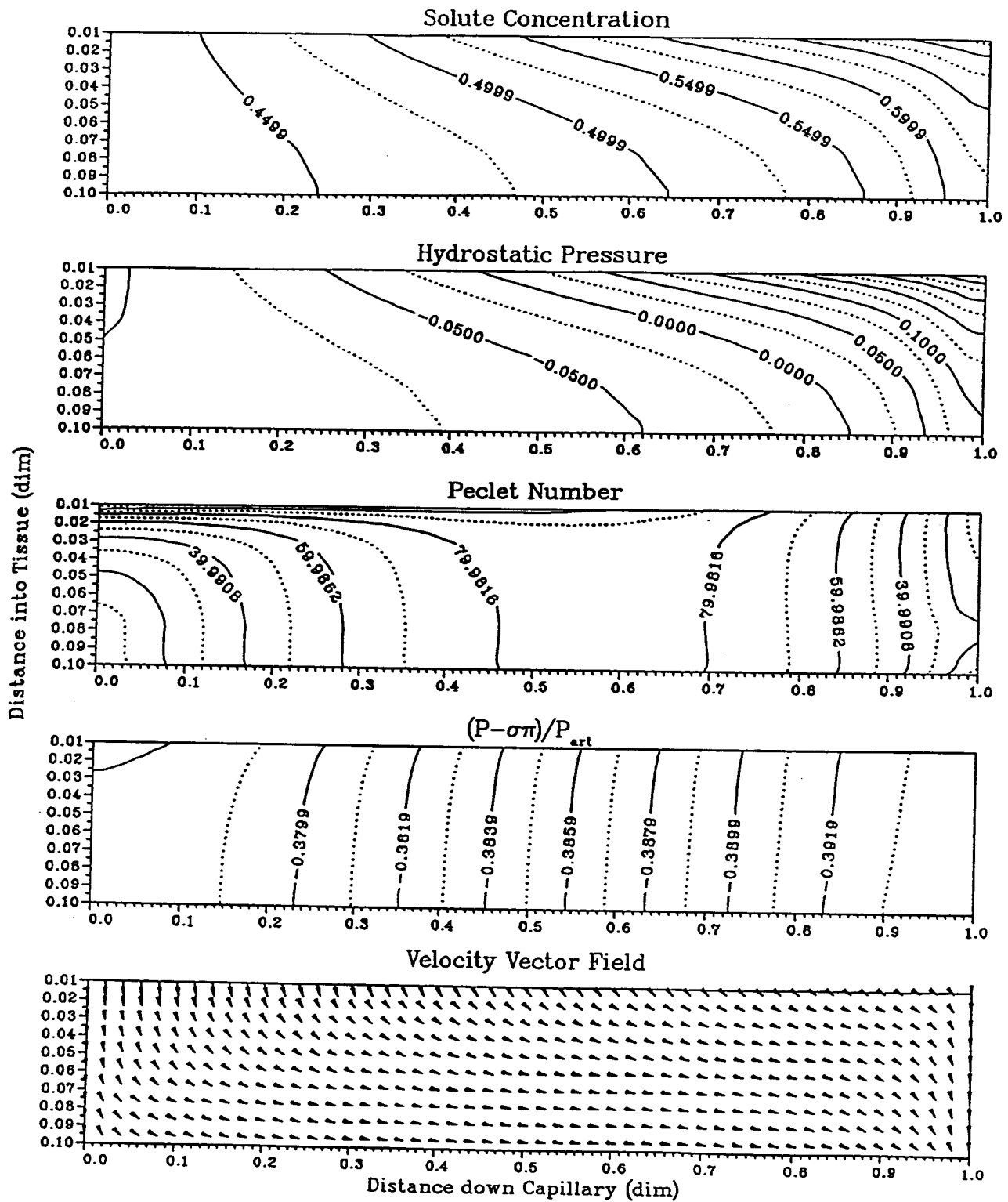


Figure 4.5: Dimensionless tissue solute concentrations, hydrostatic pressure, Peclet number, potential, and velocity vector distributions for the case with the capillary reflection coefficient, σ , equal to 0.99 at steady-state.

solute convection across the capillary wall. Solute, however, may still be transported across the wall by diffusion (the diffusive permeability PS).

Tissue Reflection Coefficient, σ_t

The effect of the tissue reflection coefficient is evaluated using the base case ($\sigma_t = 1.0$) and two other cases ($\sigma_t = 0.0$ and 0.50). Using σ_t equal to zero implies that the solute concentration distribution and gradients do not influence fluid motion and hence the hydrostatic pressure (and potential) fields within the tissue.

The range in the solute concentration distribution is slightly reduced as σ_t approaches zero. The results for $\sigma_t = 0.0$ are shown in Figure (4.6). The solute concentration gradients in the radial direction are also reduced. The concentration gradients grow more uniform within the arteriolar end and central portions of the tissue as σ_t is reduced. The dimensionless average tissue solute concentration increases very slightly to 0.5492 for $\sigma_t = 0.0$.

As a consequence of the increasingly more uniform solute concentration distribution as σ_t is reduced, the colloid osmotic pressure distribution plays a reduced role towards fluid motion. At σ_t equal to zero, the solute concentration distribution plays no role in the fluid motion. This is true within the tissue but is not, however, at the capillary wall where Starling's hypothesis still governs fluid flow across the capillary membrane. In the limit of $\sigma_t = 0.0$, the hydrostatic pressure and potential distributions are identical within the tissue. At lowered σ_t , the range of the hydrostatic pressure is greatly reduced. When $\sigma_t = 1.0$ (the base case), the dimensionless pressures range from about -0.1 to 1.0. At $\sigma_t = 0.5$, the dimensionless pressure range changes to lie between 0.1 to 0.55. The hydrostatic pressure responds to the reduced solute concentration gradients via the colloid osmotic pressure. The distribution changes from one that resembles the concentration distribution to one that resembles the potential distribution. This means that the maximum hydrostatic pressure

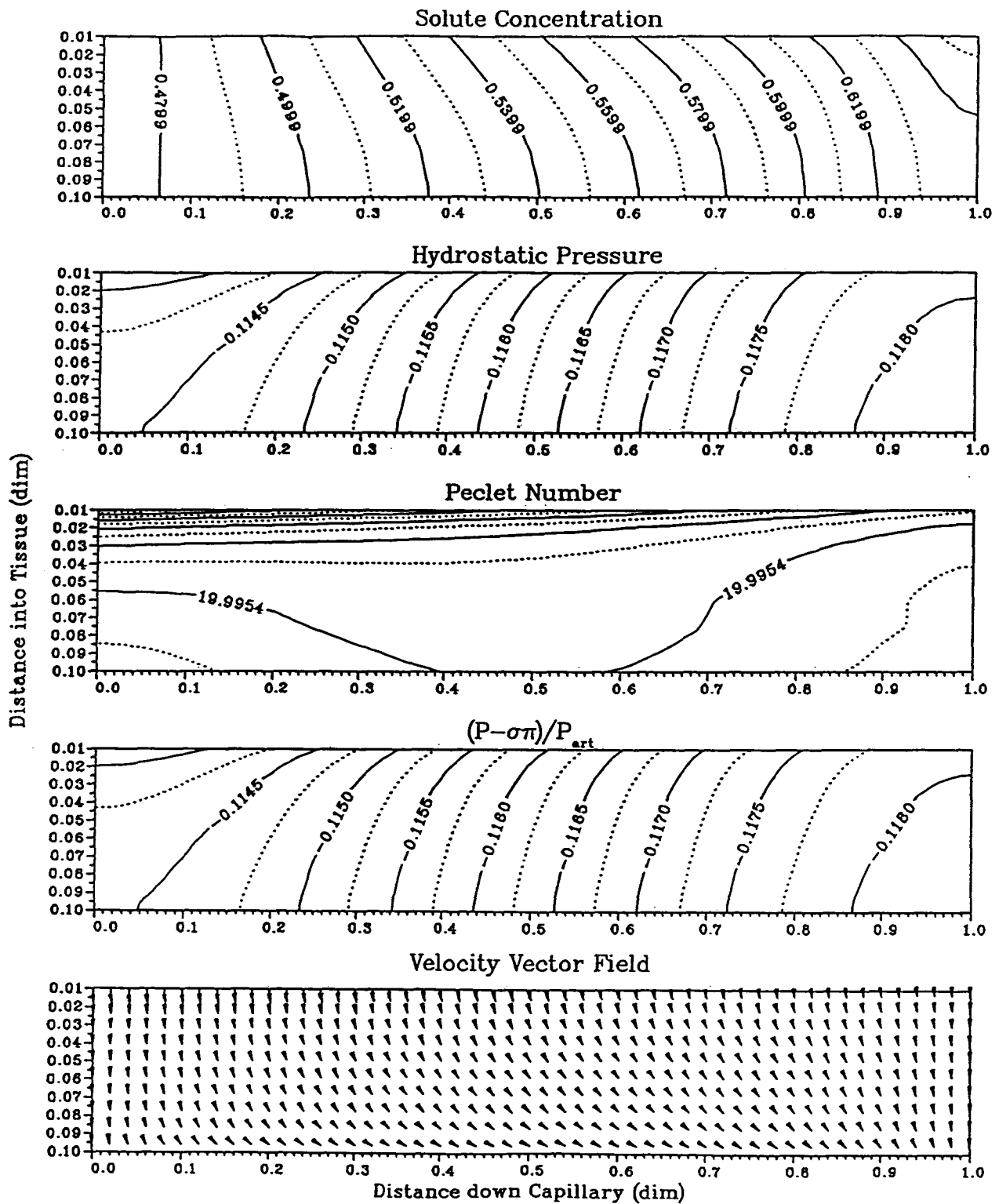


Figure 4.6: Dimensionless tissue solute concentrations, hydrostatic pressure, Peclet number, potential, and velocity vector distributions for the case with the tissue reflection coefficient, σ_p , equal to zero at steady-state.

shifts along the capillary wall towards the arteriolar end as σ_t is reduced. The average tissue hydrostatic pressure becomes more negative with reduced σ_t since it approaches the potential distribution leading to lower lymph drainage rates. For $\sigma_t = 0.0$, the dimensionless average tissue hydrostatic pressure drops to -0.1162 (-3.486 mmHg) and the lymph flow is 2.87 l/day. Correspondingly, as σ_t is reduced, the potential distribution is shifted in the positive direction and the range in its values is lowered since the solute concentration distribution range reduces.

There is no fluid reabsorption back into the capillary as σ_t is reduced and velocity magnitudes decrease substantially within the tissue space and are reduced at the arteriolar end of the capillary membrane. At the venular end of the capillary, the fluid velocities are slightly greater for reduced σ_t than the base case values. This means that there is more fluid filtering into the tissue in this region with lowered σ_t . As can be seen from the values in the Peclet number distribution, the fluid velocities in the tissue are reduced as σ_t is reduced.

Solute Diffusion Coefficient, D_{diff}

The effect the diffusion coefficient had on the system was investigated using the base case and two other cases where the diffusion coefficient was increased and decreased by an order of magnitude.

Figure (4.7) displays the results obtained with diffusion coefficient increased ten fold. An increase in the diffusion coefficient affects the results in a similar manner to the reduction of the retardation factor. The range in the solute concentration is reduced and the dimensionless average tissue solute concentration rises to 0.7151. The increase in the diffusion coefficient means that the solute can counter the convective transport to a higher degree. This means that there is very little solute washout from the arteriolar region of the

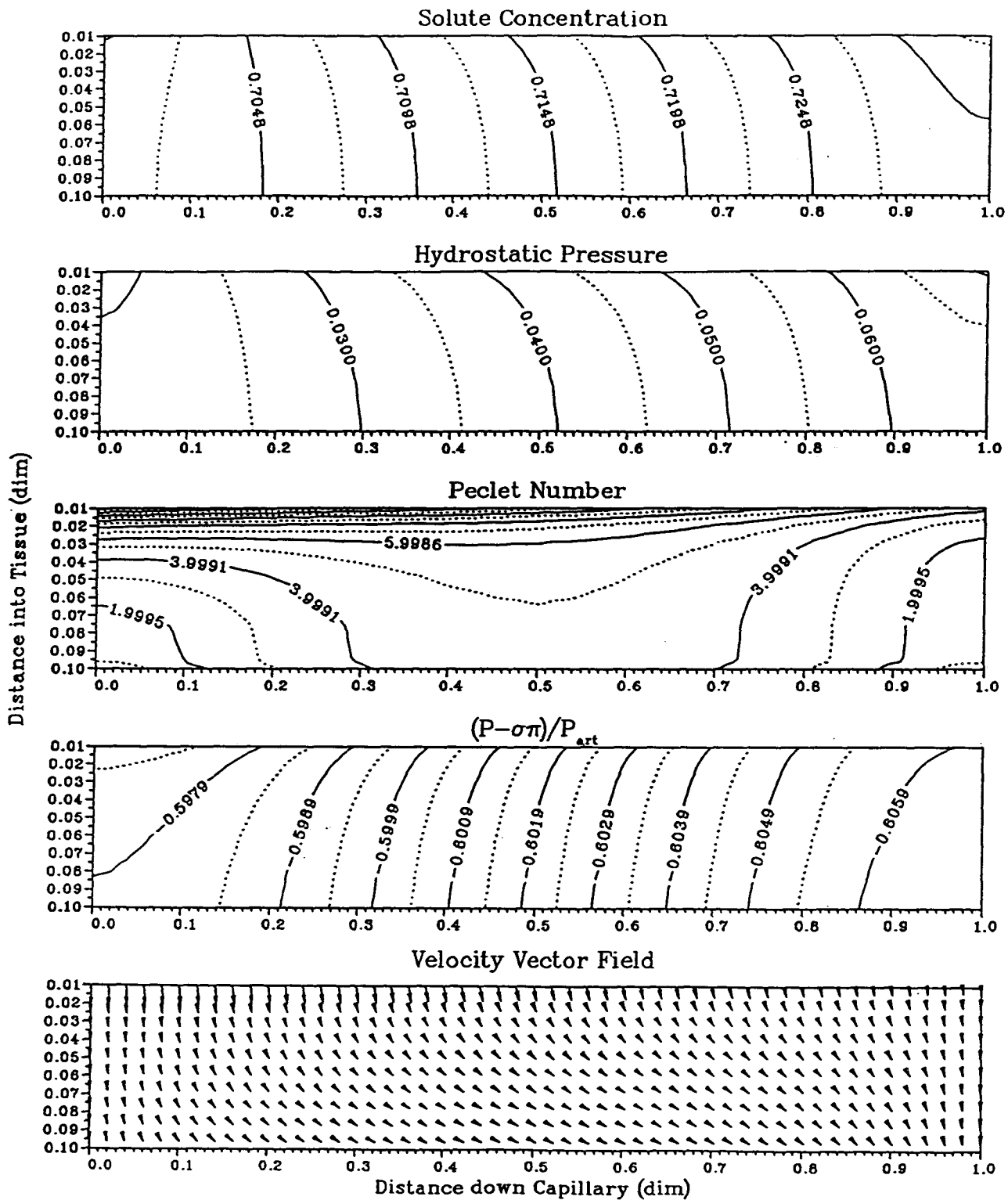


Figure 4.7: Dimensionless tissue solute concentrations, hydrostatic pressure, Peclet number, potential, and velocity vector distributions for the case with the solute molecular diffusion coefficient, D_{diff} , increased by an order of magnitude from the base value at steady-state.

capillary since solute can easily diffuse back to the capillary membrane. This leads to the more uniform solute distribution throughout the tissue clearly displayed in Figure (4.7).

The solute concentration distribution yields a similarly distributed osmotic pressure field. The hydrostatic pressure responds to the colloid osmotic pressure resulting in a distribution similar to the solute concentration distribution. Due to the higher solute concentrations, the osmotic pressure is greater throughout the tissue. This leads to more positive hydrostatic pressures throughout the tissue and therefore greater lymph flow. The average tissue hydrostatic pressure is 0.0408 (1.224 mmHg).

The potential distribution is shifted in the negative direction due to the increase in the solute concentrations via the osmotic pressure. The potential gradients are stronger in the radial direction than the base case. This is due to the greater lymph flow (8.23 l/day) caused by the more positive hydrostatic pressures in the tissue. The fluid velocities are greater throughout the tissue and at the capillary membrane.

It is interesting to note that an increase in the solute diffusion coefficient by a factor of ten has very similar transcapillary flow velocities to that when the retardation factor is reduced by a factor of ten. This is because the effect on solute transport is similar for both cases, i.e., the diffusive contribution is effectively increased by ten-fold. As expected, the drop in the range of the Peclet number indicates that the diffusive transport is increased.

Tissue Hydraulic Conductivity, K

The effect of the tissue hydraulic conductivity is tested in three cases. The base case uses the value indicated in Table (4.1). Two other cases are performed with K reduced and then enlarged by an order of magnitude respectively. The results discussed below are displayed in Figures (4.8) and (4.9) ($K \times 0.1$ and $K \times 10$ respectively).

The main effect of an adjustment in the tissue hydraulic conductivity is a change in the potential gradients within the tissue. From the results, a reduction in K by a factor of

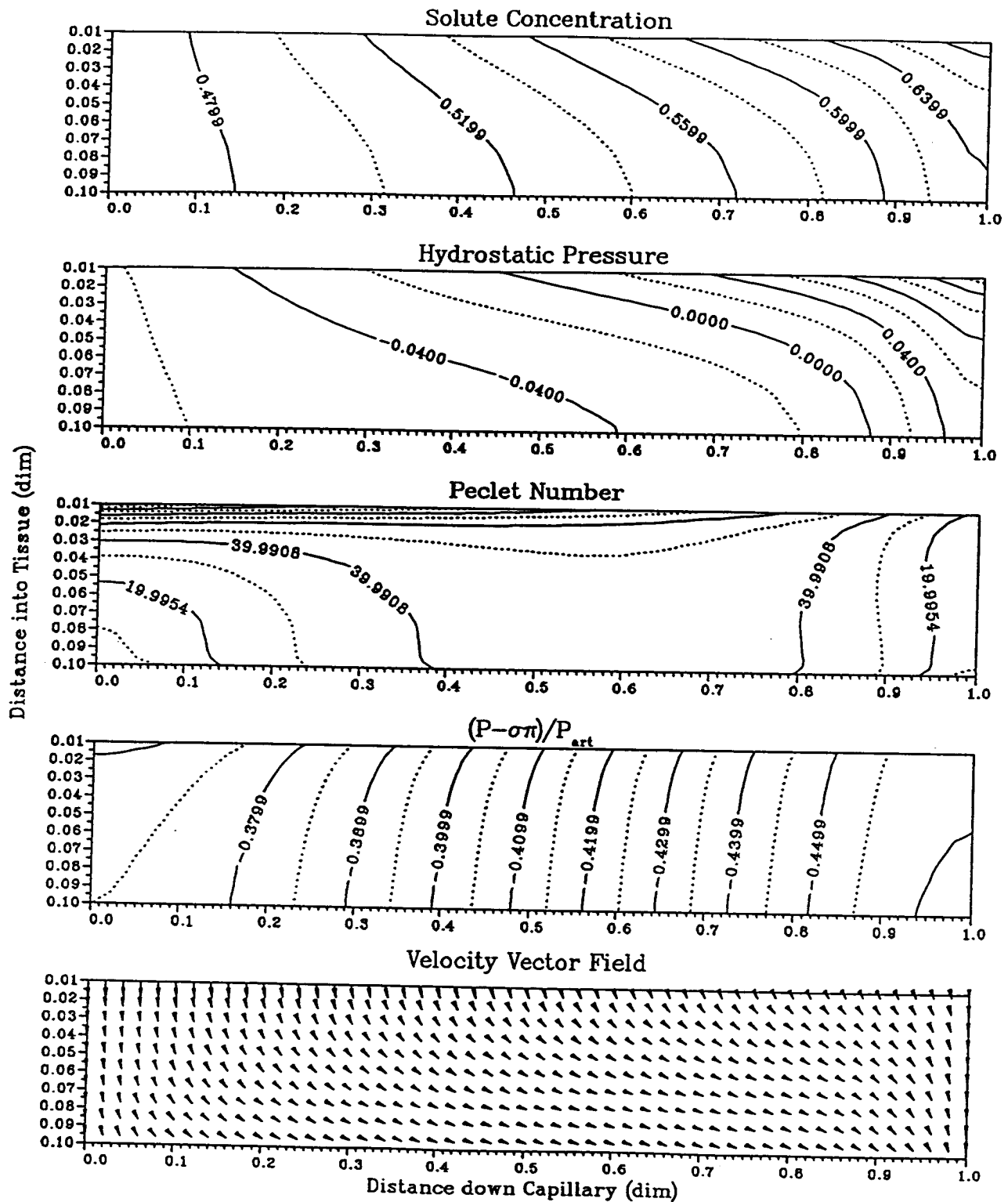


Figure 4.8: Dimensionless tissue solute concentrations, hydrostatic pressure, Peclet number, potential, and velocity vector distributions for the case with the hydraulic conductivity, K , decreased by an order of magnitude from the base value at steady-state.

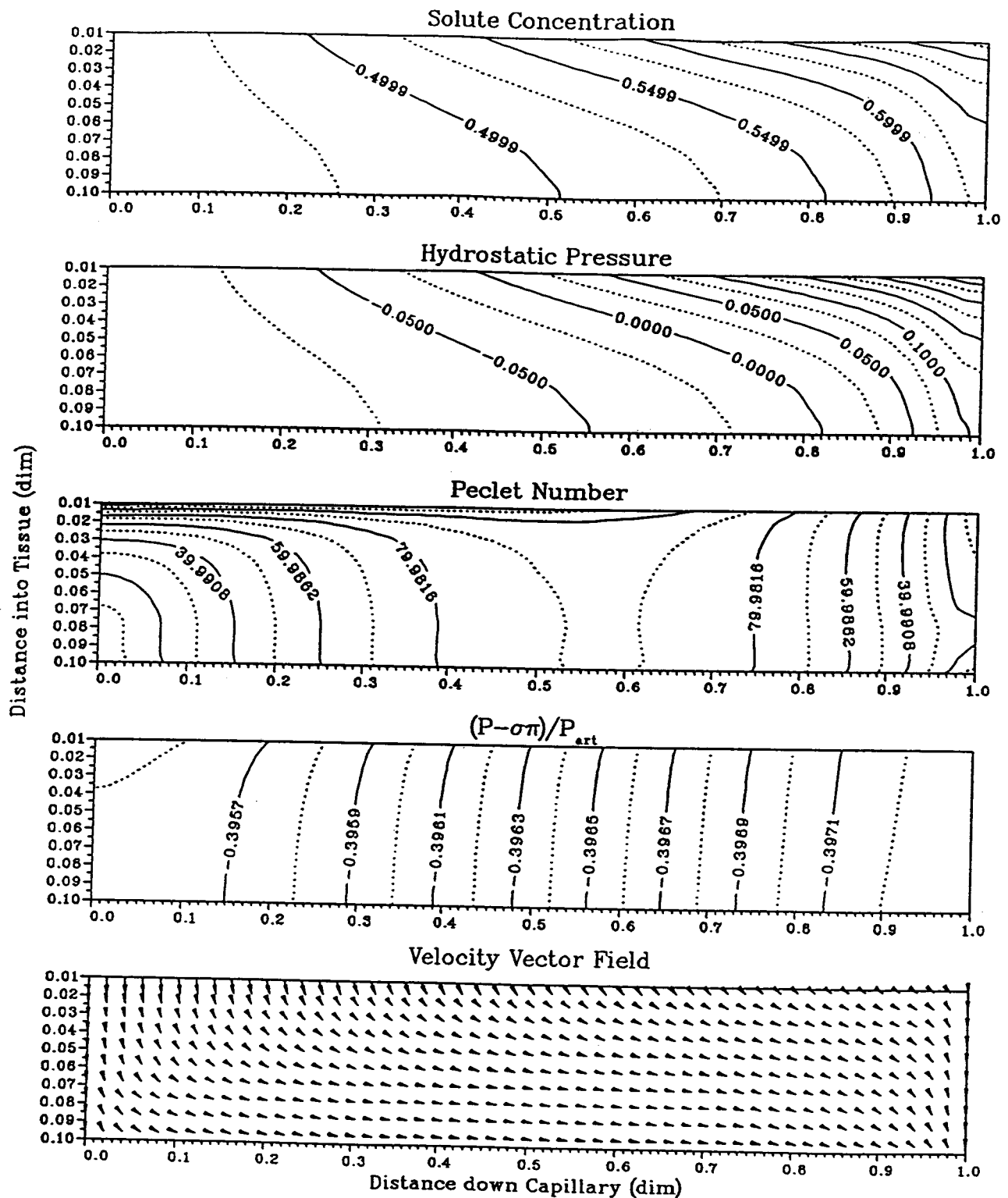


Figure 4.9: Dimensionless tissue solute concentrations, hydrostatic pressure, Peclet number, potential, and velocity vector distributions for the case with the hydraulic conductivity, K , increased by an order of magnitude from the base value at steady-state.

ten increased the range in the potential by just under a factor of ten. This is expected since this corresponds to an increase in the tissue fluid flow resistance. The combined decrease in the hydraulic conductivity and the increase in the potential gradients yield slightly lower fluid velocities throughout the tissue. This means that less solute is convected into the interstitial space. The range in the solute concentration distribution is reduced as the hydraulic conductivity is reduced. At the arteriolar end of the tissue, the solute concentrations are slightly higher than the base case values. This however, is not the case at the venular end of the tissue where the solute concentrations are slightly lower than the base case values. This produces a solute distribution with lower longitudinal and radial gradients throughout the tissue than the base case. The dimensionless average tissue solute concentration, slightly higher than the base case value, is equal to 0.5403.

The increase in K results in a lower range in the potential within the tissue. The fluid velocities increase and result in a greater solute range throughout the tissue. This produces a less uniform solute concentration distribution throughout the tissue.

The hydrostatic pressure distribution is very similar to the solute concentration distribution. For the case with decreased K , the more uniform solute concentrations throughout the tissue result in a more uniform hydrostatic pressure distribution. The range in the pressures is decreased with increasing portions of the tissue becoming subatmospheric. Hydrostatic pressure gradients are low in the central and arteriolar portions of the tissue. The dimensionless average tissue hydrostatic pressure for the reduced hydraulic conductivity case is -0.0268 (-0.8040 mmHg). The lymphatic drainage decreased to 5.27 l/day. When the hydraulic conductivity was increased by an order of magnitude, the dimensionless tissue hydrostatic pressure increased very slightly to -0.0253 (-0.7590 mmHg). The lymph drainage increased slightly to 5.51 l/day. The smaller change in the average tissue hydrostatic pressure for an order of magnitude increase in K than the order of magnitude decrease in K implies that the tissue fluid flow resistance is not dominating the fluid flow structure at the current base value of K listed in Table (4.1). As

K decreases further, the tissue potential drop increases and the hydraulic conductivity begins to control the fluid flow patterns to a greater extent. Therefore, only reductions in the tissue hydraulic conductivity (or increasing the capillary membrane filtration coefficient) would alter the flow patterns significantly.

As K is decreased, the fluid velocities within the central portions and arteriolar end of the tissue are reduced despite the increase in the potential gradients. This is reflected in the Peclet number distribution. The reason the fluid velocities are largely reduced throughout the tissue is due to the increased resistance of the tissue porous medium. The fluid velocities are similarly decreased at the capillary wall except at the extreme venular end of the capillary where fluid velocities are slightly elevated from the base case values.

Capillary Membrane Diffusive Permeability, PS

Four cases were used in evaluating the impact of the diffusive permeability through the capillary wall, PS . As well as the base case, the following cases were also investigated: $PS = 0.0$, $PS \times 100$, and $PS \times 10000$. Figure (4.10) displays the results for the last case.

Moderate changes in PS only affect the solute concentration distribution (and thus the pressure and potential distributions) slightly. Increases in PS increase the diffusive transport of solute through the capillary membrane yielding higher solute concentrations at the tissue-side of the capillary membrane and thus throughout the tissue. This is most pronounced at the venular end of the capillary. This is expected since the convective transport of solute is minimal at the venular end of the capillary. The small changes in the results for moderate changes ($\times 100$) in PS indicate that transport across the capillary membrane is convectively dominated. If there were reabsorption of fluid back into the capillary then increasing PS would most affect the central portions of the capillary near the zero point where the fluid velocities are the lowest.

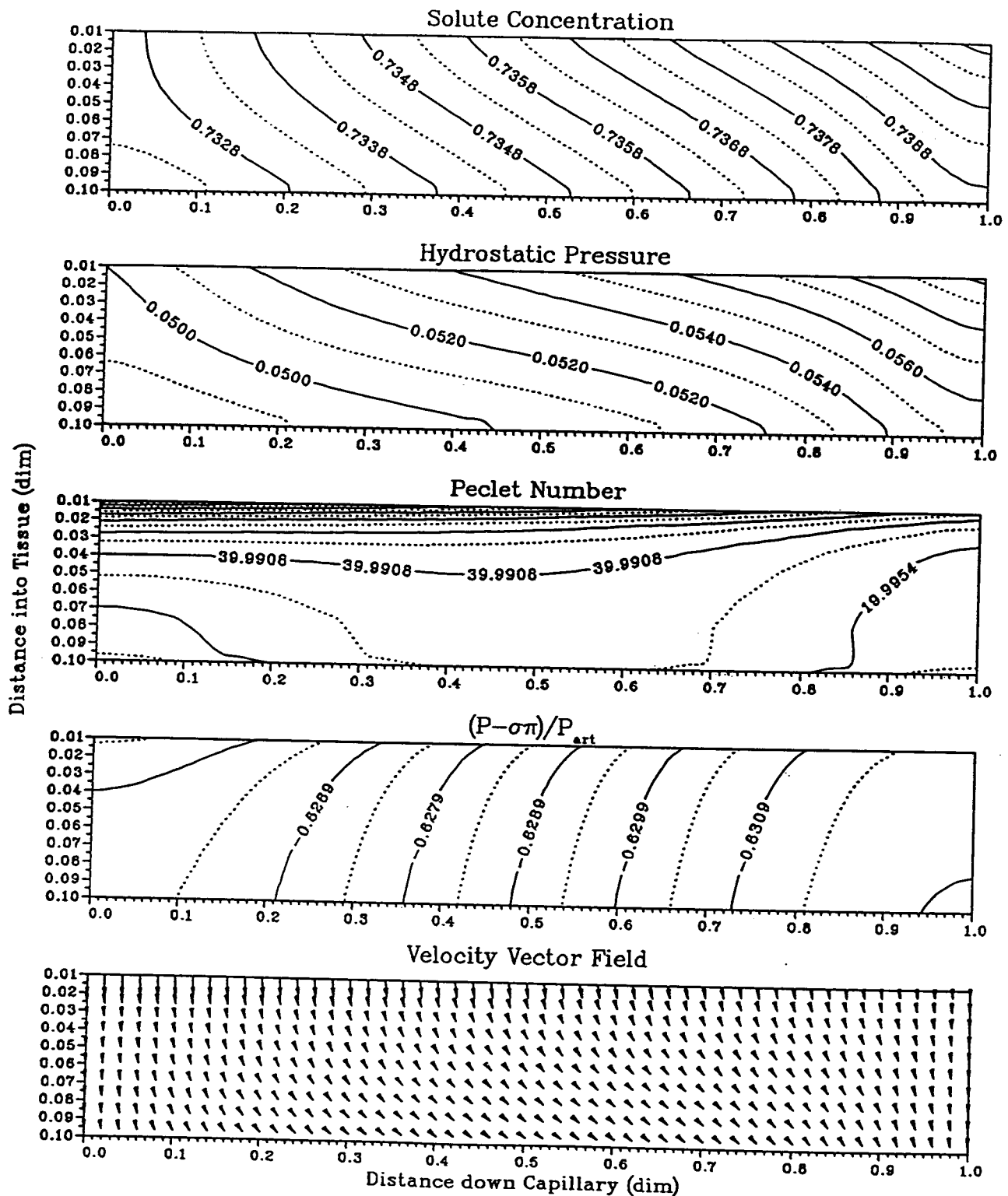


Figure 4.10: Dimensionless tissue solute concentrations, hydrostatic pressure, Peclet number, potential, and velocity vector distributions for the case with the capillary membrane diffusive permeability, PS , increased by a large amount ($\times 10000$) from the base value at steady-state.

Extreme changes in the diffusive permeability (for example, $\times 10000$) alter the solute concentration range and average tissue concentration values significantly. The solute concentration range is reduced dramatically to roughly 0.010 and gradients are reduced throughout the tissue. The increased diffusive permeability raises the dimensionless average tissue solute concentration to 0.7355. This rise in the solute concentration distribution leads in turn to a rise in the hydrostatic pressure distribution as it responds to the increased colloid osmotic pressure throughout the tissue. The dimensionless average hydrostatic pressure is 0.05209 (1.5627 mmHg). This results in an increase in the lymph drainage to 8.60 l/day. The range in the potential is largely unaffected. The main change is that the radial gradients are slightly greater throughout the tissue especially at the arteriolar end near the capillary. The potential distribution is shifted in the negative direction due to the increased solute concentration values (via the colloid osmotic pressure). Fluid velocities are greater along the capillary membrane and within the tissue due to the increased lymph flow.

Lymphatic Sink Strength, LS

The strength of the sink was varied in two other cases. In the first case, the sink strength, LS , is reduced by a factor of five while in the second case it is increased by a factor of five. This allows us to make some generalizations on the behaviour of the system with regard to the strength of the lymphatic sink.

The solute concentration distribution is increased as the sink strength is reduced. The dimensionless average solute concentration is equal to 0.5653 for the reduced value of LS . This is expected since less solute is being dragged out through the sink and less solute is being convected across the capillary membrane. The range in the solute concentration changes little with a drop in LS . These results are presented in Figure (4.11). Increasing the value of LS lowers the average solute concentration to 0.5065. The radial gradients are

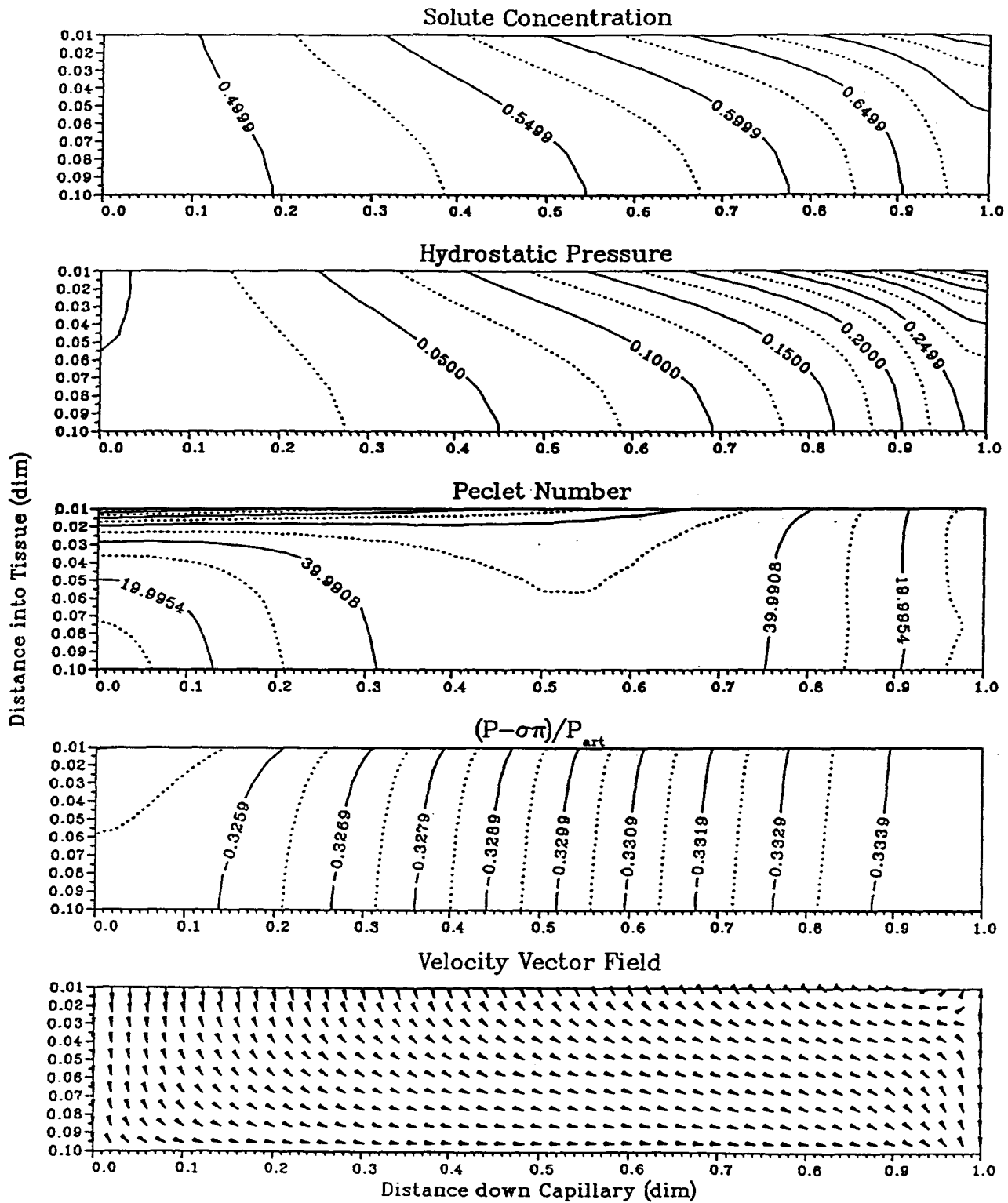


Figure 4.11: Dimensionless tissue solute concentrations, hydrostatic pressure, Peclet number, potential, and velocity vector distributions for the case with the lymphatic sink strength, LS , decreased by a factor of five from the base value at steady-state.

increased relative to the longitudinal gradients within the tissue as the sink strength is increased.

The hydrostatic pressure distributions are very similar to the solute concentration distributions. As the sink strength is increased, the pressure distribution shifts lower but is limited by the lymphatic pressure, P_L . The average tissue hydrostatic pressures are 0.0924 (2.772 mmHg) and -0.0575 (-1.725 mmHg) for the cases with LS reduced and increased by a factor of five respectively. As the sink strength is reduced, the potential distribution is shifted in the positive direction. The sink affects the fluid velocities within the tissue and at the capillary membrane. As expected, as the sink strength is reduced the zero points approaches the mid-point $z^* = 0.5$. With a sufficiently strong sink, there is no reabsorption of fluid back into the capillary and all the fluid is drained out through the lymphatics. This occurs with the base case. The case with LS reduced by a factor of five displays fluid reabsorption back into the capillary. The zero point occurs at roughly $z^* = 0.94$.

As expected, as LS is increased, the lymph flow increases. The lymph drainage flows are equal to 1.91 and 21.42 l/day for the cases where LS is decreased and increased respectively. Numerical convergence was difficult to obtain in cases where LS was increased. This is because the fluid leaving the system via the lymphatic sink is limited by the amount of fluid that can enter the system. This is dictated by the value of the capillary filtration coefficient, L_p , which is prescribed at the capillary membrane. This result indicates that, given a fixed value of the capillary filtration coefficient, there is a lymph flow limit that cannot be exceeded.

Lymphatic Sink Pressure, P_L

The base case value of the lymphatic sink pressure is -0.20 (-6 mmHg). Two other cases were performed with the lymphatic sink pressure reduced to -0.30 (-9 mmHg) and -

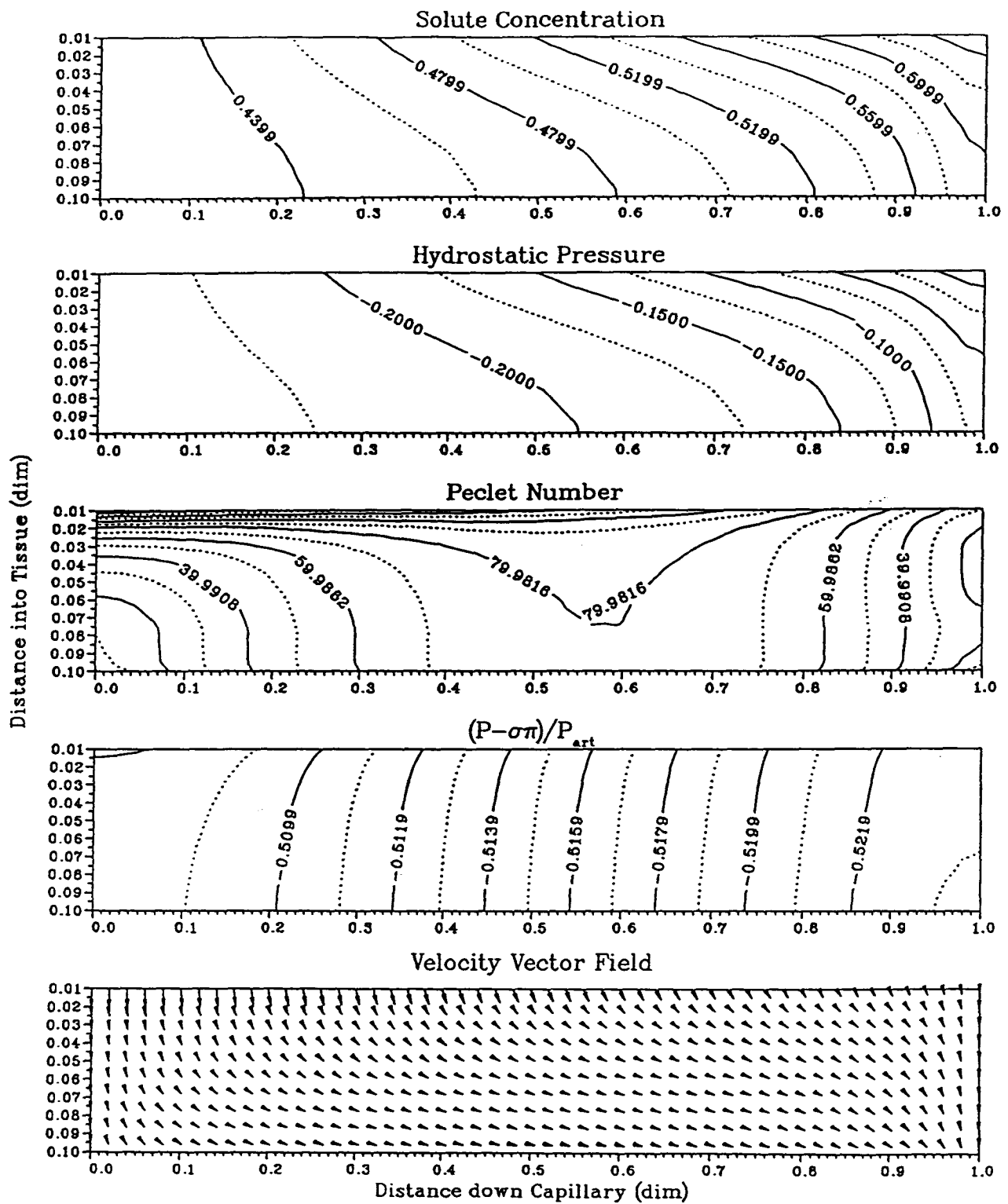


Figure 4.12: Dimensionless tissue solute concentrations, hydrostatic pressure, Peclet number, potential, and velocity vector distributions for the case with the lymphatic sink pressure, P_L^* , lowered to -0.4 (-12 mmHg) at steady-state.

0.40 (-12 mmHg). The latter case represents an extremely low lymphatic sink pressure and is presented in Figure (4.12).

Decreasing the lymphatic sink pressure increases lymph drainage (see equation (3.20)). Consequently, with more negative lymphatic sink pressures, the average solute concentrations in the tissue are slightly lower than the base case. This is especially noticeable in the tissue away from the capillary ($r^* > \sim 0.03$). In addition, the range in the solute concentrations are reduced slightly. The change in the solute concentration field causes a drop in both the hydrostatic pressure distribution and its range. The average pressure drops from -0.0255 (-0.7650 mmHg) for the base case to -0.1800 (-5.4000 mmHg) for a lymphatic sink pressure of -0.40 (-12 mmHg). As expected, the potential distribution is shifted in the negative direction and its range decreased as P_L is reduced. The velocity field is virtually unchanged in most of the tissue although fluid velocities are greater than those of the base case at the venular end of the capillary. This is a result of the increased lymph drainage. The lymph flow rises to 7.14 l/day for $P_L^* = -0.40$ (-12 mmHg). The increased lymph flow leads to lower solute concentrations within the tissue space. The dimensionless average solute concentration is equal to 0.4901 for $P_L^* = -0.40$ (-12 mmHg).

Lymphatic Sink Radial Position

The position of the sink was varied in two other cases. These two cases place the sink at the radial positions $r^* = 0.025$ and $r^* = 0.055$ (half of tissue envelope thickness). The results for the former case are shown in Figure (4.13). The sink is always maintained as parallel to the capillary. When the sink is repositioned to a reduced radius, the volume of the sink is lowered because the lymphatic sink is represented by a concentric shell of the same radial thickness about the capillary. To provide a valid comparison, either the volume of the sink or the sink strength has to be enlarged. Here, the sink strength will be increased to reflect the reduction in sink volume with lower radii. The volume of the

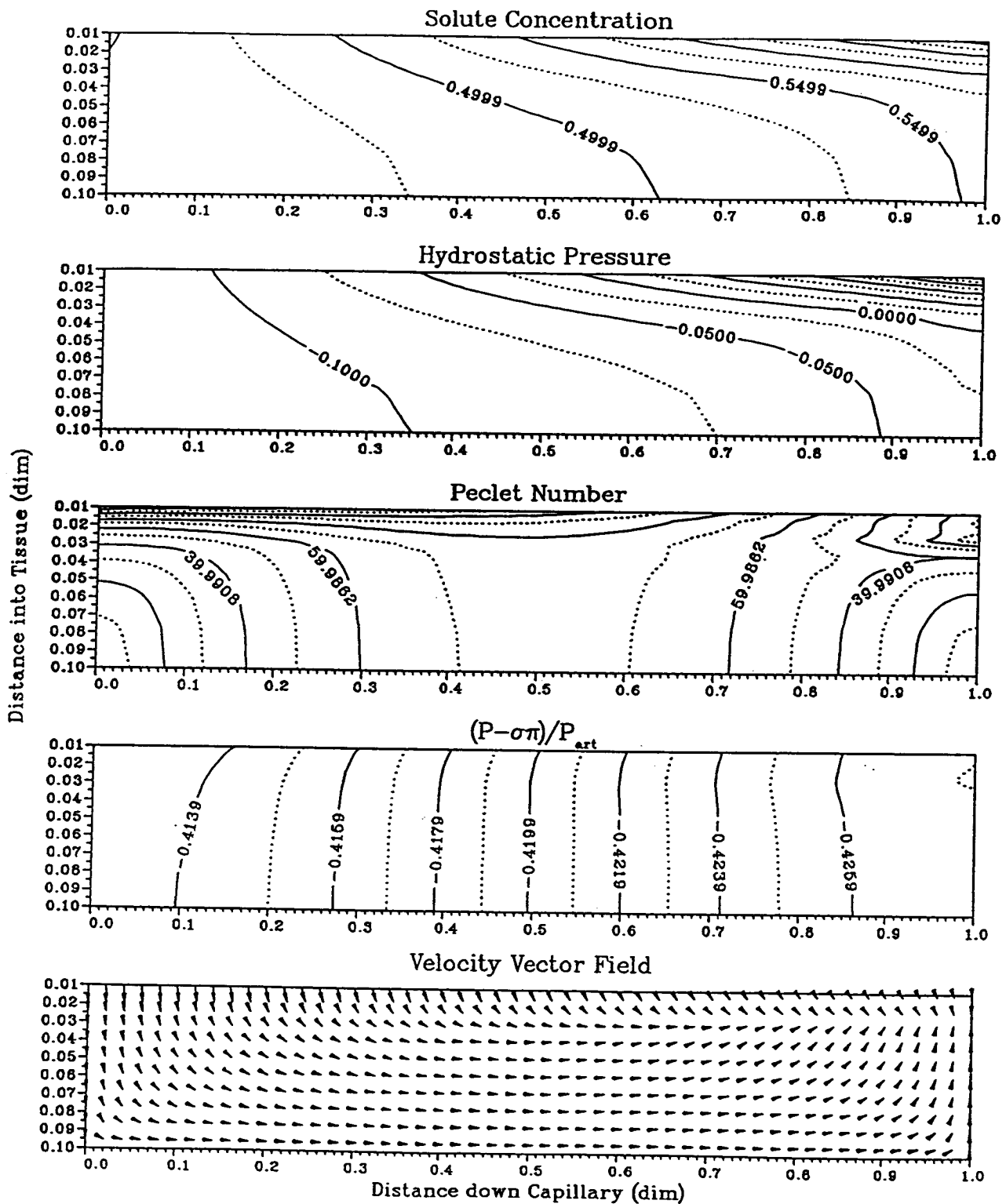


Figure 4.13: Dimensionless tissue solute concentrations, hydrostatic pressure, Peclet number, potential, and velocity vector distributions for the case with the lymphatic sink repositioned at $r^* = 0.025$ at steady-state.

sink when positioned at $r^* = 0.025$ is 3.55 times less than the volume of the sink at the outer tissue envelope. Therefore the sink located at $r^* = 0.025$, the value of LS is increased by the factor 3.55. Similarly, the sink strength for the sink located at $r^* = 0.055$ was increased by the factor 1.70.

From the results, it is seen that the solute concentration and hydrostatic pressure distributions are not affected significantly by the movement of the sink. The solute concentrations lower as the sink moves closer to the capillary. The radial gradients are greater near the venular end of the tissue and increase near the capillary as the sink moves closer to the capillary. Despite the presence of the sink, the solute and fluid can 'see' the remainder of the tissue beyond and can pass into and out of these regions. This explains why there is solute on the other side of the sink into the tissue for the two repositioned sink cases. The solute gradients in these regions are far less than the gradients that exist between the capillary and sink. The average solute concentrations are 0.5006 and 0.5167 for the $r^* = 0.025$ and $r^* = 0.055$ positioned sinks respectively.

The hydrostatic pressure distributions are very similar to the solute concentration distributions for both cases. The gradients beyond the sink diminish as the sink is moved towards the capillary. The dimensionless average tissue hydrostatic pressures for the $r^* = 0.025$ and $r^* = 0.055$ positioned sinks are -0.0761 (-2.2833 mmHg) and -0.0322 (-0.9660 mmHg) respectively. The lymph flows increase as the sink is moved towards the capillary to 18.38 and 9.69 l/day for the $r^* = 0.025$ and $r^* = 0.055$ positioned sinks respectively. It is important to bear in mind that the sink strengths have been increased for each case due to the sink geometry. This the reason the average tissue pressures for these cases are less than the base case value and yet provide more lymph flow. With increased sink strengths, the tissue beyond the sink would contain less and less solute (and lower gradients) and the hydrostatic pressure would fall to that slightly above the the lymphatic sink pressure (also with lower gradients). With a reduction of the sink strength, there is greater solute stored in the outer tissue space and the hydrostatic pressure increases.

From Figure (4.13), as the sink becomes closer to the capillary, the potential distribution shifts in the negative direction. The range of the potential distribution is similar to all the previous runs. There is a dip in the potential along the sink which becomes more pronounced at the venular end of the tissue. As can be seen from the fluid velocity plots, the sink at $r^* = 0.025$ affects the flow patterns. Fluid enters the sink from the capillary-side and from tissue-side of the lymphatic sink. The radial component of the fluid velocities increases in the neighborhood of the sink. This is indicated indirectly in the plot of the Peclet numbers. There is a local ridge of higher Peclet numbers in the vicinity of the sink reflecting the greater convective transport at the sink.

The tissue space beyond the lymphatic sink stores solute. This means that there exists the possibility to access this solute if there is a sudden shortage or that solute will still be drained via the sink even if there were none in the plasma. This would occur until the stored solute were depleted. In this manner, the tissue beyond the sink acts as a capacitance.

Capillary Membrane Filtration Coefficient, L_p

The effect of the capillary membrane filtration coefficient, L_p , on the system was examined from the base case and two other cases where it was varied as half the base value and twice the base value ($L_p \times 0.5$ and $L_p \times 2$ respectively). A reduction in the capillary membrane filtration coefficient increases the fluid flow resistance of the capillary membrane. This means that the flow rate decreases for a given potential drop across the membrane. The results for the increased and decreased filtration coefficients ($L_p \times 2$ and $L_p \times 0.5$) are shown in Figures (4.14) and (4.15) respectively.

The range in the solute concentration and gradients increase as the capillary membrane filtration coefficient is increased (or capillary fluid flow resistance is reduced). The average solute concentration decreases as L_p increases (0.4311 for $L_p \times 2$ and 0.6053

for $L_p \times 0.5$). The reduction in L_p reduces the fluid velocities across the capillary membrane. The reduction in L_p by a factor of two reduces the transcapillary flow velocities by roughly a factor of two. This means that the fluid velocities in the tissue will also be reduced and thus diffusion will play a relatively greater role for solute transport in the tissue. This explains the increased average tissue solute concentration for the case $L_p \times 0.5$.

The hydrostatic pressure distributions are very similar to the solute concentration distributions. As a consequence of the ranges in the solute concentration distributions, at increased L_p , the hydrostatic pressure range increases and high gradients occur, particularly at the venular end of the tissue near the capillary. A reduction in L_p also lowers the average tissue hydrostatic pressure. The average tissue hydrostatic pressures are -0.0205 (-0.6150 mmHg) and -0.0262 (-0.7860 mmHg) for the cases $L_p \times 2$ and $L_p \times 0.5$ respectively. This results in the following lymph flow rates : 5.76 l/day for $L_p \times 2$ and 5.37 l/day for $L_p \times 0.5$. The reduced solute removal by the lymphatic sink also explains the higher solute concentrations in the tissue for lowered values of L_p .

With enlarged L_p , the potential gradients increase and the range in the tissue rises and is shifted slightly in the positive direction. This is expected since the decrease in the capillary membrane filtration resistance will increase the potential drop throughout the tissue space relative to that in the capillary wall. In other words, the potential distribution will be less uniform. For reduced L_p , at the arteriolar end of the tissue, the velocities across the membrane are significantly lower than those for the base case. The opposite is true at the extreme venular end of the capillary where flows are slightly greater than the base case. An increase in L_p changes the flow structure significantly. As shown for the case with increased L_p , reabsorption back into the capillary starts to occur. The zero point occurs at about $z^* = 0.92$. This is expected since with increased L_p more fluid can enter the system. The transcapillary flow velocities are much greater in the arteriolar and central portions of the capillary. At the venular end of the tissue, the reabsorption is apparent. The strength of

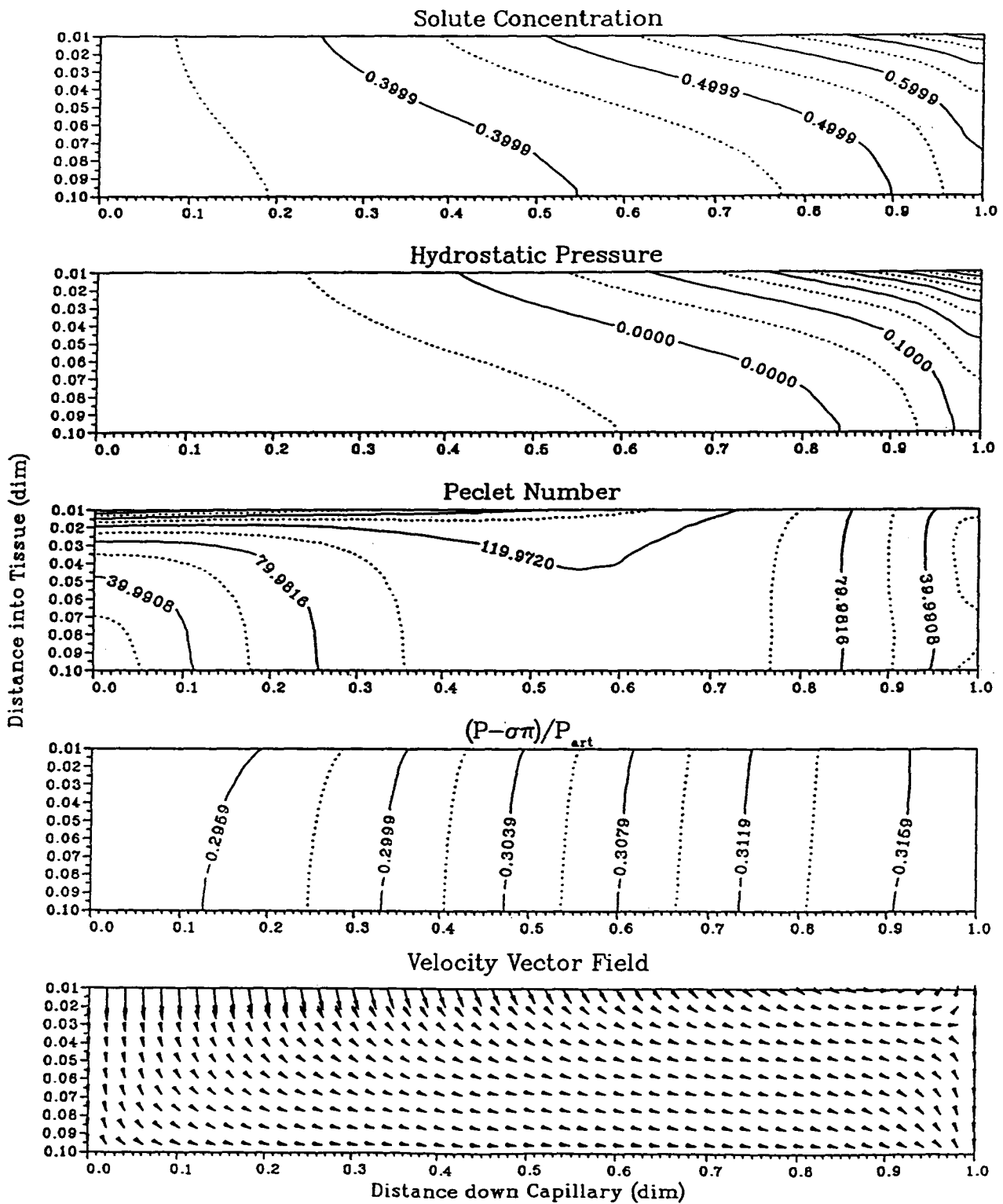


Figure 4.14: Dimensionless tissue solute concentrations, hydrostatic pressure, Peclet number, potential, and velocity vector distributions for the case with the capillary membrane filtration coefficient, L_p , increased by a factor of two from the base value at steady-state.

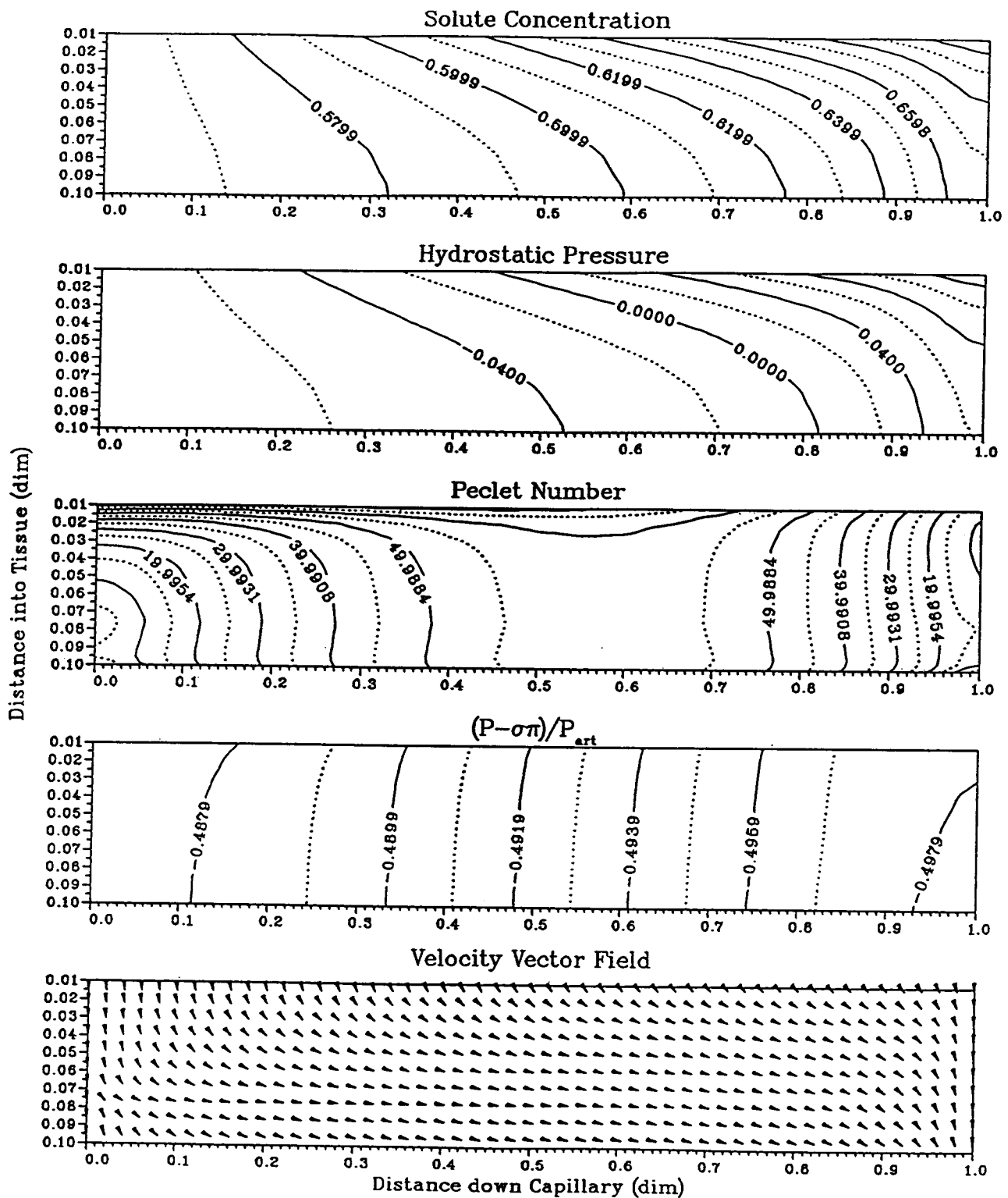


Figure 4.15: Dimensionless tissue solute concentrations, hydrostatic pressure, Peclet number, potential, and velocity vector distributions for the case with the capillary membrane filtration coefficient, L_p , decreased by a factor of two from the base value at steady-state.

the sink is constant and so fluid starts to flow back into the capillary. This shows that with the increased L_p , sufficient fluid is entering the system to allow a large amount of lymph drainage (at fixed sink strength) and reabsorption. The fluid velocity magnitudes are indirectly indicated in the Peclet number distribution. As expected, for increased L_p , the fluid velocities are greater throughout the tissue and at the capillary wall.

In summary, if L_p is increased, the fluid velocities rise due to the reduction in the resistance to flow at the membrane. This is propagated throughout the tissue. An enlarged filtration coefficient promotes convection throughout the tissue lowering the solute concentration distribution and leading to increased lymph flow. With reabsorption of fluid back into the capillary, there are higher than usual solute concentration gradients at the venular end of the tissue. This is because convective transport is operating in the opposite direction to diffusive transport in this region.

Mechanical Dispersion

The inclusion of dispersion in the problem simply increases the effective diffusion coefficient. The results are displayed in Figure (4.16). This case involves an added degree of complexity because the dispersion coefficient is a function of the local fluid velocities which are in turn a function of the solute concentrations via the osmotic pressure term. The increase in the effective diffusion coefficient lead to slightly higher solute concentration values and lower concentration gradients within the tissue. The inclusion of dispersion increases the dimensionless average tissue solute concentration to 0.6842 from 0.5258 for the base case (this is without dispersion). The solute concentration gradients are reduced within the tissue especially in the arteriolar end of the tissue. As a consequence of the increased solute concentration distribution, the hydrostatic pressure distribution responds and falls slightly. The average dimensionless tissue pressure is -0.0258 (-0.7740 mmHg) compared to the base case value of -0.0255 (-0.7650 mmHg). The lymph drainage rate

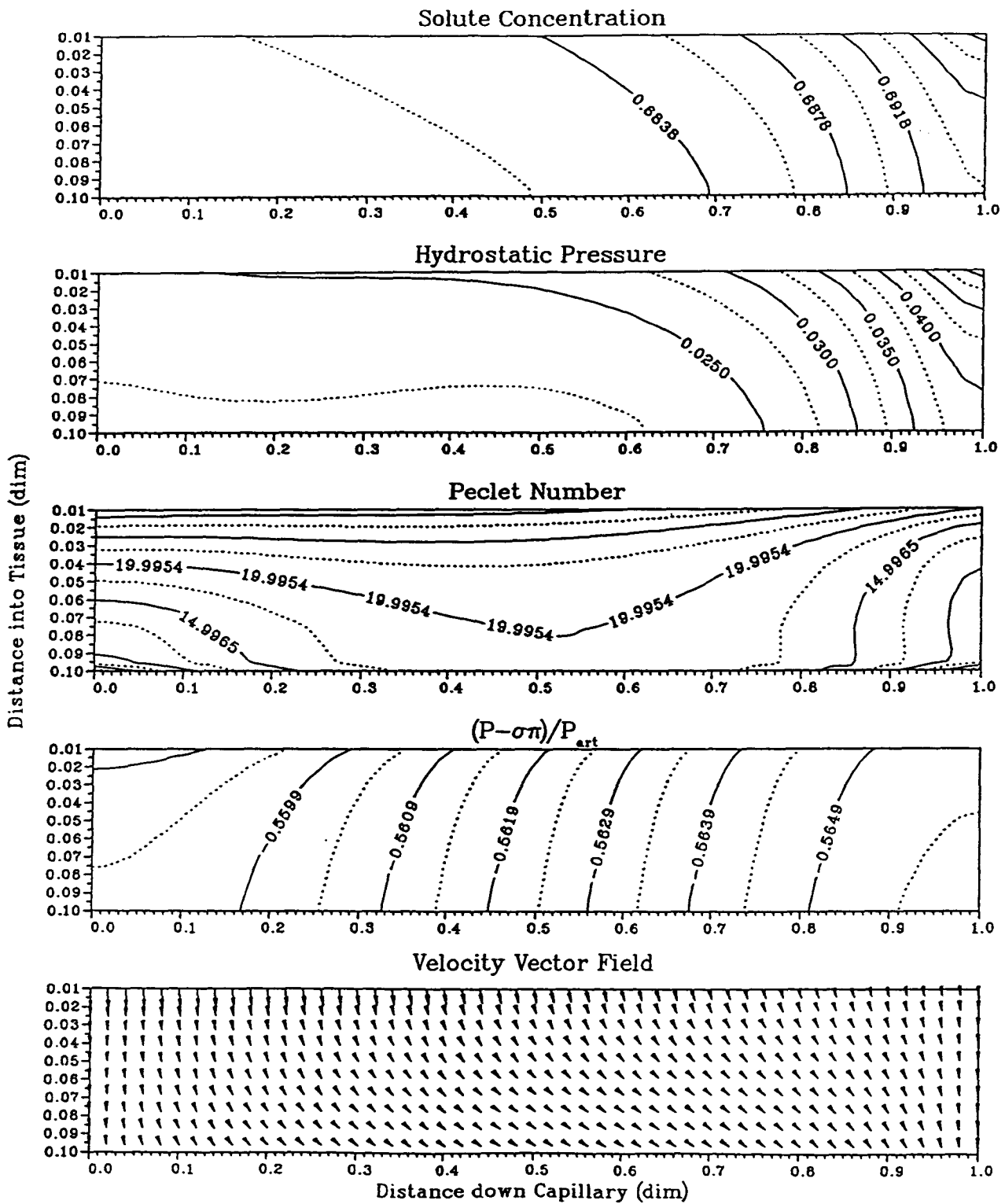


Figure 4.16: Dimensionless tissue solute concentrations, hydrostatic pressure, Peclet number, potential, and velocity vector distributions for the case with the inclusion of mechanical dispersion at steady-state.

increases as a result of the increased solute concentration to 7.70 l/day. The potential distribution is shifted in the negative direction due to the greater osmotic pressures throughout the tissue. The velocity field, although similar to the base case, has greater transcapillary velocities than the base case in response to the enlarged lymph drainage. The Peclet number distributions are difficult to compare since the effective diffusion-dispersion coefficient is a function of the local fluid velocities and is therefore a function of position. It is apparent, however, that convection plays a reduced role in solute transport from the Peclet number distribution. This is especially so at the arteriolar end of the tissue near the capillary where the highest fluid velocities are found.

4.5.3 Variable Capillary Membrane Filtration Coefficient, $L_p(z)$

In this section, the capillary membrane filtration coefficient is considered to be a known function of the length down the capillary. It is known that the capillary fluid conductance increases towards the venular end of the capillary network. This allows for more fluid and solute interchange between the circulation and the interstitial space at locations where the filtration coefficient is high.

As a first approximation, a linear function is assumed between values specified at the arteriolar and venular ends of the capillary. The value at the arteriolar end is chosen to be the base value given in Table (4.1). The value at the venular end is taken to be twice the base value. This value is arbitrary but indicates general trends for linearly increasing capillary filtration coefficient. Since L_p increases towards the venular end of the capillary, the fluid flow resistance decreases along the capillary length.

The linear function for L_p leads primarily to greater fluid velocities across the capillary membrane along its length. The results are presented in Figure (4.17). This promotes more lymph drainage in the system (5.64 l/day). The increased fluid velocities

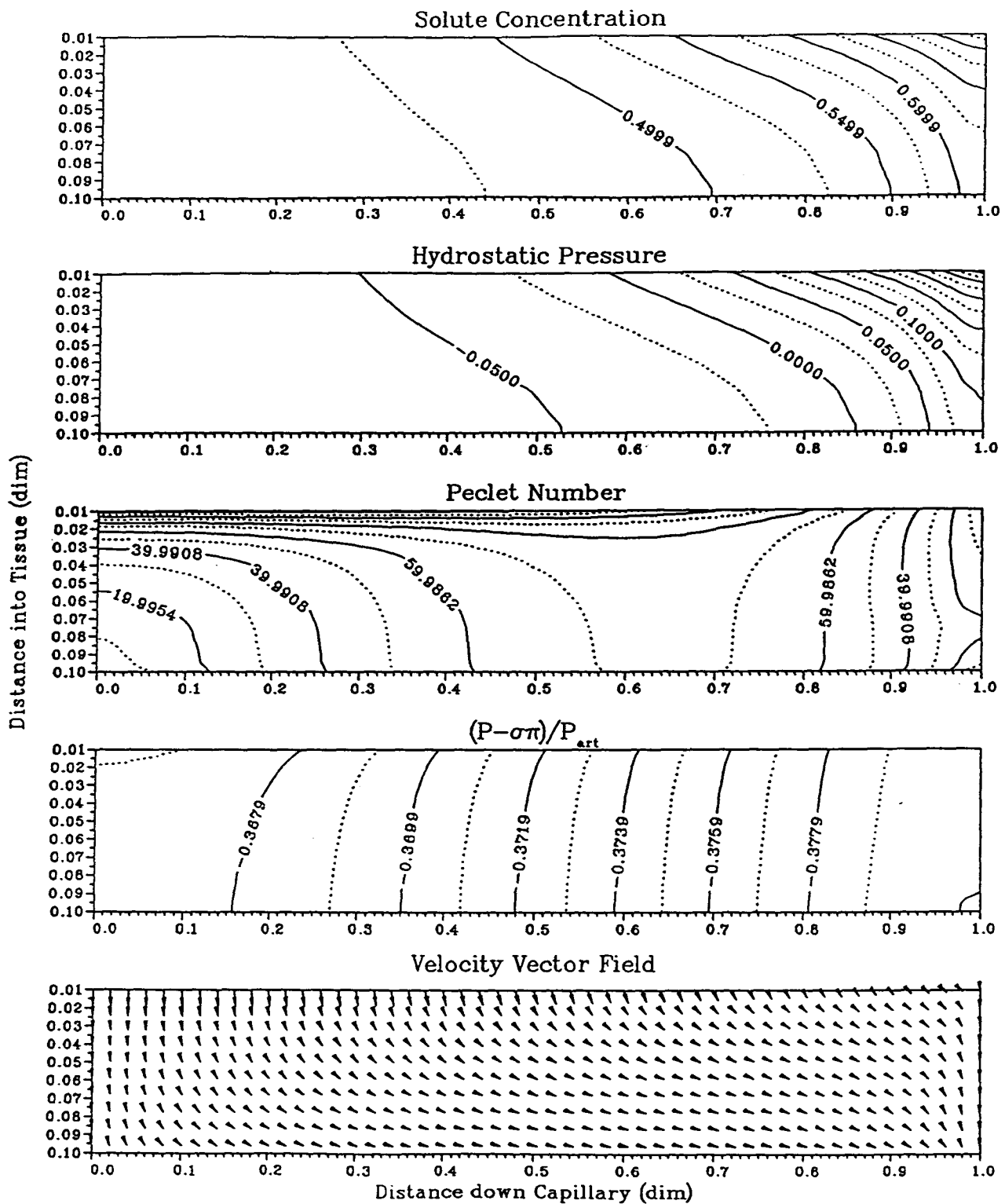


Figure 4.17: Dimensionless tissue solute concentrations, hydrostatic pressure, Peclet number, potential, and velocity vector distributions for the case with the capillary membrane filtration coefficient, L_p , varied linearly from the base value at the arteriolar end to twice the base value at the venular end of the capillary at steady-state.

are localized to near the capillary and the central portions of the tissue. At the extreme arteriolar and central portions of the tissue near the lymphatic sink, the flow velocities are largely unchanged. Although the increased flows through the capillary wall lead to higher transport of seived solutes through the membrane, the increased lymph drainage removes solute from the system. The net effect is a lowering of solute concentrations in the tissue. This is particularly noticeable in the arteriolar end of the tissue ($z^* < 0.5$) where increased solute washout drags more solute from the tissue space to the lymphatics where it is removed from the system. Although the average hydrostatic pressure increases slightly, more of the tissue is subatmospheric due to the lower solute concentrations in the tissue. The average tissue concentration and tissue hydrostatic pressure are 0.5029 and -0.0250 (-0.7500 mmHg) respectively. The dimensionless average tissue hydrostatic pressure over the region of the lymphatic sink is equal to -0.0356 (-1.068 mmHg). The average hydrostatic pressure at the sink for the base case is equal to -0.0405 (-1.2100 mmHg). The more positive value for this case explains why the lymph drainage (5.64 l/day) is greater than the base case value (5.47 l/day). As expected, the lymph flow rate for this case lies between the base case and the case $L_p \times 2$ values.

The range in the potential is largely unchanged but is shifted in the positive direction. This is due to the drop in the solute concentration distribution which leads to lower colloid osmotic pressures in the tissue.

In addition, the filtration coefficient along the capillary was also varied as a step function (at $z^* = 0.5$). It was found that the discontinuity occurring at the step caused considerable numerical difficulties. The following functional form solved this problem :

$$L_p(z^*) = L_{p,art} + \frac{(L_{p,ven} - L_{p,art})}{1 + e^{-m(z^* - 0.5)}} \quad (4.7)$$

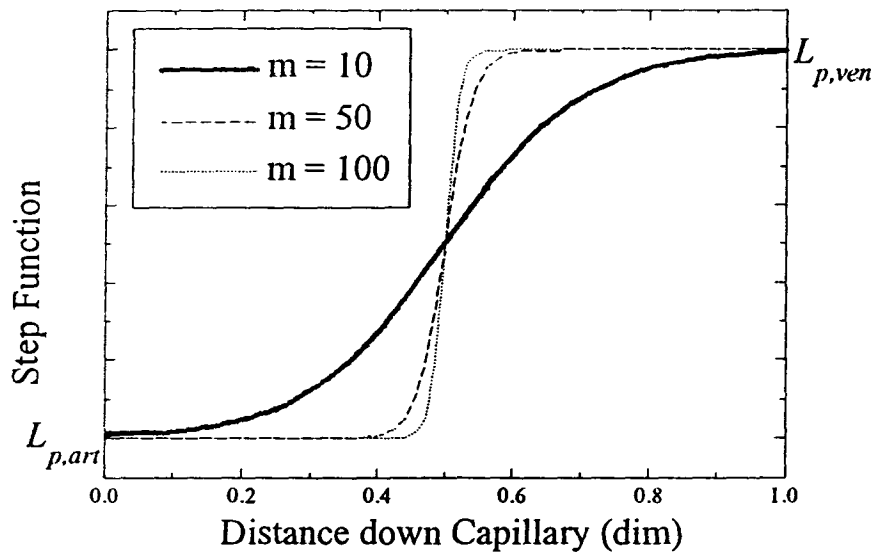


Figure 4.18: Step function for variable membrane filtration coefficient.

where m governs the quality of the step and varies typically between 10 and 100. This produces an effective step function at $z^* = 0.5$ without the discontinuity and is displayed in Figure (4.18). The arteriolar capillary filtration coefficient, $L_{p,art}$, was set to the base case value while the venular end value, $L_{p,ven}$, was set to twice the base case value. The value of the parameter m was set to 50.

The results, shown in Figure (4.19), were found to be very similar to those found for the linear case described earlier. Here, the sudden increase in the filtration coefficient resulted in a region of lower solute concentrations in the region $z^* = 0.53$ to $z^* = 0.64$. This is because of the washout of solute occurring here due to the higher fluid velocities across the membrane. The cushioned step function that exists between $z^* = 0.47$ and $z^* = 0.53$ produces a local maximum in the solute concentration at roughly $z^* = 0.50$. As can be seen in the velocity vector plot, this corresponds to a minimum in the transcapillary fluid velocity across the membrane. Thus the minimal amount of washout of the solute from the membrane occurs here. The reduction of the membrane flow resistance leads to increased fluid flow across the capillary wall after $z^* = 0.53$. This promotes more washout of solute

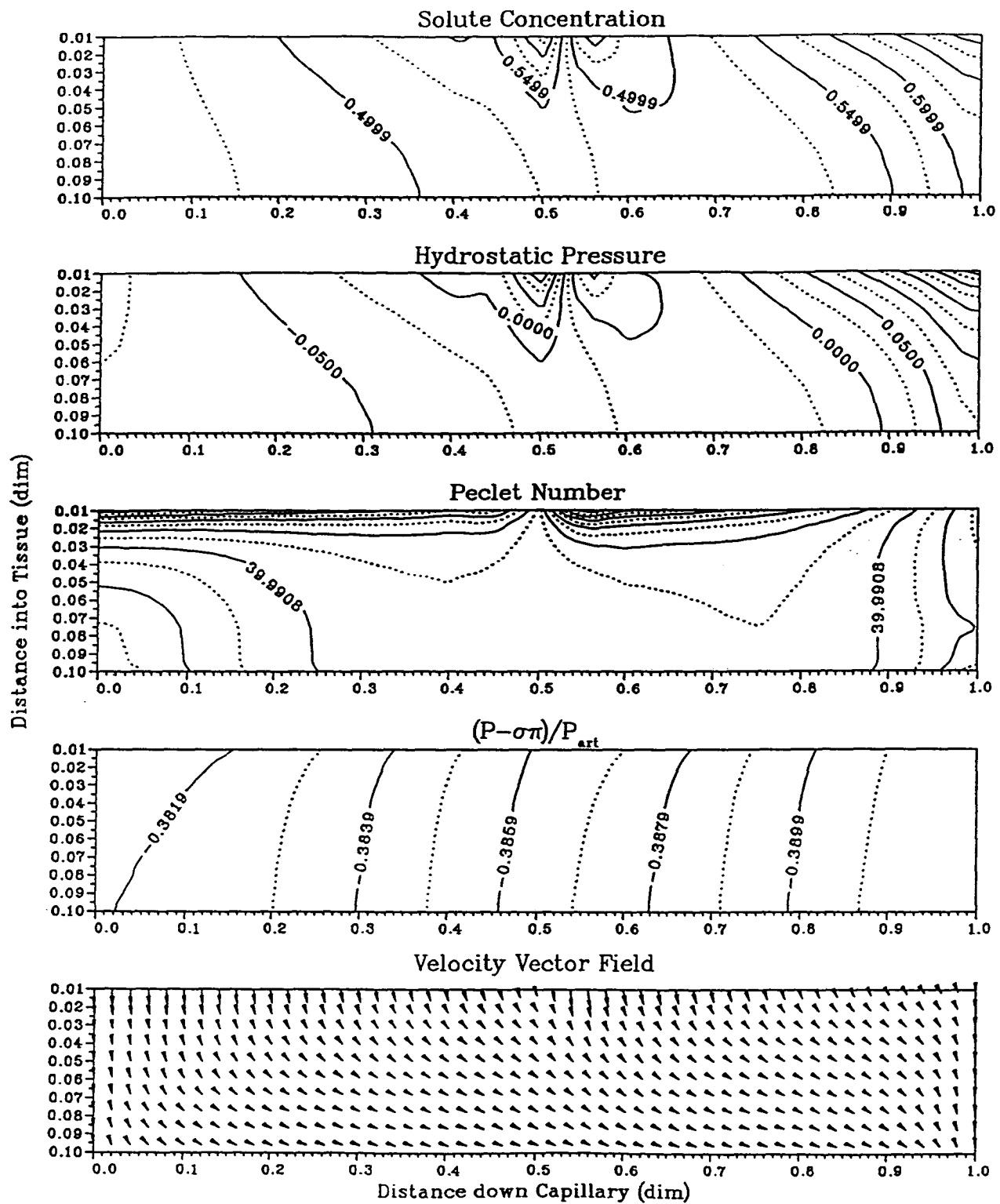


Figure 4.19: Dimensionless tissue solute concentrations, hydrostatic pressure, Peclet number, potential, and velocity vector distributions with a step change in the capillary membrane filtration coefficient, L_p , at $z^* = 0.50$ from the base value at the arteriolar end to twice the base value at the venular end of the capillary at steady-state.

from the capillary membrane and a minimum in the solute concentration at this point. This can be seen as a local solute concentration minimum at $z^* \cong 0.56$. In the region $z^* > 0.53$, the transcapillary fluid velocities decrease further down the capillary length resulting in less solute washout from the capillary. This produces a maximum in the solute concentration at the venular end of the capillary.

The lymph drainage rises to 5.71 l/day. The hydrostatic pressure distribution is, as expected, similar to the solute concentration distribution. At $z^* = 0.50$, there is a local maximum in the hydrostatic pressure. At $z^* = 0.53$, just after the step change in the filtration coefficient, there is a minimum in the hydrostatic pressure. These correspond to the maximum and minimum found in the solute concentration distribution. The average tissue solute concentration and hydrostatic pressure are 0.5161 and -0.0256 (-0.7680 mmHg) respectively. As with the case above, the increased lymph drainage rate is due to the relatively more positive dimensionless hydrostatic pressures in the lymphatic sink region (-0.0334) when compared to that of the base case (-0.0405). The increased flow velocities after the step change in L_p are reflected in the Peclet number distribution. The potential distribution rises due to the drop in the solute concentration distribution.

4.5.4 High Flow Channels

The high flow channels are implemented within the tissue as an increase of the tissue hydraulic conductivities in specified regions of the tissue space. This means that the fluid flow resistance is reduced in these regions. The spatial heterogeneity of the hydraulic conductivity requires that the fluid-pressure equation (3.6) be expanded as :

$$\begin{aligned}
& K_r \frac{\partial^2 (P_i - \sigma_i \pi_i)}{\partial r^2} + \frac{K_r}{r} \frac{\partial (P_i - \sigma_i \pi_i)}{\partial r} + K_z \frac{\partial^2 (P_i - \sigma_i \pi_i)}{\partial z^2} + \\
& \frac{\partial K_r}{\partial r} \frac{\partial (P_i - \sigma_i \pi_i)}{\partial r} + \frac{\partial K_z}{\partial z} \frac{\partial (P_i - \sigma_i \pi_i)}{\partial z} + Q(P_i) = 0
\end{aligned} \tag{4.8}$$

The two new terms thus created contain the gradients in the hydraulic conductivities and can be treated in the same way as the convective terms in the solute transport equation. When the hydraulic conductivity is constant throughout the tissue, these two extra terms reduce to zero.

Two different physical situations were simulated. The first had the high flow channel perpendicular to the capillary membrane centred at $z^* = 0.5$. The dimensionless thickness of the single high flow channel is approximately 0.10 or 10% of the length of the capillary. This may be visualized as a cylindrical fin (of higher flow conductivity) about the capillary. The second case is similar with two channels centred at $z^* = 0.3$ and $z^* = 0.7$. Each of the high flow channels is taken to be approximately 0.05 dimensionless length units thick or 5% of the capillary length. For both cases, the hydraulic conductivity in the high flow channels are set to twice the base case value.

As seen from earlier results, the primary location of the fluid flow resistance is the capillary membrane. The tissue hydraulic resistance is small compared to that across the capillary wall. This leads to the high potential drop across the membrane relative to that across the tissue. To accommodate higher velocities across the capillary membrane, the filtration coefficient was doubled where the high flow channel met the capillary membrane. The tissue hydraulic conductivity was increased by a factor of two in the high flow channels. This is sufficient to indicate the general trends. It is important to note that the high flow channels were not considered to be free flow channels but simply rather as regions with increased tissue conductivity. This means that the potential still acts as the driving force for fluid flow in the high flow channels. If the high flow channels are

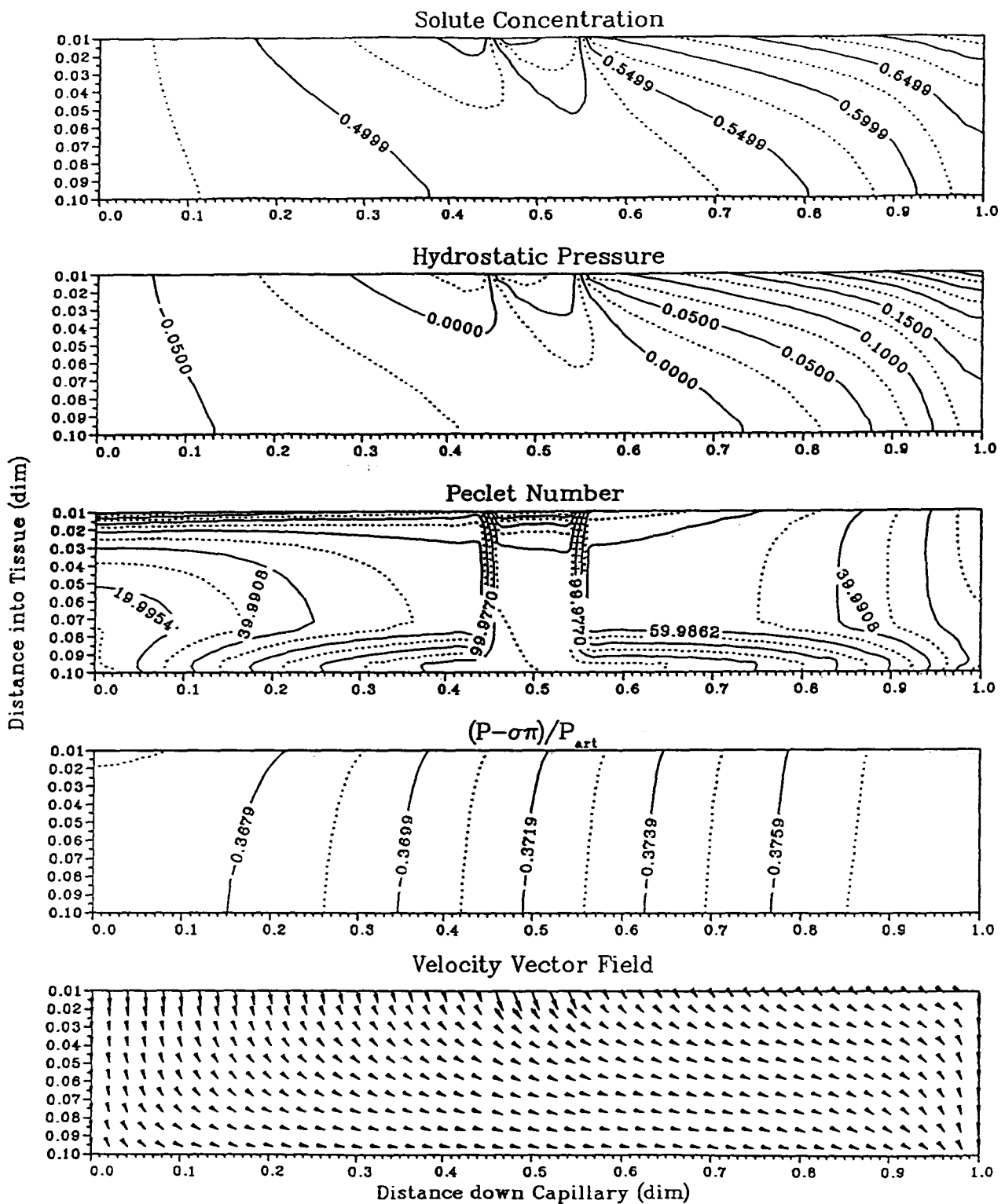


Figure 4.20: Dimensionless tissue solute concentrations, hydrostatic pressure, Peclet number, potential, and velocity vector distributions for the case with a single high flow channel centred at $z^* = 0.50$ at steady-state.

considered to be true free flow channels then the driving force for fluid motion would be the hydrostatic pressure. The lymphatic sink region is also considered to be a high flow channel. This aids in the distribution of fluid to the lymphatic sink.

As expected, the increased conductivities in the high flow regions lead to higher fluid flow velocities in the high conductivity regions. This promotes greater solute convection in these regions. With the increased flow velocities, there is greater solute washout from the capillary membrane into the tissue. This is seen in the results for the case with the single high flow region (Figure (4.20)) where the concentrations drop near the capillary membrane in the high conductivity region. The dimensionless average tissue solute concentration is equal to 0.5307. The solute leaking through the membrane is sufficient to produce a local maximum in the solute concentration in the area of $z^* \cong 0.40$ at the capillary wall. Here, fluid velocities are still limited by the base values of the capillary filtration coefficient and hydraulic conductivity. The hydrostatic pressure distribution clearly responds to the solute concentration which has a similar distribution. The dimensionless average tissue hydrostatic pressure rises to 0.0068 (0.2040 mmHg) and 0.0128 (0.3840 mmHg) for the single and double high flow channel cases respectively. The lymph flow, as expected, increases with the presence of high flow channels. The lymph flows are 6.57 and 6.78 l/day for the single and double high flow channels respectively. The potential distribution is largely unaffected by the presence of the high flow channels but does have larger radial gradients in the high flow channel as indicated by the velocity field. The magnitudes of the fluid velocities are greater in the high flow channel. This is also indicated in the Peclet number distribution where the higher Peclet numbers are in the high flow channel areas and the lymphatic sink. The results from the single high flow channel are shown in Figure (4.20).

For the case with two high flow channels, both have fluid propelled towards the lymphatic sink. The results are displayed in Figure (4.21). The trends indicated by the two channel case are very similar to that of the single channel case.

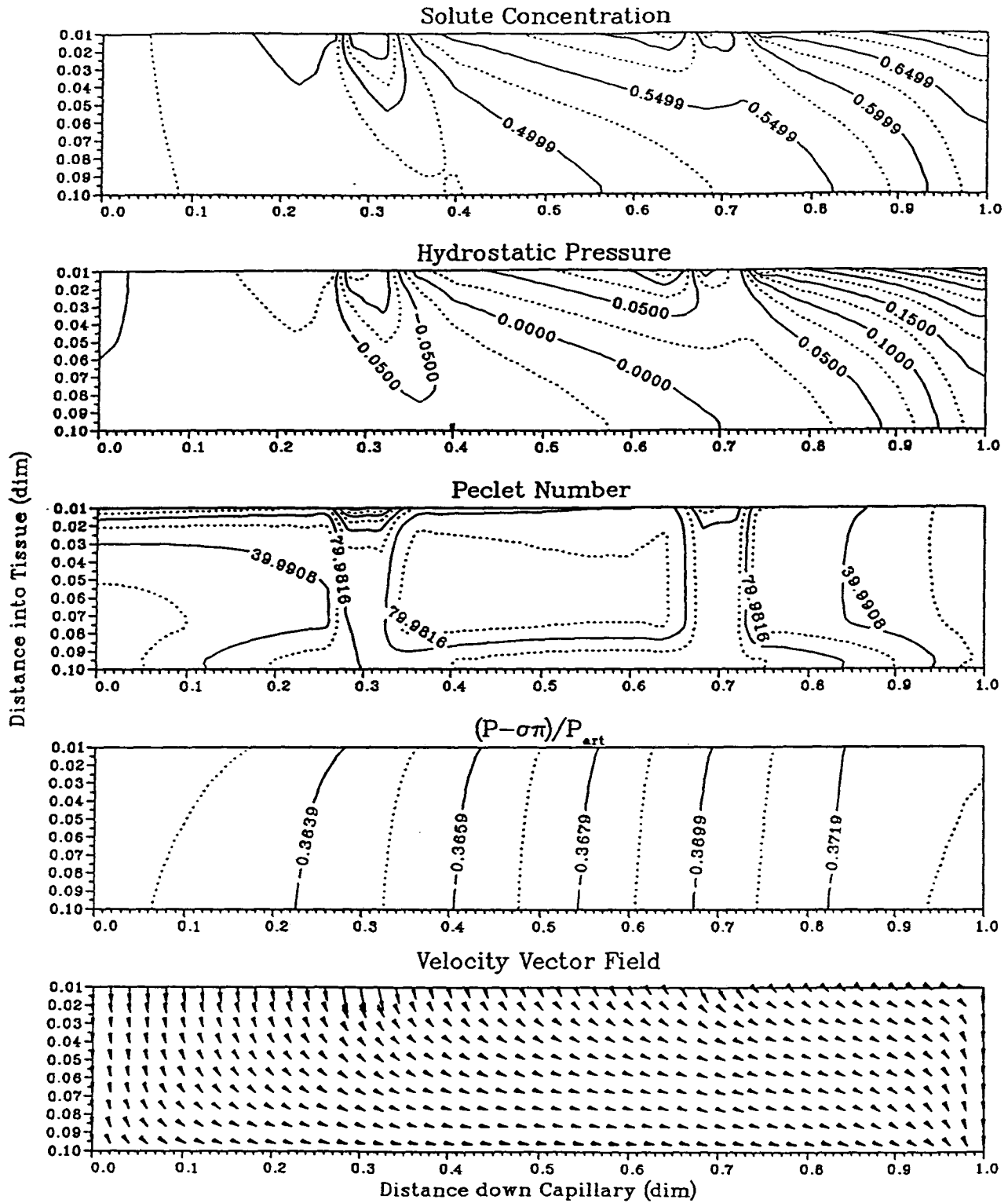


Figure 4.21: Dimensionless tissue solute concentrations, hydrostatic pressure, Peclet number, potential, and velocity vector distributions for the case with the double high flow channels centred at $z^* = 0.30$ and 0.70 at steady-state.

4.6 Conclusions

The model developed in Chapter 3 was used for steady-state analysis of fluid and solute transport in human tissue. The influence of the physiological parameters on the microvascular exchange system were examined in detail. The results from the many simulations are summarized in Table (4.3). Some conclusions based on the results above are summarized in the following.

1. The numerical simulations indicate that both convection and diffusion contribute to solute transport. Convection appears to be the dominant mode of solute transport. Solute distributions were considerably different for different values of the retardation factor and diffusion coefficient.
2. The osmotic pressure plays an important role in microvascular exchange. The differences in solute concentrations throughout the tissue yield osmotic pressure gradients which serve to reduce fluid motion. The hydrostatic pressure responds to the solute concentration distribution via the osmotic pressure. The heterogeneity of the osmotic pressure throughout the interstitium cannot be ignored and should be taken into account in any models of microvascular exchange.
3. The inclusion of the lymphatic sink provides the mechanism for negative pressures (below atmospheric) in the tissue. As the strength of the sink increases, the amount of material reabsorbed back into the capillary is reduced and the zero point shifts towards the venular end of the capillary. With a reduced sink strength, the amount of reabsorption increases. At the limit when the sink strength is equal to zero, the amount of fluid filtered into the tissue equals that being reabsorbed.

4. Dispersion plays a secondary role as a solute transport mechanism. It acts to increase the effective diffusion coefficient, thus lowering solute concentration gradients. The nature of dispersion in the interstitial space is not well understood but has been described by two parameters, the longitudinal and transverse dispersivities which are dependent on the porous medium grain size and fluid properties. It is unknown at what scale the representative grain size should be chosen.
5. Fluid pressure, solute concentration, and potential distributions are determined largely by transport properties of the capillary membrane. The range in the potential has been shown to be due to the relative fluid flow resistance of the capillary membrane to that of the tissue. The primary fluid flow resistance is located in the capillary membrane.
6. An increasing capillary membrane filtration coefficient along the length of the capillary induces greater fluid flow across the capillary membrane due to lower membrane flow resistance. This leads to increased lymph drainage and thus lower solute concentrations within the tissue. The hydrostatic pressure drops in response to the solute concentration distribution.
7. The many results indicate that the microvascular exchange system produces complex fluid flow and solute distributions which are highly reliant on the values of the physiological parameters.

Table 4.3 : Results from Various Cases.

No.	Case	Average c_f	Average P_f	Average c_f	Lymph Flow (l/day)
1	base	0.5258	-0.0255	0.5134	5.47
2	nows	0.7462	-0.1014	0.7460	3.37
3	$LS \times 0.2$	0.5653	0.0924	0.5555	1.91
6	$LS \times 5$	0.5065	-0.0575	0.4911	21.42
5	$\sigma = 0.1$	0.7150	0.0428	0.7139	8.25
6	$\sigma = 0.5$	0.5990	-0.0002	0.5922	6.51
7	$\sigma = 0.99$	0.5056	-0.0328	0.4914	5.17
8	$\xi = 0.1$	0.7132	0.0406	0.7123	8.19
9	$\xi = 0.5$	0.6137	-0.0002	0.6088	6.60
10	$PS = 0.0$	0.5258	-0.0255	0.5134	5.47
11	$PS \times 100$	0.5265	-0.0252	0.5141	5.48
14	$PS \times 10000$	0.7355	0.0521	0.7349	8.60
15	$\sigma_f = 0.0$	0.5492	-0.1162	0.5460	2.87
16	$\sigma_f = 0.5$	0.5346	-0.0710	0.5265	4.25
15	$D_{diff} \times 0.1$	0.4120	-0.1185	0.3854	2.75
16	$D_{diff} \times 10$	0.7151	0.0408	0.7148	8.23
17	disp	0.6842	0.0258	0.6836	7.70
18	$K \times 0.1$	0.5403	-0.0268	0.5327	5.27
19	$K \times 10$	0.5232	-0.0253	0.5100	5.51
20	$P_f = -0.40$	0.4901	-0.1800	0.4794	7.14
21	$P_f = -0.30$	0.5078	-0.1029	0.4961	6.30
22	$L_n \times 0.5$	0.6053	-0.0262	0.5992	5.37
23	$L_n \times 2$	0.4311	-0.0205	0.4081	5.76
24	L_n to $2L_n$ (linear)	0.5029	-0.0250	0.4940	5.64
25	L_n to $2L_n$ (step)	0.5161	-0.0256	0.5097	5.71
26	K1	0.5307	0.0068	0.5186	6.57
27	K2	0.5116	-0.0128	0.4998	6.78
28	ms3	0.5006	-0.0761	0.5251	18.38
29	ms6	0.5167	-0.0322	0.5163	9.69

Chapter 5 : Capillary - Tissue Fluid Balance and the Effects of Perturbations on Material Exchange

5.1 Introduction

The roles of the interstitial space, the lymphatic sink, and osmotic pressure have not been clearly identified in terms of the capillary-tissue fluid balance. By the capillary-tissue fluid balance, it is meant the regulation of the transcapillary fluid flows and lymph drainage. These flows affect maintenance of the interstitial space and plasma volumes.

Starling (1896) postulated that transcapillary fluid exchange is the result of differences in both the hydrostatic and osmotic pressure across the capillary membrane. The colloid osmotic pressure acts to oppose the hydrostatic pressure driving force for fluid motion. The steady-state equilibrium of the Starling forces is thus dependent on the solute concentrations within the capillary and tissue via their colloid osmotic pressure contributions. Landis (1927) experimentally confirmed Starling's hypothesis.

The thrust of the work in this area is to isolate the mechanisms of regulation of the capillary-tissue fluid balance. The microvascular exchange system is maintained in a stable state through various feedback mechanisms. This chapter makes use of the model developed in Chapter 3 to examine capillary-tissue fluid balance and its regulation. The nature of the effect the osmotic pressure, the capillary membrane, and the lymphatic sink has on controlling and maintaining fluid balance will be discussed.

The first section (5.2) will investigate fluid flow through the capillary membrane. The driving forces for fluid movement through the capillary wall will be identified and displayed for the base case and the case where the lymphatic sink conductivity, LS , has been reduced by a factor of five ($LS \times 0.2$). These two cases were also examined in Chapter 4. The second section, (5.3), will describe some transient cases that were performed in order to examine the effect on fluid balance. The final section will briefly list some conclusions based on the findings.

5.2 Transcapillary Fluid Flow

Starling's hypothesis relates the amount of fluid flowing across the capillary membrane to the driving forces and the membrane fluid conductivity. This is given by (Taylor and Townsley, 1987) :

$$v_{f,n} = L_p [P_c - P_t - \sigma(\pi_c - \pi_t)] \quad (5.1)$$

where L_p is the capillary membrane filtration coefficient, P_c and P_t are the capillary and tissue hydrostatic pressure respectively, and π_c and π_t are the capillary and tissue osmotic pressure respectively. The reflection coefficient, σ , is given by :

$$\sigma = \frac{\Delta\pi_{effective}}{\Delta\pi_{theoretical}} = \frac{\Delta\pi_{effective}}{\pi_c - \pi_t} \quad (5.2)$$

The reflection coefficient relates the value of the theoretical (measured) osmotic pressure gradient to the effective gradient operating across the membrane. If the reflection coefficient

is equal to 1, the the driving force for fluid motion across the membrane is the transcapillary potential given by :

$$\Delta T = (P_c - \pi_c) - (P_t - \pi_t) \quad (5.3)$$

This means that there is no leakage of solute across the membrane, in other words, it is 100 percent reflected from the membrane. The actual measured osmotic pressure then acts to oppose fluid motion. If there is leakage of solute across the membrane, then the osmotic gradient across the membrane is lowered. Therefore, only some fraction, σ , of the measured osmotic pressure gradient will operate across the membrane opposing fluid motion. This leads to the effective operating osmotic pressure gradient. If the reflection coefficient is equal to zero, then solute may pass unsieved through the membrane. This means there would be no osmotic pressure gradient across the membrane and the hydrostatic pressure would be the only driving force for fluid motion. Typically, in human capillaries, σ ranges between 0.75 and 0.95 (Renkin, 1977). There are some cases where the reflection coefficient is nearly zero (the liver sinusoids) and those where it is nearly 1 (the blood-brain barrier) (Ganong, 1989).

The driving force for fluid motion in the tissue is the potential given by :

$$T_t = P_t - \sigma_t \pi_t \quad (5.4)$$

where P_t and π_t are the tissue hydrostatic and colloid osmotic pressure respectively. The tissue reflection coefficient, σ_t , relates the fact that the tissue porous medium may be considered as a stack of membranes. In this sense, solute transport will be hindered in certain regions by the fibrous meshwork of biopolymers causing osmotic pressure gradients throughout the tissue. The solute can still leak throughout the tissue by the various transport mechanism, diffusion, dispersion, and convection. This means that a fraction, σ_t , of the

measured osmotic pressure gradient (the effective osmotic pressure gradient) will operate to oppose fluid motion.

In past analyses, the driving force for fluid motion in the tissue has been the hydrostatic pressure only (Taylor and Townsley, 1987). The results from Taylor (1990) and this work (see Chapter 4) have demonstrated that the colloid osmotic pressure is sufficiently large and spatially variable that it must be included in any analysis of microvascular exchange. It plays a significant role in material exchange throughout the tissue. Taylor and Townsley (1987) have used a simplistic Starling force analysis of flow across the capillary wall. This is displayed in Figure (5.1). Here the tissue hydrostatic pressure drops along the length of the membrane and the colloid osmotic pressure is considered nearly constant along the capillary. The transcapillary potential difference is seen to be constant and positive (fluid filtration) down the length of the capillary. From their analysis, they conclude that fluid reabsorption is a transient phenomenon which will not occur at steady-state. In this work, it has been found that the hydrostatic pressure increases along the length of the capillary in response to the solute profile (via the osmotic pressure) along the membrane. The solute concentrations increase along the capillary membrane due to the lower washout that occurs at the venular end of the tissue. The transcapillary potential difference does not remain constant but is maximal at the arteriolar end of the capillary and decreases along the capillary. The tissue-side potential decreases along the capillary. The hydrostatic pressures, osmotic pressures, and transcapillary potential difference are displayed in Figures (5.2) and (5.3) for the base and $LS \times 0.2$ cases.

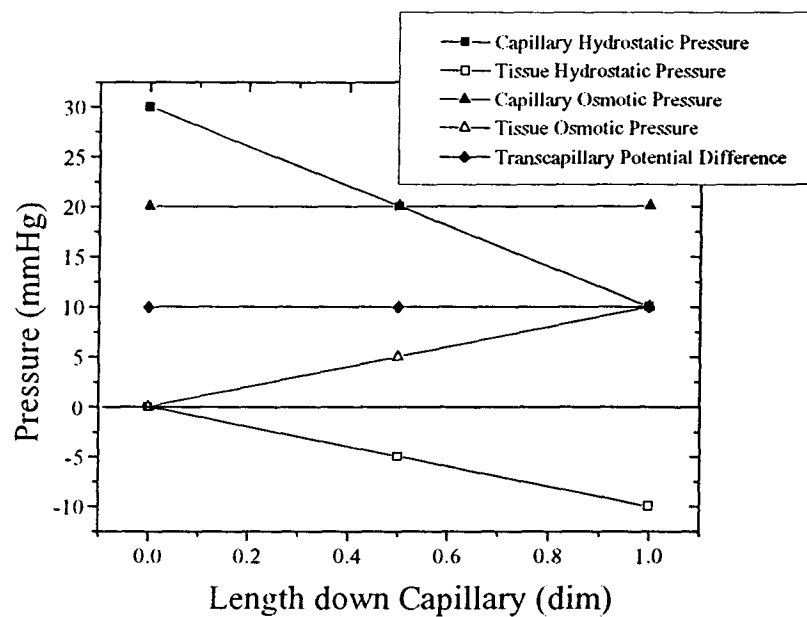


Figure 5.1: Starling forces across capillary wall. Taken from Taylor and Townsley (1987).

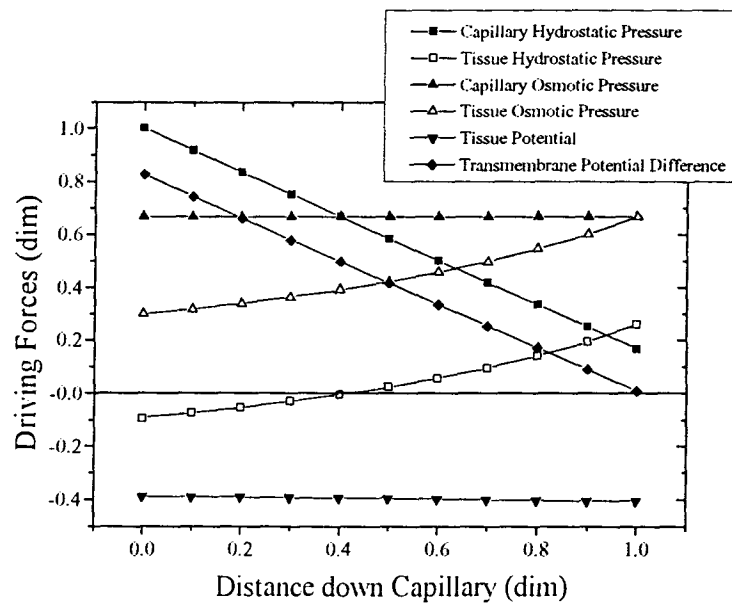


Figure 5.2: Transcapillary fluid motion : Driving forces for base case.

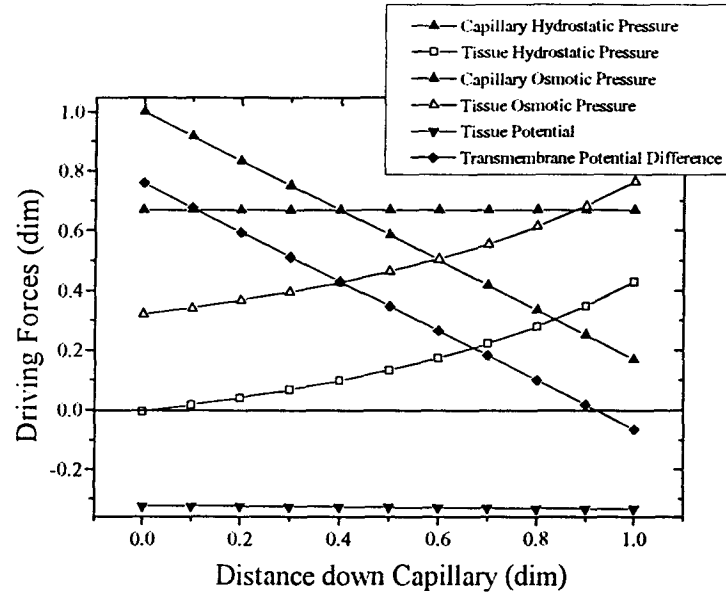


Figure 5.3: Transcapillary fluid motion : Driving forces for $LS \times 0.2$.

As can be seen from the results, the transcapillary potential difference remains positive for the base case confirming the results shown in Chapter 4 for no fluid reabsorption. The results in Figure (5.3) display clearly the fluid reabsorption occurring at the venular end of the capillary (after about $z^* = 0.92$) where the transcapillary potential difference becomes negative. Both of these results are steady-state results. The reabsorption of fluid back into the capillary for the latter case conflicts with Taylor and Townsley's suggestion that reabsorption occurs only transiently until the tissue forces equilibrate. The amount of fluid that flows across the membrane, however, is very close to the lymph drainage rates. This suggests that the amount of reabsorption is expected to be far less than fluid filtration into the tissue. This agrees well with results suggested by Intaglietta and Endrich (1979).

5.3 Capillary - Tissue Fluid Balance : Mechanisms of Regulation

The roles of material exchange across the capillary membrane, lymphatic drainage, and the osmotic pressure will be examined in this section. The goal here is to identify mechanisms of control observed from transient simulations of microvascular exchange using the model formulated in Chapter 3. These controlling features of the microvascular exchange system will be investigated by implementing several perturbations to the system. The first section will deal with a sudden drop in the tissue solute concentrations and its impact on the flow structure. The second will examine the effects of an elevated venous pressure on the system. The third section will examine the effects of a sudden drop or increase in the capillary solute concentration on the system. The final section will briefly summarize the results from two cases which examine the role of the osmotic pressure on the system. This is done by perturbing the system after it has reached steady-state (the base case) with zero plasma solute concentration. Two simulations are performed. The first includes the effects of osmotic pressure throughout the system and the second does not.

5.3.1 Perturbed Tissue Solute Concentration

The tissue solute concentration generates an osmotic pressure which opposes fluid reabsorption back into the capillary. If the solute concentration is high at a particular location in the tissue adjacent to the capillary membrane, then the corresponding osmotic pressure will reduce the local tissue potential. This will promote fluid filtration from the capillary into the tissue. The effects a lowered tissue solute concentration will have on the system will be examined in this section.

This condition was implemented in the model by dropping the capillary solute concentration but maintaining the capillary osmotic pressure at its normal values found from

normal capillary solute concentrations. This will maintain the driving forces (colloid osmotic pressure) from the capillary side for fluid exchange but will lower the concentration of solute in the tissue since there is less solute effectively passing through the membrane. This is purely a contrivance to achieve the desired conditions for lowered solute concentrations in the tissue.

Figures (5.4)-(5.6) display the transient results for the case where the effective dimensionless capillary solute concentration is equal to 0.10. The colloid osmotic pressure in the capillary is maintained at the value for a dimensionless solute concentration equal to 1.0 (the base value). This is a reduction in the solute concentration by a factor of ten which will lead to lower the solute concentrations within the tissue. This condition is implemented after the system has reached the base case steady-state conditions presented in Chapter 4.

As can be seen from the results, the drop in the effective solute concentration acting across the capillary membrane results in lower tissue solute concentrations. The solute is still washed out of the regions near the capillary to the sink and builds at the sink initially (see $t = 1800$ s). After one hour the solute concentrations are beginning to equilibrate within the tissue and the solute build-up at the sink is far reduced. At the new steady-state, the tissue solute distribution is lower (average concentration is equal to 0.0620) and there is a build-up of solute near the venular capillary wall. It is important to bear in mind that the osmotic pressures in the capillary have not been changed to correspond with the effective solute concentrations transporting across the membrane.

The transient behaviour of the hydrostatic pressure is similar to the solute concentration distributions. This is because the hydrostatic pressure responds to the solute concentration via the colloid osmotic pressure. The hydrostatic pressures become negative (subatmospheric) throughout the tissue with the maximum values at the venular end of the capillary. These shift from the lymphatic sink region early in the transient response to near the capillary at steady-state. The average tissue hydrostatic pressure at the new steady-state is -0.1288 (-3.864 mmHg).

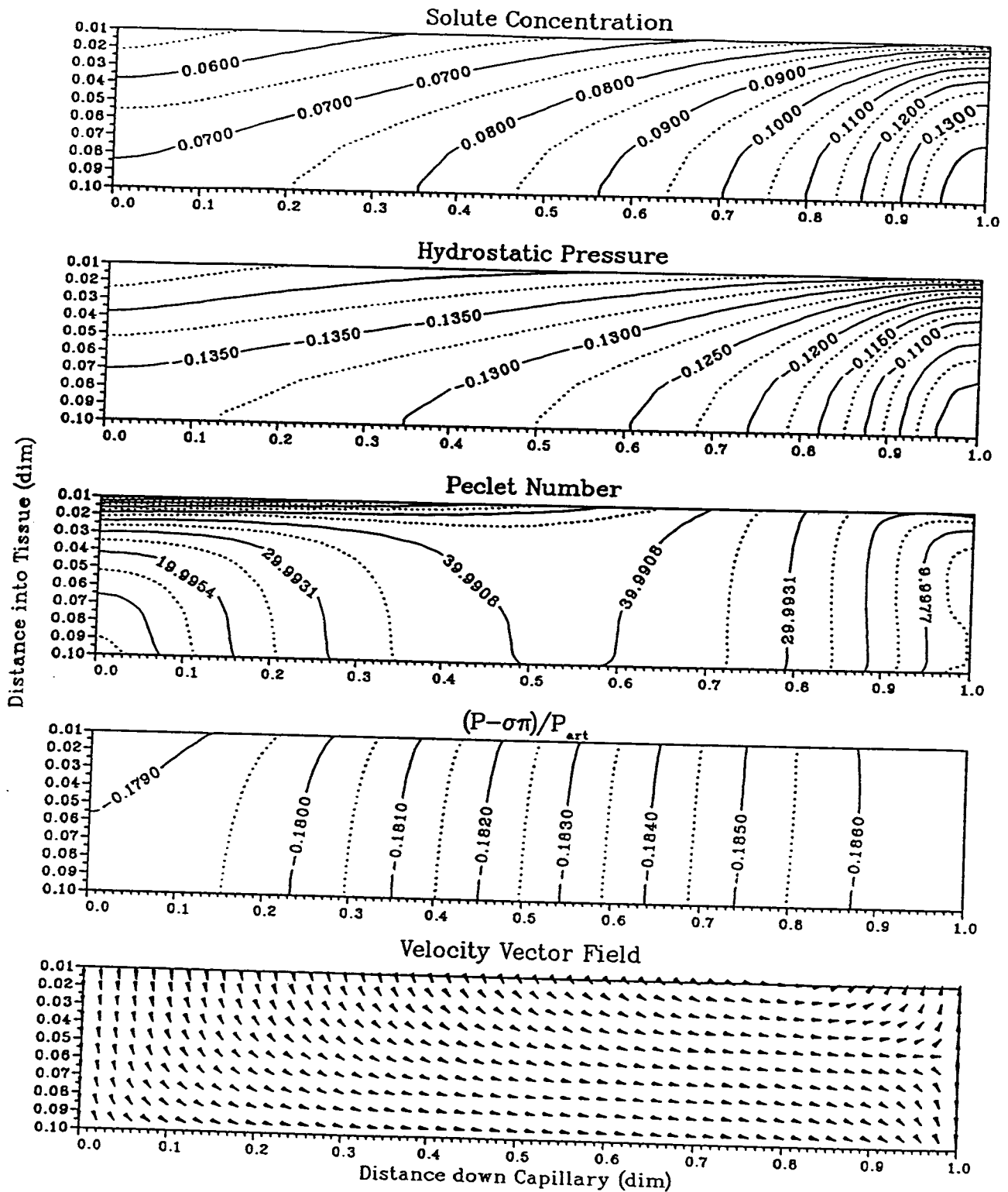


Figure 5.4: Dimensionless tissue solute concentration, hydrostatic pressure, Peclet number, potential and velocity vector distributions for the case with lowered tissue solute concentration at $t = 1800$ s.

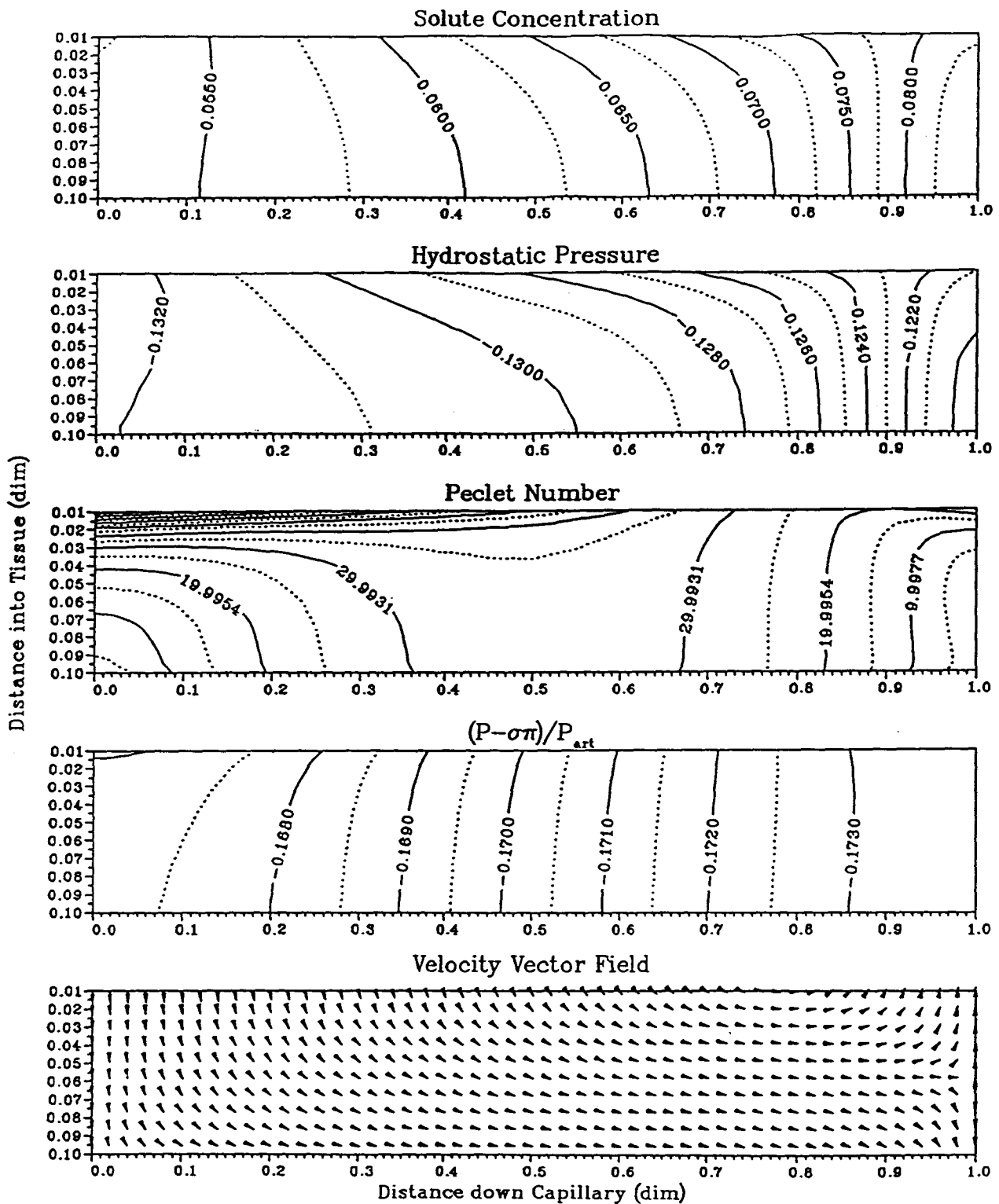


Figure 5.5: Dimensionless tissue solute concentration, hydrostatic pressure, Peclet number, potential and velocity vector distributions for the case with lowered tissue solute concentration at $t = 3600$ s.

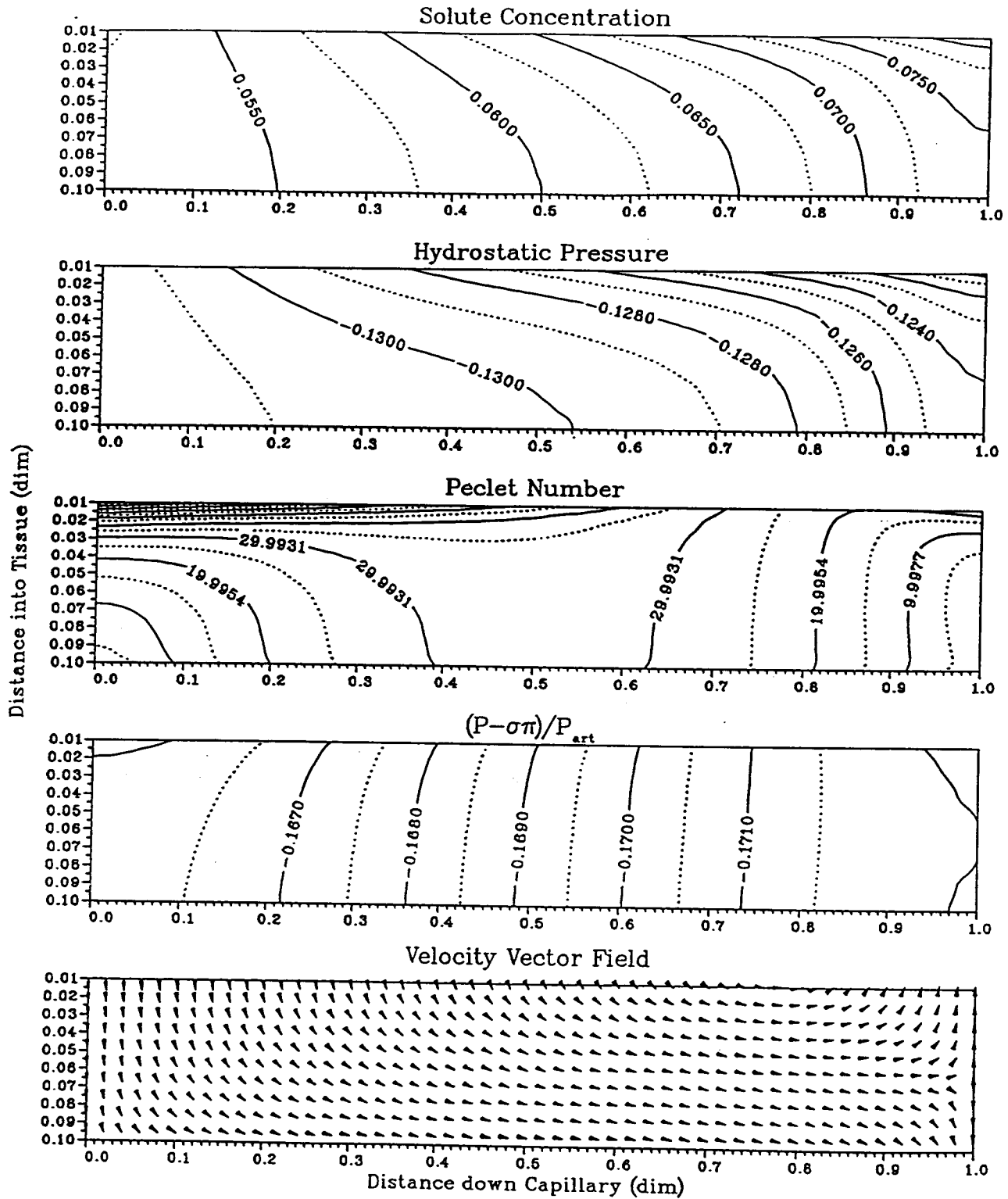


Figure 5.6: Dimensionless tissue solute concentration, hydrostatic pressure, Peclet number, potential and velocity vector distributions for the case with lowered tissue solute concentration at new steady-state.

The drop in the tissue solute concentrations lead to lower osmotic pressures throughout the tissue. This is particularly important adjacent to the capillary membrane. As can be seen in the potential distributions, the lowest potential regions shift from being entirely at the the lymphatic sink to being at the venular capillary membrane. This causes fluid reabsorption back into the capillary as can be seen in the fluid field structure. This is a direct consequence of the drop in the osmotic pressure in the tissue.

The drop in the tissue osmotic pressure causes the tissue-side potential to increase in magnitude. This then at some point exceeds the capillary potential and then fluid reabsorption occurs. As the tissue solute concentrations are further lowered transiently, the amount of reabsorption increases. This can be seen in the results as the zero point (the point on the capillary membrane where the normal fluid flow is zero) shifts up the capillary from $z^* \cong 0.82$ at 1800 s to $z^* \cong 0.79$ at the new steady-state. The increasing amount of reabsorption due to the reduction in the tissue osmotic pressures leads to lower fluid velocities across the capillary membrane. This is clearly displayed in the Peclet number distribution. The convective transport drops off into the tissue from maximum values at the arteriolar capillary membrane. There is slight increase in the region of reabsorption at the venular end of the capillary. The lymph drainage drops to 2.42 l/day at the new steady-state.

5.3.2 Perturbed Venous Hydrostatic Pressure

The venous hydrostatic pressure provides an additional controlling factor for fluid filtration and reabsorption. This can be understood if a rise in the venous pressure is considered. This will lead to a rise in the hydrostatic pressures along the capillary. Elevated venous pressures may occur because of venous obstructions or in heart failure. If the capillary solute concentration, and thus the capillary colloid osmotic pressure, is largely unchanged, then an elevated venous pressure will increase the potential to be overcome for fluid reabsorption. In fact, this would lead to increased fluid filtration and lymph drainage.

The results shown in Figure (5.7)-(5.10) are the transient results for elevated venous pressure. The venous hydrostatic pressure is increased suddenly to four times its original value. This corresponds to a venular pressure of 0.6667 (20 mmHg). Steady-state is achieved rapidly (< 2000 s) unlike the case performed in section 5.3.2 above. The initial state corresponds to the base case performed in Chapter 4.

Initially, with increased venous pressure, the fluid filtration rates across the capillary membrane increase rapidly and the tissue pressures increase. Subsequent to the perturbation, the lymph flow increases to 6.43 l/day. This leads to greater removal of solute from the tissue space and thus the solute concentration drops. This can be seen at $t = 120$ s in Figure (5.5) where the solute concentrations are dropping throughout the tissue and radial gradients have formed near the capillary wall. The maximum dimensionless hydrostatic pressures are as high as 0.1000 (3.000 mmHg) at the extreme venular end of the tissue. The dimensionless average tissue hydrostatic pressure is increased to -0.0209 (-0.6270 mmHg).

As a result of the lowered solute concentrations within the interstitium, the hydrostatic pressure begins to drop in response to the lower colloid osmotic pressures. As a consequence, the lymph drainage rates begin to fall. At $t = 240$ s, the lymph flow drops to 6.00 l/day. The fluid velocities across the capillary and within the tissue also drop. The solute concentrations and hydrostatic pressures continue to drop through time resulting in decreasing lymph flows. The new steady-state lymph flow (5.89 l/day) is higher than the initial state value (5.47 l/day).

At the new steady-state, the solute concentrations are lowered within the tissue (the dimensionless average tissue solute concentration equals 0.4997) and the range is lower than the initial state. The solute gradients appear to be more uniform throughout the tissue. The maximal gradients occur at the venular end of the tissue but they are lower than gradients in this region for the initial condition (the base case). This is because there is greater and more uniform washout of solute into the tissue along the length of the capillary. This results in the more uniform solute concentration distribution within the tissue.

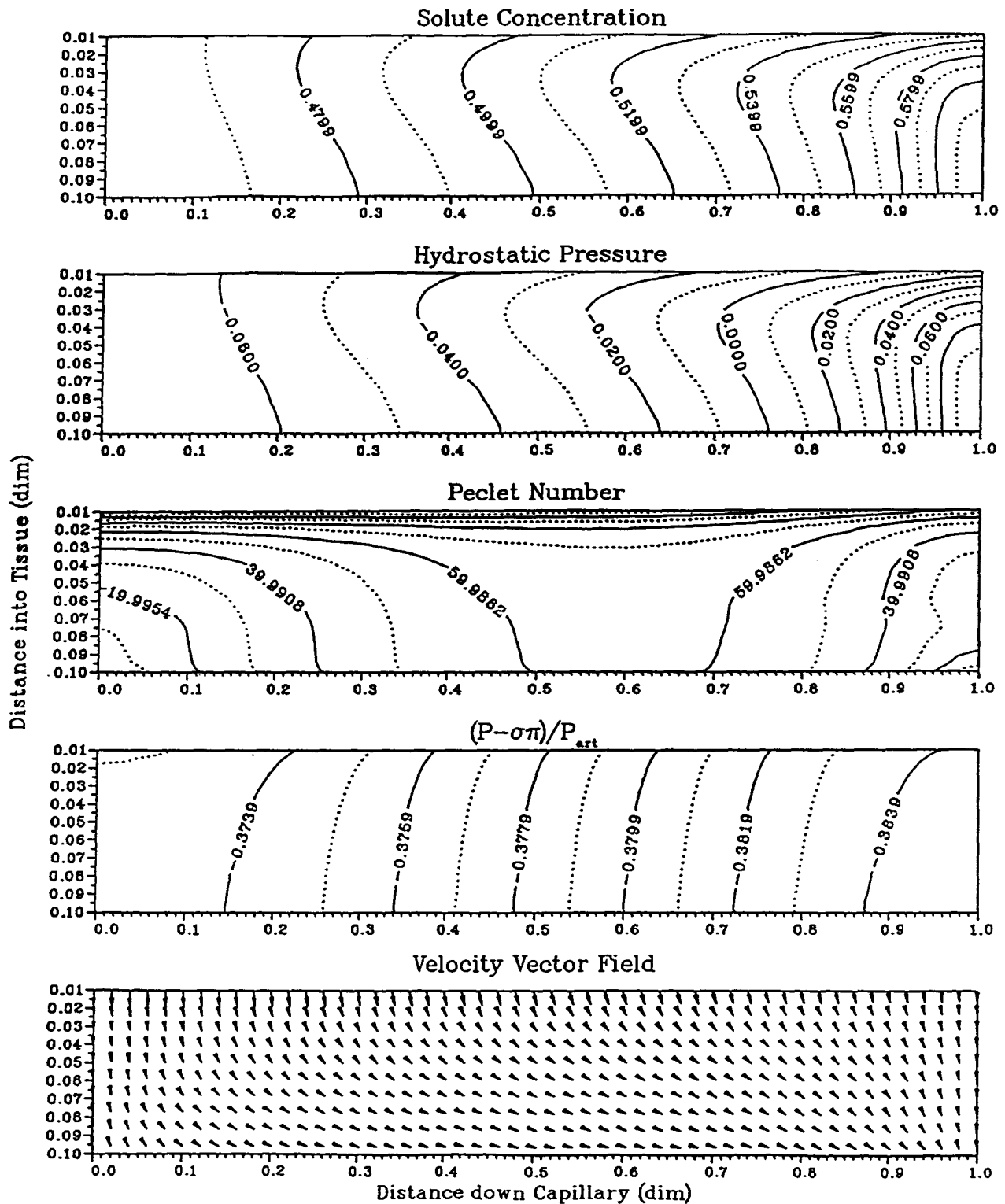


Figure 5.7: Dimensionless tissue solute concentration, hydrostatic pressure, Peclet number, potential and velocity vector distributions for the case with elevated venous hydrostatic pressure ($P_{ven}^* = 0.6667$) at $t = 120$ s.

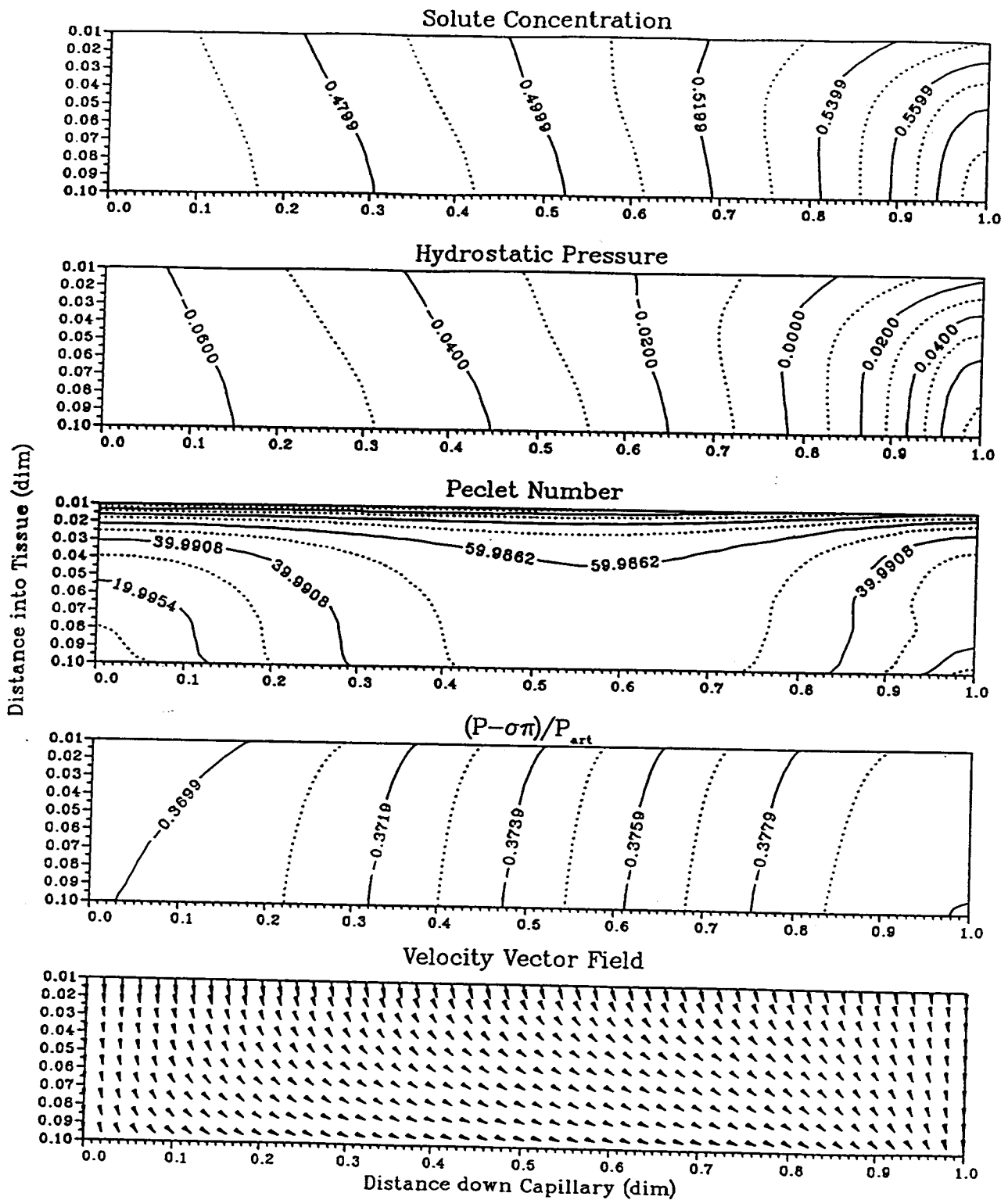


Figure 5.8: Dimensionless tissue solute concentration, hydrostatic pressure, Peclet number, potential and velocity vector distributions for the case with elevated venous hydrostatic pressure ($P_{ven}^* = 0.6667$) at $t = 240$ s.

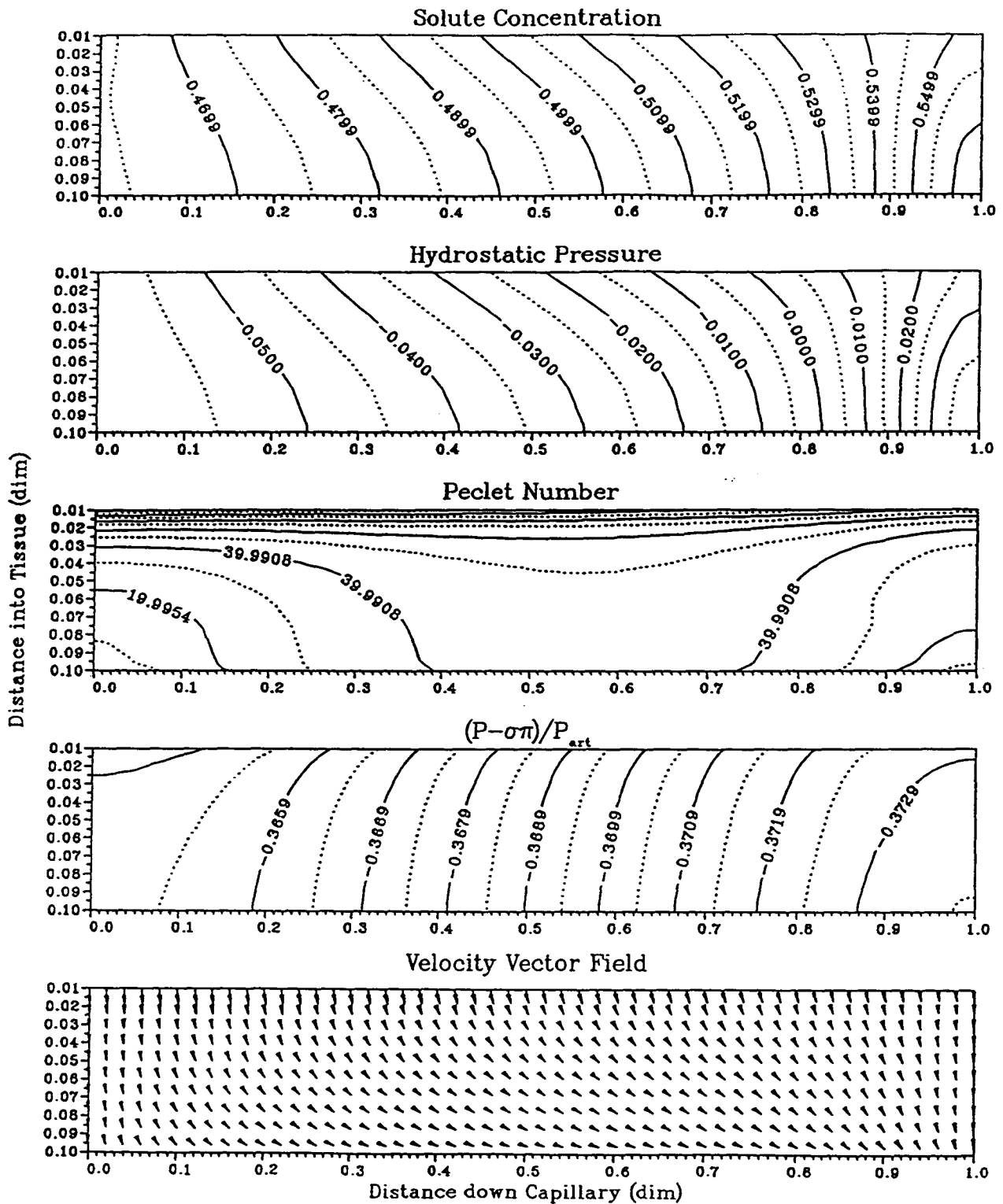


Figure 5.9: Dimensionless tissue solute concentration, hydrostatic pressure, Peclet number, potential and velocity vector distributions for the case with elevated venous hydrostatic pressure ($P_{ven}^* = 0.6667$) at $t = 600$ s.

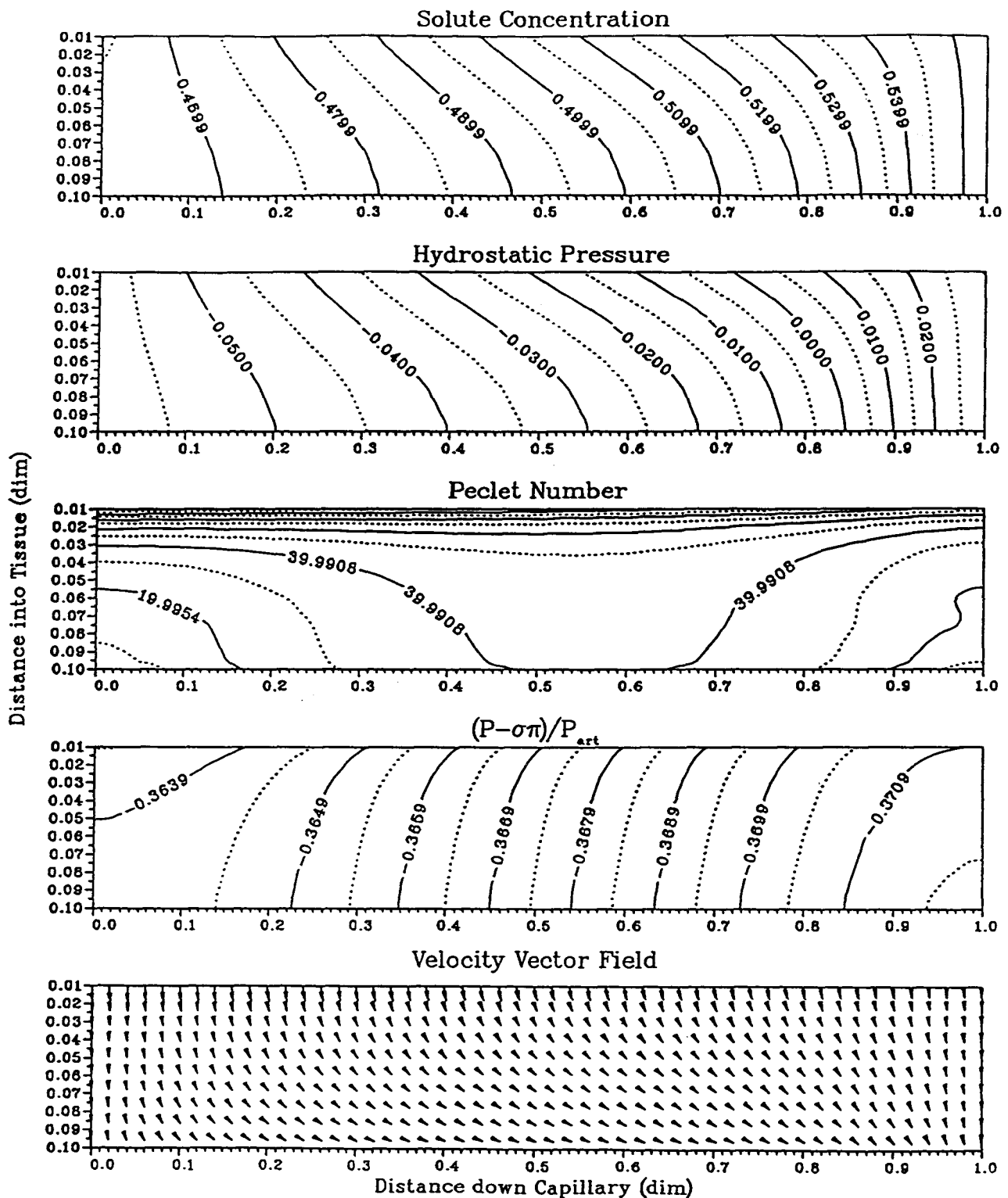


Figure 5.10: Dimensionless tissue solute concentration, hydrostatic pressure, Peclet number, potential and velocity vector distributions for the case with elevated venous hydrostatic pressure ($P_{ven}^* = 0.6667$) at steady-state.

As expected, the hydrostatic pressure distribution is very similar to the solute concentration distribution. The gradients are lower within the tissue and the range is reduced. The dimensionless average tissue hydrostatic pressure rises slightly from the initial state to -0.0251 (-0.7530 mmHg) , however, greater portions of the tissue become subatmospheric as the venous hydrostatic pressure is increased. This was not expected but can be explained by tendency of the tissue hydrostatic pressures to respond to the tissue solute concentrations. The lower, more uniform solute concentration distribution leads to a more uniform hydrostatic pressure distribution throughout the tissue. Although the average hydrostatic pressure for elevated venous pressure is higher than the initial state value, a greater portion of the tissue is subatmospheric.

The radial gradients in the potential are increased and the distribution become slightly more positive with the increase in the venous pressure . The increased radial gradients are expected since the elevated venous pressure promotes more fluid filtration at higher fluid velocities across the capillary membrane.

In summary, the results from this case illustrate that the system initially responded to the increased venous pressure by increased tissue hydrostatic pressure and associated lymph flow. This, subsequently, reduced the solute concentrations within the tissue leading transiently to lower hydrostatic pressures in the interstitium and thus lower lymph drainage. The lowered solute concentrations at the tissue-side of the capillary membrane decrease the transmembrane potential thus providing the tendency to lower fluid filtration rates across the capillary wall. These results follow trends found in experimental studies (Johnson and Richardson, 1974; Mortillaro and Taylor, 1976).

When the system had reached the new steady state, the lymph flow had reduced until it was just greater than the initial state. The system has shown that despite the large increase in the venous pressure, the solute concentration, hydrostatic pressure, and potential distributions readjust themselves to provide a modest increase in the average tissue hydrostatic pressure and lymph drainage. This safety factor mechanism against edema is

supported by the work of Johnson and Richardson (1974). It is important to bear in mind that the potential drives fluid motion throughout the system. The tissue potential distribution increases (by about 0.04) with the rise in the venous pressure. In terms of the range of the tissue potential, this is a significant amount. This further confirms that the capillary wall bears the dominant fluid flow resistance in the system. In other words, the potential drop across the capillary increases to a larger degree than the tissue potential.

5.3.3 Perturbed Capillary Solute Concentration

In this section, the results from two cases will be presented. In the first, the dimensionless capillary arteriolar solute concentration will be decreased to 0.10 (the base case value is 1.0). The corresponding capillary osmotic pressures will accordingly be reduced in response to the lower solute concentrations. In the second case, the dimensionless capillary arteriolar solute concentration will be increased to 1.2. The first case corresponds to hypoproteinemia, that is when plasma protein levels are low. This may occur because of liver disease (low hepatic protein synthesis) or nephrosis (elevated loss of protein in urine). The perturbation in the capillary solute concentration is implemented when the steady-state conditions achieved in the base case in Chapter 4 have been reached.

The transient results for the case where the blood solute concentration is dropped to 0.10 are displayed in Figures (5.11) to (5.14). As the solute concentration in the blood is reduced, the plasma colloid osmotic pressure exerted is lowered. This means that the transcapillary potential difference becomes more positive leading to greater amounts of fluid filtration. Initially this results in increased lymphatic drainage rates. In this manner, the blood volume decreases and more fluid passes through the interstitial space and out through the lymphatics. Later, the solute concentrations in the tissue begins to drop as seen at $t = 300$ s (Figure (5.11)) due to the increased lymphatic withdrawal. The maximum tissue solute concentrations occur near the lymphatic sink. The tissue hydrostatic pressure falls in

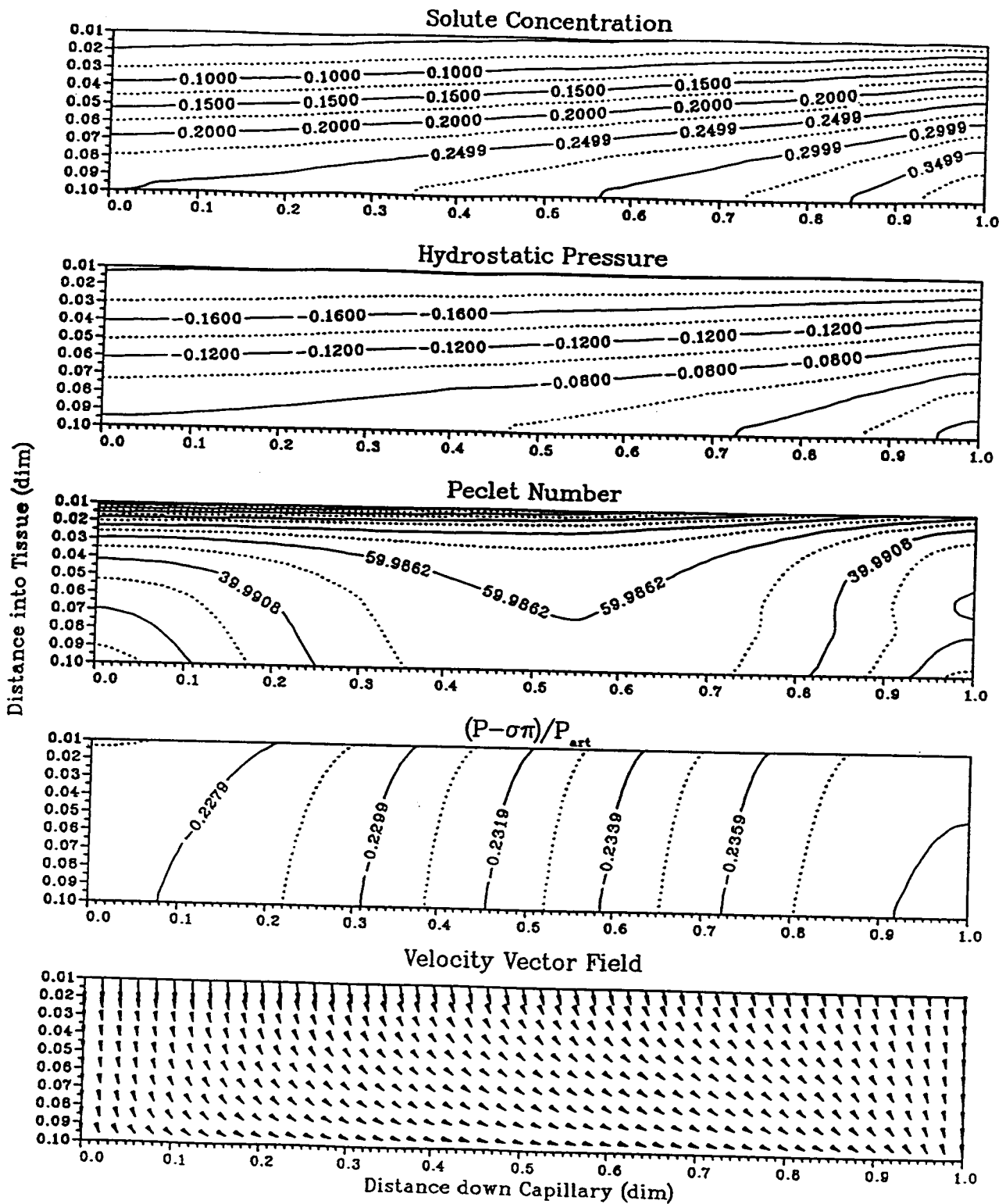


Figure 5.11: Dimensionless tissue solute concentration, hydrostatic pressure, Peclet number, potential and velocity vector distributions for the case with lowered capillary solute concentration ($c_{art}^* = 0.1000$) at $t = 300$ s.

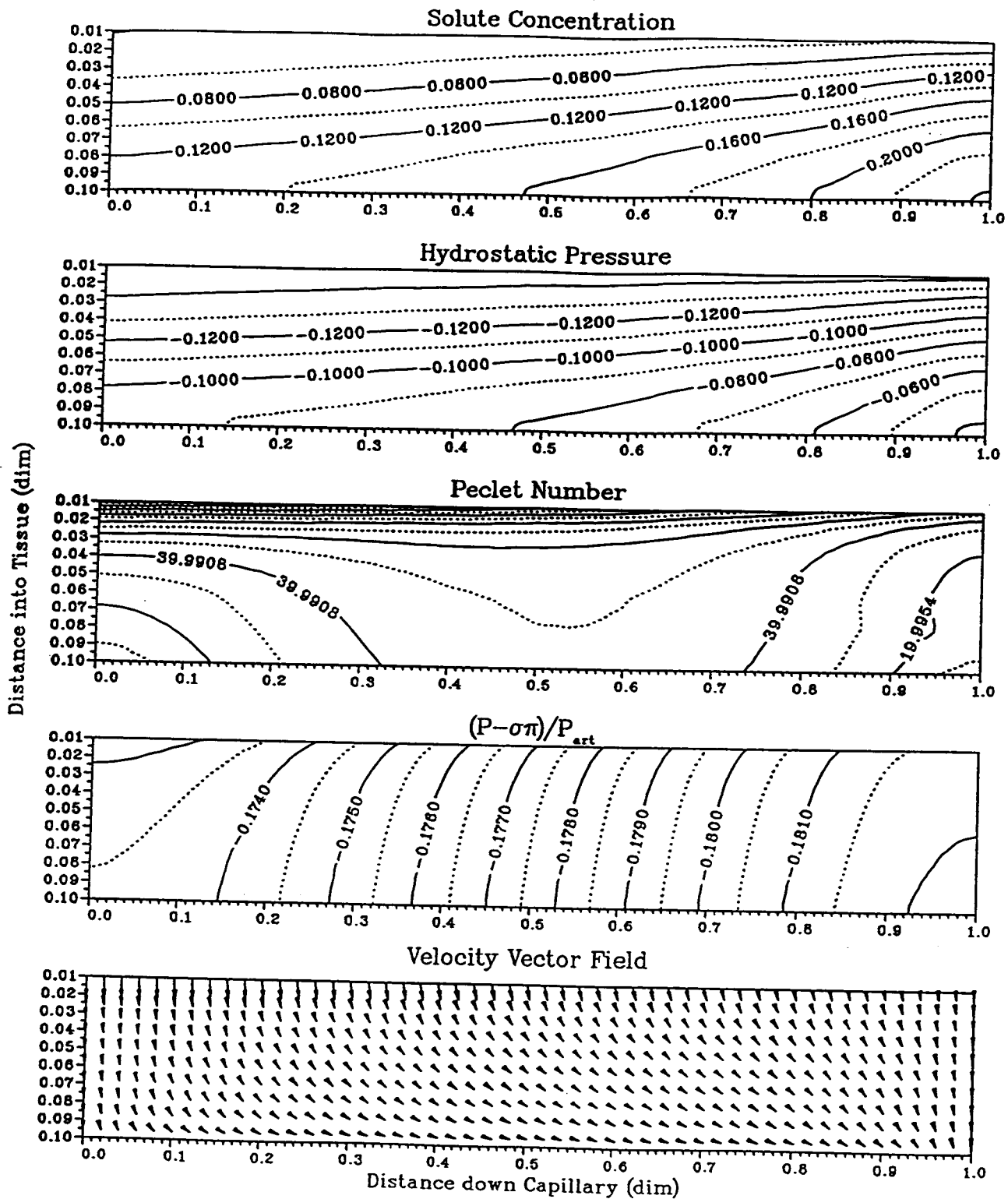


Figure 5.12: Dimensionless tissue solute concentration, hydrostatic pressure, Peclet number, potential and velocity vector distributions for the case with lowered capillary solute concentration ($c_{art}^* = 0.1000$) at $t = 600$ s.

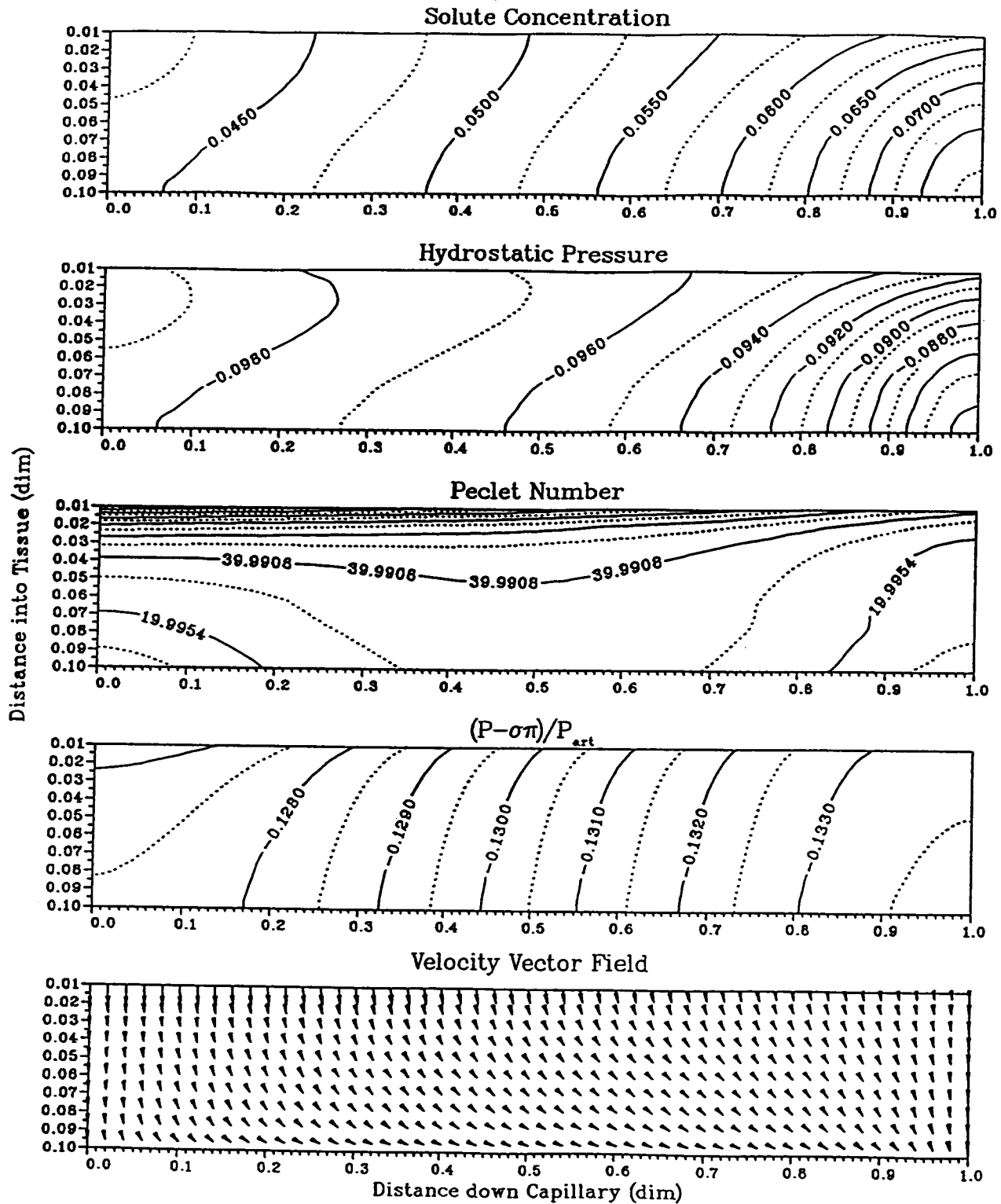


Figure 5.13: Dimensionless tissue solute concentration, hydrostatic pressure, Peclet number, potential and velocity vector distributions for the case with lowered capillary solute concentration ($c_{art}^* = 0.1000$) at $t = 1800$ s.

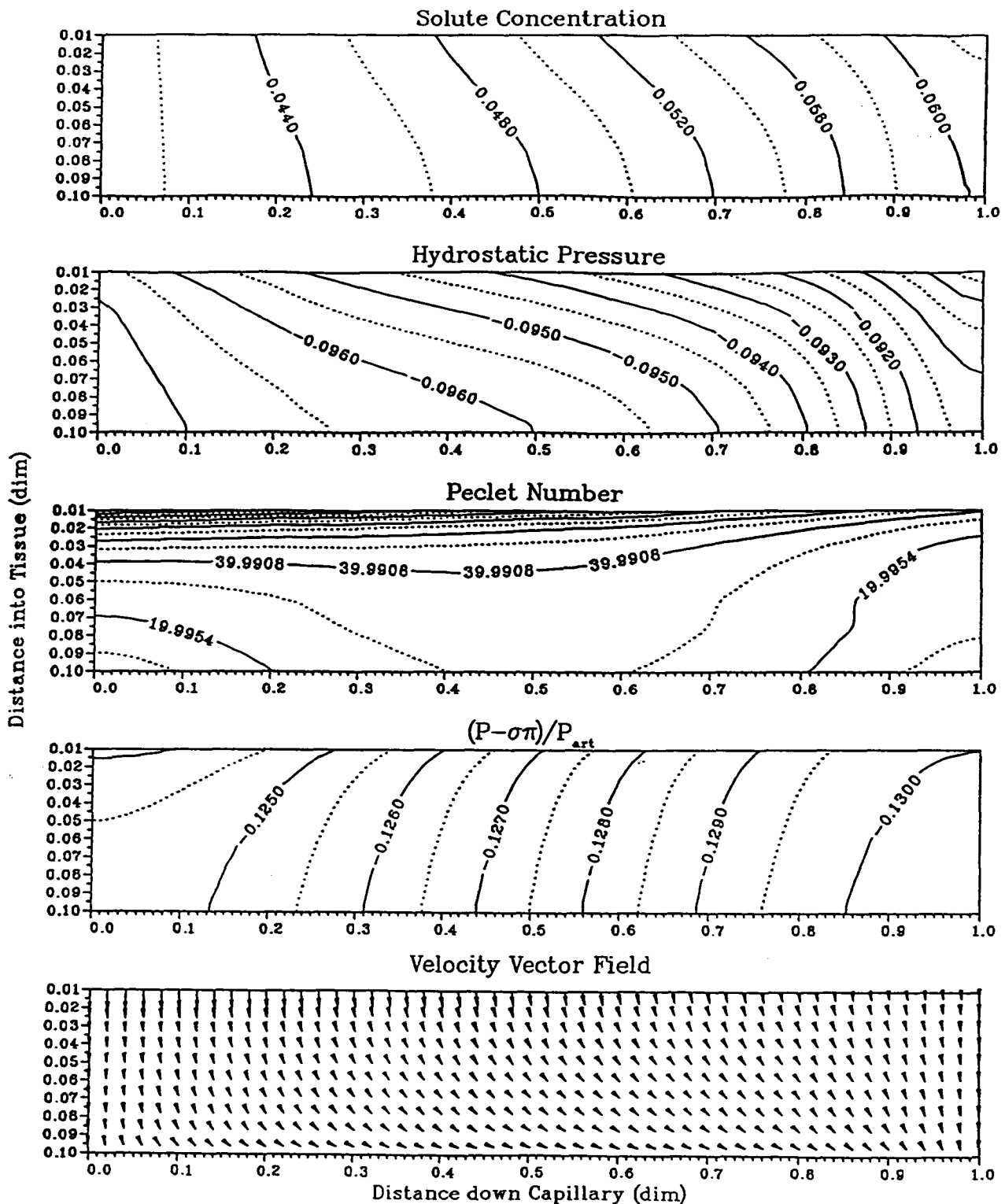


Figure 5.14: Dimensionless tissue solute concentration, hydrostatic pressure, Peclet number, potential and velocity vector distributions for the case with lowered capillary solute concentration ($c_{art}^* = 0.1000$) at new steady-state.

response to the drop in the tissue solute concentrations. At $t = 300$ s, the tissue hydrostatic pressures have become subatmospheric throughout most of the tissue. As a result the lymphatic sink removes less and less fluid and solute from the tissue thus reducing the fluid flow rates at the capillary membrane.

The solute concentrations reduce further with time. The hydrostatic pressure responds to the lowered solute concentrations by becoming increasingly more negative throughout the tissue. As a consequence, the lymph flow rates lower and therefore the transcapillary fluid velocities decrease with time. This means that solute removal rate out the lymphatics is dropping with time.

At steady-state ($t \cong 4600$ s), Figure (5.14), the maximum solute concentration of the solute distribution has shifted to the venular end of the tissue near the capillary. The excess amount of solute that had built up in the venular end of the tissue near the lymphatic sink due to the initial condition has now been depleted and solute removal is now largely dependent on the amount of solute being transported from the capillary membrane. As expected, the tissue hydrostatic pressure distribution resembles the solute concentration distribution. The low solute concentrations within the tissue cause the tissue to be entirely subatmospheric. The new steady-state solute concentration distribution has lower gradients throughout the tissue. The range is also decreased to roughly one-tenth of the initial condition values. This is reasonable since the blood solute concentration was dropped to 10% of its original value. The dimensionless average tissue solute concentration at the new steady-state is equal to 0.0495. The hydrostatic pressures are also lowered within the tissue. The dimensionless average tissue hydrostatic pressure drops to -0.0949 (-2.847 mmHg). As a result of the lower hydrostatic pressures, the lymphatic drainage rate is reduced to 3.59 l/day (from the original 5.47 l/day).

These results are confirmed by the experimental findings of Manning *et al.* (1983) in dogs. They found that the lymph flow decreased as the capillary protein content was reduced to very low levels.

The results for the increased capillary solute concentration are displayed in Figures (5.15)-(5.18). Here, the trends are opposite to those of the previous case. As expected, more solute is transported into the tissue leading to higher solute concentrations and thus elevated colloid osmotic pressures. The transmembrane potential, as a result, decreases until, near the venular end of the capillary, it eventually becomes negative. At this point, fluid reabsorption back into the capillary begins to occur. At $t = 0$, corresponding to the base case, the solute is completely filtered into the tissue space

Figure (5.18) display the results at $t = 300$ s. As can be seen, the solute concentrations are increased within the tissue. Also, the solute concentration gradients at the venular end of the tissue near the capillary increase due to the fluid reabsorption and consequent tissue-side protein filtration occurring in this region. Washout of solute from the arteriolar region of the tissue produces lower solute concentrations here with relatively lower gradients. The tissue hydrostatic pressure responds to the solute concentration distribution and has increased gradients at the venular end of the tissue near the capillary. The hydrostatic pressures become more positive. This leads to an associated increase in the lymphatic drainage. Fluid velocities increase within the tissue as a consequence of the rise in the lymph drainage. The rise in the solute concentrations within the tissue produce a drop in the potential distribution via the colloid osmotic pressures. As can be seen from the fluid flow field, fluid reabsorption is occurring. The zero point is located at $z^* \cong 0.70$.

At $t = 600$ s, Figure (5.16), the solute concentration has increased further within the tissue. The solute concentration and hydrostatic pressure gradients have increased further at the venular end of the tissue near the capillary. Also the maximum values of the concentrations and pressures occur in this region. The rise in the hydrostatic pressures results in an enlarged lymph drainage rate. This leads to a slight reduction in the fluid reabsorption back into the capillary. This is reflected by the shift in the zero point down the capillary to $z^* \cong 0.75$.

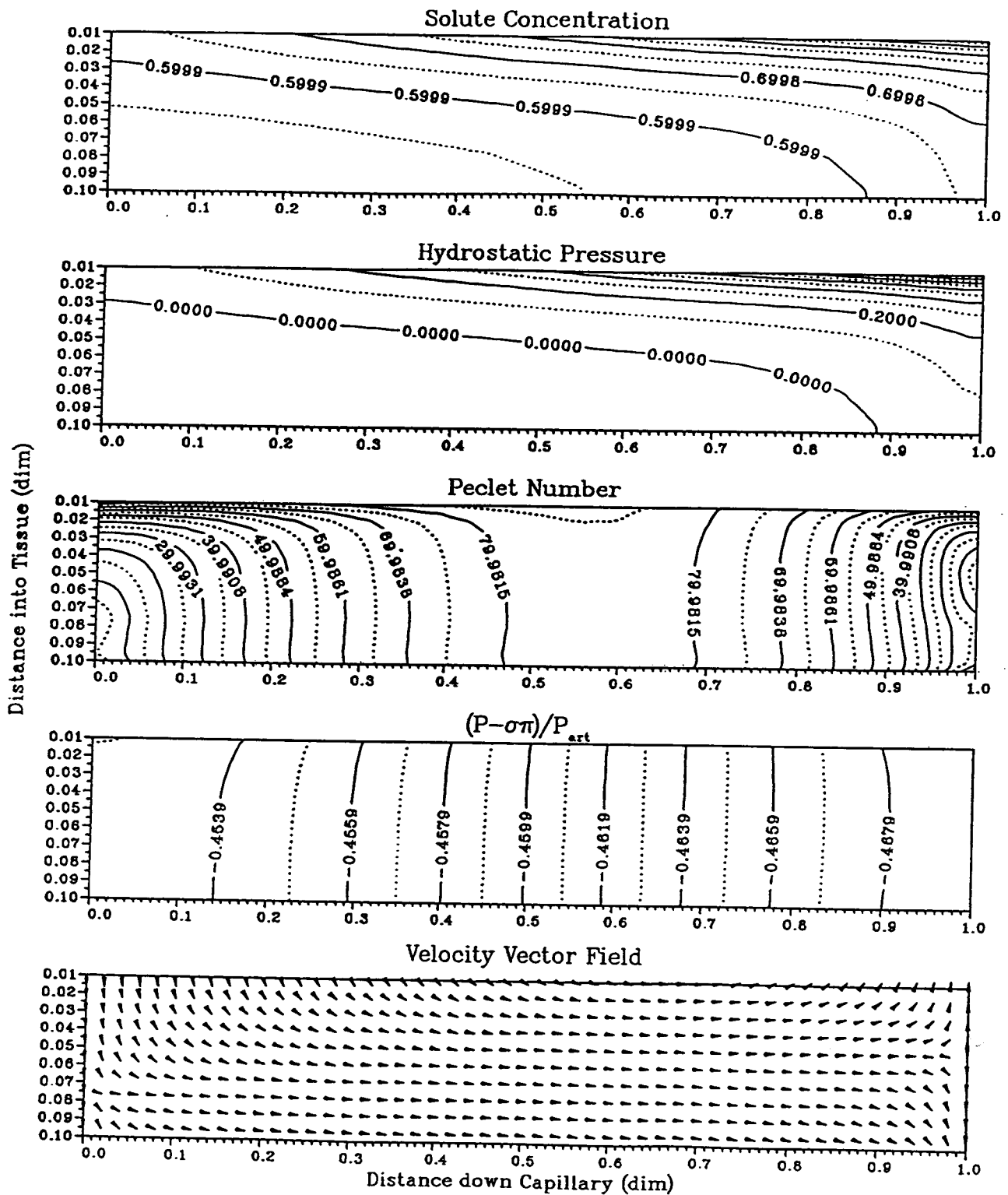


Figure 5.15: Tissue solute concentration, hydrostatic pressure, Peclet number, potential and velocity vector distributions for the case with enlarged capillary solute concentration ($c_{art}^* = 1.2000$) at $t = 300$ s.

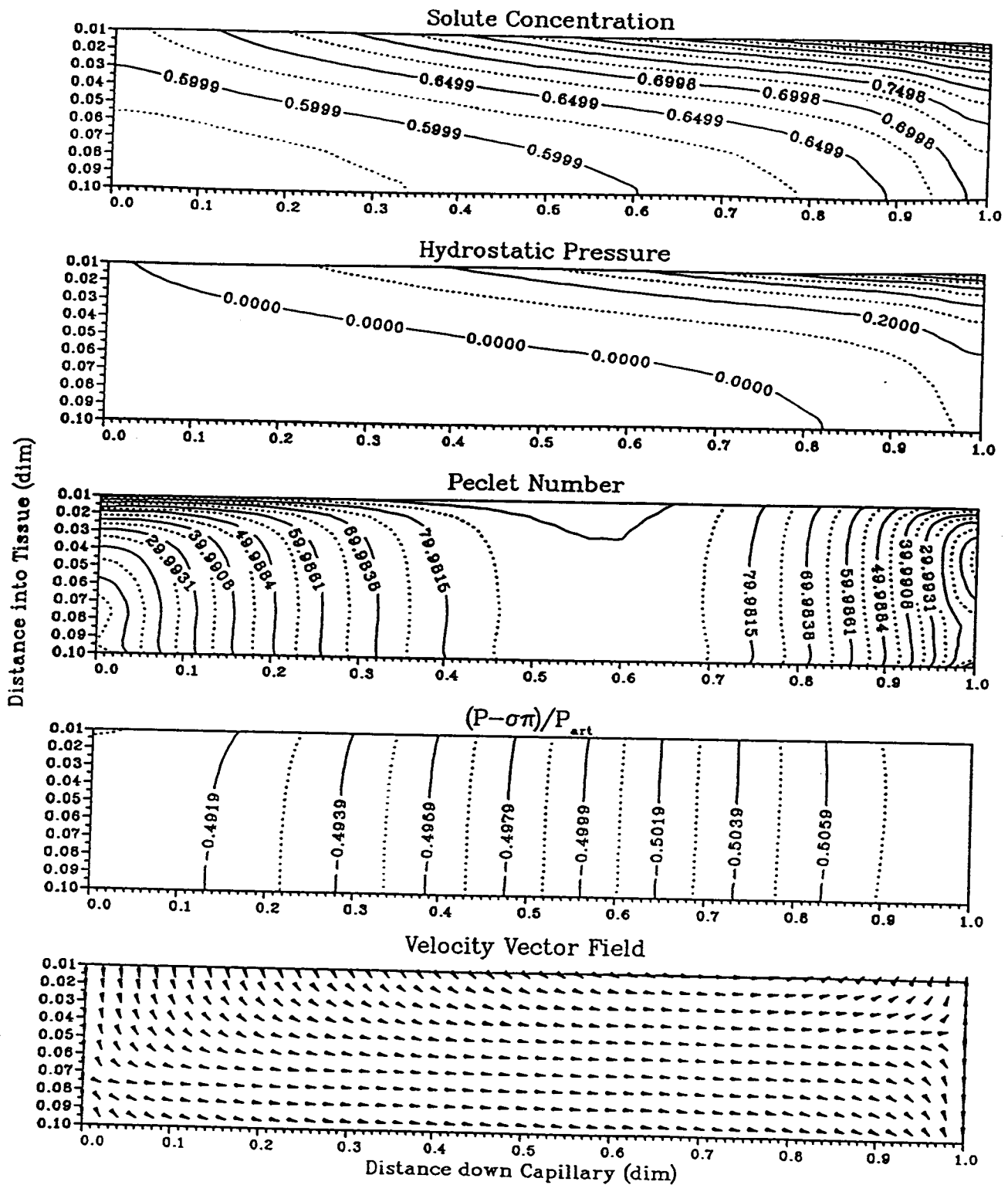


Figure 5.16: Tissue solute concentration, hydrostatic pressure, Peclet number, potential and velocity vector distributions for the case with enlarged capillary solute concentration ($c_{art}^* = 1.2000$) at $t = 600$ s.

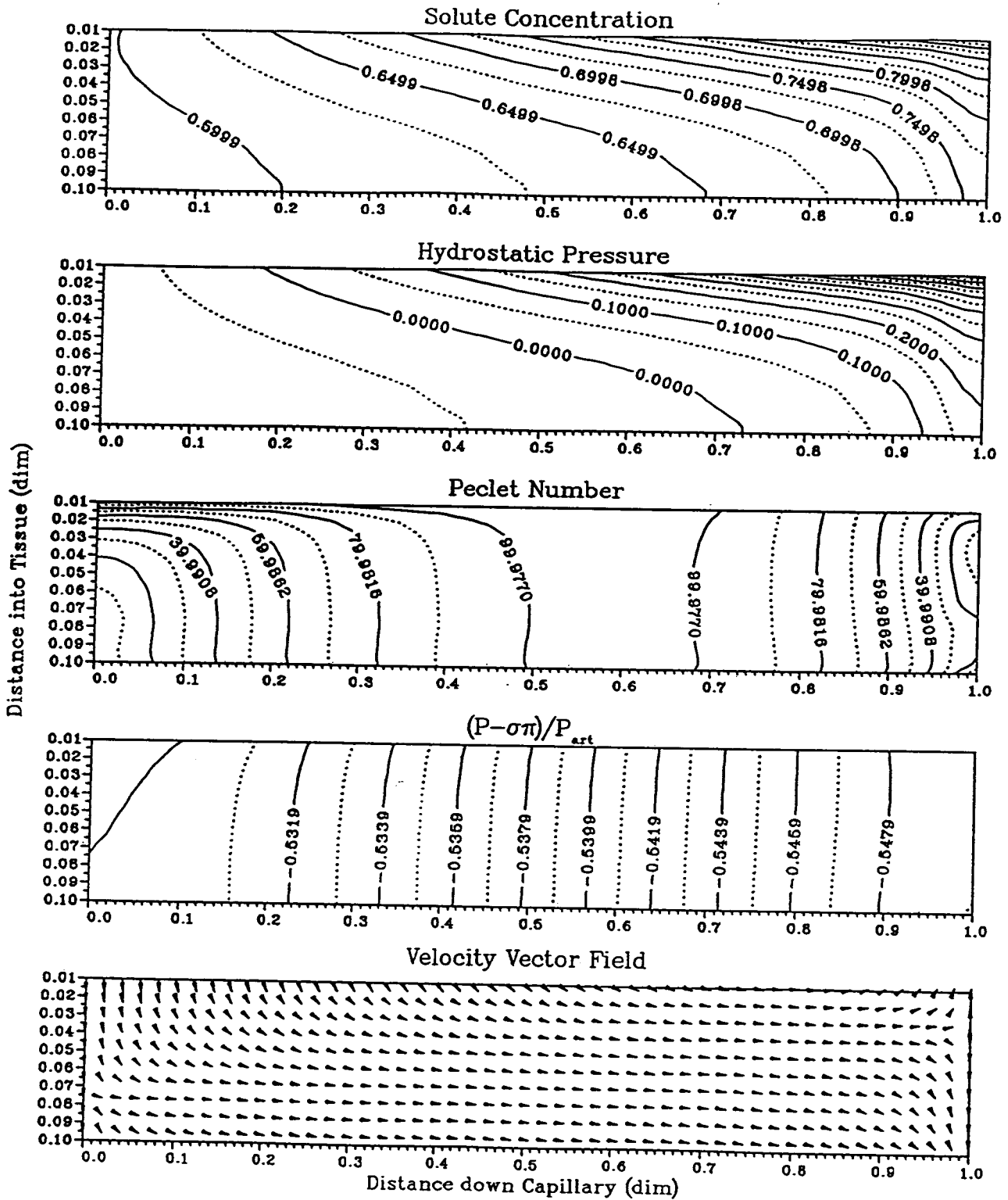


Figure 5.17: Tissue solute concentration, hydrostatic pressure, Peclet number, potential and velocity vector distributions for the case with enlarged capillary solute concentration ($c_{art}^* = 1.2000$) at $t = 1800$ s.

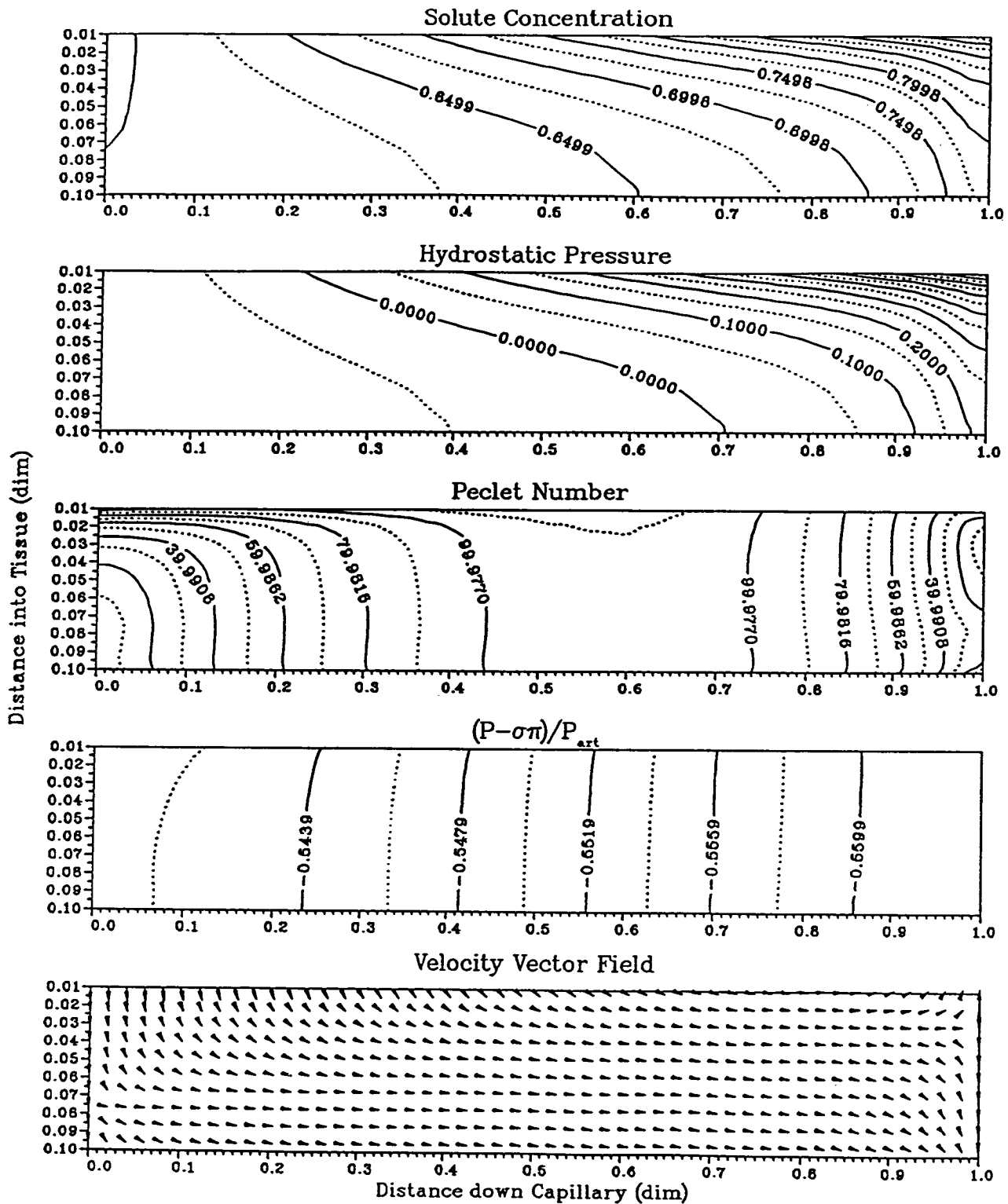


Figure 5.18: Tissue solute concentration, hydrostatic pressure, Peclet number, potential and velocity vector distributions for the case with enlarged capillary solute concentration ($c_{art}^* = 1.2000$) at steady-state.

The solute continues to build-up, although more slowly, with time at the venular end of the tissue near the capillary membrane. The associated increase in the colloid osmotic pressure at the tissue-side of the capillary membrane results in a increasingly more positive transmembrane potential. As a consequence, the tendency for fluid reabsorption begins to lessen and the zero point continues to move down the capillary. At $t = 1800$ s, the zero point is at $z^* \cong 0.80$. At steady-state, Figure (5.18), the solute concentration distribution has higher gradients than the initial state, especially at the venular end of the tissue near the capillary. The hydrostatic pressure distribution resembles the solute concentration distribution. The gradients are particularly steep at the extreme venular end of the tissue adjacent to the membrane. The Peclet numbers are higher throughout the tissue than the initial state indicating increased fluid velocities and thus a higher degree of convective transport. At the new steady-state, the dimensionless average tissue solute concentration is equal to 0.6881. The average hydrostatic pressure is equal to 0.0189 (0.5670 mmHg) and the resulting lymph drainage is 6.34 l/day.

From the above simulations it is clear that the lymphatic sink also plays a role in fluid balance regulation. When reabsorption occurs due to the elevated capillary solute concentrations (via its colloid osmotic pressure), then less fluid is withdrawn from the tissue via the lymphatic sink. As the solute concentration builds-up at the capillary wall, the transmembrane potential becomes more positive and the amount of reabsorption decreases and the hydrostatic pressures rise. The lymph drainage increases as a result. An equilibrium is established based on the fact that the increased solute removal by the lymphatics offsets the high solute flux across the capillary membrane. The amount of reabsorption is dependent on the transmembrane potential which is in turn is a function of the solute concentrations within the tissue. With a sufficiently strong sink, solute concentrations would be lowered leading to fluid reabsorption.

5.3.4 Transient Analysis of the Effects of Osmotic Pressure

The influence of the osmotic pressure on the system was examined in this section. Two cases were performed; the first including colloid osmotic pressure effects and the second without any colloid osmotic pressure driving terms throughout the system. The system was perturbed at steady-state (the base case solution) by resetting the capillary solute concentration to zero. This means that there is no longer any solute entering the system and thus solute concentrations will fall in the tissue due to the lymphatic drainage.

The average tissue and lymphatic fluid solute concentrations are displayed in Figure (5.19). As can be seen, the solute concentrations drop rapidly to zero. For the case where the effects of the osmotic pressure are not included, the osmotic pressure gradients may be taken as equal to zero. For the case under the influence of the colloid osmotic pressure effects, fluid is dragged out through the lymphatics causing relatively high gradients in the osmotic pressure, especially at the venular end of the tissue. The hydrostatic pressures throughout the tissue begins to fall in response to the depletion of solute. Consequently, the lymphatic drainage drops therefore lowering fluid velocities throughout the interstitium and across the membrane. Initially, the hydrostatic pressures are greater throughout the tissue for the case with osmotic pressure than the case without it. This means during these times, lymphatic drainage is greater in the case with osmotic pressure than the case without. This is why the solute concentrations for the case with osmotic pressure are lower, i.e., initially, the solute is dragged out of the tissue at a faster rate than the case without the osmotic pressure.

As the solute concentrations drop within the tissue, the colloid osmotic pressure plays a smaller role in determining the hydrostatic pressure and the profiles become indistinguishable.

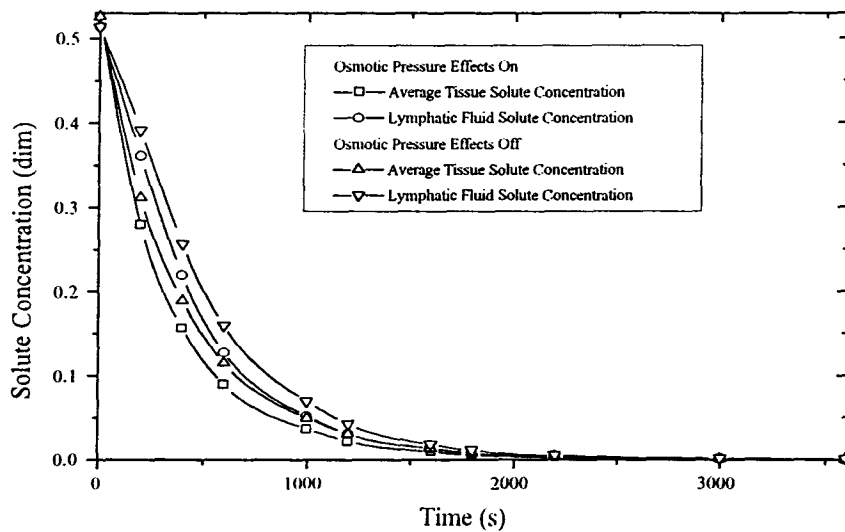


Figure 5.19 : Average tissue and lymphatic fluid solute concentrations through time.

From Figure (5.19), it appears that the colloid osmotic pressure enhances solute removal from the system at early times for higher solute concentrations.

The transient contour plots for the case with colloid osmotic pressure effects included are displayed in Figure (5.20)-(5.24). The initial state is the steady-state base case distributions presented in Chapter 4. The solute removal by the lymphatic sink creates a strongly radial solute concentration distribution. Also the relatively greater washout of solute at the arteriolar end of the tissue promotes lower solute concentrations at the arteriolar end of the tissue near the capillary membrane.

Initially in the transient response, the hydrostatic pressure distributions are similar to the solute concentration distributions. At low solute concentrations, the hydrostatic pressure distribution approaches the potential distribution. This is because the colloid osmotic pressure approaches zero. For the case without osmotic pressure effects, the hydrostatic pressure distribution is constant through time and is identical to the potential distribution. The potential distribution for the case with osmotic pressure shifts in the positive direction as

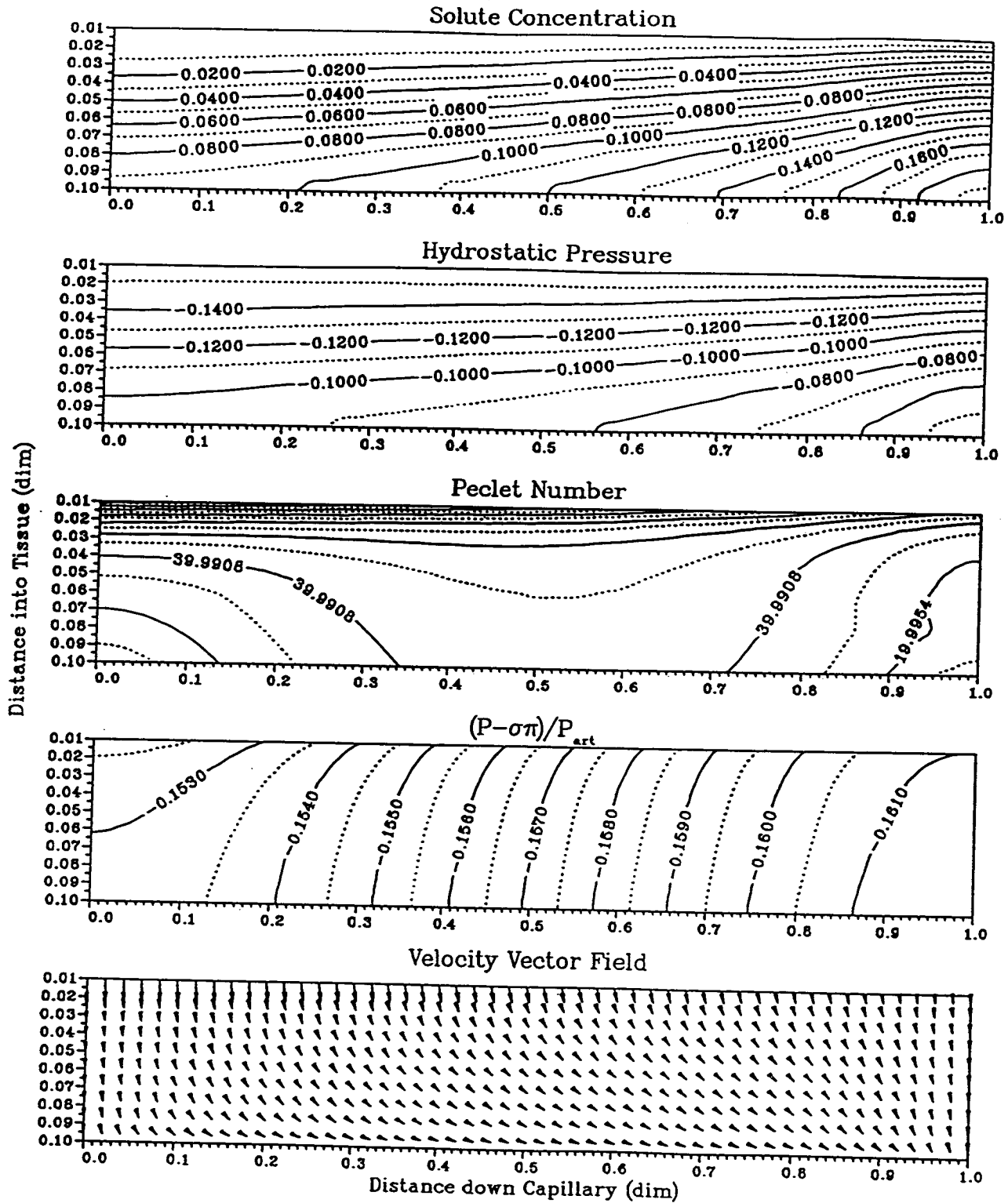


Figure 5.20: Dimensionless tissue solute concentration, hydrostatic pressure, Peclet number, potential and velocity vector distributions for the case with colloid osmotic pressure effects throughout the system and zero arteriolar capillary solute concentration ($c_{art}^* = 0.0000$) at $t = 600$ s.

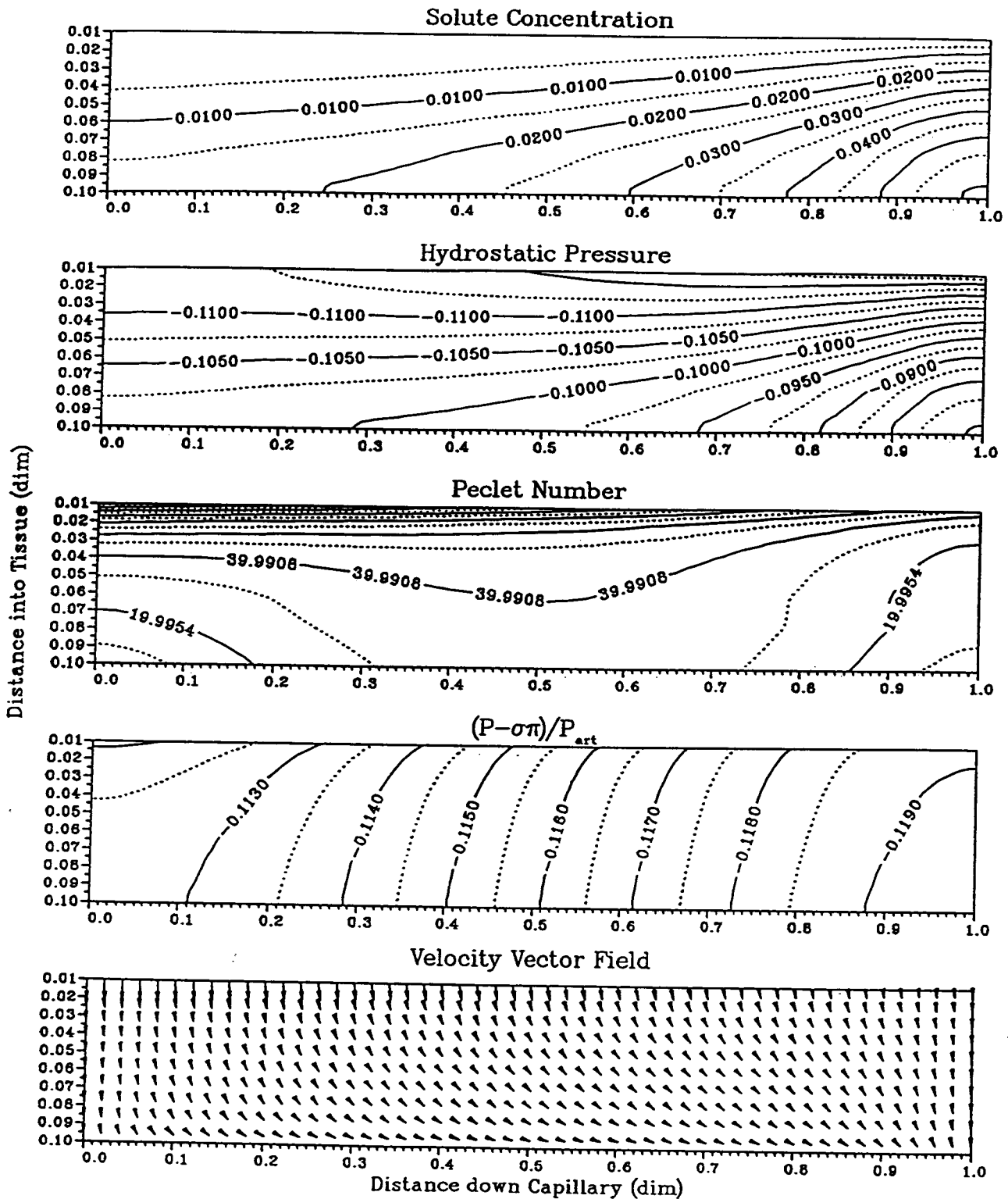


Figure 5.21: Dimensionless tissue solute concentration, hydrostatic pressure, Peclet number, potential and velocity vector distributions for the case with colloid osmotic pressure effects throughout the system and zero arteriolar capillary solute concentration ($c_{art}^* = 0.0000$) at $t = 1200$ s.

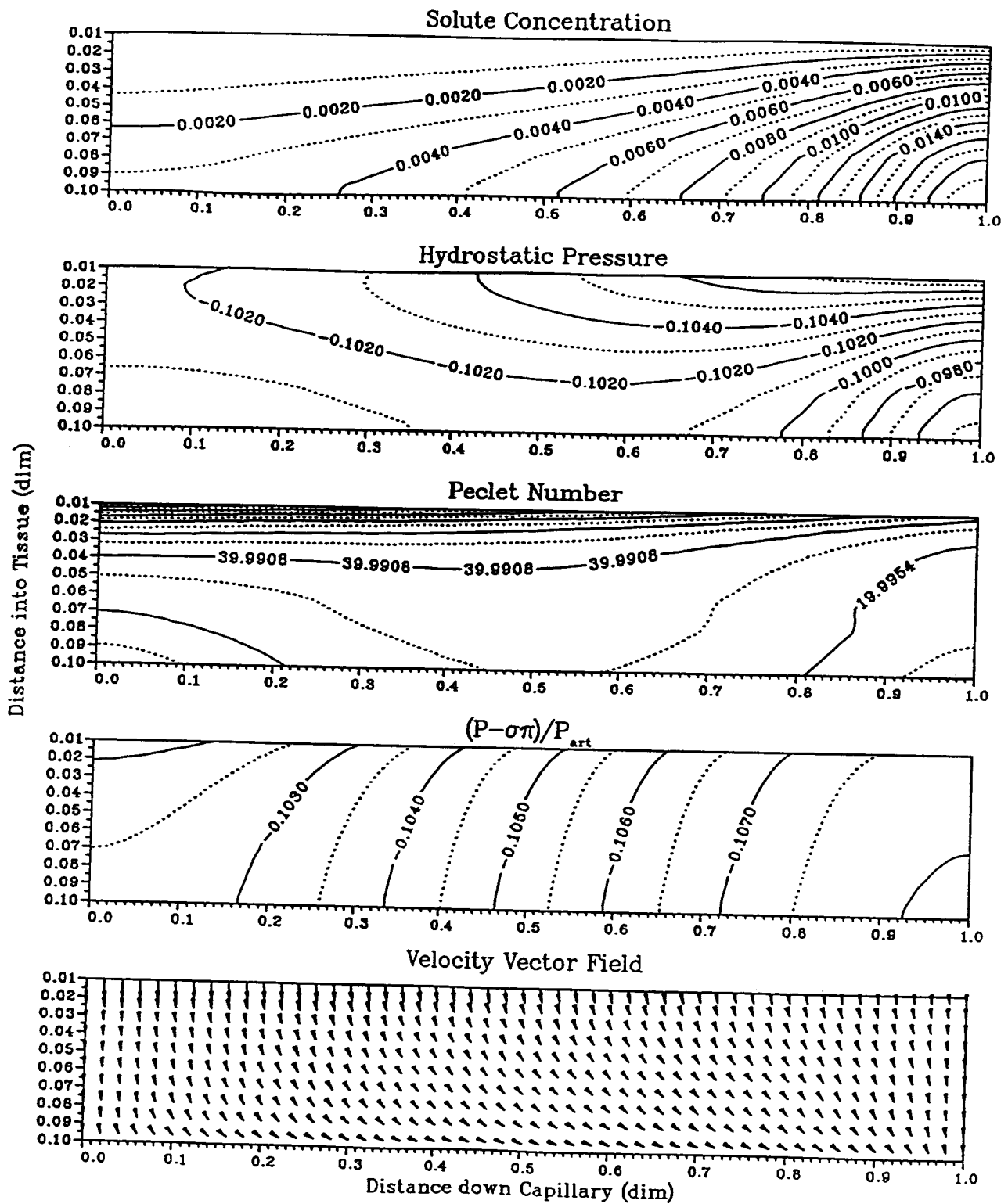


Figure 5.22: Dimensionless tissue solute concentration, hydrostatic pressure, Peclet number, potential and velocity vector distributions for the case with colloid osmotic pressure effects throughout the system and zero arteriolar capillary solute concentration ($c_{art}^* = 0.0000$) at $t = 1800$ s.

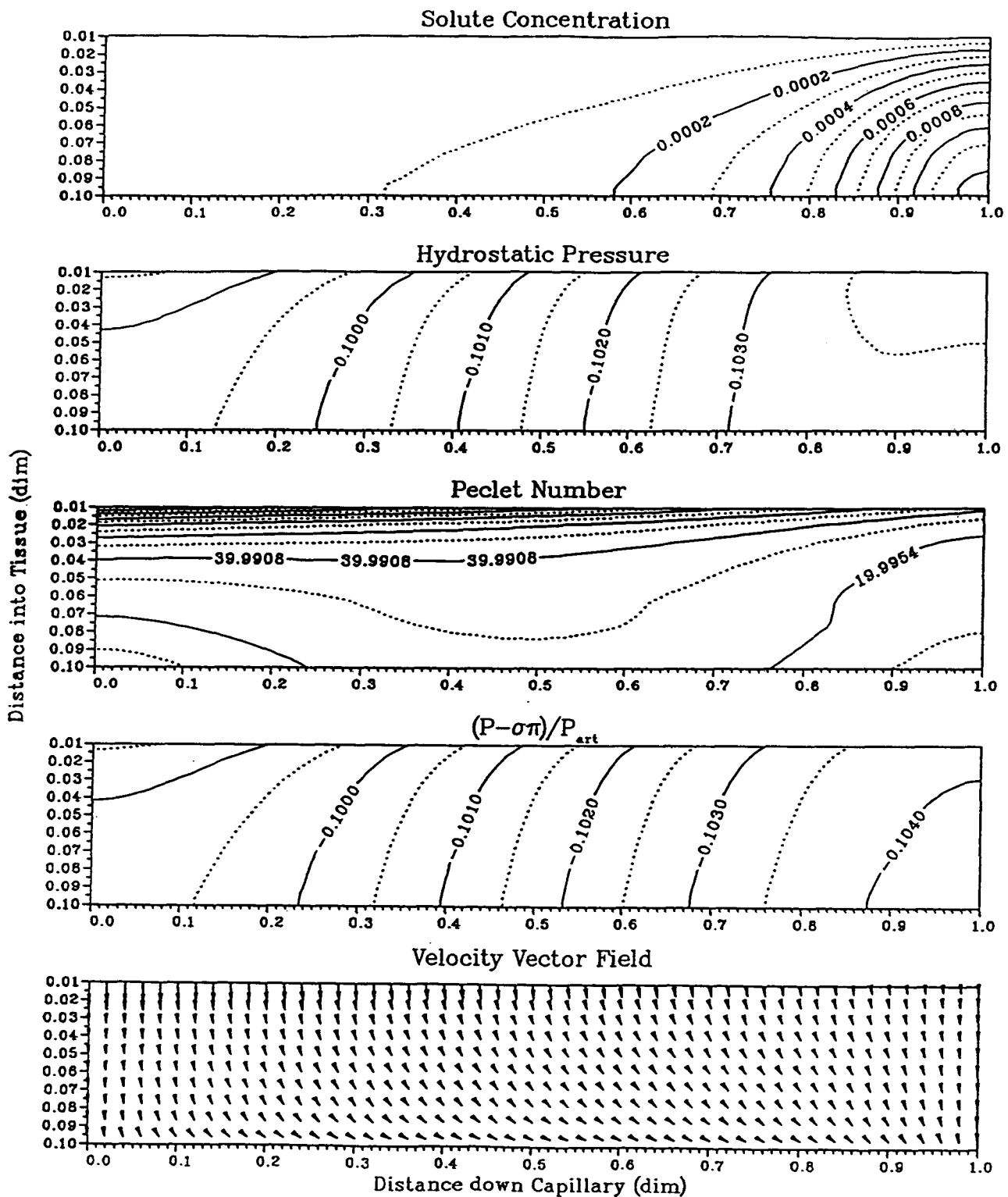


Figure 5.23: Dimensionless tissue solute concentration, hydrostatic pressure, Peclet number, potential and velocity vector distributions for the case with colloid osmotic pressure effects throughout the system and zero arteriolar capillary solute concentration ($c_{art}^* = 0.0000$) at $t = 3600$ s.

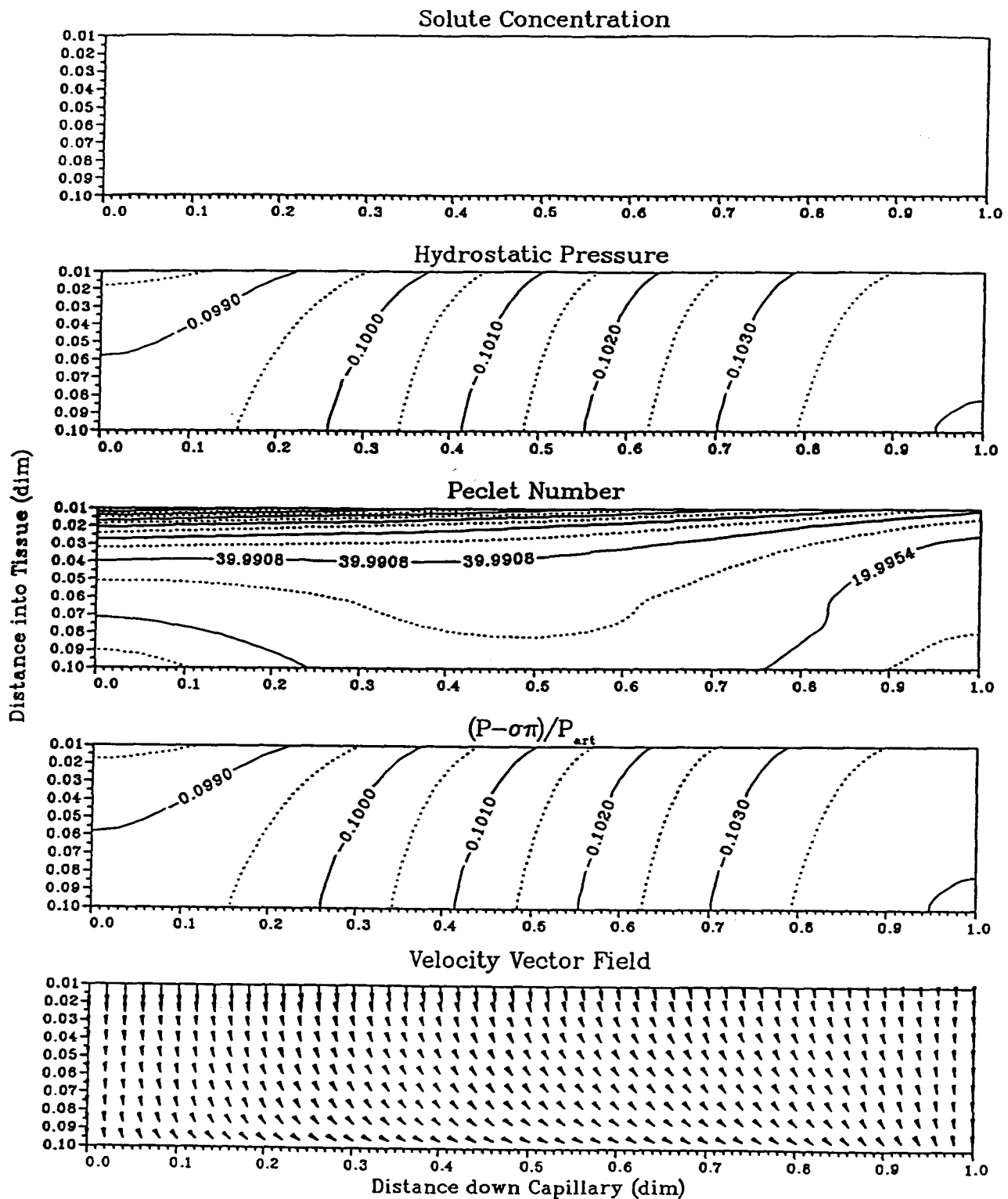


Figure 5.24: Dimensionless tissue solute concentration, hydrostatic pressure, Peclet number, potential and velocity vector distributions for the case with colloid osmotic pressure effects throughout the system and zero arteriolar capillary solute concentration ($c_{art}^* = 0.0000$) at new steady-state.

the solute concentrations decrease. This is a direct result of the reduction of the osmotic pressure and its gradients within the tissue through time. The velocity vector pattern is similar through time. There is no fluid reabsorption during the simulations.

5.4 Discussion and Conclusions

The average tissue solute concentration and hydrostatic pressures, lymphatic solute concentrations, and lymph drainage rates for the cases performed in this Chapter are listed in Table (5.1). These values are those at the new steady-state established after the perturbation.

Table 5.1: Results summary for transient cases performed at new steady-state.

Case	Average c_t	Average P_t	Average c_l	Lymph Flow (l/day)
$P_{ven}^* = 0.6667$	0.4997	-0.0251	0.4971	5.90
c_t^* lowered	0.0620	-0.1289	0.0612	2.42
$c_{art}^* = 0.10$	0.0495	-0.0949	0.0490	3.59
$c_{art}^* = 1.20$	0.6881	0.0189	0.6492	6.34
$c_{art}^* = 0.0$ Osmotic Pr. On	0.0000	-0.1014	0.0000	3.37
$c_{art}^* = 0.0$ Osmotic Pr. Off	0.0000	-0.1014	0.0000	3.37

Elevated venous hydrostatic pressure leads to higher tissue hydrostatic pressures. This means that the lymphatic sink will drain more material from the system. The fact that the lymphatic sink can accommodate large flow rates points to it being a regulator of the fluid balance. As the tissue hydrostatic pressure increases, there is increased lymph drainage. This allows for the removal of excess fluid in the interstitial space which would increase tissue pressures. As pointed out by Guyton *et al.* (1987), the lymph drainage may increase

up to 20 times before edema occurs. It then levels off as indicated by the work of Taylor *et al.* (1973). This supports the idea that the lymphatic sink initially handles the increase in the fluid filtration through the capillary membrane maintaining the fluid balance and tissue volume. Once the tissue hydrostatic pressures are sufficiently positive, the lymph flow does not increase further indicating that it is saturated. The reason for this is not understood. It is important to remember that the model does not take into account tissue swelling. With venous pressure elevation it is expected that tissue swelling would occur. This may explain the modest decrease in the solute concentration in the tissue. Mortillaro and Taylor (1976) observed that the lymphatic protein concentration fell about 20% for a similar elevation of venous pressure as performed in this work. This indicates a reduction in the interstitial protein concentration. Elevated venous pressure would expectedly lead to tissue swelling resulting in enlarged tissue hydration. This would lower observed tissue protein concentrations.

The lymphatic sink is also instrumental in providing the negative pressures throughout the tissue and lowering the solute concentrations within the tissue space. With sufficient sink drainage, the solute concentrations would be reduced to low values in the tissue. This is because the transcapillary exchange of solute is limited by the capillary filtration and reflection coefficients. Eventually, the tissue solute concentrations will be low enough that fluid reabsorption occurs. This is because of the phenomenon due to lowered tissue-side capillary membrane osmotic pressures discussed above. Once fluid reabsorption occurs, eventually, the hydrostatic pressure will drop in the tissue. Thus the lymphatic drainage will be reduced and then consequently, the solute concentrations in the tissue will start to increase once again. This will lead to a reduction in fluid reabsorption back into the capillary and tissue fluid hydrostatic pressures will start to increase. The cycle of control is then repeated as the lymph sink starts to drain more fluid and solute again. The solute concentration acting through the osmotic pressure provides the feedback signal to the system to adjust the flow pattern. The signal that controls the lymphatic sink drainage is the tissue

hydrostatic pressure. Any increase in the tissue hydrostatic pressure leads to an increased lymph drainage and thus a lowered solute concentration. Lower tissue solute concentrations lead to lower tissue osmotic pressures which in turn then result in higher tissue hydrostatic pressures via the transport through the capillary membrane phenomenon.

The control of the interstitial fluid balance is closely tied with that of the blood volume. The lymphatic sink and capillary membrane through their transport properties regulate the flow of fluid and solute between the plasma and tissue compartments. The osmotic pressure, as mentioned earlier, provides a negative feedback signal controlling the fluid balance across the capillary wall via the transcapillary potential difference. This leads to the control of the blood volume. When the venous pressure rises, more fluid filters into the interstitial space. This in itself reduces the blood volume. As the tissue solute concentrations are lowered due to removal by the lymphatic sink, this promotes increased fluid reabsorption. This will increase the blood volume.

The following conclusions can be made :

1. The osmotic pressure plays an important role as a feedback signal for fluid balance regulation. It serves to regulate the amount of fluid reabsorption into the capillary.
2. The controlling mechanisms for capillary-tissue fluid balance arise from the cycling effects of the hydrostatic pressure and solute concentrations within the tissue and the capillary. This can be established as follows. Lowered tissue solute concentrations result in a reduction of the tissue hydrostatic pressure due to fluid reabsorption. This means less flow exits via the lymphatics and thus the solute concentrations increase leading to less fluid reabsorption. The hydrostatic pressure rises because of both the lesser reabsorption and as a consequence of its response to the increasing osmotic pressure. This leads to greater lymph drainage and eventually lower solute concentrations.
3. The lymphatic sink serves as a controlling feature of the capillary-tissue fluid balance. Its role is to remove excess fluid and solute from the interstitial space. The regulation of the solute concentrations in the tissue are key for the occurrence of fluid reabsorption

back into the capillary. This is directly dependent on the local tissue hydrostatic pressure.

Chapter 6 : Conclusions and Recommendations

A transient, spatially distributed two-dimensional model of the microvascular exchange system has been developed and successfully implemented in cylindrical coordinates. For the base case parameters selected, the calculated values for the average tissue solute concentrations, hydrostatic pressures, and lymph drainage are in the range of values expected for human tissue. The effect of these physiological parameters on the system have been investigated. It appears that some of the parameters have a larger impact on the system than others.

In particular, the capillary membrane filtration coefficient and lymphatic sink strength dominate the fluid flow structure of the system. The capillary membrane filtration coefficient limits the amount of fluid entering the system. The high fluid flow resistance of the membrane relative to that in the tissue suggests that fluid flow is controlled entirely by the capillary filtration coefficient. This is clearly shown by the significantly greater potential drop across the membrane relative to that across the tissue. The strength of the lymphatic sink in combination with the high flow resistance of the capillary membrane provides the opportunity for negative hydrostatic pressures (subatmospheric) within the interstitial space. The lymphatic sink also provides the primary mechanism for removal of solute from the tissue. Fluid reabsorption may be promoted based on the values of LS , P_L , and L_p . The average tissue solute concentration, hydrostatic pressure, and potential distributions are largely functions of the transport properties of the capillary membrane and the lymphatic sink.

Dispersion was not found to play a major role as a transport mechanism based on the assumed dispersivity values. This was found despite the highly convective nature of the solute transport across the capillary membrane and within the tissue. High convective transport promotes greater dispersion.

From the results, the colloid osmotic pressure cannot be ignored in any formulation of microvascular exchange. Gradients in the colloid osmotic pressure are significant in the tissue and contribute to the fluid motion. The hydrostatic pressure distributions are usually quite similar to the solute concentration distributions. This is because the hydrostatic pressure responds directly to the solute concentrations via the osmotic pressure. This would occur for σ_t greater than zero. Of course, as the tissue reflection coefficient is reduced, the effect of the colloid osmotic pressure on hydrostatic pressure distribution would diminish. The fluid potential is the driving force for fluid movement throughout the system.

The capillary-tissue fluid balance is regulated by a combination of the osmotic pressure, the lymphatic sink, and transport through the capillary membrane. The colloid osmotic pressure serves as a negative feedback signal controlling the influx of fluid into the interstitial space by maintaining the transcapillary potential difference. The lymphatic sink also acts as a regulatory mechanism for fluid balance. It serves to reduce solute concentrations within the tissue thus reducing the transcapillary potential and promoting fluid reabsorption. This lowers the hydrostatic pressures within the interstitial space thus reducing the lymph drainage, which would eventually lead to higher solute concentrations and therefore less reabsorption. The hydrostatic pressure would then begin to increase once again. This is intimately tied to maintenance of the blood plasma volume.

The following recommendations are made for possible future efforts as extensions of the present work :

1. The model is limited in that the tissue is assumed rigid and nondeformable. This means the effects of hydration and fluid accumulation on the fluid balance cannot be studied. This does not permit the observation of edema within the tissue. The inclusion of swelling in the model formulation would enhance the model's utility and aid in observing the regulation of interstitial fluid volume. This may be implemented as a first approximation as being one dimensional swelling in the radial direction. This could be averaged over the entire length of the tissue thus producing a radial increase or decrease in volume depending on the compliance relationships and fluid balance. In this manner, the need for calculating stresses at each element in the tissue is avoided simplifying the problem greatly.
2. The description of the lymphatic sink may be extended to be more realistic. In the present model, it is assumed as a simple linear function of the local tissue hydrostatic pressure. This may be too simple in that there is no limit on the lymphatic flow which is observed experimentally (Taylor *et al.*, 1973).
3. The tissue reflection coefficient and the implications of such a parameter should be examined from a theoretical and experimental viewpoint. The emphasis would be on deriving or approximating the relationship between the tissue reflection coefficient and the retardation factor and volume exclusion fractions and its impact on osmotically active solute particles moving through a fibrous porous medium.
4. It is also felt that existing models describing microvascular exchange should first be validated by experimental work. The construction of more complex and elaborate models may not be adding new understanding to the mechanisms of solute and fluid exchange in the microvascular system unless experiments are done validating them. At present, there is little experimental data to draw from for model validation.

Nomenclature

Symbol	Description	Units
α	Dispersivity	m
A	Area	m^2
c	Solute concentration	$kg\ m^{-3}$
dim	Dimensionless	
D	Solute diffusion coefficient	$m^2\ s^{-1}$
δ	Dirac delta function or small distance	
f	Volume fraction	
g	Acceleration due to gravity	$m\ s^{-2}$
j	Solute flux	$kg\ m^{-2}\ s^{-1}$
k	Anisotropic porous medium permeability	m
K	Fluid hydraulic conductivity	$m^2\ Pa^{-1}\ s^{-1}$
L	Length	m
L_p	Capillary fluid filtration coefficient	$m\ Pa^{-1}\ s^{-1}$
LS	Lymphatic sink strength	$m^3\ fl\ m^{-3}\ tis\ Pa^{-1}\ s^{-1}$
μ	Fluid viscosity	$Pa\ s^{-1}$

n	Outward normal direction	
π	Colloid osmotic pressure	Pa
P	Hydrostatic pressure	Pa
Pe	Peclet number	
PS	Solute capillary wall diffusive permeability	m s^{-1}
Q	Lymphatic sink drainage or volumetric flow rate	s^{-1} $\text{m}^3 \text{s}^{-1}$
ρ	Fluid density	kg m^{-3}
r	Radial coordinate direction	
R	Capillary or tissue radius	m
σ	Solute reflection coefficient if no subscript, then for capillary membrane if subscript t then for tissue	
t	Time	s
τ	Dimensionless time	
T	Fluid driving potential, $(P - \sigma\pi)$	Pa
θ	Tissue porosity	
v	Velocity	m s^{-1}
W	General variable	
ξ	Retardation factor	
z	Longitudinal coordinate direction	

Appendices

Symbol	Description	Units
A	Vector or matrix of elemental function, $a(s)$, values	
α	Upwinding parameter	
C	Convective matrix	
D	Diffusion coefficient	$\text{m}^2 \text{s}^{-1}$
f	Function defined in solution domain	
F	Vector of elemental function, f , values	
γ	Elemental Peclet number	
h	Elemental characteristic length	m
$h(s)$	Function defined along element boundary	
H	Vector of elemental function, $h(s)$, values	
K	Stiffness matrix	
Λ	Eigenvalues	
n	Basis or trial functions	
N	Vector of elemental trial functions	
p	Perturbation (upwinding) function	
s	Coordinate along boundary segment	
t	Interpolation function	
T	Transient matrix	
u	General unknown variable	
U	Vector of elemental unknown variables	

v	Fluid velocity	m s^{-1}
w	Weighting or test function	
ω	Relaxation factors	
x	x-direction	
y	y-direction	

Subscripts and Superscripts (including Appendices)

Symbol Description

art	Arteriolar capillary quantity
av	Available volume fraction seen by fluid
c	Capillary quantity
d	Combined diffusive and dispersive components
$diff$	Diffusive component
$disp$	Dispersive component
Da	Darcy's law
e	Elemental quantity
eff	Effective quantity
ex	Excluded volume fraction
f	Fluid quantity
G	Global matrix quantity
i	i^{th} direction
im	Immobile fluid volume fraction

<i>j</i>	<i>j</i> th direction
<i>k</i>	<i>k</i> th direction or dummy iteration variable
<i>l</i>	<i>l</i> th direction
<i>L</i>	Lymphatic quantity
<i>long</i>	Longitudinal direction
<i>m</i>	Membrane quantity
<i>n</i>	Outward normal direction
<i>r</i>	Radial coordinate direction
<i>ref</i>	Reference quantity
<i>s</i>	Solute quantity
<i>so</i>	Solid volume fraction
<i>st</i>	Volume fraction solute can see
<i>St</i>	Starling's hypothesis
<i>t</i>	Tissue quantity
<i>tran</i>	Transverse direction
<i>ven</i>	Venular capillary quantity
<i>z</i>	Longitudinal coordinate direction
*	Dimensionless quantity

References

- Apelblat, A., A. Katzir-Katchalsky, and A. Silberberg. A mathematical analysis of capillary-tissue fluid exchange. *Biorheology*. **11** : 1-49 (1974).
- An, K.-N., and E.P. Salathe. The effect of variable capillary radius and filtration coefficient on fluid exchange. *Biorheology*. **13** : 367-378 (1976).
- Aukland, K. Interstitial fluid balance in experimental animals and man. *Adv. Microcirc.* **13** : 110-123 (1987).
- Bassingthwaighe, J.B., C.Y. Wang, and L.S. Chan. Blood tissue exchange via transport and transformation by capillary endothelial cells. *Circulation Research*. **65** : 997-1020 (1989)
- Baxter, L.T., and R.K. Jain. Transport of fluid and macromolecules in tumours. I. Role of interstitial pressure and convection. *Microvascular Research*. **37** : 77-104 (1989).
- Baxter, L.T., and R.K. Jain. Transport of fluid and macromolecules in tumours. II. Role of heterogeneous perfusion and lymphatics. *Microvascular Research*. **40** : 246-263 (1990).
- Baxter, L.T., and R.K. Jain. Transport of fluid and macromolecules in tumours. III. Role of binding and metabolism. *Microvascular Research*. **41** : 5-23 (1991a).
- Baxter, L.T., and R.K. Jain. Transport of fluid and macromolecules in tumours. III. A microvascular model of the perivascular distribution. *Microvascular Research*. **41** : 252-272 (1991b).
- Benoit, J.N., C.A. Navia, A.E. Taylor, and D.N. Granger. Mathematical model of transcapillary fluid and protein exchange. In : A.P. Shepherd and D.N. Granger (eds.), *Physiology of the Internal Circulation*, N.Y.: Raven Press, 275-287 (1984).
- Bear, J. Dynamics of fluids in porous media. N.Y. : Elsevier, 579-663 (1972).
- Bert, J.L., and R.H. Pearce. The interstitium and microvascular exchange. In : (E.M. Renkin and C.C. Michel (eds.), *Handbook of Physiology - Cardiovascular System*,

- Volume IV - Microcirculation, Chapter 12, Bethesda, Md : American Physiological Society (1984).
- Bert, J.L., B.D. Bowen, and R.K. Reed. Microvascular exchange and interstitial volume control in the rat : model validation. *Am. J. Physiol.* **254** : H384-H399 (1988).
- Bert, J.L., B.D. Bowen, X. Gu, T. Lund, and R.K. Reed. Microvascular exchange during burn injury. II : Formulation and validation of a mathematical model. *Circulatory Shock.* **28** : 199-219 (1989).
- Bickford, W.B. A first course in the finite element method. Irwin Inc. Boston. (1990).
- Bird, R.B., W.E. Stewart, and E.N. Lightfoot. Transport Phenomena. John Wiley and Sons. N.Y. : (1960).
- Blake, T.R., and J.F. Gross. A mathematical model of fluid exchange from an array of capillaries. *Microvascular Research.* **19** : 80-98 (1980).
- Blake, T.R., and J.F. Gross. Analysis of coupled intra- and extraluminal flows for single and multiple capillaries. *Math. Biosci.* **59** : 173-236 (1982).
- Bowen, B.D., J.L. Bert, X. Gu, T. Lund, and R.K. Reed. Microvascular exchange during burn injury. III : Implications of the model. *Circulatory Shock.* **28** : 221-233 (1989).
- Brenner, H., and L.J. Gaydos. The constrained Brownian movement of spherical particles in cylindrical pores of comparable radius. *J. Colloid Interface Sci.* **58** : 312-356 (1977).
- Brooks, A.N., and T.J.R. Hughes. Streamline upwind/Petrov-Galerkin formulations for convection dominated flows with particular emphasis on the incompressible Navier-Stokes equations. *Comp. Meth. Appl. Mech. Eng.* **32** : 199-259 (1982).
- Chapple, C. A compartmental model of microvascular exchange in humans. M.A.Sc. thesis. Department of Chemical Engineering, The University of British Columbia. (1990).
- Curry, F.E. Mechanics and thermodynamics of transcapillary exchange. In : (E.M. Renkin and C.C. Michel (eds.), *Handbook of Physiology - Cardiovascular System*, Volume IV - Microcirculation, Chapter 8, Bethesda, Md : American Physiological Society (1984).
- Dietrich, H.H., and K. Tyml. Capillary as a communicating medium in the microvasculature. *Microvascular Research.* **43** : 87-99 (1992).
- Donea, J. A Taylor-Galerkin method for convective transport problems. *Int. J. Num. Meth. Eng.* **20** : 101-119 (1984).

- Flessner, M.F., R.L. Dedrick, and J.S. Schultz. A distributed model of peritoneal-plasma transport: analysis of experimental data in the rat. *Am. J. Physiol.* **248** : F413-F424 (1985).
- Friedman, J.J., and S. Witte. The radial protein concentration in the interstitial space of the rat ileal mesentery. *Microvascular Research.* **31** : 277-287 (1986).
- Fry, D.L. Mathematical models of arteriolar transmural transport. *Am. J. Physiol.* **248** : H240-H263 (1985).
- Ganong, W.F. Review of medical physiology. Fourteenth Edition. Lange Medical Publications. (1989).
- Gerlowski, L.E., and R.K. Jain. Microvascular permeability of normal and neoplastic tissues. *Microvascular Research.* **31** : 288-305 (1986).
- Guyton, A.C., T.H. Adair, R.D. Manning, and J. Valenzuela-Rendon. Fluid dynamics and control in the interstitial-lymph system. *Adv. Microcirc.* **13** : 95-109 (1987).
- Intaglietta, M. and B.W. Zweifach. Geometrical model of the microvasculature of rabbit omentum from *in vivo* measurements. *Circulation Research.* **28** : 593-600 (1971).
- Johnson, P.C., and D.R. Richardson. The influence of venous pressure on filtration forces in the intestine. *Microvascular Research.* **7** : 296-306 (1974).
- Heinrich, J.C., and C.-C. Yu. Finite element simulation of buoyancy-driven flows with emphasis on natural convection in a horizontal circular cylinder. *Comp. Meth. Appl. Mech. Eng.* **69** : 1-27 (1988).
- Hughes, T.J.R. A simple scheme for developing 'upwind' finite elements. *Int. J. Num. Meth. Eng.* **12** : 1359-1365 (1978).
- Iida, N. Effects of vasomotion and venous pressure elevation on capillary-tissue fluid exchange across heteroporous membrane. *Biorheology.* **27** : 205-224 (1990).
- Intaglietta, M., and E.P. de Plomb. Fluid exchange in tunnel and tube capillaries. *Microvascular Research.* **6** : 153-168 (1973).
- Intaglietta, M., and B.A. Endrich. Experimental and quantitative analysis of microcirculatory water exchange. *Acta. Physiol. Scand. Suppl.* **463** : 59-66 (1979).
- Katz, M.A., and R.C. Schaeffer. Convection of macromolecules is the dominant mode of transport across horizontal 0.4 and 0.3 μm filters in diffusion chambers : significance for biologic monolayer permeability assessment. *Microvascular Research.* **41** : 149-163 (1991).

- Klitzman, B., and P.C. Johnson. Capillary network geometry and red cell distribution in hamster cremaster muscle. *Am. J. Physiol.* **11** : H211-H219 (1982).
- Krogh, A. The number and distribution of capillaries in muscles with calculation of the oxygen pressure head necessary for supplying the tissue. *J. Physiol. (London)*. **52** : 409-415 (1919).
- Landis, E.M. Microinjection studies of capillary permeability II. The relationship between capillary pressure and the rate at which fluid passes through the walls of single capillaries. *Am. J. Physiol.* **82** : 217-238 (1927).
- Lanir, Y. Constitutive equations for fibrous connective tissues. *J. Biomechanics*. **16** : 1-12 (1983).
- Laurent, T.C. Structure, function and turnover of the extracellular matrix. *Adv. Microcirc.* **13** : 13-34 (1987).
- Levick, J.R. Flow through interstitium and other fibrous matrices. *Quart. J. Exp. Physiol.* **72** : 409-438 (1987).
- Lund, T., J.L. Bert, H. Onarheim, B.D. Bowen, and R.K. Reed. Microvascular exchange during burn injury. I : A review. *Circulatory Shock*. **28** : 179-197 (1989).
- Manning, R., and A.C. Guyton. Effects off hypoproteinemia on fluid volumes and arterial pressure. *Am. J. Physiol.* **245** : H285-H293 (1983).
- Mortillaro, N.A., and A.E. Taylor. Interaction of capillary and tissue forces in the cat small intestine. *Circulation Research*. **39** : 348-358 (1976).
- Ogston, A.G., and C.C. Michel. General descriptions of passive transport of neutral solute and solvent through membranes. *Prog. Biophys. Molec. Biol.* **34** : 197-217 (1978).
- Orbach, O., and C.M. Crowe. Convergence promotion in the simulation of chemical processes with recycle - the dominant eigenvalue method. *C.J.Ch.E.* **49** : 509-513 (1971).
- Patlak, C.S., D.A. Goldstein, and J.F. Hoffman. The flow of solute and solvent across a two-membrane system. *J. Theoret. Biol.* **5** : 426-442 (1963).
- Press, W.H., B.P. Flannery, S.A. Teukolsky, and W.T. Vetterling. Numerical Recipes - The art of scientific computing. Cambridge University Press. Cambridge (1986).
- Renkin, E.M. Some consequences of capillary permeability to macromolecules : Starling's hypothesis reconsidered. *Am. J. Physiol.* **250** : H706-H710 (1986).

- Richtmyer, R.D., and K.W. Morton. Difference methods for initial-value problems. (2nd Ed.) Interscience. N.Y. (1967).
- Salathe, E.P., and K.N. An. A mathematical analysis of fluid movement across capillary walls. *Microvascular Research*. **11** : 1-23 (1976).
- Salathe, E.P., and R. Venkataraman. Role of extravascular protein in capillary-tissue exchange. *Am. J. Physiol.* **234** : H52-H58 (1978).
- Schmidt-Schonbein, G.W. Microlymphatics and lymph flow. *Physiological Reviews*. **70**(4) October 1990.
- Silberberg, A. Structure of the interendothelial cell cleft. *Biorheology*. **25** : 303-318 (1988).
- Smith, L. Transport phenomena in porous media : Geological Sciences 564 course notes. University of British Columbia. (1990).
- Sorbie, K.S. Depleted layer effects in polymer flow through porous media. I. Single capillary calculations. *J. Colloid Interface Sci.* **139** : 299-323 (1990).
- Sorbie, K.S., and Y. Huang. Rheological and transport in the flow of low concentration xanthan solution through porous media. *J. Colloid Interface Sci.* **145** : 74-89 (1991).
- Starling, E.H. On the absorption of fluid from the connective tissue spaces. *J. Physiol. (London)*. **19** : 312-326 (1896).
- Taylor, A., W. Gibson, H. Granger, and A.C. Guyton. The interaction between intracapillary forces in the overall regulation of interstitial fluid volume. *Lymphology*. **6** : 192-208 (1973).
- Taylor, A.E., and M.I. Townsley. Evaluation of the Starling fluid flux equation. NIPS Volume 2/April : 48-52 (1987).
- Taylor, D.G. A mathematical model of interstitial transport. Ph.D. thesis. Department of Chemical Engineering. The University of British Columbia. (1990a).
- Taylor, D.G., J.L. Bert, and B.D. Bowen. A mathematical model of interstitial transport. I. Theory. *Microvascular Research*. **39** : 253-278 (1990b).
- Taylor, D.G., J.L. Bert, and B.D. Bowen. A mathematical model of interstitial transport. II. Microvascular exchange in mesentery. *Microvascular Research*. **39** : 279-306 (1990c).
- Wiederhielm, C.A. Dynamics of capillary fluid exchange : A nonlinear computer simulation. *Microvascular Research*. **18** : 48-82 (1979).

- Yu, C.-C., and J.C. Heinrich. Petrov-Galerkin methods for the time-dependent convective-transport equation. *Int. J. Num. Meth. Eng.* **23** : 883-901 (1986).
- Yu, C.-C., and J.C. Heinrich. Petrov-Galerkin method for multidimensional, time-dependent, convective-diffusion equations. *Int. J. Num. Meth. Eng.* **24** : 2201-2215 (1987).

Appendices

Appendix A : The Finite Element Method and the Petrov-Galerkin Method.

Appendix B : Solution algorithm and under-relaxation technique.

Appendix C : Program Listing.

Appendix A : The Finite Element Method and the Petrov-Galerkin Upwinding Method.

A.1 The Galerkin Finite Element Method

In this section, a brief introduction of the basic theory of the Galerkin finite element method will be presented. The Galerkin finite element method applies the method of weighted residuals (MWR). The general procedure for implementing the finite element method is presented by applying the method to two-dimensional transient solute transport equation in rectangular coordinates . The treatment the equivalent equation in cylindrical coordinates will then be discussed. A detailed introduction of the finite element method may be found in Bickford (1990).

The two dimensional transient solute transport equation, an elliptic partial differential equation, is stated as follows :

$$\frac{\partial u}{\partial t} + v_x \frac{\partial u}{\partial x} + v_y \frac{\partial u}{\partial y} = D \left(\frac{\partial^2 u}{\partial x^2} + \frac{\partial^2 u}{\partial y^2} \right) + f(u, x, y) \quad \text{in } \Omega \quad (\text{A.1})$$

$$u = g(s) \quad \text{on } L_1 \quad (\text{A.2})$$

$$\frac{\partial u}{\partial n} + a(s)u = h(s) \quad \text{on } L_2 \quad (\text{A.3})$$

where u is the unknown variable which is sought and $f(x,y)$ is an arbitrary function prescribed within the solution domain Ω . The first and second terms are the temporal and

convective terms respectively. The third term is the diffusive-dispersive component and the last term may be considered as a source term. The essential boundary conditions (Dirichlet boundary condition) are specified at the boundary segment L_1 . The natural boundary conditions (Robins boundary condition) are specified along the boundary segments L_2 . If $a(s)$ is set to zero, then this is referred to as a Neumann boundary condition. The general geometry of the problem is described in Figure (A.1).

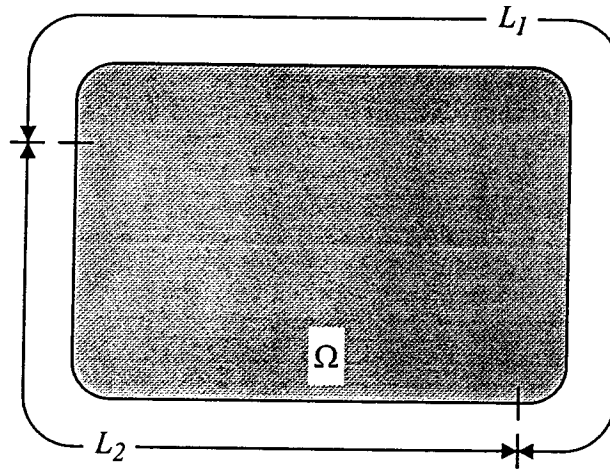


Figure A.1: General description of elliptic boundary value problem.

The general procedure for implementing the finite element method can be approached in five steps (Bickford, 1990) : 1) discretization, 2) interpolation, 3) weak formulation, 4) formation of elemental matrices, 5) solution of resulting algebraic equation.

Discretization

The finite element method, like the finite difference method, approximates the solute of the differential equation at a finite set of point (or nodes) in the solute domain. The objective of these methods is to set up an approximate algebraic form of the differential equation at each node. It is required that the position of nodes be chosen (discretization)

within the solution domain. In the finite element method, the differential equation is satisfied locally within subregions called elements. There is then a requirement that at the boundary of two elements, for instance, the differential equation is satisfied for both elements and at the mutual boundary. At the absolute boundary of the solution domain, the boundary conditions (A.2) and (A.3) have to be satisfied. A typical discretization for the geometry above is displayed in Figure (A.2).

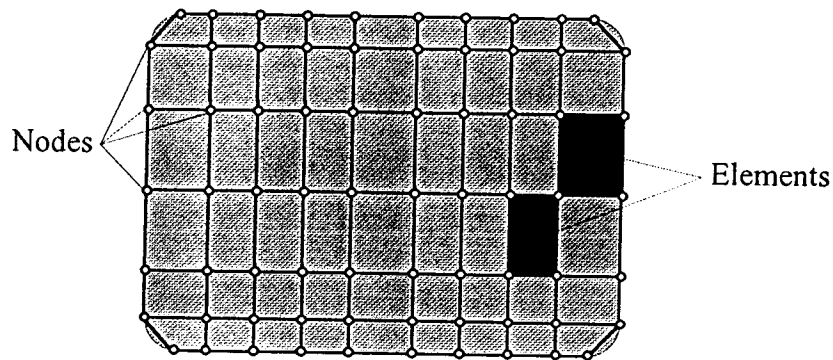


Figure A.2: Discretized geometry using linearly interpolated rectangular elements.

The region is discretized using linearly interpolated rectangular elements. This means that curved boundaries have to be approximated with straight line segments. This introduces an inherent approximation error into the formulation. More nodes are placed within regions expecting relatively high gradients.

The elements are constructed from any number of nodes (> 3 for two-dimensional problems). For linearly interpolated elements, three node elements are known as triangular elements whereas four node elements are known as rectangular elements. With additional nodes within an element, say eight in a rectangular element, the degree of accuracy increases and the element boundary may follow a quadratic function shape. For this work, linearly interpolated rectangular elements were used.

Interpolation

The solution at any particular location within each element is approximated by an interpolation scheme using the values of the solution at the nodes. The linear interpolation functions are the simplest to implement. This can be visualized as a plane (the solution surface) above the element. This is shown in Figure (A.3).

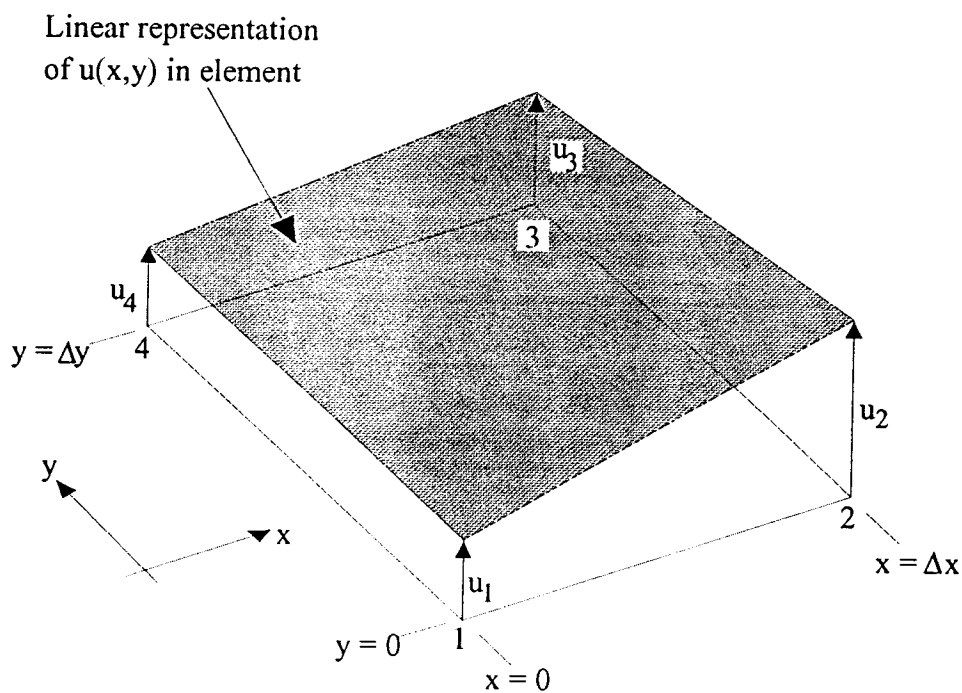


Figure A.3: Rectangular element with linear interpolation.

The approximation to the solution within the element, $u_e(x,y)$, is expressed mathematically (Yu and Heinrich, 1987) as :

$$u_e(x,y) = \sum_{i=1}^4 n_i u_i \quad (\text{A.4})$$

where u_i is the solution value at node i and n_i is the interpolation function (also known as the shape or trial function) of node i . For the space trial functions defined over the element region $0 \leq x \leq \Delta x$, $0 \leq y \leq \Delta y$, the interpolation functions are given by (Yu and Heinrich, 1987) :

$$\begin{aligned} n_1(x, y) &= t_1(x)t_2(y) \\ n_2(x, y) &= t_2(x)t_1(y) \\ n_3(x, y) &= t_2(x)t_1(y) \\ n_4(x, y) &= t_1(x)t_2(y) \end{aligned} \tag{A.5}$$

where the numbers refer to the nodes in Figure (A.3) and the functions $t_i(\cdot)$ is the interpolation function along the boundary for each node and are given by :

$$\begin{aligned} t_1(z) &= \left(1 - \frac{z}{\Delta z}\right) \\ t_2(z) &= \frac{z}{\Delta z} \end{aligned} \tag{A.6}$$

It is here that linear interpolation is being used to define the variation of the unknown variable, u , within the element. If more nodes are placed within the element, then higher order interpolation functions may be used.

Weak formulation

The weak formulation is found by first multiplying the differential equation by an appropriate test function, $w(x, y)$, and then integrating it over the solution domain :

$$\iint_{\Omega} w(x,y) \left[\frac{\partial u}{\partial t} + v_x \frac{\partial u}{\partial x} + v_y \frac{\partial u}{\partial y} - D \left(\frac{\partial^2 u}{\partial x^2} + \frac{\partial^2 u}{\partial y^2} \right) - f(u,x,y) \right] d\Omega = 0 \quad (\text{A.7})$$

This equation satisfies the differential in an average sense within the solution region. It does not require that the differential equation be satisfied exactly at every point. In this manner, equation (A.7) is a weaker statement of the problem than equation (A.1). The test function is any arbitrary continuous function since at the solution, the term in the square brackets vanishes. However, the test function must hold to the property that it vanishes on L_1 , i.e., the portion of the boundary at which essential boundary conditions apply. From Green's first identity (the two-dimensional form of the divergence theorem), we have (Bickford, 1990) :

$$\iint_{\Omega} w \left(\frac{\partial^2 u}{\partial x^2} + \frac{\partial^2 u}{\partial y^2} \right) d\Omega = \int_L w \frac{\partial u}{\partial n} ds - \iint_{\Omega} w \left(\frac{\partial w}{\partial x} \frac{\partial u}{\partial x} + \frac{\partial w}{\partial y} \frac{\partial u}{\partial y} \right) d\Omega \quad (\text{A.8})$$

where n is the outward pointing normal and L is the line segment bounding the region. Substituting equation (A.8) into equation (A.7) gives :

$$\begin{aligned} \iint_{\Omega} w \frac{\partial u}{\partial t} d\Omega + \iint_{\Omega} w \left(v_x \frac{\partial u}{\partial x} + v_y \frac{\partial u}{\partial y} \right) d\Omega + \\ D \iint_{\Omega} \left(\frac{\partial w}{\partial x} \frac{\partial u}{\partial x} + \frac{\partial w}{\partial y} \frac{\partial u}{\partial y} \right) d\Omega = \int_L w \frac{\partial u}{\partial n} ds + \iint_{\Omega} w f d\Omega \end{aligned} \quad (\text{A.9})$$

The bounding segment, L , is composed of the two segments L_1 and L_2 . Since the test function vanishes on L_1 then the first term on the right hand side in equation (A.9) only applies about the line segment L_2 . The imposed boundary condition, equation (A.3) may then be substituted into equation (A.9) resulting in :

$$\iint_{\Omega} w \frac{\partial u}{\partial t} d\Omega + \iint_{\Omega} w \left(v_x \frac{\partial u}{\partial x} + v_y \frac{\partial u}{\partial y} \right) d\Omega +$$

$$D \iint_{\Omega} \left(\frac{\partial w}{\partial x} \frac{\partial u}{\partial x} + \frac{\partial w}{\partial y} \frac{\partial u}{\partial y} \right) d\Omega = \int_{L_2} w (h(s) - a(s)u) ds + \iint_{\Omega} wf d\Omega \quad (\text{A.10})$$

or

$$\iint_{\Omega} w \frac{\partial u}{\partial t} d\Omega + \iint_{\Omega} w \left(v_x \frac{\partial u}{\partial x} + v_y \frac{\partial u}{\partial y} \right) d\Omega +$$

$$D \iint_{\Omega} \left(\frac{\partial w}{\partial x} \frac{\partial u}{\partial x} + \frac{\partial w}{\partial y} \frac{\partial u}{\partial y} \right) d\Omega + \int_{L_2} w a u ds = \int_{L_2} w h ds + \iint_{\Omega} wf d\Omega \quad (\text{A.11})$$

This is the final weak form of the differential equation. It includes the natural boundary conditions that may exist if there are any natural boundary conditions on the boundary. Using the appropriate interpolation functions for the variable u and test functions, w , it is possible to generate a set of algebraic equations describing the system. This is performed in the next section.

Formation of elemental matrices

The unknown variable u is approximated by equation (A.4). This may be rewritten in matrix notation as :

$$u_e(x, y) = \sum_{i=1}^4 n_i u_i = U_e^T N = N^T U_e \quad (\text{A.12})$$

In the Galerkin method, the test function is taken to be the same as the unknown variable, thus equation (A.11) becomes :

$$\begin{aligned} \iint_{\Omega} u \frac{\partial u}{\partial t} d\Omega + \iint_{\Omega} u \left(v_x \frac{\partial u}{\partial x} + v_y \frac{\partial u}{\partial y} \right) d\Omega + \\ D \iint_{\Omega} \left(\frac{\partial u}{\partial x} \right)^2 + \left(\frac{\partial u}{\partial y} \right)^2 d\Omega + \int_{L_2} a u^2 ds = \int_{L_2} u h ds + \iint_{\Omega} u f d\Omega \end{aligned} \quad (\text{A.13})$$

Substitution of the interpolated approximations, equation (A.12), into equation (A.13) yields the following discrete form :

$$\begin{aligned} \iint_{\Omega} U_e^T N \frac{\partial N^T}{\partial t} U_e d\Omega + \iint_{\Omega} U_e^T N \left(v_x \frac{\partial N^T}{\partial x} + v_y \frac{\partial N^T}{\partial y} \right) U_e d\Omega + \\ D \iint_{\Omega} \left(U_e^T \frac{\partial N}{\partial x} \frac{\partial N^T}{\partial x} U_e + U_e^T \frac{\partial N}{\partial y} \frac{\partial N^T}{\partial y} U_e \right) d\Omega + \\ \int_{L_2} U_e^T N a N^T U_e ds = \int_{L_2} U_e^T N h ds + \iint_{\Omega} U_e^T N f d\Omega \end{aligned} \quad (\text{A.14})$$

The unknown variable, U_e , may be taken outside of the integrals resulting in a system of four equations for each node in an element. This is written as :

$$\begin{aligned} \left[\iint_{\Omega} N \frac{\partial N^T}{\partial t} d\Omega + \iint_{\Omega} N \left(v_x \frac{\partial N^T}{\partial x} + v_y \frac{\partial N^T}{\partial y} \right) d\Omega + \right. \\ \left. D \iint_{\Omega} \left(\frac{\partial N}{\partial x} \frac{\partial N^T}{\partial x} + \frac{\partial N}{\partial y} \frac{\partial N^T}{\partial y} \right) d\Omega + \int_{L_2} N a N^T ds \right] U_e = \\ \int_{L_2} N h ds + \iint_{\Omega} N f d\Omega \end{aligned} \quad (\text{A.15})$$

The function f can be approximated by its interpolant within the element, i.e.,

$$f = N^T F \quad (\text{A.16})$$

Also, $a(s)$ and $h(s)$ may be approximated by their linear interpolants along the boundary segments, i.e.,

$$\begin{aligned} a &= a_i n_i + a_j n_j = N^T A \\ h &= h_i n_i + h_j n_j = N^T H \end{aligned} \quad (\text{A.17})$$

where nodes i and j are along the boundary segment. These approximations may be substituted into equation (A.15) to give :

$$\begin{aligned} & \left[\iint_{\Omega} N \frac{\partial N^T}{\partial t} d\Omega + \iint_{\Omega} N \left(v_x \frac{\partial N^T}{\partial x} + v_y \frac{\partial N^T}{\partial y} \right) d\Omega + \right. \\ & \quad \left. D \iint_{\Omega} \left(\frac{\partial N}{\partial x} \frac{\partial N^T}{\partial x} + \frac{\partial N}{\partial y} \frac{\partial N^T}{\partial y} \right) d\Omega + \int_L NN^T AN^T ds \right] U_e = \\ & \quad \int_L NN^T H ds + \iint_{\Omega} NN^T F d\Omega \end{aligned} \quad (\text{A.18})$$

or

$$[T_e] \dot{U}_e + [C_e + K_e + A_e] U_e = [F_e + H_e] \quad (\text{A.19})$$

where T_e , C_e , K_e , and A_e are the temporal matrix, convective, stiffness, and natural boundary condition matrices respectively. F_e and H_e are the load and natural boundary condition vectors respectively. The dot signifies the time derivative of the unknown variable. The

integration of the interpolation functions in equation (A.18) is handled easily by a Gauss quadrature method (Press *et al.*, 1986).

The temporal derivative may be handled by a finite difference backward or Crank-Nicolson method. If a backward difference method is used, then (A.19) is rewritten as :

$$\left[\frac{T_e}{\Delta t} + C_e + K_e + A_e \right] U_e^{t+\Delta t} = \left[\frac{T_e}{\Delta t} U_e^t + F_e + H_e \right] \quad (\text{A.20})$$

The unknown variable may be evaluated from this equation for the nodes within an element. However, since each node may have communication with other nodes outside the particular element, then the equations have to be solved simultaneously for all other elements. For four-node, rectangular elements, each node will be in communication with four nodes. This is displayed schematically in Figure (A.4).

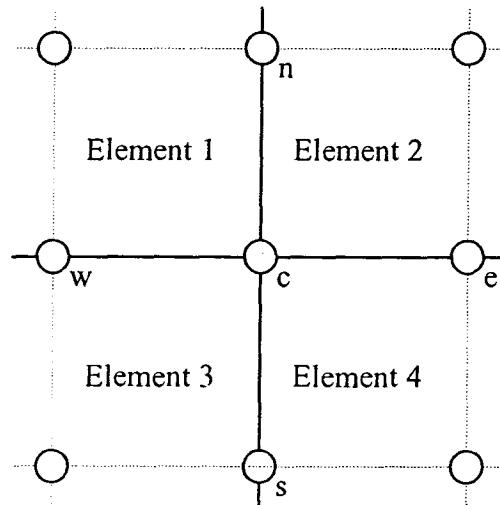


Figure A.4: Node communication.

This means that the center node *c* will form four separate equations with the four elements 1, 2, 3, and 4. Each equation will form elemental entries which apply globally to the entire

system and thus they are incorporated into a global stiffness matrix. In this manner, the global stiffness equations are formed from the sum of the elemental matrices :

$$[K_G]U_G^{t+\Delta t} = Q_G^t \quad (\text{A.21})$$

where

$$K_G = \sum_{\text{elements}} \left(\frac{T_e}{\Delta t} + C_e + K_e \right) + \sum_{\substack{\text{elements on} \\ \text{boundary} \\ \text{segments}}} A_e \quad (\text{A.22})$$

and

$$Q_G^t = \sum_{\text{elements}} \left(\frac{T_e}{\Delta t} U_e^t + F_e \right) + \sum_{\substack{\text{elements on} \\ \text{boundary} \\ \text{segments}}} H_e \quad (\text{A.23})$$

Solution of the resulting algebraic equations

The system of equations described in equation (A.20) may be solved using any of the direct or iterative system of equations solvers (Press *et al.*, 1986; Bickford, 1990). For this work, a banded direct method solver (Gauss-Jordan elimination) was used.

Natural boundary conditions are automatically dealt with in the Galerkin finite element method. Essential boundary conditions have to be implemented separately. Since the value of u is known at the boundary segment for an essential boundary condition, then the equation associated with this node may be eliminated and the global stiffness matrices adjusted to reflect this change. On the other hand, the equation may be retained but manipulated such that it solves for the specified boundary value. This is discussed further in Smith, 1990.

Cylindrical Geometry and Variable Properties

The problem for cylindrical geometry can be handled in a similar manner to the above formulation for rectangular coordinates. Deriving the problem in cylindrical coordinates introduces an additional term :

$$\frac{1}{r} \frac{\partial u}{\partial r}$$

which can be simply treated as a convective-like term in the formulation. This is similar to the situation with spatially variant properties. As can be seen from equation (4.8), this introduces two convective-like terms into the formulation.

A.2 The Petrov-Galerkin Upwinding Method

It was found that the straight-forward Galerkin finite element method was insufficient to solve the solute transport problem due to the high convection within the system. The dominance of the convective terms alter the nature of the differential equation from that of elliptic to that of hyperbolic-like. Its effect was observed in the form of 'wiggles' and large scale oscillations in the calculated solutions. Convective dominance produces large gradients in the solution which can only be dealt with by making the finite element mesh very fine or by implementing an upwinding method. Upwinding techniques have been the most popular method employed for convection dominated finite difference problems (Richtmyer and Morton, 1967).

The upwinding formalism developed by Yu and Heinrich (1986) is used in this work. This is largely based on the streamline upwinding technique first implemented by Brooks

and Hughes (1982). Artificial diffusion is added in the direction of flow. The method will simply be presented here. Detailed theoretical justification of the Petrov-Galerkin upwinding formulation may be found elsewhere (Brooks and Hughes, 1982; Yu and Heinrich, 1986; Donea, 1984).

The upwinding technique is implemented as a modification of the weighting function of the convective term. This modified weighting function vanishes for the other terms and so can be applied to all terms thus defining a consistent finite element formulation. The weighting functions are considered to be of the form :

$$w_i = n_i + p_i \quad (\text{A.24})$$

where n are the interpolation functions given by equation (A.5) and p is a perturbation function that adds the appropriate amount of artificial diffusion. Yu and Heinrich (1987) give the perturbation function as :

$$p_i = \alpha \frac{h}{2\|v\|} \left(v_x \frac{\partial n_i}{\partial x} + v_y \frac{\partial n_i}{\partial y} \right) \quad (\text{A.25})$$

where h is a characteristic element length, α is a parameter which optimizes the size of the perturbation function, and $\|v\|$ is the Euclidean norm of the average velocity in the element. Equation (A.25) represents additional anisotropic diffusion added to the convective term of the solute transport equation of the form :

$$\frac{\alpha v h}{2} \frac{\partial^2 u}{\partial \zeta^2}$$

where ζ is the coordinate in the flow direction. This can be arrived at by substituting the weighting function in equation (A.24) into the finite element equation (A.18). The optimal value of the parameter α has been found to be given by (Yu and Heinrich, 1987) as :

$$\alpha = \coth\left(\frac{\gamma}{2}\right) - \frac{2}{\gamma} \quad (\text{A.26})$$

where γ is defined for each element as :

$$\gamma = \frac{\|v\|h}{D} \quad (\text{A.27})$$

where D is the local diffusion coefficient. The characteristic element length for rectangular finite elements is given by (Yu and Heinrich, 1987) :

$$h = \frac{1}{\|v\|} (|v_x|\Delta x + |v_y|\Delta y) \quad (\text{A.28})$$

where Δx and Δy are shown in Figure (A.3).

The perturbed weighting functions are easily incorporated into the program and integrated along with the other terms in the finite element equation (A.18). The upwinding routines incorporated into the program constructed for this work were tested successfully against the examples provided in Yu and Heinrich (1987).

Appendix B : The solution algorithm and under-relaxation scheme.

B.1 The Solution Algorithm

The solution algorithm is presented in Table (B.1). The convergence tolerance was set as 10^{-6} for both the solute concentrations and the hydrostatic pressures. If the problem did not converge within 100 iterations, the procedure was terminated.

Table B.1: Overall solution algorithm.

	Step
0.	Set initial estimates for the solute concentrations and hydrostatic pressures within the tissue space.
1.	Calculate the colloid osmotic pressure throughout the interstitium.
2.	Obtain the tissue potential by solving the fluid conservation equation using the hydrostatic pressures for the sink drainage term.
3.	Evaluate the fluid velocities within the tissue and across the capillary wall.
4.	Calculate the hydrostatic pressure distribution throughout the interstitium.
5.	Obtain the solute concentrations by solving the solute transport equation throughout the tissue space. Use the last estimates of the solute concentrations for the sink drainage term.
6.	Compare the solute concentrations and hydrostatic pressures from the previous estimates and if they differ by less than the tolerance, then the procedure is complete and this time step is complete. If not, go to step 1. and repeat the process.

This procedure has to be repeated for each time step. The initial guess of the values at the following time step may be estimated from the first two terms of the Taylor's series expansion :

$$u^{t+\Delta t} \cong u^t + \Delta t \frac{\partial u}{\partial t} \quad (\text{B.1})$$

where u may be the solute concentrations or the hydrostatic pressures. This provides a rough estimate of the variable at the next time step. This is not very efficient at the first few time steps since the estimate of the temporal derivative is not very good. At later times when a good estimate of the time derivative has been evaluated, equation (B.1) accelerates the process to steady-state.

If the hydrostatic pressure in the capillary is not assumed linear, then the solution of the fluid conservation equation, equation (3.6), coupled with Starling's hypothesis, equation (3.33), has to be performed iteratively. This is because the the capillary hydrostatic pressure is required as a known value in the Starling hypothesis for the membrane boundary condition for the solution of the fluid conservation equation. On the other hand, the capillary pressure is a function of the tissue-side membrane hydrostatic pressure and requires its value for the solution of the capillary hydrostatic pressure. The solution algorithm used for this work is listed in Table (B.2).

Table B.2: Capillary hydrostatic pressure-tissue hydrostatic pressure solution algorithm.

	Step
1.	Using prior estimates of the tissue-side (from the last time step or overall iteration), solve for the capillary hydrostatic pressure using equation (3.36).
2.	Using the newly evaluated capillary hydrostatic pressure, solve for the tissue hydrostatic pressure distribution obtained from the solution of the fluid conservation equation.
3.	Repeat steps 1. and 2. until the tissue-side membrane hydrostatic pressures are less than the specified tolerance.

If the solute concentration is allowed to vary down the capillary, the identical solution is adopted as above for the capillary and tissue hydrostatic pressures. Here the solute transport equation and Patlak equation have to be satisfied as well as the solute depletion or addition to the capillary.

B.2 The Under-relaxation technique

The fluid conservation and solute transport equation are coupled due to the colloid osmotic pressure. The osmotic pressure is a non-linear function of the solute concentration. This can cause problems for successful convergence and so an under-relaxation method was adopted to attempt to ensure convergence if possible. The technique used was the dominant eigenvalue method suggested by Orback and Crowe (1971). This method often accelerates the convergence of the problem. The method is presented as follows. At two consecutive iterations k and $k+1$, the change in the solution may be given by the vectors du^k and du^{k+1} . The general variable u may be the solute concentrations or hydrostatic pressures. The vector du^{k+1} , for example, is evaluated as the difference in the solution between the k and $(k+1)$ st iterations. The general dominant eigenvalue method of Orbach and Crowe (1971) suggests that the dominant eigenvalues of the solution matrix can be roughly estimated from these consecutive differences :

$$\Lambda_i = \frac{du_i^{k+1}}{du_i^k} \quad (\text{B.2})$$

where Λ_i are the estimated eigenvalues. The relaxation factors are then calculated from :

$$\omega_i = \frac{1}{1 - \Lambda_i} \quad (\text{B.3})$$

and the accelerated solution evaluated from :

$$\hat{u}_i^{k+1} = (1 - \omega_i)u_i^{k+1} + \omega_i u_i^k \quad (\text{B.4})$$

This solution is then used in the next iteration. As the residual difference between the iterations diminishes as convergence is achieved, the eigenvalues approach zero and thus the relaxation parameters approach unity. This acceleration procedure was implemented in the program constructed as part of this work.

Appendix C : Program Listing.

The program constructed was written in C and run on both an IBM 3090 using the Metaware High C compiler and then on a IBM RS/6000 using the standard IBM C compiler supplied with the unit.

```

/*
    ***** M V E . C

    AXISYMMETRIC PROBLEM - SOLVES 2D ADVECTIVE DISPERSION
    EQUATION TRANSIENTLY IN POROUS MEDIA USING THE PETROV-
    GALERKIN FINITE ELEMENT METHOD OSMOTIC PRESSURE
    EFFECTS TAKEN INTO ACCOUNT.

    THE ARGUMENTS TO THIS PROGRAM ARE AS FOLLOWS :

    mve cvpd b l

    WHERE :

        c IS THE CONCENTRATION OUTPUT RESULTS
        v IS THE VELOCITY FIELD OUTPUT RESULTS
        p IS THE PRESSURE OUTPUT RESULTS
        d IS THE PECLET OUTPUT RESULTS
        b IS THE CAPILLARY PRESSURE RESULTS FILE NAME
        l IS THE LOG FILE NAME

        cvpd IS A SINGLE FILE

    WRITTEN BY IAN GATES
    CHEMICAL ENGINEERING
    UNIVERSITY OF BRITISH COLUMBIA
    MAY 1992
*/

#include <stdio.h>
#include <stdlib.h>
#include <math.h>
#include <float.h>
#define I int
#define F float
#define D double
#define C char
#define V void
#define PI 3.14159265352
#define PI2 6.28318530704
/*
    PROGRAM CONSTANTS :

    NM : NUMBER OF NODES
    EM : NUMBER ELEMENTS
    MM : NUMBER OF NODES ABOUT DOMAIN PERIMETER (ON BOUNDARIES)
    IM : NUMBER OF NODES ON CAPILLARY WALL (>nz)
    NJ : NUMBER OF COMMUNICATION INTERVALS ALONG CAPILLARY WALL (>IM)
    HM : NUMBER OF ODE'S TO SOLVE IN BVP SOLVER (DO NOT ADJUST)
    RW : NUMBER OF NODES IN R DIRECTION FOR RESULTS
    ZW : NUMBER OF NODES IN Z DIRECTION FOR RESULTS
*/
#define NM 615
#define EM 545
#define MM 280
#define IM 65
#define NJ 103

```

```

#define HM 4
#define RW 25
#define ZW 105

/*
   DEFINED DATA STRUCTURES
*/

typedef struct {
    I error, nf, k;
    D err, t, x[HM], tt[NJ], xx[NJ]; } M;
typedef struct {
    I iter;
    D p[NM], r[NM], z[NM], pt[NM], pcap[IM], qcap[IM]; } N;
typedef struct {
    I iter;
    D c[NM], ccap[IM], ctis[IM], fmem[IM], mpe[IM]; } O;
typedef struct {
    D m[NM][NM], v[NM]; } U;
typedef struct {
    I typ_lp, mmod[IM];
    D asq, c_art, sigma, pi_cap, ps, ps_d, diff,
      lp0, lpl, lref, cref, pref, wall_th, wall_th_d,
      r[IM], z[IM], hp[IM], op[IM], vm[IM], cp[IM], ct[IM]; } membr;
typedef struct {
    I osm;
    D mu, rho, por, hind, ls, vol_tis, alfl, alft, diff, sigmag,
      plymph, jo, fex, fst, fav, fs, fim, lref, cref, pref, kref,
      hi_k, lo_k; } media;
typedef struct {
    D q[NJ], r[NJ], s[NJ]; } vec3;
typedef struct {
    D rr[NM], rz[NM], zz[NM]; } vdiff;
typedef struct {
    D v[6]; } W;

/*
   GENERAL DATA CHECKING ROUTINES
*/

I safechk(I, I, I, I, I, I);
I datachk(I*);

/*
   FINITE ELEMENT STIFFNESS MATRICES ROUTINES
*/

D* stif(I, I, I, I, D*, D*, I*, D*, D*, D*, D*, D*, D*, D*, D*, D, I, I, I, I);

/*
   MODIFY STIFFNESS ROUTINE FOR BC'S
*/

U modstif(I, I*, D*, D*, I*, D*, D*, I*, I*, D*, D*, D*, I, I);

/*
   DIFFUSION AND DISPERSION MATRICES
*/

vdiff dspc(I, D, D, D, D*, D*, I);

/*
   FLUID PRESSURE AND VELOCITY ROUTINES
*/

N itpruruz2d(I, I, I, I, I, I, I, I, I, media, membr, I*, I*, D*, D*, D*, D*,
  D*, D*, I*, D*, I*, I*, D*, D*, I*, I*, I*, D, D, D, D, I, I, I, I);
D *cmpd(I, membr, D, D);
D *mempr(membr, D, D*, D, D);

/*
   SOLUTE CONCENTRATION ROUTINES
*/

O itcscap2d(I, I, I, I, I, I, I, I, I, media, membr, I*, D*, D*, D*, D*,
  D*, D*, D*, D*, D*, D*, I*, D*, I*, I*, D*, D*, I*, I*, I*,
  D, D, I, I, I, I);
D *cmcd(I, membr);
D *memcs(membr, D, D*, D, D, D);

/*
   USER DEFINED lp() FUNCTION.

```

```

*/
D lp(I, D, D, D);
/*
    MASS BALANCE
*/
V massb(I, I, I, I, media, membr, I*, I*, D*, D*, D*, D*, D*, D, D, I, I);
/*
    AVERAGE QUANTITIES FOR SOLUTION DOMAIN
*/
V domavg(I, media, I*, D*, D*, D*, D*, I, I);
/*
    COLLOID OSMOTIC PRESSURE ROUTINE
*/
D *osmopr(I, media, D*);
/*
    ODE AND BVP SOLVER ROUTINES (PRED-CORR ODE SOLVER)
*/
M pdcr(I, membr, D*, D, D, I, vec3, vec3, vec3, I, I);
D *rk4(I, membr, D, D, D*, D, D, D, I);
/*
    CUBIC SPLINE ROUTINES
*/
vec3 fspl(I, D*, D*, I, I, D, D);
D *tridiag(I, D*, D*, D*, D*);
D evalcs(I, vec3, D*, D*, D);
D devalcs(I, vec3, D*, D);
D d2evalcs(I, vec3, D*, D);
D ddpoly(D*, D*);
/*
    MATH FUNCTION ROUTINES
*/
D sq(D x)
    { x *= x; return x; }
D norm(D x, D y)
    { D z = sqrt(sq(x)+sq(y)); return z; }
D coth(D x)
{
    D q1, q2;
    if (x == 0.0) {
        puts(" E: coth()-> Domain error.\n");
        exit(0); }
    if (fabs(x) > 10.0)
        { x = 1.0; }
    else {
        q1 = exp(x);
        q2 = exp(-x);
        if (q1 != q2)
            { x = (q1+q2)/(q1-q2); }
        else
            { x = 1.0/x; } }
    return x;
}
/*
    DATA RECORDING ROUTINES
*/
V outdata(I, I, I, I, I, I, I*, I*, F*, F*, D*, D*, D*, D*, I, D, C*, D*, FILE*);
V outuv2d(I, I, I, I, I, I, I*, I*, F*, F*, D*, D*, D*, D*, I, D, C*, D*, D*, FILE*);
V outcoll(I, I, I, D, D*, D*, D*, C*, FILE*);
V outcapp(I, I, D, D*, D*, D*, D*, D*, D*, D*, C*, FILE*);
V contour(I, I, I, I, I, D*, D, C*, FILE*);
V header(D, D, D, membr, media, FILE*);
/*
    MATRIX ROUTINES AND ITERATIVE SOLVERS
*/

```

```

D *solver(I, I, D*, D*);
D *matvecbw(I, I, I, D*, D*);

/*
    ELEMENTAL STIFFNESS MATRIX INTEGRATION AND CONSTRUCTION ROUTINES
*/

D l1(D, D);
D l2(D, D);
D l3(D, D);
D dl1(D, D);
D dl2(D, D);
D dl3(D, D);
D d2l1(D, D);
D d2l2(D, D);
D d2l3(D, D);
W fmrzt(D, D, D, D);
W fmrzt(D, D, D, D);
W fwrzt(D, W, W, W, W, W);
W fdndr(D, D, D, D);
W fdndz(D, D, D, D);
W fdmdr(D, D, D, D);
W fdmdz(D, D, D, D);
W fd2mdr2(D, D, D, D);
W fd2mdrdz(D, D, D, D);
W fd2mdz2(D, D, D, D);
W fd3mdr2dz(D, D, D, D);
W fd3mdrdz2(D, D, D, D);
D gw(I, I);
D gp(I, I);
D gw2(I);
D gw3(I);
D gw4(I);
D gw6(I);
D gw8(I);
D gw16(I);
D gp2(I);
D gp3(I);
D gp4(I);
D gp6(I);
D gp8(I);
D gp16(I);

/*
    M A I N ( )
    READS IN DATA AND IMPLEMENTS SOLUTIONS OF EQUATIONS AT EACH
    TIME STEP. RECORDS CONVERGED SOLUTION INTO A TEMPORARY FILE
    IN CASE OF SYSTEM SHUTDOWN.
*/

main(I argc, C *argv[])
(
    I i, j, k, l, m, n, ii, jj, bw, cdt, ndt, ict, crz, disp, doitpr,
    ic=1, irec, geom, ihof, ndnm, ndnmout, elnm,
    nncbc, necbc, nnpbc, nepbc, nesink, nrec, nr, nz,
    nrout, nzout, ngp, cmaxit, vmaxit, icontour, lincap, wtf,
    relax, relaxp, ss, pert, pert_osmp;
    I drec[20], inchk[50];
    I cbcnod[MM], cbcelev[MM], cbcgrp[MM], cbc1[MM], cbc2[MM],
    pbcnod[MM], pbcelev[MM], pbcgrp[MM], pbc1[MM], pbc2[MM],
    isink[EM], iout[RW*ZW], nsink[NM], eldef[EM][6];
    I flow[NM];
    F w1, w2, w3, w4, w5;
    F rot[IM], zot[IM];
    D avgas, ctol, co, dd, ddt, dgamma, dr, dz, dt, dto, dti,
    dtmax, dtmin, effvol, en, eo, hc, hh, p_art, p_ven,
    pert_p_art, pert_p_ven, pert_c_art, pert_c_osmp, pn, ndvel,
    maxcc, maxco, maxpe, maxop, maxdc, maxdp, lref2d,
    t, ti, tf, rg, rg2, zg, ur, uu, uz, vtol, uc, ww, xm;
    D trec[20];
    D cbcndv[MM], cbceva[MM][3], cbcevh[MM][3],
    pbcndv[MM], pbceva[MM][3], pbcevh[MM][3];
    D edr[EM], edz[EM];
    D r[NM], z[NM], pe[NM], hp[NM], op[NM], cm[NM], cn[NM], dc[NM],
    drreff[NM], drzeff[NM], dzzeff[NM];
    D *p_q;
    C line[80], title[80];
    FILE *in, *outr, *outb, *outl, *outq, *outu, *tmpf;
    vdiff d;
    media pp;
    membr mem;

```

```

N pruruz;
O cs;
/* */
puts(" mve() :\n");
if ((argc == 2) || (argc == 5))
    { ic = 0; }
if (ic == 1) {
    puts(" F: mve MODEL_f PRES_POTL_PECCL_CONC_VEL_f CAP_f LOG_f.\n");
    puts(" MODEL_f = input model file");
    puts(" PRES = Pressure results");
    puts(" POTL = Potential results");
    puts(" PECCL = Peclet number results");
    puts(" CONC = Concentration results");
    puts(" VEL = Velocity results");
    puts(" CAP_f = Capillary data file");
    puts(" LOG_f = Log file");
    exit(0); }
/*
OPEN INPUT
*/
if ((in = fopen(argv[1], "r")) == NULL) {
    printf("\n E: mve()-> %s not found. \n", argv[1]);
    exit(0); }
/*
INITIALIZE VARIABLES AND VECTORS
*/
ict = ic = 1;
ndnm = ndnmout = elnm = nr = nz = 0;
nncbc = necbc = nnpbc = nepbc = nesink = pert = pert_ospm = 0;
bw = cdt = ndt = crz = disp = doitpr = jj = ss = 0;
geom = ihof = cmaxit = vmaxit = ngp = 0;
irec = nrec = icontour = wtf = relaxc = relaxp = 0;
pert_p_ven = pert_p_art = pert_c_art = pert_c_ospm = 0.0;
dgamma = avgas = co = p_art = p_ven = pn = 0.0;
dr = dz = ddt = dt = dto = dti = dtmax = dtmin = 0.0;
t = ti = tf = lref2d = effvol = ndvel = 0.0;
dd = hc = hh = uc = ur = uu = uz = ww = xm = 0.0;
ctol = vtol = 0.0;
maxcc = maxco = maxdc = maxdp = maxpe = maxop = 0.0;
for (i=0;i<50;i++)
    { inchk[i] = 0; }
for (i=0;i<NM;i++) {
    nsink[i] = flow[i] = 0;
    r[i] = z[i] = op[i] = hp[i] = 0.0;
    d.xr[i] = d.rz[i] = d.zz[i] = 0.0;
    drreff[i] = drzeff[i] = dzzeff[i] = 0.0;
    cn[i] = cs.c[i] = cm[i] = dc[i] = 0.0;
    pruruz.r[i] = pruruz.z[i] = pruruz.p[i] = 0.0; }
for (i=0;i<MM;i++) {
    cbc1[i] = cbc2[i] = pbc1[i] = pbc2[i] = 0;
    cbcele[i] = pbcele[i] = 0;
    cbcnod[i] = pbcnod[i] = 0;
    cbcgrp[i] = pbcgrp[i] = 0;
    cbcndv[i] = pbcndv[i] = 0.0;
    for (j=0;j<3;j++) {
        cbceva[i][j] = cbcevh[i][j] = 0.0;
        pbceva[i][j] = pbcevh[i][j] = 0.0; } }
for (i=0;i<EM;i++) {
    isink[i] = 0;
    edr[i] = edz[i] = 0.0;
    for (j=0;j<6;j++)
        { eldef[i][j] = 0; } }
for (i=0;i<RW*ZW;i++)
    { iout[i] = 0; }
puts(" Work vectors and matrices initialized.");
/*
READ MODEL DATA
*/
ic = 0;
while ((feof(in) == 0) && (ic < 120)) {
    /* */
    fgets(line, 80, in);
    /* */
    if (strncmp(line, "$end input", 10) == 0) {
        inchk[0] = 1; }
    else
    if (strncmp(line, "$beg input", 10) == 0) {
        inchk[1] = 1;
        fgets(title, 80, in);
        puts(title); }
    else

```

```

if (strncmp(line, "$prob size", 10) == 0) {
    inchk[2] = 1;
    fscanf(in, "%d %d %d %d %f %f", &ndnm, &elnm, &nr, &nz); }
else
if (strncmp(line, "$transient", 10) == 0) {
    inchk[4] = 1;
    fscanf(in, "%d %f %f %f", &ss, &w1, &w2, &w3);
    t = ti = w1;
    tf = w2;
    dt = dto = dti = w3;
    fscanf(in, "%e %e %d", &w1, &w2, &ndt);
    dtmax = w1;
    dtmin = w2; }
else
if (strncmp(line, "$max iterations", 15) == 0) {
    inchk[5] = 1;
    fscanf(in, "%d %d", &cmaxit, &vmaxit); }
else
if (strncmp(line, "$dispersivity", 13) == 0) {
    inchk[6] = 1;
    fscanf(in, "%e %e %e %d", &w1, &w2, &w3, &crz);
    pp.alfl = w1;
    pp.alft = w2;
    pp.diff = mem.diff = w3;
    if ((pp.alfl != 0.0) || (pp.alft != 0.0))
        { disp = 1; }
    else
        { disp = 0; } }
else
if (strncmp(line, "$fluid sink LS", 14) == 0) {
    inchk[7] = 1;
    fscanf(in, "%e", &w1);
    pp.ls = w1; }
else
if (strncmp(line, "$porosity", 9) == 0) {
    inchk[8] = 1;
    fscanf(in, "%f", &w1);
    pp.por = w1; }
else
if (strncmp(line, "$fluid viscosity", 16) == 0) {
    inchk[9] = 1;
    fscanf(in, "%f", &w1);
    pp.mu = w1; }
else
if (strncmp(line, "$relaxation", 11) == 0) {
    inchk[10] = 1;
    fscanf(in, "%d %d", &relaxc, &relaxp); }
else
if (strncmp(line, "$hydraulic cond", 15) == 0) {
    inchk[11] = 1;
    fscanf(in, "%e %e", &w1, &w2);
    pp.lo_k = w1;
    pp.hi_k = w2; }
else
if (strncmp(line, "$conc sink", 10) == 0) {
    inchk[12] = 1;
    nesink = 0;
    for (i=0;i<elnm;i++) {
        fscanf(in, "%d %d", &j, &k);
        isink[j] = k;
        if (k == 1)
            { nesink++; } }
    printf(" %d elemental sinks specified.\n", nesink); }
else
if (strncmp(line, "$mem refl coef", 14) == 0) {
    inchk[13] = 1;
    fscanf(in, "%f", &w1);
    mem.sigma = w1; }
else
if (strncmp(line, "$fluid density", 14) == 0) {
    inchk[14] = 1;
    fscanf(in, "%f", &w1);
    pp.rho = w1; }
else
if (strncmp(line, "$tis refl coef", 14) == 0) {
    inchk[3] = 1;
    fscanf(in, "%f", &w1);
    pp.sigmag = w1; }
else
if (strncmp(line, "$diff mem PS", 12) == 0) {
    inchk[15] = 1;

```

```

        fscanf(in, "%e", &w1);
        mem.ps = w1; }
else
if (strncmp(line, "$geometry", 9) == 0) {
    inchk[16] = 1;
    fscanf(in, "%d", &geom);
    switch (geom) {
        case 0: puts(" Rectangular Coord w/o Upwinding.");
                break;
        case 1: puts(" Cylindrical Coord w/o Upwinding.");
                break;
        case 2: puts(" Rectangular Coord w/ Upwinding.");
                break;
        case 3: puts(" Cylindrical Coord w/ Upwinding.");
                break; } }
else
if (strncmp(line, "$cap osm pr", 11) == 0) {
    inchk[17] = 1;
    fscanf(in, "%f", &w1);
    mem.pi_cap = w1; }
else
if (strncmp(line, "$node definitions", 17) == 0) {
    inchk[18] = 1;
    for (i=0;i<ndnm;i++) {
        fscanf(in, "%d %f %f %d", &j, &w1, &w2, &k);
        r[j] = w1;
        z[j] = w2;
        flow[j] = k; }
    printf(" %d node definitions set.\n", ndnm); }
else
if (strncmp(line, "$elem definitions", 17) == 0) {
    inchk[19] = 1;
    for (i=0;i<elnm;i++) {
        fscanf(in, "%d %d %d %d %d", &j, &k, &l, &m, &n);
        eldef[j][0] = k;
        eldef[j][1] = l;
        eldef[j][2] = m;
        eldef[j][3] = n; }
    printf(" %d element definitions set.\n", elnm); }
else
if (strncmp(line, "$conc node bc", 13) == 0) {
    inchk[20] = 1;
    i = 0;
    while(strncmp(fgets(line, 80,in), "$e", 2) != 0) {
        sscanf(line, "%d %e", &j, &w1);
        cbcnod[i] = j;
        cbendv[i] = w1;
        i++; }
    nncbc = i;
    printf(" %d concentration nodal BC's specified.\n", nncbc); }
else
if (strncmp(line, "$conc elem bc", 13) == 0) {
    inchk[21] = 1;
    i = 0;
    while(strncmp(fgets(line, 80, in), "$e", 2) != 0) {
        sscanf(line, "%d %d %d %d %e %e %e %e", &j, &k, &l, &m, &w1,
&w2, &w3, &w4);
        cbcele[i] = j;
        cbcgrp[i] = k;
        cbc1[i] = l;
        cbc2[i] = m;
        cbceva[i][0] = w1;
        cbcevh[i][0] = w2;
        cbceva[i][1] = w3;
        cbcevh[i][1] = w4;
        i++; }
    necbc = i;
    printf(" %d concentration elemental BC's specified.\n", necbc); }
else
if (strncmp(line, "$conc node ic", 13) == 0) {
    inchk[22] = 1;
    fgets(line, 80, in);
    if (strncmp(line, "$$file", 6) == 0) {
        for (i=0;i<ndnm;i++) {
            fscanf(in, "%d %e", &j, &w1);
            cn[j] = cm[j] = w1; } }
    else
    if (strncmp(line, "$$init", 6) == 0) {
        fscanf(in, "%e", &w1);
        for (i=0;i<ndnm;i++)
            { cn[i] = cm[i] = w1; } }

```

```

        printf(" %d concentration IC's specified.\n", ndnm); }
else
if (strncmp(line, "$cap conditions", 15) == 0) {
    inchk[33] = 1;
    fscanf(in, "%f %f %f %d", &w1, &w2, &w3, &lincap);
    mem.c_art = w1;
    p_art = w2;
    p_ven = w3; }
else
if (strncmp(line, "$pres node bc", 13) == 0) {
    inchk[23] = 1;
    i = 0;
    while(strncmp(fgets(line, 80, in), "$e", 2) != 0) {
        sscanf(line, "%d %e", &j, &w1);
        pbcnod[i] = j;
        pbcndv[i] = w1;
        pruruz.p[j] = w1;
        i++; }
    nnpbc = i;
    printf(" %d pressure nodal BC's specified.\n", nnpbc); }
else
if (strncmp(line, "$pres elem bc", 13) == 0) {
    inchk[24] = 1;
    i = 0;
    while(strncmp(fgets(line, 80, in), "$e", 2) != 0) {
        sscanf(line, "%d %d %d %d %e %e %e %e", &j, &k, &l, &m, &w1,
&w2, &w3, &w4);
        pbcele[i] = j;
        pbcgrp[i] = k;
        pbc1[i] = l;
        pbc2[i] = m;
        pbceva[i][0] = w1;
        pbcevh[i][0] = w2;
        pbceva[i][1] = w3;
        pbcevh[i][1] = w4;
        i++; }
    nepbc = i;
    printf(" %d pressure elemental BC's specified.\n", nepbc); }
else
if (strncmp(line, "$write results", 14) == 0) {
    inchk[25] = 1;
    switch (ss) {
        case 0 :
            nrec = 1;
            for (i=0; i<20; i++) {
                drec[i] = 1;
                trec[i] = 0.0; }
            break;
        default :
            fscanf(in, "%d", &nrec);
            for (i=0; i<nrec; i++) {
                fscanf(in, "%f", &w1);
                trec[i] = w1;
                if (trec[i] == 0.0)
                    { drec[i] = 1; }
                else
                    { drec[i] = 0; } }
            break; } }
else
if (strncmp(line, "$contour", 8) == 0) {
    inchk[26] = 1;
    fscanf(in, "%d", &icontour); }
else
if (strncmp(line, "$ref values", 11) == 0) {
    inchk[27] = 1;
    fscanf(in, "%e %e %e %e", &w1, &w2, &w3, &w4);
    pp.lref = mem.lref = w1;
    pp.cref = mem.cref = w2;
    pp.pref = mem.pref = w3;
    pp.kref = w4;
    puts(" Reference values set."); }
else
if (strncmp(line, "$tolerance", 10) == 0) {
    inchk[28] = 1;
    fscanf(in, "%e %e", &w1, &w2);
    ctol = w1;
    vtol = w2; }
else
if (strncmp(line, "$frac volumes", 13) == 0) {
    inchk[29] = 1;
    fscanf(in, "%f %f %f %f %f", &w1, &w2, &w3, &w4, &w5);

```

```

        pp.fex = w1;
        pp.fst = w2;
        pp.fav = w3;
        pp.fs = w4;
        pp.fim = w5; }
else
if (strncmp(line, "$conv hindrance", 15) == 0) {
    inchk[30] = 1;
    fscanf(in, "%f", &w1);
    pp.hind = w1; }
else
if (strncmp(line, "$gauss points", 13) == 0) {
    inchk[31] = 1;
    fscanf(in, "%d", &ngp);
    i = 0;
    switch(ngp) {
        case 2 :
        case 3 :
        case 4 :
        case 6 :
        case 8 :
        case 16: i = 1; break; }
    printf(" Using Gaussian integration of order %d.\n", ngp);
    if (i == 0) {
        puts("\n E: mve()-> Incorrect Gauss Points (2,3,4,6,8,16
allowed).\n");
        exit(0); } }
else
if (strncmp(line, "$asq", 4) == 0) {
    inchk[32] = 1;
    fscanf(in, "%e", &w1);
    mem.asq = w1; }
else
if (strncmp(line, "$hof", 4) == 0) {
    inchk[34] = 1;
    fscanf(in, "%d", &ihof);
    switch (ihof) {
        case 0: puts(" Using lower order trial functions.");
            break;
        case 1: puts(" Using higher order trial functions.");
            break; } }
else
if (strncmp(line, "$node results", 13) == 0) {
    inchk[35] = 1;
    fgets(line, 80, in);
    if (strncmp(line, "$$coll", 6) == 0) {
        wtf = 1;
        nrout = nr;
        nzout = nz;
        ndnmout = ndnm;
        puts(" Record nodal results at collocation points."); }
    else
    if (strncmp(line, "$$file", 6) == 0) {
        wtf = 0;
        fscanf(in, "%d", &nrout);
        for (i=0; i<nrout; i++)
            { fscanf(in, "%f", &rot[i]); }
        fscanf(in, "%d", &nzout);
        for (i=0; i<nzout; i++)
            { fscanf(in, "%f", &zot[i]); }
        ndnmout = nrout*nzout;
        puts(" Record nodal results at specified points."); } }
else
if (strncmp(line, "$osm pres", 9) == 0) {
    inchk[36] = 1;
    fscanf(in, "%d", &pp.osm); }
else
if (strncmp(line, "$dgamma", 7) == 0) {
    inchk[37] = 1;
    fscanf(in, "%f", &w1);
    dgamma = w1; }
else
if (strncmp(line, "$lymph cond", 11) == 0) {
    inchk[38] = 1;
    fscanf(in, "%f %e", &w1, &w2);
    pp.plymph = w1;
    pp.jo = w2; }
else
if (strncmp(line, "$wall th", 7) == 0) {
    inchk[40] = 1;
    fscanf(in, "%e", &w1);

```

```

        mem.wall_th = w1; }
    else
    if (strncmp(line, "$perturbation", 13) == 0) {
        inchk[41] = 1;
        fscanf(in, "%d %f %f %f %f %d", &pert, &w1, &w2, &w3, &w4, &pert_osmp);
        pert_p_art = w1;
        pert_p_ven = w2;
        pert_c_art = w3;
        pert_c_osmp = w4;
        if (pert != 0)
            { puts(" System perturbation will occur after SS reached."); }
        else
            { puts(" No specified system perturbation."); }
    }
    else
    if (strncmp(line, "$cap wall Lp", 12) == 0) {
        inchk[39] = 1;
        fscanf(in, "%d %e %e", &mem.typ_lp, &w1, &w2);
        mem.lp0 = w1;
        mem.lp1 = w2;
        if ((mem.lp0 == 0.0) && (mem.lp1 == 0.0)) {
            puts("\n E: mve()-> Lp = Zero.\n");
            exit(0); }
    }

ic++; }
fclose(in);
/* */
if (safchk(ndnm, elnm, nr, nz, nrout, nzout) != 0) {
    puts("\n Run Aborted.");
    exit(0); }
if ((ic = datachk(&inchk[0])) != 0) {
    printf("\n E: mve()-> %d input items missing. Run aborted.\n", ic);
    exit(0); }
/* */
puts("\n Model input data check passed.\n");
if (argc == 2) {
    puts("\n T: mve()-> Data check. No analysis performed.\n");
    exit(0); }
/*
MEMBRANE NODE NUMBER, LOCATION, AND ESTIMATED PRESSURE
*/
xm = (p_art-p_ven);
for (i=0;i<nz;i++) {
    k = i*nr;
    mem.mnod[i] = k;
    mem.r[i] = r[k];
    mem.z[i] = z[k];
    mem.hp[i] = p_art-xm*mem.z[i]; }
/*
TISSUE OUTER RADIUS
*/
rg = r[nr-1];
zg = mem.z[nz-1]-mem.z[0];
rg2 = sq(rg);
/*
GET dr[] AND dz[] VECTORS
*/
for (i=0;i<elnm;i++) {
   edr[i] = fabs(r[eldef[i][1]]-r[eldef[i][0]]);
    edz[i] = fabs(z[eldef[i][3]]-z[eldef[i][0]]); }
/*
ASSIGN OUTPUT ELEMENTS FOR OUTPUT NODE LOCATIONS
*/
for (i=0;i<elnm;i++) {
    for (j=0;j<nzout;j++) {
        for (k=0;k<nrout;k++) {
            l = j*nrout+k;
            if (iout[l] == 0) {
                if ((rot[k] >= r[eldef[i][0]])
                    && (rot[k] <= r[eldef[i][2]])
                    && (zot[j] >= z[eldef[i][0]])
                    && (zot[j] <= z[eldef[i][2]]))
                    { iout[l] = i; } } } }
puts(" Assigned output element-node numbering.");
/*
DATA CONVERSIONS TO MAINTAIN CORRECT UNIT DIMENSIONS
*/
bw = 2*nr+1;
/*
DIMENSIONING TERMS
*/
lref2d = sq(pp.lref)/pp.diff;
ndvel = pp.hind*pp.fst/pp.fav;

```

```

mem.ps_d = mem.ps*mem.lref/mem.diff;
mem.wall_th_d = mem.wall_th/mem.lref;
/*
ASSIGN NODAL SINK VALUES AND GET AVERAGE SINK AREA
*/
avgas = 0.0;
for (i=0;i<elnm;i++) {
    if (isink[i] == 1) {
        avgas += (edr[i]*edz[i]);
        for (j=0;j<4;j++)
            { nsink[eldef[i][j]] = 1; } }
if (nesink != 0)
    { avgas *= sq(pp.lref)/((D)(nesink)); }
else
    { avgas = 0.0; }
printf(" Lymphatic sink area = %10.6e\n", avgas);
/*
GET EFFECTIVE VOLUME AND TOTAL TISSUE VOLUME
*/
effvol = (1.0-pp.fs)/pp.fst;
pp.vol_tis = 0.0;
for (i=0;i<nz-1;i++) {
    dr = 0.5*(mem.r[i]+mem.r[i+1]);
    dz = (mem.z[i+1]-mem.z[i]);
    pp.vol_tis += dz*(rg2-sq(dr)); }
pp.vol_tis *= (pp.lref*pp.lref*pp.lref*PI);
printf(" Total tissue volume = %10.6e\n", pp.vol_tis);
/*
OPEN OUTPUT FILES
*/
outr = fopen(argv[2], "w+");
outb = fopen(argv[3], "w+");
/*
WRITE (DISSPLA) HEADER DATA TO OUTPUT FILES
*/
fprintf(outr, " %d\n", nrec);
header(rg, zg, pp.lo_k, mem, pp, outr);
header(rg, zg, pp.lo_k, mem, pp, outb);
/*
CLOSE FILES
*/
fclose(outr);
fclose(outb);
switch (ss) {
    case 0 :
        printf(" Steady-state run. \n");
        break;
    default :
        if (ss == 1)
            { puts(" Temporal stability requirement (Co < 1) enforced."); }
        else
            { puts(" Temporal stability requirement (Co < 1) not
enforced."); }
        printf(" Initial time = %10.4f\n Final time = %10.4f\n", ti, tf);
        printf(" Time step will be increased every %d cycles.\n", ndt);
        break; }
printf("\n %s Run start.\n", title);
if (ss != 0) {
    outl = fopen(argv[4], "w+");
    fputs(title, outl);
    fputs("\n Model Run Log :\n\n", outl);
    fputs("      TOT t      INC t      MAXCO      MAXPE      MAXDC:N
MAXDP:N\n", outl);
    fputs("      -----
----\n", outl);
    fclose(outl); }
/*
START MODEL RUN
*/
ii = cdt = 0;
/* */
do {
    raku:
    ii++;
    cdt++;
    irec = 0;
    ti = t;
    puts("\n*****");
    if (ss != 0)
        { printf("Time Step %4d :\n", ii); }
    /*
SWITCH OFF ALL OSMF EFFECTS IN TIS AND CAP IF DESIRED

```

```

*/
if (pp.osm == 0)
    { mem.sigma = pp.sigmag = 0.0; }
/*
CHECK IF TO RECORD THIS TIME STEP
*/
switch (ss) {
    case 0 :
        irec = 1;
        dt = ddt = 0.0;
        break;
    default :
        if (pert == 0) {
            if ((t+dt) > tf) {
                irec = 1;
                dto = dt;
                dt = tf-t; }
            for (i=nrec-1;i>-1;i--) {
                if (((t+dt) > trec[i]) && (drec[i] == 0)) {
                    irec = 1;
                    dto = dt;
                    dt = trec[i]-t;
                    for (j=i;j>-1;j--)
                        { drec[j] = 1; } } }

            if (dt > dtmax) {
                irec = 0;
                dt = dtmax; }
            if (dt <= 0.0) {
                irec = 0;
                printf("\n W: mve()-> dt <= Zero. Reset to dtmax.\n");
                dt = dtmax; }
            ddt = dt/lref2d;
            break; }

/*
SET PREDICTOR VALUES AND PRESSURE AT TIME t+dt
*/
for (i=0;i<ndnm;i++)
    { cs.c[i] = cm[i] = cn[i]+ddt*dc[i]; }
/*
START ITERATIVE SCHEME
*/
jj = 0;
eo = 1.0e-02;
do {
    jj++;
    doitpr = 0;
    maxco = maxdc = maxop = maxpe = 0.0;
    printf(" Conc Iter %3d :\n", jj);
    /*
    OSMOTIC PRESSURE EFFECT
    */
    j = 0;
    p_q = osmopr(ndnm, pp, &cs.c[0]);
    for (i=0;i<ndnm;i++) {
        op[i] = *p_q++;
        if (op[i] > maxop) {
            maxop = op[i];
            j = i; } }
    printf(" Max Osmotic Pressure = %10.6f at node %d.\n", maxop, j);
    /*
    SET MEMBRANE OSMOTIC PRESSURE
    */
    for (i=0;i<nz;i++)
        { mem.op[i] = op[mem.mnod[i]]; }
    /*
    PRESSURE DISTRIBUTION AND FLUID VELOCITY FIELD
    */
    if (pp.osm != 0)
        { doitpr = 1; }
    else
        { doitpr = 0; }
    if (ii < 2)
        { doitpr = 1; }
    switch (doitpr) {
        case 0 :
            puts(" Membrane-Tissue Pressure-Velocity variables
converged.");
            break;
        case 1 :
            pruruz = itpruruz2d(ndnm, elnm, nnpbc, nepbc,
nr, nz, bw, vmaxit, pp, mem,

```

```

&pbcevh[0][0],
&pbcevh[0][0],

&eldef[0][0], &flow[0], &edr[0], &edz[0],
&r[0], &z[0], &op[0], &hp[i], &pbcnod[0],

&pbcele[0], &pbgrp[0], &pbceva[0][0],

&pbcl[0], &pbcl2[0], &nsink[0],
p_art, p_ven, ctol, vtol,
lincap, relaxp, ihof, geom, ngp);

/*
SET IMPROVED NODAL PRESSURE BOUNDARY CONDITIONS
*/
for (i=0;i<nnpbc;i++)
    { pbcevh[i] = pruruz.p[pbcnod[i]]; }
/*
SET MEMBRANE FLUID VELOCITIES
*/
for (i=0;i<nz;i++) {
    mem.vh[i] = pruruz.r[mem.mnod[i]];
    mem.hp[i] = pruruz.p[mem.mnod[i]]; }
break; }

/*
CALCULATE VIRTUAL DIFFUSION COEFFICIENTS
*/
if ((disp == 1) || (ii < 2)) {
    d = dspc(ndnm, pp.alf1, pp.alf2, pp.diff,
    &pruruz.r[0], &pruruz.z[0], crz);
    /*
    GET DIMENSIONLESS DIFF-DISP COEFFICIENTS
    */
    for (i=0;i<ndnm;i++) {
        drreff[i] = pp.fst*d.rr[i]/pp.diff;
        if (crz == 1)
            { drzeff[i] = pp.fst*d.rz[i]/pp.diff; }
        dzzeff[i] = pp.fst*d.zz[i]/pp.diff; } }

/*
GET MAX COURANT AND PECLET ELEMENTAL NUMBERS
AND CHECK MAX PERMISSABLE dt FOR STABILITY
*/
k = 1 = 0;
for (i=0;i<elnm;i++) {
    dr = dz = ur = uz = 0.0;
    for (j=0;j<4;j++) {
        dr += pp.fst*d.rr[eldef[i][j]];
        dz += pp.fst*d.zz[eldef[i][j]];
        ur += ndvel*fabs(pruruz.r[eldef[i][j]]);
        uz += ndvel*fabs(pruruz.z[eldef[i][j]]); }
    dr *= 0.25;
    dz *= 0.25;
    ur *= 0.25;
    uz *= 0.25;
    uu = norm(ur, uz);
    dd = norm(dr, dz);
    if (uu != 0.0) {
        hh = pp.lref*(ur*edr[i]+uz*edz[i])/uu;
        co = uu*dt/hh;
        pn = uu*hh/dd; }
    else {
        co = pn = 0.0; }
    if (co > maxco) {
        maxco = co;
        uc = uu;
        hc = hh;
        k = i; }
    if (pn > maxpe) {
        maxpe = pn;
        l = i; } }
printf("\n Max Peclet number = %10.6f at element %3d.\n", maxpe, l);
if (ss != 0) {
    printf(" Max Courant number = %10.6f at element %3d.\n", maxco,
k);

    if ((maxco > 0.95) && (ss == 1)) {
        puts(" Stability violation (Max Co < 1.0).");
        ii--;
        dt = 0.9*hc/uc;
        t = ti;
        if (dt < dtmin) {
            outl = fopen(argv[8], "a+");
            puts("\n E: mve()-> Time increment too small.
Run aborted.\n");
            fputs("\n E: mve()-> Time increment too small.
Run aborted.\n", outl);

```

```

                                fclose(out1);
                                goto aljo; )
                                printf("\n W: mve()-> Reducing time increment to dt =
%10.6f.\n", dt);
                                goto raku; })
/*
USE ITERATIVE SOLVER WITH SINK TERMS ON THE
RIGHT HAND SIDE FOR SOLUTE DISTRIBUTION
*/
cs = itcscap2d(ndnm, elnm, nncbc, necbc, nr, nz, bw,
              cmaxit, pp, mem, &eldef[0][0],
              &edr[0], &edz[0], &r[0], &z[0],
              &drreff[0], &drzeff[0], &dzzeff[0],
              &pruruz.r[0], &pruruz.z[0],
              &pruruz.p[0], &cn[0],
              &cbcnod[0], &cbcnodv[0],
              &cbcele[0], &cbcgrp[0], &cbceva[0][0], &cbcevh[0][0],
              &cbc1[0], &cbc2[0],
              &nsink[0], ctol, ddt, crz, ss, ihof, geom, ngp);
/*
SET IMPROVED NODAL CONCENTRATION BOUNDARY CONDITIONS
*/
for (i=0;i<nncbc;i++)
    { cbcndv[i] = cs.c[cbcnod[i]]; }
/*
SET CAPILLARY AND TISSUE-SIDE MEMBRANE CONCENTRATIONS
*/
for (i=0;i<nz;i++) {
    mem.ct[i] = cs.c[mem.mnod[i]];
    mem.cp[i] = cs.ccap[i]; }
/*
GET DEVIATION AND THEN APPLY RELAXATION
*/
for (i=0;i<ndnm;i++) {
    dc[i] = fabs(cs.c[i]-cm[i]);
    if (dc[i] > maxdc)
        { maxdc = dc[i]; }
if (relaxc != 0) {
    en = 0.0;
    for (i=0;i<ndnm;i++)
        { en += fabs(dc[i]); }
    ww = dgamma/(1.0+en/eo);
    if ((eo = en) == 0.0)
        { eo = 1.0e-02; }
    for (i=0;i<ndnm;i++) {
        cs.c[i] = ww*cs.c[i]+(1.0-ww)*cm[i];
        cm[i] = cs.c[i]; }
else {
    for (i=0;i<ndnm;i++)
        { cm[i] = cs.c[i]; }
/* */
printf(" Conc Iter %3d : MDeltaC = %7.3e\n", jj, maxdc);
} while ((maxdc > ctol) && (jj < cmaxit));
if (jj >= cmaxit) {
    puts(" Did not converge. Possibly try smaller time step");
    puts(" or implement relaxation parameter.\n Program terminated.\n");
    exit(0); }
/*
SOLUTION CONVERGED
*/
for (i=0;i<ndnm;i++) {
    if (cs.c[i] < 0.0)
        { cs.c[i] = 0.0; }}
switch (ss) {
case 0 :
    printf("Steady-state solution completed in %3d iterations.\n",
jj);
    break;
default :
    t += dt;
    printf("Solution completed in %3d iterations.\n", jj);
    printf("Time Step %4d : t = %10.6f : dt = %10.6f completed.\n",
11, t, dt);
    break; }
/*
CALCULATE MAX CHANGE IN CONCENTRATION SOLUTION THROUGH TIME
*/
if (ss != 0) {
    maxcc = maxdc = maxdp = 0.0;
    for (i=0;i<ndnm;i++) {
        uc = cs.c[i]-cn[i];

```

```

uu = pruruz.p[i]-hp[i];
if (fabs(cs.c[i]) > maxcc)
    { maxcc = cs.c[i]; }
if (fabs(uc) > fabs(maxdc)) {
    k = i;
    maxdc = uc; }
if (fabs(uu) > fabs(maxdp)) {
    l = i;
    maxdp = uu; }
if (ddt != 0.0)
    { dc[i] = uc/ddt; }
else
    { dc[i] = 0.0; }
cn[i] = cs.c[i];
hp[i] = pruruz.p[i];
cs.c[i] /= effvol; }
if (maxcc != 0.0)
    { uc = fabs(maxdc/maxcc); }
else
    { uc = fabs(maxdc); }
if ((uc < ctol) && (ss != 0)) {
    printf(" Max temporal relative change in solute conc. = %10.6e\n", uc);
    puts(" Solute steady-state distribution has been achieved.\n");
    puts(" Will output steady-state data to amod.inp input file.");
    puts(" Will implement perturbation if specified.");
    printf(" Time to steady-state = %10.6f\n", t);
    irec = 1;
    jj = ss;
    ss = 3;
    ti = 0.0;
    dt = dti; }
/*
CALCULATE PECKET NUMBER - THIS IS NOT THE ELEMENTAL
PECKET NUMBER (USES REFERENCE LENGTH r[0]*pp.lref)
*/
xm = pp.hind*pp.fst/pp.fav;
for (i=0;i<ndnm;i++) {
    uu = xm*norm(pruruz.r[i], pruruz.z[i]);
    dd = pp.fst*norm(d.rr[i], d.zz[i]);
    if (uu != 0.0)
        { pe[i] = uu*pp.lref/dd; }
    else
        { pe[i] = 0.0; } }
/*
MASS BALANCE FOR FLUID AND SOLUTE
*/
massb(elnm, nr, nz, nesink, pp, mem, &eldef[0][0], &isink[0],
    &edr[0], &edz[0], &cs.c[0], &pruruz.p[0], &cs.fmem[0],
    pruruz.qcap[0], avgas, ngp, geom);
/*
GET TISSUE AVERAGE PRESSURE AND SOLUTE CONCENTRATION
*/
domavg(elnm, pp, &eldef[0][0], &edr[0], &edz[0], &cs.c[0],
    &pruruz.p[0], ngp, geom);
/*
CONTOUR OUTPUT DATA
*/
if (icontour != 0) {
    outq = fopen("zcon.dat", "w+");
    contour(0, ss, ndnm, nr, nz, &cs.c[0], t, title, outq);
    contour(1, ss, ndnm, nr, nz, &pruruz.p[0], t, title, outq);
    if (pp.osm != 0) {
        contour(2, ss, ndnm, nr, nz, &op[0], t, title, outq);
        contour(3, ss, ndnm, nr, nz, &pruruz.pt[0], t, title, outq); }
    printf(" contour()");
    fclose(outq); }
/*
OUTPUT CONVERGED RESULTS
*/
if ((nrec == 0) || (irec == 1)) {
    printf(" Recording data : ");
    outr = fopen(argv[2], "a+");
    outb = fopen(argv[3], "a+");
    switch (wtf) {
        case 0:
            outdata(0, ss, ndnmout, nrout, nzout, &iout[0],
                &eldef[0][0],
                &rot[0], &zot[0], &r[0], &z[0], &edr[0],
                &edz[0],
                ihof, t, title, &cs.c[0], outr);

```

```

                                outdata(1, ss, ndnmout, nrout, nzout, &iout[0],
                                &rot[0], &zot[0], &r[0], &z[0], &edr[0],
&eldef[0][0],
                                ihof, t, title, &pruruz.p[0], outr);
&edz[0],
                                outdata(2, ss, ndnmout, nrout, nzout, &iout[0],
                                &rot[0], &zot[0], &r[0], &z[0], &edr[0],
&eldef[0][0],
                                ihof, t, title, &pe[0], outr);
&edz[0],
                                outdata(3, ss, ndnmout, nrout, nzout, &iout[0],
                                &rot[0], &zot[0], &r[0], &z[0], &edr[0],
&eldef[0][0],
                                &rot[0], &zot[0], &r[0], &z[0], &edr[0],
&edz[0],
                                ihof, t, title, &pruruz.pt[0], outr);
                                break;
                                case 1:
                                outcoll(0, ss, ndnmout, t, &r[0], &z[0], &cs.c[0],
                                outcoll(1, ss, ndnmout, t, &r[0], &z[0], &pruruz.p[0],
                                outcoll(2, ss, ndnmout, t, &r[0], &z[0], &pe[0], title,
                                outcoll(3, ss, ndnmout, t, &r[0], &z[0], &pruruz.pt[0],
                                break; )
                                outuv2d(wtf, ss, ndnmout, nrout, nzout, &iout[0], &eldef[0][0],
                                &rot[0], &zot[0], &r[0], &z[0], &edr[0], &edz[0],
                                ihof, t, title, &pruruz.r[0], &pruruz.z[0], outr);
                                outcapp(nz, ss, t, &mem.z[0], &pruruz.pcap[0], &pruruz.qcap[0],
                                &cs.ccap[0], &cs.mpe[0], &cs.fmem[0], title, outb);
                                fclose(outr);
                                fclose(outb);
                                printf(".\n"); }
/*
OUTPUT TO RUN LOG FILE
*/
if (ss != 0) {
    outl = fopen(argv[4], "a+");
    fprintf(outl, "%3d %10.4f %10.4f %6.3e %6.3e %6.3e:%3d %6.3e:%3d",
            ict++, t, dt, maxco, maxpe, maxdc, k, maxdp, l);
    if (pert == 0) {
        switch(irec) {
            case 0: break;
            case 1: fprintf(outl, " R");break; }
        fprintf(outl, "\n");
        fclose(outl); }
if (ss == 3)
    { ss = 0; }
/*
WRITE RESULTS TO INTERMEDIATE FILE IN CASE OF SHUTDOWN
OR FOR NEW START-UP FILE FOR OTHER RUNS
*/
tmpf = fopen("zmod.tmp", "w+");
/*
*/
fputs("$beg input\n", tmpf);
fputs(title, tmpf);
fputs("$prob size\n", tmpf);
fprintf(tmpf, "%d %d %d %d\n", ndnm, elnm, nr, nz);
fputs("$transient\n", tmpf);
fprintf(tmpf, "%d %f %f %f\n%e %e %d\n",
        ss, ti, tf, dt, dtmax, dtmin, ndt);
fputs("$max iterations\n", tmpf);
fprintf(tmpf, "%d %d\n", cmaxit, vmaxit);
fputs("$dispersivity\n", tmpf);
fprintf(tmpf, "%e %e %e %d\n", pp.alfl, pp.alft, pp.diff, crz);
fputs("$fluid sink LS\n", tmpf);
fprintf(tmpf, "%e\n", pp.lsl);
fputs("$porosity\n", tmpf);
fprintf(tmpf, "%f\n", pp.por);
fputs("$fluid viscosity\n", tmpf);
fprintf(tmpf, "%f\n", pp.mu);
fputs("$fluid density\n", tmpf);
fprintf(tmpf, "%f\n", pp.rho);
fputs("$relaxation\n", tmpf);
fprintf(tmpf, "%d %d\n", relaxc, relaxp);
fputs("$geometry\n", tmpf);
fprintf(tmpf, "%d\n", geom);
fputs("$dgamma\n", tmpf);
fprintf(tmpf, "%f\n", dgamma);

```

```

fputs("$lymph cond\n", tmpf);
fprintf(tmpf, "%f %e\n", pp.plymph, pp.jo);
fputs("$wall th\n", tmpf);
fprintf(tmpf, "%e\n", mem.wall_th);
fputs("$cap wall Lp\n", tmpf);
fprintf(tmpf, "%d %e %e\n", mem.typ_lp, mem.lp0, mem.lp1);
fputs("$osm pres\n", tmpf);
fprintf(tmpf, "%d\n", pp.osm);
fputs("$mem refl coef\n", tmpf);
fprintf(tmpf, "%f\n", mem.sigma);
fputs("$tis refl coef\n", tmpf);
fprintf(tmpf, "%f\n", pp.sigmag);
fputs("$diff mem PS\n", tmpf);
fprintf(tmpf, "%e\n", mem.ps);
fputs("$cap osm pr\n", tmpf);
fprintf(tmpf, "%f\n", mem.pi_cap);
fputs("$ref values\n", tmpf);
fprintf(tmpf, "%e %e %e %e\n",
        pp.lref, pp.cref, pp.pref, pp.kref);
fputs("$tolerance\n", tmpf);
fprintf(tmpf, "%e %e\n", ctol, vtol);
fputs("$frac volumes\n", tmpf);
fprintf(tmpf, "%f %f %f %f %f\n",
        pp.fex, pp.fst, pp.fav, pp.fs, pp.fim);
fputs("$conv hindrance\n", tmpf);
fprintf(tmpf, "%f\n", pp.hind);
fputs("$gauss points\n", tmpf);
fprintf(tmpf, "%d\n", ngp);
fputs("$contour\n", tmpf);
fprintf(tmpf, "%d\n", icontour);
fputs("$asq\n", tmpf);
fprintf(tmpf, "%e\n", mem.asq);
fputs("$hof\n", tmpf);
fprintf(tmpf, "%d\n", ihof);
fputs("$perturbation\n", tmpf);
fprintf(tmpf, "%d %f %f %f %f %d\n",
        1, pert_p_art, pert_p_ven, pert_c_art, pert_c_osmp, pert_osmp);
fputs("$hydraulic cond\n", tmpf);
fprintf(tmpf, "%10.6e %10.6e\n", pp.lo_k, pp.hi_k);
fputs("$conc sink\n", tmpf);
for (i=0;i<elnm;i++)
    { fprintf(tmpf, "%d %d\n", i, isink[i]); }
fputs("$node definitions\n", tmpf);
for (i=0;i<ndnm;i++)
    { fprintf(tmpf, "%4d %10.6f %10.6f %4d\n", i, r[i], z[i], flow[i]); }
fputs("$elem definitions\n", tmpf);
for (i=0;i<elnm;i++)
    { fprintf(tmpf, "%4d %4d %4d %4d\n",
        i, eldef[i][0], eldef[i][1], eldef[i][2], eldef[i][3]); }
fputs("$conc node bc\n", tmpf);
for (i=0;i<nncbc;i++)
    { fprintf(tmpf, "%4d %10.6e\n", cbcnod[i], cbcdv[i]); }
fputs("$e\n", tmpf);
fputs("$conc elem bc\n", tmpf);
for (i=0;i<necbc;i++) {
    fprintf(tmpf, "%4d %4d %4d %4d",
        i, cbcgrp[i], cbc1[i], cbc2[i]);
    for (j=0;j<2;j++)
        { fprintf(tmpf, " %10.6e %10.6e",
            cbceva[i][j], cbcevh[i][j]); }
    fprintf(tmpf, "\n"); }
fputs("$e\n", tmpf);
fputs("$conc node ic\n", tmpf);
fputs("$file\n", tmpf);
for (i=0;i<ndnm;i++)
    { fprintf(tmpf, "%4d %10.6e\n", i, cs.c[i]); }
fputs("$cap conditions\n", tmpf);
fprintf(tmpf, "%10.6f %10.6f %10.6f %d\n",
        mem.c_art, p_art, p_ven, lincap);
fputs("$pres node bc\n", tmpf);
for (i=0;i<nnpbc;i++)
    { fprintf(tmpf, "%4d %10.6e\n", pbcnod[i], pbcndv[i]); }
fputs("$e\n", tmpf);
fputs("$pres elem bc\n", tmpf);
for (i=0;i<nepbc;i++) {
    fprintf(tmpf, "%4d %4d %4d %4d",
        i, pbcgrp[i], pbc1[i], pbc2[i]);
    for (j=0;j<2;j++)
        { fprintf(tmpf, " %10.6e %10.6e",
            pbceva[i][j], pbcevh[i][j]); }
    fprintf(tmpf, "\n"); }

```

```

fputs("$e\n", tmpf);
fputs("$write results\n", tmpf);
switch (ss) {
  case 0 :
    break;
  default :
    fprintf(tmpf, "%d\n", nrec);
    for (i=0;i<nrec;i++)
      { fprintf(tmpf, "%10.6f\n", trec[i]); }
    break; }
fputs("$node results\n", tmpf);
switch (wtf) {
  case 0: fputs("$$file\n", tmpf);
    fprintf(tmpf, "%d\n", nrout);
    for (i=0;i<nrout;i++)
      { fprintf(tmpf, "%f\n", rot[i]); }
    fprintf(tmpf, "%d\n", nzout);
    for (i=0;i<nzout;i++)
      { fprintf(tmpf, "%f\n", zot[i]); }
    break;
  case 1: fputs("$$coll\n", tmpf);
    break; }
fputs("$end input\n", tmpf);
/* */
fclose(tmpf);
/*
ENLARGE TIME INCREMENT EVERY ndt TIME STEP CYCLES
*/
if (ss != 0) {
  if (irec == 1)
    { dt = dto; }
  if (cdt == ndt) {
    cdt = 0;
    dt *= 2.0; }
  ddt = dt/lref2d; }
if ((pert != 0) && (ss == 0)) {
  puts(" Initiating perturbation in Part, Pven, Cart, and Osmp.");
  ss = jj;
  pert = ii = 0;
  t = 0.0;
  p_art = pert_p_art;
  p_ven = pert_p_ven;
  mem.c_art = pert_c_art;
  mem.pi_cap = pert_c_osmp;
  pp.osm = pert_osmp;
  printf(" P_art          = %10.6f\n", p_art);
  printf(" P_ven          = %10.6f\n", p_ven);
  printf(" C_art          = %10.6f\n", mem.c_art);
  printf(" Osmp_cap       = %10.6f\n", mem.pi_cap);
  switch (pp.osm) {
    case 0 : printf(" Osmotic effects off.\n");break;
    case 1 : printf(" Osmotic effects on.\n");break; }}
  /* */
} while ((t < tf) && (ss != 0));
/* */
outl = fopen(argv[4], "a+");
fputs("\n Model run complete.\n", outl);
fclose(outl);
rename("zmod.tmp", "amod.inp");
aljo: /* */
printf(" %s Run complete.\n", title);
}
O itcscap2d(I ndnm, I elnm, I nncbc, I necbc, I nr, I nz, I bw, I cmaxit,
media pp, membr mem,
I *pe, D *rd, D *zd, D *pr, D *pz,
D *rr, D *rz, D *zz, D *ur, D *uz, D *ph, D *co,
I *bn, D *bv, I *be, I *bg, D *ba, D *bh, I *bl, I *b2,
I *sk, D ctol, D ddt, I crz, I ss, I ihof, I geom, I ngp)
(
I i, j, k, l, n, m;
I bcn[NM], bce[MM], bcg[MM], bcl[MM], bc2[MM];
I nsk[NM], eldef[EM][6];
D aa, bb, cc, dd, isigmas, lref2d, lsvol, jovol, ndvel, mcerr, xm, *p_q;
D edr[EM], edz[EM], bcv[MM], bca[MM][3], bch[MM][3];
D r[NM], z[NM], drr[NM], drz[NM], dzz[NM], qt[NM],
per[NM], pez[NM], vr[NM], vz[NM], hp[NM], qlymph[NM];
O cs;
U cln;
/* */
for (i=0;i<NM;i++) {
  r[i] = *pr++;
}

```

```

        z[i] = *pz++;
        nsk[i] = *sk++;
        drr[i] = *rr++;
        drz[i] = *rz++;
        dzz[i] = *zz++;
        vr[i] = *ur++;
        vz[i] = *uz++;
        hp[i] = *ph++;
        qt[i] = *co++;
        for (j=0;j<NM;j++)
            { cln.m[i][j] = 0.0; }
    for (i=0;i<EM;i++) {
        edr[i] = *rd++;
        edz[i] = *zd++;
        for (j=0;j<6;j++)
            { eldef[i][j] = *pe++; }
    for (i=0;i<MM;i++) {
        bc1[i] = *b1++;
        bc2[i] = *b2++;
        bce[i] = *be++;
        bcn[i] = *bn++;
        bcg[i] = *bg++;
        bcv[i] = *bv++;
        for (j=0;j<3;j++) {
            bca[i][j] = *ba++;
            bch[i][j] = *bh++; }
    /* */
    puts(" itcscap()");
    isigmas = 1.0-mem.sigma;
    lref2d = sq(pp.lref)/pp.diff;
    ndvel = pp.lref*pp.hind*pp.fst/(pp.fav*pp.diff);
    lsvol = pp.pref*lref2d*pp.ls;
    jovol = lref2d*pp.jo;
    /*
    GET DIMENSIONLESS EFFECTIVE CONVECTIVE VELOCITIES
    */
    for (i=0;i<ndnm;i++) {
        per[i] = ndvel*vr[i];
        pez[i] = ndvel*vz[i]; }
    /*
    GET NODAL LYMPH FLOW
    */
    if (pp.ls != 0.0) {
        for (i=0;i<ndnm;i++) {
            if (nsk[i] != 0) {
                if ((xm = lsvol*(hp[i]-pp.plymph)) > 0.0)
                    { qlymph[i] = jovol+xm; }
                else
                    { qlymph[i] = jovol; }
            }
            else
                { qlymph[i] = 0.0; } }
    }
    else {
        for (i=0;i<ndnm;i++)
            { qlymph[i] = 0.0; }
    }
    /*
    TEMPORAL AND/OR SINK MATRIX
    */
    p_q = stif(2, ndnm, elnm, bw, &r[0], &z[0], &eldef[0][0], &edr[0], &edz[0],
        &drr[0], &drz[0], &dzz[0], &per[0], &pez[0], &per[0],
        pp.lref, crz, ihof, geom, ngp);
    for (i=0;i<NM;i++) {
        for (j=0;j<NM;j++)
            { cln.m[i][j] = *p_q++; }
    }
    /*
    PREVIOUS TIME STEP CONTRIBUTION
    */
    if (ss != 0) {
        p_q = matvecbw(0, ndnm-1, bw, &cln.m[0][0], &qt[0]);
        for (i=0;i<ndnm;i++)
            { qt[i] = (*p_q+)/ddt; }
    }
    else {
        for (i=0;i<ndnm;i++)
            { qt[i] = 0.0; }
    }
    /*
    SUM TEMPORAL AND SINK MATRICES
    */
    if (pp.ls != 0.0) {
        for (i=0;i<NM;i++) {
            for (j=0;j<NM;j++) {
                if (ss != 0)
                    { cln.m[i][j] *= (1.0/ddt+qlymph[i]); }
            }
        }
    }

```

```

        else
            { cln.m[i][j] *= qlymph[i]; }) }
/*
SUM DIFF-DISP STIFFNESS AND TEMPORAL-SINK MATRICES
*/
p_q = stif(0, ndnm, elnm, bw, &r[0], &z[0], &eldef[0][0], &edr[0], &edz[0],
    &drr[0], &drz[0], &dzz[0], &per[0], &pez[0], &per[0],
    pp.lref, crz, ihof, geom, ngp);
for (i=0;i<NM;i++) {
    for (j=0;j<NM;j++)
        { cln.m[i][j] += *p_q++; } }
/*
SUM TEMPORAL-SINK-DIFF-DISP AND CONVECTIVE MATRICES
*/
p_q = stif(1, ndnm, elnm, bw, &r[0], &z[0], &eldef[0][0], &edr[0], &edz[0],
    &drr[0], &drz[0], &dzz[0], &per[0], &pez[0], &per[0],
    pp.lref, crz, ihof, geom, ngp);
for (i=0;i<NM;i++) {
    for (j=0;j<NM;j++)
        { cln.m[i][j] += *p_q++; } }
/*
GET MEMBRANE PECELET NUMBER
*/
for (i=0;i<nz;i++) {
    cs.mpe[i] = fabs(vr[mem.mnod[i]]*isigmas/mem.ps);
    cs.ccap[i] = mem.cp[i]; }
/* */
puts("\n Membrane-Tissue Concentration Iterations :");
k = l = m = n = 0;
do {
    mcerr = 0.0;
    printf(" %3d:", l+1);
    /*
    GET TISSUE-SIDE SOLUTE CONCENTRATION USING INTEGRATED
    PATLAK EQUATION
    */
    for (i=0;i<nz;i++) {
        if (cs.mpe[i] > 1.0e-06) {
            if (cs.mpe[i] > 100.0)
                { aa = 0.0; }
            else
                { aa = mem.ps_d*cs.mpe[i]/(exp(cs.mpe[i])-1.0); } }
        else
            { aa = mem.ps_d; }
        if (mem.vd[i] >= 0.0) {
            bb = aa+per[mem.mnod[i]]*isigmas;
            cc = aa+per[mem.mnod[i]];
            dd = cc*mem.wall_th_d/drr[mem.mnod[i]];
            xm = bb/cc;
            mem.ct[i] = (xm+(1.0-xm)*exp(-dd))*mem.cp[i]; }
        else {
            bb = per[mem.mnod[i]]-aa;
            cc = per[mem.mnod[i]]*isigmas-aa;
            dd = cc*mem.wall_th_d/drr[mem.mnod[i]];
            xm = bb/cc;
            mem.ct[i] = (xm+(1.0-xm)*exp(dd))*mem.cp[i]; } }
    /*
    CAPILLARY MEMBRANE CONCENTRATION DISTRIBUTION
    */
    p_q = cmcd(nz, mem);
    for (i=0;i<nz;i++) {
        if ((mem.cp[i] = *p_q++) < 0.0)
            { mem.cp[i] = 0.0; } }
    /* */
    for (i=0;i<nz;i++) {
        if (fabs(mem.cp[i]-cs.ccap[i]) > mcerr)
            { mcerr = fabs(mem.cp[i]-cs.ccap[i]); }
        cs.ccap[i] = mem.cp[i]; }
    printf(" mcerr=%6.3e\n", mcerr);
    l++;
} while ((mcerr > ctol) && (l < cmaxit));
cs.iter = l;
/* */
for (i=0;i<nz;i++)
    { cs.c[mem.mnod[i]] = mem.ct[i]; }
/*
SET TISSUE NODAL BC
*/
for (i=0;i<nz;i++) {
    for (j=0;j<nncbc;j++) {
        if (bcn[j] == mem.mnod[i])

```

```

        { bcv[j] = mem.ct[i]; })
/*
SET TYPE 3 BOUNDARY CONDITION VALUES FOR
MEMBRANE BC AND WALLS.
*/
for (i=0;i<necbc;i++) {
    switch(bcg[i]) {
        case 0: /* RO<r<RG, z=0 */
            for (j=0;j<2;j++) {
                switch (j) {
                    case 0 : k = bc1[i];break;
                    case 1 : k = bc2[i];break; }
                bca[i][j] = -pez[k]/dzz[k];
                bch[i][j] = 0.0; }
            break;
        case 1: /* RO<r<RG, z=L */
            for (j=0;j<2;j++) {
                switch (j) {
                    case 0 : k = bc1[i];break;
                    case 1 : k = bc2[i];break; }
                bca[i][j] = -pez[k]/dzz[k];
                bch[i][j] = 0.0; }
            break;
        case 2: /* r=RG, 0<z<L */
            for (j=0;j<2;j++) {
                switch (j) {
                    case 0 : k = bc1[i];break;
                    case 1 : k = bc2[i];break; }
                bca[i][j] = -per[k]/drr[k];
                bch[i][j] = 0.0; }
            break;
        case 3: /* r=RO, 0<z<L, MEMBRANE BC */
            for (j=0;j<2;j++) {
                switch (j) {
                    case 0 : k = bc1[i];break;
                    case 1 : k = bc2[i];break; }
                for (m=0;m<nz;m++) {
                    if (mem.mnod[m] == k)
                        { n = m; } }
                if (cs.mpe[n] > 1.0e-06) {
                    if (cs.mpe[n] > 100.0)
                        { xm = 0.0; }
                    else
                        { xm = cs.mpe[n]/(exp(cs.mpe[n])-1.0); }
                }
                else
                    { xm = mem.ps_d; }
                if (per[k] > 0.0) {
                    bca[i][j] = -pp.lref*(per[k]+mem.ps_d*xm);
                    bch[i][j] = -
pp.lref*(per[k]*isigmas+mem.ps_d*xm)*cs.ccap[n]; }
                else {
                    bca[i][j] = -pp.lref*(per[k]*isigmas-
mem.ps_d*xm);
                    bch[i][j] = -pp.lref*(per[k]-
mem.ps_d*xm)*cs.ccap[n]; } }
            break;
        case 4 : /* PRESCRIBED AT INPUT */
            break; } }
/*
MODIFY CONC STIFFNESS MATRIX FOR ELEMENTAL BOUNDARY CONDITIONS
*/
if (necbc != 0) {
    cln = modstif(necbc, &eldef[0][0], &r[0], &z[0],
&bce[0], &bca[0][0], &bch[0][0], &bc1[0], &bc2[0],
&edr[0], &edz[0], &cln.m[0][0], ihof, ngp); }
/*
SUM TYPE 3 BC VECTOR AND PREVIOUS TIME STEP VECTOR
*/
for (i=0;i<ndnm;i++)
    { cln.v[i] += qt[i]; }
/*
NODAL BOUNDARY CONDITIONS (TYPE 1)
*/
for (i=0;i<nncbc;i++) {
    for (j=0;j<ndnm;j++) {
        if (j == bcn[i]) {
            cln.m[bcn[i]][j] = 1.0e+15;
            cln.v[bcn[i]] = 1.0e+15*bcv[i]; }
        else
            { cln.m[bcn[i]][j] = 0.0; } } }

```

```

/*
GET CONCENTRATION DISTRIBUTION
*/
p_q = solver(ndnm, bw, &cln.m[0][0], &cln.v[0]);
for (i=0;i<ndnm;i++)
  { cs.c[i] = *p_q++; }
/*
*/
for (i=0;i<nz;i++) {
  cs.ctis[i] = cs.c[mem.mnod[i]];
  cs.ccap[i] = mem.cp[i]; }
/*
SOLUTE FLOW ACROSS MEMBRANE
*/
for (i=0;i<nz;i++) {
  if (cs.mpe[i] > 1.0e-06) {
    if (cs.mpe[i] > 100.0)
      { xm = 0.0; }
    else
      { xm = cs.mpe[i]/(exp(cs.mpe[i])-1.0); }
  }
  else
    { xm = mem.ps; }
  cs.fmem[i] = vr[mem.mnod[i]]*isigmas*mem.cp[i]+mem.ps*xm*(cs.ccap[i]-
cs.ctis[i]); }
/* */
return cs;
}
N itpruruz2d(I ndnm, I elnm, I nnpbc, I nepbc, I nr, I nz, I bw, I vmaxit,
media pp, membr mem, I *pe, I *fl, D *rd, D *zd, D *pr, D *pz,
D *po, D *ph, I *bn, D *bv, I *be, I *bg, D *ba, D *bh, I *b1, I *b2, I *sk,
D p_art, D p_ven, D ptol, D vtol, I lincap,
I relaxp, I ihof, I geom, I ngp)
{
  I i, j, k, l, m, n, hiflow;
  I bcn[MM], bce[MM], bcg[MM], bcl[MM], bc2[MM];
  I nsk[NM], flow[NM], eldef[EM][6];
  D en, eo, ls_d, jo_d, lref2k, piatemu, prefl, mperr, mverr, xm, ww, *p_q;
  D xx[IM], yy[IM], verr[IM], vmem[IM], vtis[IM], edr[EM], edz[EM];
  D bcv[MM], bca[MM][3], bch[MM][3];
  D dp[NM], r[NM], z[NM], dkrr[NM], dkzz[NM], krr[NM], kzz[NM],
  kkr[NM], kkz[NM], op[NM], lsk[NM], ld[NM], hp[NM], sig[NM];
  D ln[NM][NM];
  N pruruz;
  U pln;
  vec3 v_p;
  /* */
  for (i=0;i<NM;i++) {
    nsk[i] = *sk++;
    flow[i] = *fl++;
    r[i] = *pr++;
    z[i] = *pz++;
    op[i] = *po++;
    hp[i] = *ph++; }
  for (i=0;i<EM;i++) {
    edr[i] = *rd++;
    edz[i] = *zd++;
    for (j=0;j<6;j++)
      { eldef[i][j] = *pe++; }}
  for (i=0;i<MM;i++) {
    bcl[i] = *b1++;
    bc2[i] = *b2++;
    bce[i] = *be++;
    bcn[i] = *bn++;
    bcg[i] = *bg++;
    bcv[i] = *bv++;
    for (j=0;j<3;j++) {
      bca[i][j] = *ba++;
      bch[i][j] = *bh++; }}
  /* */
  switch (geom) {
  case 0: /* NO UPWINDING - RECT */
    geom = 0;
    break;
  case 1: /* NO UPWINDING - CYL */
    geom = 1;
    break;
  case 2: /* UPWINDING - RECT */
    geom = 0;
    break;
  case 3: /* UPWINDING - CYL */
    geom = 1;
    break; }
}

```

```

/* */
puts(" itpruruz()");
hiflow = 0;
lref2k = sq(pp.lref)/pp.kref;
prefl = pp.pref/(pp.lref);
ls_d = lref2k*pp.ls;
jo_d = lref2k*pp.jo;
/*
HYDRAULIC CONDUCTIVITY
*/
for (i=0;i<ndnm;i++) {
    switch (flow[i]) {
        case 0 : /* LO FLOW CHANNEL */
            default :
                krr[i] = kzz[i] = pp.lo_k;
                kkr[i] = kkz[i] = pp.lo_k/pp.kref;
                sig[i] = pp.sigmag;
                break;
        case 1 : /* HI FLOW CHANNEL */
            hiflow = 1;
            krr[i] = kzz[i] = pp.hi_k;
            kkr[i] = kkz[i] = pp.hi_k/pp.kref;
            sig[i] = pp.sigmag;
            break;
        case 2 : /* SINK REGION */
            krr[i] = kzz[i] = pp.hi_k;
            kkr[i] = kkz[i] = pp.hi_k/pp.kref;
            sig[i] = pp.sigmag;
            break; } }

for (i=0;i<ndnm;i++)
    { sig[i] *= op[i]; }
/*
GRADIENTS IN HYDRAULIC CONDUCTIVITY :
Krr IN r DIRECTION
Kzz IN z DIRECTION
*/
if (hiflow != 0) {
    for (i=0;i<nz;i++) {
        for (j=0;j<nr;j++) {
            k = i*nr+j;
            xx[j] = r[k];
            yy[j] = krr[k]; }
        v_p = fspl(nr, &xx[0], &yy[0], 0, 0, 0.0, 0.0);
        for (j=0;j<nr;j++) {
            k = i*nr+j;
            dkrr[k] = devalcs(nr, v_p, &xx[0], r[k]); } }
    for (i=0;i<nr;i++) {
        for (j=0;j<nz;j++) {
            k = j*nr+i;
            xx[j] = z[k];
            yy[j] = kzz[k]; }
        v_p = fspl(nz, &xx[0], &yy[0], 0, 0, 0.0, 0.0);
        for (j=0;j<nz;j++) {
            k = j*nr+i;
            dkzz[k] = devalcs(nz, v_p, &xx[0], z[k]); } }
    printf(" dkrr()/dkzz()"); }
/*
GET CONDUCTIVITY STIFFNESS MATRIX
*/
p_q = stif(0, ndnm, elnm, bw, &r[0], &z[0], &eldef[0][0], &edr[0], &edz[0],
&kkrr[0], &kkz[0], &kkz[0], &dkrr[0], &dkzz[0], &kkz[0],
pp.lref, 0, ihof, geom, ngp);
for (i=0;i<NM;i++) {
    for (j=0;j<NM;j++)
        { ln[i][j] = *p_q++; } }
/*
SUM CONDUCTIVITY AND ANISOTROPIC CONDUCTIVITY (CONVECTIVE-LIKE) MATRICES
*/
if (hiflow != 0) {
    p_q = stif(1, ndnm, elnm, bw, &r[0], &z[0], &eldef[0][0], &edr[0], &edz[0],
&kkrr[0], &kkz[0], &kkz[0], &dkrr[0], &dkzz[0], &kkz[0],
pp.lref, 0, ihof, geom, ngp);
    for (i=0;i<NM;i++) {
        for (j=0;j<NM;j++)
            { ln[i][j] -= lref2k*(*p_q++); } } }
/* */
puts("\n Membrane-Tissue Pressure-Velocity Iterations :");
eo = 1.0e-02;
k = l = m = n = pruruz.iter = 0;
do {
    mperr = mverr = 0.0;

```

```

printf(" %3d:", l+1);
/*
CAPILLARY MEMBRANE PRESSURE DISTRIBUTION
*/
if (lincap != 0) {
    xm = (p_art-p_ven)/(mem.z[0]-mem.z[nz-1]);
    for (i=0;i<nz;i++)
        { pruruz.pcap[i] = p_art+xm*mem.z[i]; }
else {
    p_q = compd(nz, mem, p_art, p_ven);
    for (i=0;i<nz;i++)
        { pruruz.pcap[i] = *p_q++; }
/*
SET POTENTIAL TYPE 3 BOUNDARY CONDITIONS d(hP-sigmag*oP)/dn = 0.0
*/
for (i=0;i<nepbc;i++) {
    switch(bcg[i]) {
        case 0: /* RO<r<RG, z=0 */
            for (j=0;j<2;j++) {
                switch (j) {
                    case 0 : k = bc1[i];break;
                    case 1 : k = bc2[i];break; }
                bca[i][j] = 0.0;
                bch[i][j] = 0.0; }
            break;
        case 1: /* RO<r<RG, z=L */
            for (j=0;j<2;j++) {
                switch (j) {
                    case 0 : k = bc1[i];break;
                    case 1 : k = bc2[i];break; }
                bca[i][j] = 0.0;
                bch[i][j] = 0.0; }
            break;
        case 2: /* r=RG, 0<z<L */
            for (j=0;j<2;j++) {
                switch (j) {
                    case 0 : k = bc1[i];break;
                    case 1 : k = bc2[i];break; }
                bca[i][j] = 0.0;
                bch[i][j] = 0.0; }
            break;
        case 3: /* MEMBRANE BC */
            for (j=0;j<2;j++) {
                switch (j) {
                    case 0 : k = bc1[i];break;
                    case 1 : k = bc2[i];break; }
                for (m=0;m<nz;m++) {
                    if (mem.mnod[m] == k)
                        { n = m; }}
                switch (flow[k]) {
                    case 0 :
                    default :
                        xm = lref2k*lp(mem.typ_lp,
mem.lp0, mem.lp1, z[k]);
                    break;
                    case 1 :
                        xm = lref2k*lp(0, mem.lp1,
mem.lp1, z[k]);
                    break; }
                bca[i][j] = xm;
                bch[i][j] = xm*((pruruz.pcap[n]-
mem.sigma*mem.pi_cap)+(mem.sigma-pp.sigmag)*op[k]); }
            break;
        case 4 : /* PRESCRIBED AT INPUT */
            break; }
    }
/*
MODIFY PRESSURE STIFFNESS MATRIX
*/
if (nepbc != 0) {
    pln = modstif(nepbc, &eldef[0][0], &r[0], &z[0],
&bce[0], &bca[0][0], &bch[0][0], &bc1[0], &bc2[0],
&edr[0], &edz[0], &ln[0][0], ihof, ngp); }
/*
SUM CONDUCTIVITY AND SINK MATRICES
*/
if (pp.ls != 0.0) {
    /*
    SINK MATRIX CONTRIBUTION
    */
    for (i=0;i<ndnm;i++) {
        if (nsk[i] != 0)

```

```

        { lsk[i] = ls_d; }
    else
        { lsk[i] = 0.0; }
    p_q = stif(3, ndnm, elnm, bw, &r[0], &z[0], &eldef[0][0], &edr[0],
&edz[0],
        &kkz[0], &kkz[0], &kkz[0], &kkz[0], &kkz[0], &kkz[0],
        pp.lref, 0, ihof, geom, ngp);
    for (i=0;i<NM;i++) {
        for (j=0;j<NM;j++)
            { pln.m[i][j] += lsk[i]*(p_q++); }
    /*
    SINK VECTOR CONTRIBUTION (TAKEN FROM LHS OF FEM EQN)
    */
    for (i=0;i<ndnm;i++) {
        if (nsk[i] != 0)
            { lsk[i] = ls_d*(pp.plymph-sig[i])-jo_d; }
        else
            { lsk[i] = 0.0; }
    p_q = stif(4, ndnm, elnm, bw, &r[0], &z[0], &eldef[0][0], &edr[0],
&edz[0],
        &kkz[0], &kkz[0], &kkz[0], &kkz[0], &kkz[0], &lsk[0],
        pp.lref, 0, ihof, geom, ngp);
    for (i=0;i<NM;i++)
        { lsk[i] = (p_q++); }
    for (i=0;i<ndnm;i++) {
        if (nsk[i] != 0)
            { pln.v[i] += lsk[i]; } }
    /*
    NODAL BOUNDARY CONDITIONS (TYPE 1)
    */
    for (i=0;i<nnpbc;i++) {
        for (j=0;j<ndnm;j++) {
            if (j == bcn[i]) {
                pln.m[bcn[i]][j] = 1.0e+15;
                pln.v[bcn[i]] = 1.0e+15*(bcv[i]-sig[j]); }
            else
                { pln.m[bcn[i]][j] = 0.0; } }
    /*
    GET PRESSURE (hP) AND POTENTIAL (hP-sigma*oP) DISTRIBUTIONS
    */
    p_q = solver(ndnm, bw, &pln.m[0][0], &pln.v[0]);
    for (i=0;i<ndnm;i++) {
        pruruz.pt[i] = p_q++;
        pruruz.p[i] = pruruz.pt[i]+sig[i]; }
    /*
    FLUID FLOW VELOCITY FIELD
    */
    for (i=0;i<nz;i++) {
        for (j=0;j<nr;j++) {
            k = i*nr+j;
            xx[j] = r[k];
            yy[j] = pruruz.pt[k]; }
        v_p = fspl(nr, &xx[0], &yy[0], 2, 1, 0.0, 0.0);
        for (j=0;j<nr;j++) {
            k = i*nr+j;
            pruruz.r[k] = -krr[k]*prefl*devalcs(nr, v_p, &xx[0], r[k]); }
    for (i=0;i<nr;i++) {
        for (j=0;j<nz;j++) {
            k = j*nr+i;
            xx[j] = z[k];
            yy[j] = pruruz.pt[k]; }
        v_p = fspl(nz, &xx[0], &yy[0], 1, 1, 0.0, 0.0);
        for (j=0;j<nz;j++) {
            k = j*nr+i;
            pruruz.z[k] = -kzz[k]*prefl*devalcs(nz, v_p, &xx[0], z[k]); }
    printf(" uv2d()");
    /*
    CHECK FLUID CONTINUITY ACROSS MEMBRANE
    */
    for (i=0;i<nz;i++) {
        k = mem.mnod[i];
        vmem[i] = lp(mem.typ_lp, mem.lp0, mem.lp1, z[k])*pp.pref*(pruruz.p[k]-
pruruz.pcap[i]-mem.sigma*(op[k]-mem.pi_cap));
        vtis[i] = pruruz.r[k];
        verr[i] = (vmem[i]-vtis[i]);
        if (fabs(verr[i]) > fabs(mverr))
            { mverr = verr[i]; }
    /*
    GET PRESSURE DEVIATION AND THEN APPLY RELAXATION
    */
    for (i=0;i<ndnm;i++) {

```

```

        dp[i] = pruruz.p[i]-hp[i];
        if (fabs(dp[i]) > mperr)
            { mperr = fabs(dp[i]); }
    if (relaxp != 0) {
        en = 0.0;
        for (i=0;i<ndnm;i++)
            { en += fabs(dp[i]); }
        ww = 1.0/(1.0+en/eo);
        if ((eo = en) == 0.0)
            { eo = 1.0e-02; }
        for (i=0;i<ndnm;i++) {
            pruruz.p[i] = ww*pruruz.p[i]+(1.0-ww)*hp[i];
            hp[i] = pruruz.p[i]; }
    else {
        for (i=0;i<ndnm;i++)
            { hp[i] = pruruz.p[i]; }
    /*
    SET MEMBRANE HYDROSTATIC PRESSURE
    */
    for (i=0;i<nz;i++)
        { mem.hp[i] = pruruz.p[mem.mnod[i]]; }
    /*
    CHECK IF PRESSURES ARE BELOW SINK PRESSURE LIMIT AND SWITCH
    OFF SINK IF THIS IS CASE AND SET PRESSURES FOR THOSE NODES
    EQUAL TO LYMPHATIC SINK LIMIT VALUE
    */
    k = 0;
    for (i=0;i<ndnm;i++) {
        if (nsk[i] != 0) {
            if ((pruruz.p[i]-pp.plymph) < 0.0) {
                k = 1;
                bcn[nnpbc] = i;
                bcv[nnpbc] = pp.plymph;
                nnpbc++;
                nsk[i] = 0; }}}
    /* */
    if ((mperr < ptol) || (fabs(mverr) < vtol))
        { pruruz.iter = 1; }
    else
        { pruruz.iter = 0; }
    if (lincap != 0)
        { pruruz.iter = 1; }
    if (k != 0)
        { pruruz.iter = 0; }
    /* */
    if (k != 0)
        { puts(" Recycle - sink pressure violation."); }
    else
        { printf(" mperr=%6.3e mverr=%+6.3e\n", mperr, mverr); }
    l++;
} while ((pruruz.iter == 0) && (l < vmaxit));
pruruz.iter = 1;
if (l >= vmaxit) {
    puts(" W: itpruruz()-> Convergence not achieved.");
    puts("          Try different Lp or K values.");
    puts("          Node List : ");
    for (i=0;i<ndnm;i++) {
        if (fabs(dp[i]) > ptol)
            { printf("          Node : %4d : Deviation = %+10.6e\n", mem.mnod[i],
dp[i]); }
        printf("          Max pressure deviation          = %10.6e\n", mperr);
        printf("          Max velocity deviation           = %+10.6e\n", mverr); }
    /*
    GET FLUID FLOW RATE ALONG CAPILLARY
    */
    if (lincap != 0) {
        piatemu = (PI*pp.pref/(8.0*pp.mu*pp.lref))*(p_art-p_ven)/(mem.z[0]-mem.z[nz-
1]);
        for (i=0;i<nz;i++) {
            xm = pow(pp.lref*mem.r[i], 4.0);
            pruruz.qcap[i] = -piatemu*xm; }
    else {
        piatemu = PI*pp.pref/(8.0*pp.mu*pp.lref);
        for (i=0;i<nz;i++) {
            xx[i] = z[mem.mnod[i]];
            yy[i] = pruruz.pcap[i]; }
        v_p = fspl(nz, &xx[0], &yy[0], 2, 2, 0.0, 0.0);
        for (i=0;i<nz;i++) {
            xm = pow(pp.lref*mem.r[i], 4.0);
            pruruz.qcap[i] = -piatemu*xm*devalcs(nz, v_p, &xx[0], mem.z[i]); }
    /*
    */

```

```

    return pruruz;
}
D *stif(I lct, I ndnm, I elnm, I bw, D *pr, D *pz, I *pe, D *rd, D *zd,
      D *rrd, D *rzd, D *zsd, D *ur, D *uz, D *pf,
      D lref, I crz, I ihof, I geom, I ngp)
{
    I i, j, k, ii, jj, wind;
    I eldef[EM][6];
    D aa, alpha, gam, vavg, vzavg, dravg, dzavg, unorm, dnorm,
      hh, rr, zz, rp, zp, rw, zw, dr2, dz2, drdz, ww, ro, *p_q;
    D estif[6][6];
    D edr[EM], edz[EM];
    D f[NM], drr[NM], drz[NM], dzz[NM], r[NM], z[NM], vr[NM], vz[NM];
    D stifn[NM][NM];
    W nrzt, wrzt, dndr, dndz, edrr, edrz, edzz, evr, evz;
    /* */
    for (i=0;i<NM;i++) {
        f[i] = *pf++;
        r[i] = *pr++;
        z[i] = *pz++;
        drr[i] = *rrd++;
        if (crz == 1)
            { drz[i] = *rzd++; }
        dzz[i] = *zsd++;
        vr[i] = *ur++;
        vz[i] = *uz++; }
    for (i=0;i<EM;i++) {
        edr[i] = *rd++;
        edz[i] = *zd++;
        for (j=0;j<6;j++)
            { eldef[i][j] = *pe++; } }
    /*
    INITIALIZE VARIABLES, MATRICES, AND VECTORS
    */
    wind = 0;
    aa = ro = 0.0;
    for (i=0;i<NM;i++) {
        for (j=1;j<NM;j++)
            { stifn[i][j] = stifn[j][i] = 0.0; }}
    /*
    STIFFNESS MATRIX AT t=t
    */
    switch (geom) {
        case 0: /* NO UPWINDING - RECT */
            geom = 0;
            wind = 0;
            break;
        case 1: /* NO UPWINDING - CYL */
            geom = 1;
            wind = 0;
            break;
        case 2: /* UPWINDING - RECT */
            geom = 0;
            wind = 1;
            break;
        case 3: /* UPWINDING - CYL */
            geom = 1;
            wind = 1;
            break; }
    /*
    FORM ELEMENTAL STIFFNESS MATRIX
    */
    switch (lct) {
        case 0 : /* LAPLACE */
            for (i=0;i<elnm;i++) {
                /* */
                dr2 = 0.5*edr[i];
                dz2 = 0.5*edz[i];
                drdz = dr2*dz2;
                for (j=0;j<6;j++) {
                    for (k=j;k<6;k++)
                        { estif[j][k] = estif[k][j] = 0.0; }}
                for (j=0;j<4;j++) {
                    edrr.v[j] = drr[eldef[i][j]];
                    edrz.v[j] = drz[eldef[i][j]];
                    edzz.v[j] = dzz[eldef[i][j]]; }
                /* */
                for (k=0;k<ngp;k++) {
                    zp = gp(ngp, k);
                    zw = gw(ngp, k);
                    zz = dz2*(zp+1.0);

```

```

for (j=0;j<ngp;j++) {
  rp = gp(ngp, j);
  rw = gw(ngp, j);
  rr = dr2*(rp+1.0);
  /* */
  ww = rw*zw;
  if (geom == 1)
    { ro = r[eldef[i][0]]+rr; }
  /* */
  if (ihof == 1) {
    nrzt = fmrzt(rr, zz, edr[i], edz[i]);
    dndr = fdmnr(rr, zz, edr[i], edz[i]);
    dndz = fdmndz(rr, zz, edr[i], edz[i]); }
  else {
    nrzt = fnrzt(rr, zz, edr[i], edz[i]);
    dndr = fdndr(rr, zz, edr[i], edz[i]);
    dndz = fdndz(rr, zz, edr[i], edz[i]); }
  /* */
  for (i1=0;i1<4;i1++) {
    for (j1=0;j1<4;j1++) {
      estif[i1][j1] +=
(ww*edrr.v[i1]*dndr.v[i1]*dndr.v[j1]);
      if (crz == 1) {
(ww*edrz.v[i1]*dndr.v[i1]*dndz.v[j1]);
      estif[i1][j1] +=
(ww*edrz.v[i1]*dndz.v[i1]*dndr.v[j1]); }
      estif[i1][j1] +=
(ww*edzz.v[i1]*dndz.v[i1]*dndz.v[j1]);
      if (geom == 1)
        { estif[i1][j1] -=
(ww*edrr.v[i1]*nrzt.v[i1]*dndr.v[j1]/ro); } } } }
  /*
  SCALE TO INTEGRATION DOMAIN
  */
  for (i1=0;i1<4;i1++) {
    for (j1=0;j1<4;j1++)
      { estif[i1][j1] *= drdz; }
  /*
  INCORPORATE INTO GLOBAL STIFFNESS MATRIX AT
  */
  for (j=0;j<4;j++) {
    for (k=0;k<4;k++)
      { stifn[eldef[i][j]][eldef[i][k]] +=
estif[j][k]; } }
  printf(" lapl()");
  break;
case 1 : /* CONVECTIVE */
  for (i=0;i<elnm;i++) {
    /* */
    dr2 = 0.5*edr[i];
    dz2 = 0.5*edz[i];
    drdz = dr2*dz2;
    for (j=0;j<6;j++) {
      for (k=j;k<6;k++)
        { estif[j][k] = estif[k][j] = 0.0; } }
    for (j=0;j<4;j++) {
      evr.v[j] = vr[eldef[i][j]];
      evz.v[j] = vz[eldef[i][j]];
      edrr.v[j] = drr[eldef[i][j]];
      edrz.v[j] = drz[eldef[i][j]];
      edzz.v[j] = dzz[eldef[i][j]]; }
    /* */
    if (wind == 1) {
      vrag = vzag = drag = dzag = 0.0;
      for (j=0;j<4;j++) {
        vrag += fabs(evr.v[j]);
        vzag += fabs(evz.v[j]);
        drag += edrr.v[j];
        dzag += edzz.v[j]; }
      vrag *= 0.25;
      vzag *= 0.25;
      drag *= 0.25;
      dzag *= 0.25;
      unorm = norm(vrag, vzag);
      dnorm = norm(drag, dzag);
      if (unorm != 0.0) {
        hh =
lref*(fabs(vrag)*edr[i]+fabs(vzag)*edz[i])/unorm;
        gam = 0.5*unorm*hh/dnorm;
        alpha = coth(gam)-1.0/gam;

```

```

                                aa = alpha*hh/(2.0*unorm); }
else
    { aa = 0.0; }
else
    { aa = 0.0; }
/* */
for (k=0;k<ngp;k++) {
    zp = gp(ngp, k);
    zw = gw(ngp, k);
    zz = dz2*(zp+1.0);
    for (j=0;j<ngp;j++) {
        rp = gp(ngp, j);
        rw = gw(ngp, j);
        rr = dr2*(rp+1.0);
        /* */
        ww = rw*zw;
        /* */
        if (ihof == 1) {
            nrzt = fmrzt(rr, zz, edr[i], edz[i]);
            dndr = fdndr(rr, zz, edr[i], edz[i]);
            dndz = fdmdz(rr, zz, edr[i], edz[i]); }
        else {
            nrzt = fnrzt(rr, zz, edr[i], edz[i]);
            dndr = fdndr(rr, zz, edr[i], edz[i]);
            dndz = fdmdz(rr, zz, edr[i], edz[i]); }
        if (wind == 1)
            { wrzt = fwrzt(aa, evr, evz, nrzt, dndr,
dndz); }
        else
            { wrzt = nrzt; }
        /* */
        for (ii=0;ii<4;ii++) {
            for (jj=0;jj<4;jj++) {
                estif[ii][jj] +=
                estif[ii][jj] +=
                (ww*evr.v[ii]*wrzt.v[ii]*dndr.v[jj]);
                (ww*evz.v[ii]*wrzt.v[ii]*dndz.v[jj]); } } }
        /*
        SCALE TO INTEGRATION DOMAIN
        */
        for (ii=0;ii<4;ii++) {
            for (jj=0;jj<4;jj++)
                { estif[ii][jj] *= drdz; } }
        /*
        INCORPORATE INTO GLOBAL STIFFNESS MATRIX
        */
        for (j=0;j<4;j++) {
            for (k=0;k<4;k++)
                { stifn[eldef[i][j]][eldef[i][k]] +=
estif[j][k]; } } }
    printf(" conv()");
    break;
case 2 : /* TEMPORAL STIFFNESS MATRIX */
case 3 : /* SINK STIFFNESS MATRIX */
case 4 : /* LOAD VECTOR STIFFNESS MATRIX */
    for (i=0;i<elnm;i++) {
        /* */
        dr2 = 0.5*edr[i];
        dz2 = 0.5*edz[i];
        drdz = dr2*dz2;
        for (j=0;j<6;j++) {
            for (k=j;k<6;k++)
                { estif[j][k] = estif[k][j] = 0.0; } }
        /* */
        for (k=0;k<ngp;k++) {
            zp = gp(ngp, k);
            zw = gw(ngp, k);
            zz = dz2*(zp+1.0);
            for (j=0;j<ngp;j++) {
                rp = gp(ngp, j);
                rw = gw(ngp, j);
                rr = dr2*(rp+1.0);
                /* */
                ww = rw*zw;
                /* */
                if (ihof == 1)
                    { nrzt = fmrzt(rr, zz, edr[i], edz[i]); }
                else
                    { nrzt = fnrzt(rr, zz, edr[i], edz[i]); }
                /* */
                for (ii=0;ii<4;ii++) {

```

```

                                for (jj=0;jj<4;jj++)
                                  { estif[i1][jj] +=
(ww*nrzt.v[i1]*nrzt.v[jj]); } } )
/*
SCALE TO INTEGRATION DOMAIN
*/
for (i1=0;i1<4;i1++) {
  for (jj=0;jj<4;jj++)
    { estif[i1][jj] *= drdz; }
/*
INCORPORATE INTO GLOBAL STIFFNESS MATRIX AT t
*/
for (j=0;j<4;j++) {
  for (k=0;k<4;k++)
    { stifn[eldef[i][jj]][eldef[i][k]] +=
estif[j][k]; } } )
switch (lct) {
case 2 :
case 3 : printf(" temp()/sink()");break;
case 4 : printf(" func()");break; }
break; }
/* */
if (lct == 4) {
  p_q = matvecbw(0, ndnm-1, bw, &stifn[0][0], &f[0]);
  for (i=0;i<NM;i++)
    { f[i] = *p_q++; }
  return &f[0]; }
/* */
return &stifn[0][0];
}
U modstif(I nebc, I *pe, D *pr, D *pz, I *be, D *ba, D *bh, I *b1, I *b2,
D *rd, D *zd, D *st, I ihof, I ngp)
{
  I i, j, k, i1, jj;
  I lnod[3], gnod[3], bce[MM], bcl[MM], bc2[MM];
  I eldef[EM][6];
  D gamma, cgamma, sgamma, ss, rr, zz, sp, sw, sqnl2, ds, ds2, ww;
  D edr[EM], edz[EM], r[NM], z[NM];
  D he[3], se[3][3], ae[4][4], bca[MM][3], bch[MM][3];
  W nrzt;
  U mv;
  /* */
  for (i=0;i<NM;i++) {
    r[i] = *pr++;
    z[i] = *pz++;
    for (j=0;j<NM;j++)
      { mv.m[i][j] = *st++; }
  }
  for (i=0;i<MM;i++) {
    bcl[i] = *b1++;
    bc2[i] = *b2++;
    bce[i] = *be++;
    for (j=0;j<3;j++) {
      bca[i][j] = *ba++;
      bch[i][j] = *bh++; }
  }
  for (i=0;i<EM;i++) {
    edr[i] = *rd++;
    edz[i] = *zd++;
    for (j=0;j<6;j++)
      { eldef[i][j] = *pe++; }
  }
  /*
INITIALIZE VARIABLES
*/
  for (i=0;i<3;i++)
    { lnod[i] = gnod[i] = 0; }
  for (i=0;i<NM;i++)
    { mv.v[i] = 0.0; }
  /*
INCORPORATE TYPE 3 BOUNDARY CONDITIONS
*/
  for (i=0;i<nebc;i++) {
    for (j=0;j<4;j++) {
      if (bcl[i] == eldef[bce[i1][j]]) {
        lnod[0] = j;
        gnod[0] = bcl[i]; }
      if (bc2[i] == eldef[bce[i1][j]]) {
        lnod[1] = j;
        gnod[1] = bc2[i]; }
    }
    for (j=0;j<3;j++) {
      he[j] = 0.0;
      for (k=j;k<3;k++)
        { ae[j][k] = ae[k][j] = se[j][k] = se[k][j] = 0.0; }
    }
  }

```

```

/*      */
ds = sqrt(sq(r[bc1[i]]-r[bc2[i]])+sq(z[bc1[i]]-z[bc2[i]]));
ds2 = 0.5*ds;
if (r[bc1[i]] == r[bc2[i]]) {
    gamma = 0.5*PI;
    cgamma = 0.0;
    sgamma = 1.0; }
else
if (z[bc1[i]] == z[bc2[i]]) {
    gamma = 0.0;
    cgamma = 1.0;
    sgamma = 0.0; }
else {
    gamma = atan(fabs(r[bc1[i]]-r[bc2[i]])/fabs(z[bc1[i]]-z[bc2[i]]));
    cgamma = cos(gamma);
    sgamma = sin(gamma); }
for (j=0;j<ngp;j++) {
    sp = gp(ngp, j);
    sw = gw(ngp, j);
    ss = ds2*(sp+1.0);
    rr = ss*cgamma;
    zz = ss*sgamma;
    ww = sw;
    /*      */
    if (ihof == 1)
        { nrzt = fmrzt(rr, zz, edr[bce[i]], edz[bce[i]]); }
    else
        { nrzt = fnrzt(rr, zz, edr[bce[i]], edz[bce[i]]); }
    sqnl2 = sq(nrzt.v[lnod[0]]+sq(nrzt.v[lnod[1]]);
    /*      */
    for (ii=0;ii<2;ii++) {
        for (jj=0;jj<2;jj++) {
            se[ii][jj] += (ww*nrzt.v[lnod[ii]]*nrzt.v[lnod[jj]]);
            ae[ii][jj] += (ww*bca[i][ii]*nrzt.v[lnod[ii]]*sqnl2);
        }
    }
} }

/*
SCALE TO INTEGRATION DOMAIN
*/
for (ii=0;ii<2;ii++) {
    for (jj=0;jj<2;jj++) {
        se[ii][jj] *= ds2;
        ae[ii][jj] *= ds2; }}

/*
GET h CONTRIBUTION
*/
for (ii=0;ii<2;ii++) {
    for (jj=0;jj<2;jj++)
        { he[ii] += se[ii][jj]*bch[i][jj]; }}

/*
INCORPORATE INTO STIFFNESS MATRIX AND RHS VECTOR
*/
for (ii=0;ii<2;ii++) {
    mv.v[gnod[ii]] += he[ii];
    for (jj=0;jj<2;jj++)
        { mv.m[gnod[ii]][gnod[jj]] += ae[ii][jj]; }} }

/*      */
printf(" modstif()");
/*      */
return mv;
}
vdiff dspc(I ndnm, D a1, D a2, D diff, D *vr, D *vz, I crz)
(
    I i;
    D vel, vrz, vr2, vz2;
    vdiff d;
    /*      */
    if ((a1 == 0.0) && (a2 == 0.0)) {
        for (i=0;i<ndnm;i++) {
            d.rr[i] = diff;
            d.rz[i] = 0.0;
            d.zz[i] = diff; }}
    else {
        for (i=0;i<ndnm;i++) {
            vrz = fabs(vr[i]*vz[i]);
            vr2 = sq(vr[i]);
            vz2 = sq(vz[i]);
            vel = sqrt(vr2+vz2);
            if (vel == 0.0) {
                d.rr[i] = diff;
                d.rz[i] = 0.0;
                d.zz[i] = diff; }
        }
    }
}

```

```

        else {
            d.rr[i] = (a2*vz2+a1*vr2)/vel+diff;
            if (crz == 1)
                { d.rz[i] = (a1-a2)*vrz/vel; }
            else
                { d.rz[i] = 0.0; }
            d.zz[i] = (a2*vr2+a1*vz2)/vel+diff; } } }

/*      */
printf(" dspc()");
/*      */
return d;
}
/*
USER DEFINED lp() FUNCTION.
*/
D lp(I typ, D lp0, D lp1, D x)
{
    D lp=0.0;
    switch (typ) {
        case 0 :
            lp = lp0;
            break;
        case 1 :
            lp = (1.0-x)*lp0+x*lp1;
            break;
        case 2 :
            if (x <= 0.50)
                { lp = lp0; }
            else
                { lp = lp1; }
            break;
        case 3 :
            if ((x < 0.90) || (x > 0.95))
                { lp = lp0; }
            else
                { lp = lp1; }
            break;
        case 4 :
            lp = lp0+(lp1-lp0)/(1.0+exp(-50.0*(x-0.5)));
            break; }
    return lp;
}
/*
MASS BALANCE
*/
V massb(I elnm, I nr, I nz, I nesink, media pp, membr mem, I *pe, I *sn, D *rd, D *zd,
D *pc, D *ph, D *pf, D qcap, D avgas, I ngp, I geom)
{
    I i, j, k, l, er, ez;
    I isink[EM], eldef[EM][6];
    D dr2, dz2, lref3, uc, uu, rr, rp, rw, zz, zp, zw,
    xm, fqm, sqm, qf1, qfo, qmf, qms, qsi, qso, qsf, qss, p, c,
    pa, ca, va, pavg, cavg, vavg, vol, ww;
    D fmem[IM], edr[EM], edz[EM], co[NM], hp[NM];
    W epr, ecs, nrzt;
    /*      */
    for (i=0;i<NM;i++) {
        co[i] = *pc++;
        hp[i] = *ph++; }
    for (i=0;i<EM;i++){
        isink[i] = *sn++;
        edr[i] = *rd++;
        edz[i] = *zd++;
        for (j=0;j<6;j++)
            { eldef[i][j] = *pe++; } }
    for (i=0;i<IM;i++)
        { fmem[i] = *pf++; }
    er = nr-1;
    ez = nz-1;
    switch (geom) {
        case 0: /* NO UPWINDING - RECT */
            geom = 0;
            break;
        case 1: /* NO UPWINDING - CYL */
            geom = 1;
            break;
        case 2: /* UPWINDING - RECT */
            geom = 0;
            break;
        case 3: /* UPWINDING - CYL */
            geom = 1;
    }
}

```

```

        break; }

/*
FLUID AND SOLUTE MASS BALANCE
*/
puts(" Mass Balance : ");
lref3 = pp.lref*pp.lref*pp.lref;
qfi = qfo = qmf = qms = qsi = qso = qsf = qss = 0.0;
/*
MEMBRANE FLUID FLOW AND SOLUTE TRANSPORT
qfi, qfo : m3/s
qsi, qso : Kg/s
*/
for (i=0;i<ez;i++) {
    k = i*er;
    xm = edz[k]*pp.lref;
    rr = 0.5*(mem.r[i]+mem.r[i+1])*pp.lref;
    uu = 0.5*(mem.vm[i]+mem.vm[i+1]);
    uc = 0.5*(fmem[i]+fmem[i+1]);
    fqm = PI2*uu*rr*xm;
    sqm = PI2*uc*rr*xm*pp.cref;
    qmf += fqm;
    qms += sqm;
    if (fqm >= 0.0) {
        qfi += fqm;
        qsi += sqm; }
    else {
        qfo += fqm;
        qso += sqm; }}

/* */
printf(" Fluid into membrane           = %+10.6e\n", qfi);
printf(" Fluid out of membrane          = %+10.6e\n", qfo);
printf(" Net fluid into membrane           = %+10.6e\n", qmf);
printf(" Solute into membrane               = %+10.6e\n", qsi);
printf(" Solute out of membrane             = %+10.6e\n", qso);
printf(" Net solute into membrane           = %+10.6e\n", qms);
printf(" Fractional fluid flow into membrane = %+10.6e\n", qfi/qcap);
/*
SINK FLUID FLOW AND SOLUTE TRANSPORT
qsf : m3/s
qss : Kg/s
*/
pavg = cavg = vol = 0.0;
for (i=0;i<elnm;i++) {
    if (isink[i] == 1) {
        dr2 = 0.5*edr[i];
        dz2 = 0.5*edz[i];
        xm = dr2*dz2;
        for (j=0;j<4;j++) {
            epr.v[j] = hp[eldef[i][j]];
            ecs.v[j] = cc[eldef[i][j]]; }
        pa = ca = va = 0.0;
        for (k=0;k<ngp;k++) {
            zp = gp(ngp, k);
            zw = gw(ngp, k);
            zz = dz2*(zp+1.0);
            for (j=0;j<ngp;j++) {
                rp = gp(ngp, j);
                rw = gw(ngp, j);
                rr = dr2*(rp+1.0);
                /* */
                ww = rw*zw;
                nrzt = fnrzt(rr, zz, edr[i], edz[i]);
                p = c = 0.0;
                for (l=0;l<4;l++) {
                    p += epr.v[l]*nrzt.v[l];
                    c += ecs.v[l]*nrzt.v[l]; }
                switch (geom) {
                    case 0 :
                        pa += ww*p;
                        ca += ww*c;
                        va += ww;
                        break;
                    case 1 :
                        pa += ww*PI2*rr*p*pp.lref;
                        ca += ww*PI2*rr*c*pp.lref;
                        va += ww*PI2*rr*pp.lref;
                        break; } })
            pavg += (lref3*xm*pa);
            cavg += (lref3*xm*ca);
            vol += (lref3*xm*va); } }
/* */

```

```

if ((avgas != 0.0) && (vol != 0.0)) {
    pavg /= vol;
    cavg /= vol;
    if ((pa = pp.pref*pp.ls*(pavg-pp.plymph)) > 0.0)
        { qsf = -pp.vol_tis*(pa+pp.jo); }
    else
        { qsf = -pp.vol_tis*pp.jo; }
    qss = qsf*cavg*pp.cref;
    vavg = qmf/((D)nesink)*avgas;
    printf(" Net fluid out sink           = %+10.6e\n", qsf);
    printf(" Net solute out sink             = %+10.6e\n", qss);
    printf(" Avg solute conc out sink           = %+10.6e\n", cavg);
    printf(" Avg conv velocity out sink        = %+10.6e\n", vavg);
    printf(" Avg tissue pressure at sink       = %+10.6e\n", pavg);
    printf(" Volume of sink                     = %+10.6e\n", vol); }
else
    { puts(" No sinks in geometry."); }
printf(" Fluid Mass Balance Residual = %10.6e\n", qmf-qsf);
printf(" Solute Mass Balance Residual = %10.6e\n", qms-qss);
}
V domavg(I elnm, media pp, I *pe, D *rd, D *zd, D *pc, D *ph, I ngp, I geom)
{
    I i, j, k, l;
    I eldef[EM][6];
    D dr2, dz2, lref2, rr, rp, rw, zz, zp, zw, xm, p, c,
    pa, ca, va, pavg, cavg, vol, ww;
    D edr[EM], edz[EM], co[NM], hp[NM];
    W epr, ecs, nrzt;
    /* */
    for (i=0;i<NM;i++) {
        co[i] = *pc++;
        hp[i] = *ph++; }
    for (i=0;i<EM;i++){
        edr[i] = *rd++;
        edz[i] = *zd++;
        for (j=0;j<6;j++)
            { eldef[i][j] = *pe++; } }
    switch (geom) {
        case 0: /* NO UPWINDING - RECT */
            geom = 0;
            break;
        case 1: /* NO UPWINDING - CYL */
            geom = 1;
            break;
        case 2: /* UPWINDING - RECT */
            geom = 0;
            break;
        case 3: /* UPWINDING - CYL */
            geom = 1;
            break; }
    /*
    GET AVERAGE QUANTITIES IN SOLUTION DOMAIN
    */
    lref2 = pp.lref*pp.lref;
    /* */
    pavg = cavg = vol = 0.0;
    for (i=0;i<elnm;i++) {
        dr2 = 0.5*edr[i];
        dz2 = 0.5*edz[i];
        xm = dr2*dz2;
        for (j=0;j<4;j++) {
            epr.v[j] = hp[eldef[i][j]];
            ecs.v[j] = co[eldef[i][j]]; }
        pa = ca = va = 0.0;
        for (k=0;k<ngp;k++) {
            zp = gp(ngp, k);
            zw = gw(ngp, k);
            zz = dz2*(zp+1.0);
            for (j=0;j<ngp;j++) {
                rp = gp(ngp, j);
                rw = gw(ngp, j);
                rr = dr2*(rp+1.0);
                /* */
                ww = rw*zw;
                nrzt = fnrzt(rr, zz, edr[i], edz[i]);
                p = c = 0.0;
                for (l=0;l<4;l++) {
                    p += epr.v[l]*nrzt.v[l];
                    c += ecs.v[l]*nrzt.v[l]; }
                switch (geom) {
                    case 0 :

```

```

        pa += ww*p;
        ca += ww*c;
        va += ww;
        break;
    case 1 :
        pa += ww*PI2*rr*p*pp.lref;
        ca += ww*PI2*rr*c*pp.lref;
        va += ww*PI2*rr*pp.lref;
        break; } })
    pavg += lref2*xm*pa;
    cavg += lref2*xm*ca;
    vol += lref2*xm*va; }
    pavg /= vol;
    cavg /= vol;
    printf(" Average Tissue Solute Concentration = %10.6e\n", cavg);
    printf(" Average Tissue Pressure = %10.6e\n", pavg);
}
/*
OSMOTIC PRESSURE ROUTINE.
USE EFFECTIVE SOLUTE CONCENTRATION (DUE TO VOLUME EXCLUSION).
THIS IS THE CONCENTRATION BEING CALCULATED (SO NO ADJUSTMENT).
*/
D *osmopr(I n, media pp, D *pc)
{
    I i, j;
    D cr, a[5], c[NM], op[NM];
    /* */
    for (i=0; i<NM; i++) {
        c[i] = *pc++;
        op[i] = 0.0; }
    /*
    CONVERT TO EFFECTIVE CONCENTRATION IN AVAILABLE FLUID VOLUME
    */
    if (pp.osm != 0) {
        a[0] = 0.0;
        cr = pp.cref/pp.pref;
        a[1] = 57.18198*cr;
        cr *= pp.cref;
        a[2] = -1.238832*cr;
        cr *= pp.cref;
        a[3] = 0.050849*cr;
        /*
        DIMENSIONLESS FORMS of c[] and op[]
        */
        for (i=0; i<n; i++) {
            op[i] = a[3];
            for (j=2; j>-1; j--)
                { op[i] = op[i]*c[i]+a[j]; } }
        printf(" osmp()");
        /* */
        return &op[0];
    }
}
D *cmpd(I n, membr m, D p_art, D p_ven)
{
    I i, j, maxit;
    D bc, err, tol, xm;
    D xbc[3], fbc[3], p[HM], pm[IM];
    M s_f;
    vec3 v_f, v_p;
    /* */
    maxit = 200;
    tol = 1.0e-6;
    /* */
    v_p = fspl(n, &m.z[0], &m.hp[0], 2, 2, 0.0, 0.0);
    v_f = fspl(n, &m.z[0], &m.op[0], 2, 2, 0.0, 0.0);
    /* */
    p[0] = p_art;
    p[1] = (p_art-p_ven)/(m.z[0]-m.z[n-1]);
    bc = p_ven;
    /*
    GET FIRST TWO VALUES
    */
    for (j=0; j<2; j++) {
        s_f = pdcr(2, m, &p[0], m.z[0], m.z[n-1], NJ-2, v_f, v_p, v_p, n, 1);
        if (s_f.error == 1) {
            printf("\n E: pdcr()-> Failed beyond t = %10.6f.\n", s_f.t);
            exit(0); }
        err = bc-s_f.x[0];
        xbc[j] = p[1];
        fbc[j] = s_f.x[0];
        p[1] *= 0.9; }
}

```

```

if (fabs(terr) < tol) goto done;
/*
SECANT METHOD UNTIL CONVERGENCE
*/
j = 2;
do {
    j++;
    if ((xm = fbc[1]-fbc[0]) != 0.0)
        { p[1] = xbc[1]-(fbc[1]-bc)*(xbc[1]-xbc[0])/xm; }
    else
        { p[1] = xbc[1]; }
    s_f = pdcr(2, m, &p[0], m.z[0], m.z[n-1], NJ-2, v_f, v_p, v_p, n, 1);
    if (s_f.error == 1) {
        printf("\n E: pdcr()-> Failed beyond t = %10.6f.\n", s_f.t);
        exit(0); }
    err = bc-s_f.x[0];
    xbc[0] = xbc[1];
    fbc[0] = fbc[1];
    xbc[1] = p[1];
    fbc[1] = s_f.x[0];
} while((fabs(terr) > tol) && (j < maxit));
if (j > maxit) {
    printf("\n Not converged after %d iterations.\n", maxit);
    exit(0); }
done: /*
*/
if (s_f.error == 1) {
    printf("\n E: pdcr()-> Failed beyond t = %10.6f.\n", s_f.t);
    exit(0); }
err = bc-s_f.x[0];
/* */
v_f = fspl(s_f.k, &s_f.tt[0], &s_f.xx[0], 2, 2, 0.0, 0.0);
/* */
for (i=0;i<n;i++)
    { pm[i] = evalcs(s_f.k, v_f, &s_f.tt[0], &s_f.xx[0], m.z[i]); }
/* */
if (fabs(s_f.err) > tol)
    { printf(" cmpd(merr=%6.3e)", fabs(s_f.err)); }
else
    { printf(" cmpd()"); }
/* */
return &pm[0];
}
D *cmcd(I n, membr m)
{
    I i;
    D c[HM], ccap[IM];
    M s_f;
    vec3 v_u, v_v, v_w;
    /* */
    v_u = fspl(n, &m.z[0], &m.cp[0], 2, 2, 0.0, 0.0);
    v_v = fspl(n, &m.z[0], &m.ct[0], 2, 2, 0.0, 0.0);
    v_w = fspl(n, &m.z[0], &m.v[0], 2, 2, 0.0, 0.0);
    /* */
    c[0] = m.c_art;
    /* */
    s_f = pdcr(1, m, &c[0], m.z[0], m.z[n-1], NJ-2, v_u, v_v, v_w, n, 0);
    /* */
    v_u = fspl(s_f.k, &s_f.tt[0], &s_f.xx[0], 2, 2, 0.0, 0.0);
    /* */
    for (i=0;i<n;i++)
        { ccap[i] = evalcs(s_f.k, v_u, &s_f.tt[0], &s_f.xx[0], m.z[i]); }
    /* */
    printf(" cmcd()");
    /* */
    return &ccap[0];
}
/*
PREDICTOR-CORRECTOR ODE INTEGRATION ROUTINES
s_f = CONTAINS ANY ERROR CONDITIONS, THE NUMBER OF FUNCTION
EVALUATIONS, k, THE SOLUTION AT tf, AND THE tt AND xo
VECTORS.
*/
M pdcr(I n, membr m, D *p_x, D tt, D tf, I nci, vec3 v_f, vec3 v_p, vec3 v_q,
I nn, I pc)
{
    I i, j;
    D err, nerr, t[6], ci, ci24, xm;
    D pi[6], hp[6], cp[6], ct[6], vm[6], f[6][HM], x[6][HM], x4p[HM];
    M s_f;
    /* */
    s_f.err = 0.0;

```

```

s_f.error = s_f.nf = s_f.k = 0;
xm = 19.0/270.0;
ci = fabs(tf-tt)/((D)(nci)-1.0);
ci24 = ci/24.0;
for (i=0;i<n;i++)
    { x[0][i] = *p_x++; }
s_f.xx[s_f.k] = x[0][0];
s_f.k++;
for (i=0;i<nci;i++)
    { s_f.tt[i] = (D)(i)*ci; }
/*
FOURTH ORDER RUNGE KUTTA ROUTINE FOR FIRST FOUR POINTS
*/
for (j=0;j<3;j++) {
    tt += ci;
    switch (pc) {
        case 0 :
            cp[j] = evalcs(nn, v_f, &m.z[0], &m.cp[0], tt-ci);
            ct[j] = evalcs(nn, v_p, &m.z[0], &m.ct[0], tt-ci);
            vm[j] = evalcs(nn, v_q, &m.z[0], &m.vm[0], tt-ci);
            p_x = rk4(n, m, tt-ci, ci, &x[j][0], cp[j], ct[j], vm[j], pc);
            break;
        case 1 :
            hp[j] = evalcs(nn, v_p, &m.z[0], &m.hp[0], tt-ci);
            pi[j] = evalcs(nn, v_f, &m.z[0], &m.op[0], tt-ci);
            p_x = rk4(n, m, tt-ci, ci, &x[j][0], pi[j], hp[j], 0.0, pc);
            break; }
    s_f.nf += 4;
    for (i=0;i<n;i++)
        { x[j+1][i] = *p_x++; }
    s_f.xx[s_f.k] = x[j+1][0];
    s_f.k++; }
/*
PREDICTOR-CORRECTOR INTEGRATION ROUTINE
*/
for (i=4;i>-1;i--) {
    t[i] = tt+(D)(i-3)*ci;
    switch (pc) {
        case 0 :
            cp[i] = evalcs(nn, v_f, &m.z[0], &m.cp[0], t[i]);
            ct[i] = evalcs(nn, v_p, &m.z[0], &m.ct[0], t[i]);
            vm[i] = evalcs(nn, v_q, &m.z[0], &m.vm[0], t[i]);
            break;
        case 1 :
            hp[i] = evalcs(nn, v_p, &m.z[0], &m.hp[0], t[i]);
            pi[i] = evalcs(nn, v_f, &m.z[0], &m.op[0], t[i]);
            break; }
    for (j=0;j<4;j++) {
        switch (pc) {
            case 0 :
                p_x = memcs(m, t[j], &x[j][0], cp[j], ct[j], vm[j]);
                break;
            case 1 :
                p_x = membr(m, t[j], &x[j][0], pi[j], hp[j]);
                break; }
        s_f.nf++;
        for (i=0;i<n;i++)
            { f[j][i] = *p_x++; } }
/*
*/
while (tt < (tf-ci)) {
    err = nerr = 0.0;
    t[4] = tt+ci;
    switch (pc) {
        case 0 :
            cp[4] = evalcs(nn, v_f, &m.z[0], &m.cp[0], t[4]);
            ct[4] = evalcs(nn, v_p, &m.z[0], &m.ct[0], t[4]);
            vm[4] = evalcs(nn, v_q, &m.z[0], &m.vm[0], t[4]);
            p_x = memcs(m, t[4], &x4p[0], cp[4], ct[4], vm[4]);
            break;
        case 1 :
            hp[4] = evalcs(nn, v_p, &m.z[0], &m.hp[0], t[4]);
            pi[4] = evalcs(nn, v_f, &m.z[0], &m.op[0], t[4]);
            p_x = membr(m, t[4], &x4p[0], pi[4], hp[4]);
            break; }
    s_f.nf++;
    for (i=0;i<n;i++)
        { f[4][i] = *p_x++; }
    for (i=0;i<n;i++)
        { x4p[i] = x[3][i]+ci24*(55.*f[3][i]-59.*f[2][i]+37.*f[1][i]-
9.*f[0][i]); }
    /* x[4][i] = x4c[i] */
}

```

```

    for (i=0;i<n;i++) {
        x[4][i] = x[3][i]+ci24*(9.*f[4][i]+19.*f[3][i]-5.*f[2][i]+f[1][i]);
        /*
        ABSOLUTE ERROR ESTIMATE
        */
        nerr = xm*fabs(x4p[i]-x[4][i]);
        if (nerr > err)
            { err = nerr; }
        if (err > s_f.err)
            { s_f.err = err; }
        tt += ci;
        s_f.xx[s_f.k] = x[4][0];
        s_f.k++;
        for (j=0;j<4;j++) {
            t[j] = t[j+1];
            for (i=0;i<n;i++) {
                x[j][i] = x[j+1][i];
                f[j][i] = f[j+1][i]; } }
        for (i=0;i<n;i++)
            { s_f.x[i] = x[4][i]; }
        /*
        */
        return s_f;
    }
    /*

```

rk4() IS THE STANDARD FOURTH ORDER RUNGE-KUTTA SYSTEM OF ORDINARY DIFFERENTIAL EQUATION INTEGRATION ROUTINE. THIS IS REQUIRED FOR THE PREDICTOR-CORRECTOR ROUTINE SINCE IT IS A MULTI-STEP ALGORITHM.

```

    /*
    D *rk4(I n, membr m, D t, D ci, D *p_x, D x1, D x2, D x3, I pc)
    (
        I i;
        D ci2, ci6;
        D z[HM], g[HM], sm[HM], q[HM];
        /*
        */
        ci2 = ci/2.0;
        ci6 = ci/6.0;
        /*
        */
        for (i=0;i<n;i++) {
            z[i] = *p_x++;
            sm[i] = 0.0; }
        switch (pc) {
            case 0 :
                p_x = memcs(m, t, &z[0], x1, x2, x3);
                break;
            case 1 :
                p_x = membr(m, t, &z[0], x1, x2);
                break; }
        for (i=0;i<n;i++)
            { q[i] = *p_x++; }
        for (i=0;i<n;i++) {
            sm[i] += q[i];
            g[i] = z[i]+ci2*q[i]; }
        switch (pc) {
            case 0 :
                p_x = memcs(m, t+ci2, &g[0], x1, x2, x3);
                break;
            case 1 :
                p_x = membr(m, t+ci2, &g[0], x1, x2);
                break; }
        for (i=0;i<n;i++)
            { q[i] = *p_x++; }
        for (i=0;i<n;i++) {
            sm[i] += 2.0*q[i];
            g[i] = z[i]+ci2*q[i]; }
        switch (pc) {
            case 0 :
                p_x = memcs(m, t+ci2, &g[0], x1, x2, x3);
                break;
            case 1 :
                p_x = membr(m, t+ci2, &g[0], x1, x2);
                break; }
        for (i=0;i<n;i++)
            { q[i] = *p_x++; }
        for (i=0;i<n;i++) {
            sm[i] += 2.0*q[i];
            g[i] = z[i]+ci*q[i]; }
        switch (pc) {
            case 0 :
                p_x = memcs(m, t+ci, &g[0], x1, x2, x3);
                break;

```

```

        case 1 :
            p_x = membr(m, t+ci, &g[0], x1, x2);
            break; }
        for (i=0;i<n;i++)
            { q[i] = *p_x++; }
        for (i=0;i<n;i++) {
            sm[i] += q[i];
            z[i] += ci6*sm[i]; }
        return &z[0];
    }
D *membr(membr m, D t, D *px, D pi_mem, D p_tiss)
{
    I i;
    D p, x[HM], dxdt[HM];
    /* */
    for (i=0;i<HM;i++)
        { x[i] = *px++; }
    /* */
    p = p_tiss-m.sigma*(pi_mem-m.pi_cap);
    /* */
    asq*lp*(p_tiss-p_cap-sigma*(pi_mem-pi_cap)
    /* */
    dxdt[0] = x[1];
    dxdt[1] = m.asq*lp(m.typ_lp, m.lp0, m.lp1, t)*(p-x[0]);
    printf("**, x[0],x[1],dxdt[0],dxdt[1]);
    /* */
    return &dxdt[0];
}
D *memcs(membr m, D t, D *px, D c_cap, D c_tis, D v_mem)
{
    I i;
    D pe, isigmas, xm, x[HM], dxdt[HM];
    /* */
    for (i=0;i<HM;i++)
        { x[i] = *px++; }
    /* */
    Js = (PS.Pe/(e(Pe)-1))(c_cap-c_tis)+Jv(1-sigmas)c_cap
    /* */
    isigmas = 1.0-m.sigma;
    xm = PI2*m.r[0]*m.lref;
    pe = fabs(v_mem*isigmas/m.ps_d);
    if (pe > 1.0e-06) {
        if (pe > 100.0)
            { dxdt[0] = -(v_mem*isigmas*c_cap)*xm; }
        else
            { dxdt[0] = -(m.ps_d*(c_cap-c_tis)*pe/(exp(pe)-
1.0)+v_mem*isigmas*c_cap)*xm; }
        else
            { dxdt[0] = -(m.ps_d*(c_cap-c_tis)+v_mem*isigmas*c_cap)*xm; }
    printf("**, x[0],dxdt[0]);
    /* */
    return &dxdt[0];
}
/*
    NATURAL, CLAMPED, OR FITTED END POINTS CUBIC SPLINE. IF n < 6
    THEN ONLY NATURAL OR CLAMPED BOUNDARY CONDITIONS CAN BE APPLIED.
    0 : NATURAL
    1 : CLAMPED (1ST DERIVATIVE SPECIFIED : ldv, udv)
    2 : FITTED END POINTS
*/
vec3 fspl(I n, D *px, D *py, I lbc, I ubc, D ldv, D udv)
{
    I i, k, kp, km, nm=n-1, nmm=n-2;
    D a[NJ], b[NJ], c[NJ], d[NJ], h[NJ], x[NJ], y[NJ], *p_f;
    vec3 v_f;
    /* */
    for (i=0;i<NJ;i++) {
        x[i] = *px++;
        y[i] = *py++; }
    /* */
    if ((n < 6) && (lbc == 2)) lbc = 0;
    if ((n < 6) && (ubc == 2)) ubc = 0;
    /* */
    for (i=0;i<nm;i++)
        { h[i] = x[i+1]-x[i]; }
    a[0] = 0.0;
    switch (lbc) {
        case 0:
            b[0] = 1.0;
            c[0] = 0.0;
            d[0] = 0.0;

```

```

        break;
    case 1:
        b[0] = 2.0*h[0];
        c[0] = h[0];
        d[0] = 3.0*((y[1]-y[0])/h[0]-ldv);
        break;
    case 2:
        b[0] = -h[0];
        c[0] = h[0];
        d[0] = 3.0*sq(h[0])*ddpoly(&x[0], &y[0]);
        break; }
for (k=1;k<nm;k++) {
    kp = k+1;
    km = k-1;
    a[k] = h[km];
    b[k] = 2.0*(h[km]+h[k]);
    c[k] = h[k];
    d[k] = 3.0*((y[kp]-y[k])/h[k]-(y[k]-y[km])/h[km]); }
c[nm] = 0.0;
switch (ubc) {
    case 0:
        a[nm] = 0.0;
        b[nm] = 1.0;
        d[nm] = 0.0;
        break;
    case 1:
        a[nm] = h[nmm];
        b[nm] = 2.0*h[nmm];
        d[nm] = -3.0*((y[nm]-y[nmm])/h[nmm]-udv);
        break;
    case 2:
        a[nm] = h[nmm];
        b[nm] = -h[nmm];
        d[nm] = -3.0*sq(h[nmm])*ddpoly(&x[n-4], &y[n-4]);
        break; }
/*
TRIDIAGONAL LINEAR EQUATION SOLVER
*/
p_f = tridiag(n, &a[0], &b[0], &c[0], &d[0]);
/*
*/
for (i=0;i<n;i++)
    { v_f.r[i] = *p_f++; }
for (k=0;k<nm;k++) {
    kp = k+1;
    v_f.q[k] = (y[kp]-y[k])/h[k]-h[k]*(2.0*v_f.r[k]+v_f.r[kp])/3.0;
    v_f.s[k] = (v_f.r[kp]-v_f.r[k])/(3.0*h[k]); }
/*
*/
return v_f;
}
D *tridiag(I n, D *a, D *b, D *c, D *d)
{
    I i, im, nm=n-1;
    D xmt, x[NJ], p[NJ], q[NJ];
    /*
    */
    a++;
    p[0] = -(*c++)/(*b);
    q[0] = (*d++)/(*b++);
    for (i=1;i<n;i++) {
        im = i-1;
        xmt = (*a)*p[im]+(*b++);
        p[i] = -(*c++)/xmt;
        q[i] = ((*d++)-(*a++)*q[im])/xmt; }
    x[nm] = q[nm];
    for (i=nm-1;i>-1;i--)
        { x[i] = p[i]*x[i+1]+q[i]; }
    /*
    */
    return &x[0];
}
D evalcs(I n, vec3 v, D *px, D *py, D zz)
{
    I i, j, k, nm=n-1;
    D xt, zy, x[NJ], y[NJ];
    C *mssg;
    mssg = "\n W: evalcs()-> %f out of range.\n";
    /*
    */
    for (i=0;i<NJ;i++) {
        x[i] = *px++;
        y[i] = *py++; }
    /*
    PLUS-MINUS TWO PERCENT OF RANGE
    */
}

```

```

xt = 0.02*(x[nm]-x[0]);
if (zz < (x[0]-xt)) {
    i = 1;
    printf(mssg, zz); }
else
if (zz > (x[nm]+xt)) {
    i = n-2;
    printf(mssg, zz); }
else { i = 0;
    j = nm;
    while (j > i+1) {
        k = (i+j)/2.0;
        if (zz < x[k]) j = k;else i = k; } }
zy = zz-x[i];
zy = y[i]+zy*(v.q[i]+zy*(v.r[i]+zy*(v.s[i])));
/* */
return zy;
}
D devalcs(I n, vec3 v, D *px, D zz)
{
    I i, j, k, nm=n-1;
    D xt, zy, x[NJ];
    C *mssg;
    mssg = "\n W: devalcs()-> %f out of range.\n";
    /* */
    for (i=0;i<NJ;i++)
        { x[i] = *px++; }
    /*
    PLUS-MINUS TWO PERCENT OF RANGE
    */
    xt = 0.02*(x[nm]-x[0]);
    if (zz < (x[0]-xt)) {
        i = 1;
        printf(mssg, zz); }
    else
    if (zz > (x[nm]+xt)) {
        i = n-2;
        printf(mssg, zz); }
    else { i = 0;
        j = nm;
        while (j > i+1) {
            k = (i+j)/2.0;
            if (zz < x[k]) j = k;else i = k; } }
    zy = zz-x[i];
    zy = v.q[i]+zy*(2.0*v.r[i]+zy*(3.0*v.s[i]));
    /* */
    return zy;
}
D d2evalcs(I n, vec3 v, D *px, D zz)
{
    I i, j, k, nm=n-1;
    D xt, zy, x[NJ];
    C *mssg;
    mssg = "\n W: d2evalcs()-> %f out of range.\n";
    /* */
    for (i=0;i<NJ;i++)
        { x[i] = *px++; }
    /*
    PLUS-MINUS TWO PERCENT OF RANGE
    */
    xt = 0.02*(x[nm]-x[0]);
    if (zz < (x[0]-xt)) {
        i = 1;
        printf(mssg, zz); }
    else
    if (zz > (x[nm]+xt)) {
        i = n-2;
        printf(mssg, zz); }
    else { i = 0;
        j = nm;
        while (j > i+1) {
            k = (i+j)/2.0;
            if (zz < x[k]) j = k;else i = k; } }
    zy = zz-x[i];
    zy = 2.0*v.r[i]+zy*3.0*v.s[i];
    /* */
    return zy;
}
/*
ddpoly() SUPPLIES THE THIRD DERIVATIVE OF THE FITTED NEWTON'S
DIVIDED DIFFERENCE POLYNOMIAL. INSTEAD OF SETTING UP A DIVIDED

```

```

DIFFERENCE TABLE, ONLY THE REQUIRED COEFFICIENTS DESCRIBING THE
INTERPOLATING POLYNOMIAL ARE CALCULATED. THIS REDUCES MEMORY USE
AND CALCULATIONS.
*/
D ddpoly(D *px, D *py)
{
    I i, j;
    D x[6], y[6];
    for (i=1; i<5; i++) {
        x[i] = *px++;
        y[i] = *py++;
    }
    for (j=1; j<4; j++) {
        for (i=4; i>j; i--)
            ( y[i] = (y[i]-y[i-1])/(x[i]-x[i-j]); );
    }
    /*
    RETURN THIRD DERIVATIVE/6.0
    */
    return y[4];
}
D *solver(I n, I bw, D *pa, D *pb)
{
    I i, j, k=0, nm=n-1, ink, index[NM], ierror=0;
    D max, xm;
    D x[NM], b[NM], maxr[NM], a[NM][NM];
    char *mssg;
    mssg = "\n ERROR: solver()-> Diagonal element = 0.0";
    for (i=0; i<NM; i++) {
        b[i] = *pb++;
        for (j=0; j<NM; j++)
            ( a[i][j] = *pa++; );
    }
    /*
    */
    for (i=0; i<n; i++) {
        index[i] = i;
        max = 0.0;
        for (j=i; j<i+bw; j++) {
            if (fabs(a[i][j]) > max)
                ( max = fabs(a[i][j]); );
        }
        maxr[i] = max;
    }
    for (i=0; i<nm; i++) {
        max = 0.0;
        for (j=i; j<n; j++) {
            if (fabs(a[index[j]][i])/maxr[index[j]] > max) {
                k = j;
                max = fabs(a[index[j]][i])/maxr[index[j]];
            }
        }
        ink = index[k];
        index[k] = index[i];
        index[i] = ink;
        for (j=i+1; j<n; j++) {
            xm = a[index[j]][i]/a[ink][i];
            for (k=i+1; k<i+bw; k++)
                ( a[index[j]][k] -= xm*a[ink][k]; );
            b[index[j]] -= xm*b[index[i]];
            a[index[j]][i] = 0.0;
        }
        for (j=nm; j>0; j--) {
            for (i=j-1; i>-1; i--) {
                xm = a[index[i]][j]/a[index[j]][j];
                a[index[i]][j] -= xm*a[index[j]][j];
                b[index[i]] -= xm*b[index[j]];
            }
        }
        for (i=0; i<n; i++) {
            if (a[index[i]][i] == 0.0)
                { ierror = 1; continue; }
            x[i] = b[index[i]]/a[index[i]][i];
        }
        if (ierror == 1) {
            puts(mssg);
            exit(0);
        }
    }
    /*
    */
    return &x[0];
}
D *matvecbw(I nb, I ne, I bw, D *pa, D *pv)
{
    I i, j, bw2p;
    D b[NM], v[NM], a[NM][NM];
    bw2p = bw/2+2;
    for (i=0; i<NM; i++) {
        v[i] = *pv++;
        b[i] = 0.0;
        for (j=0; j<NM; j++) {
            a[i][j] = *pa++;
        }
    }
    /*
    */
    for (i=nb; i<ne; i++) {
        for (j=i-bw2p; j<=i+bw2p; j++) {

```

```

        if (j < nb) continue;
        if (j > ne) continue;
        b[i] += a[i][j]*v[j]; })
    return &b[0];
}
D l1(D x, D dx)
{
    D y = 1.0-x/dx;
    return y;
}
D l2(D x, D dx)
{
    D y = x/dx;
    return y;
}
D l3(D x, D dx)
{
    D y = 4.0*(x/dx)*(1.0-x/dx);
    return y;
}
D dl1(D x, D dx)
{
    D y = -1.0/dx;
    return y;
}
D dl2(D x, D dx)
{
    D y = 1.0/dx;
    return y;
}
D dl3(D x, D dx)
{
    D y = (4.0/dx)*(1.0-2.0*(x/dx));
    return y;
}
D d211(D x, D dx)
{
    D y = 0.0;
    return y;
}
D d212(D x, D dx)
{
    D y = 0.0;
    return y;
}
D d213(D x, D dx)
{
    D y = -8.0/sq(dx);
    return y;
}
W fmrzt(D r, D z, D dr, D dz)
{
    D l1r, l2r, l1z, l2z;
    W v;
    l1r = l1(r, dr);
    l2r = l2(r, dr);
    l1z = l1(z, dz);
    l2z = l2(z, dz);
    /* */
    v.v[0] = l1r*l1z;
    v.v[1] = l2r*l1z;
    v.v[2] = l2r*l2z;
    v.v[3] = l1r*l2z;
    return v;
}
W fmrzt(D r, D z, D dr, D dz)
{
    D l1r, l2r, l1z, l2z;
    W v;
    l1r = l1(r, dr)+l3(r, dr);
    l2r = l2(r, dr)+l3(r, dr);
    l1z = l1(z, dz)+l3(z, dz);
    l2z = l2(z, dz)+l3(z, dz);
    /* */
    v.v[0] = l1r*l1z;
    v.v[1] = l2r*l1z;
    v.v[2] = l2r*l2z;
    v.v[3] = l1r*l2z;
    return v;
}
W fwrzt(D aa, W evr, W evz, W przt, W dpdr, W dpdz)

```

```

{
  I i;
  W a, v;
  /* */
  for (i=0;i<4;i++) {
    a.v[i] = aa*(evr.v[i]*dpdr.v[i]+evz.v[i]*dpdz.v[i]);
    v.v[i] = przt.v[i]+a.v[i]; }
  /* */
  return v;
}
W fdndr(D r, D z, D dr, D dz)
{
  D dl1r, dl2r, l1z, l2z;
  W v;
  dl1r = dl1(r, dr);
  dl2r = dl2(r, dr);
  l1z = l1(z, dz);
  l2z = l2(z, dz);
  /* */
  v.v[0] = dl1r*l1z;
  v.v[1] = dl2r*l1z;
  v.v[2] = dl2r*l2z;
  v.v[3] = dl1r*l2z;
  return v;
}
W fdndz(D r, D z, D dr, D dz)
{
  D l1r, l2r, dl1z, dl2z;
  W v;
  l1r = l1(r, dr);
  l2r = l2(r, dr);
  dl1z = dl1(z, dz);
  dl2z = dl2(z, dz);
  /* */
  v.v[0] = l1r*dl1z;
  v.v[1] = l2r*dl1z;
  v.v[2] = l2r*dl2z;
  v.v[3] = l1r*dl2z;
  return v;
}
W fdmdr(D r, D z, D dr, D dz)
{
  D dl1r, dl2r, l1z, l2z;
  W v;
  dl1r = dl1(r, dr)+dl3(r, dr);
  dl2r = dl2(r, dr)+dl3(r, dr);
  l1z = l1(z, dz)+l3(z, dz);
  l2z = l2(z, dz)+l3(z, dz);
  /* */
  v.v[0] = dl1r*l1z;
  v.v[1] = dl2r*l1z;
  v.v[2] = dl2r*l2z;
  v.v[3] = dl1r*l2z;
  return v;
}
W fdmdz(D r, D z, D dr, D dz)
{
  D l1r, l2r, dl1z, dl2z;
  W v;
  l1r = l1(r, dr)+l3(r, dr);
  l2r = l2(r, dr)+l3(r, dr);
  dl1z = dl1(z, dz)+dl3(z, dz);
  dl2z = dl2(z, dz)+dl3(z, dz);
  /* */
  v.v[0] = l1r*dl1z;
  v.v[1] = l2r*dl1z;
  v.v[2] = l2r*dl2z;
  v.v[3] = l1r*dl2z;
  return v;
}
W fd2m2r(D r, D z, D dr, D dz)
{
  D d211r, d212r, l1z, l2z;
  W v;
  d211r = d211(r, dr)+d213(r, dr);
  d212r = d212(r, dr)+d213(r, dr);
  l1z = l1(z, dz)+l3(z, dz);
  l2z = l2(z, dz)+l3(z, dz);
  /* */
  v.v[0] = d211r*l1z;
  v.v[1] = d212r*l1z;
}

```

```

    v.v[2] = d212r*12z;
    v.v[3] = d211r*12z;
    return v;
}
W fd2mdrdz(D r, D z, D dr, D dz)
{
    D dl1r, dl2r, dl1z, dl2z;
    W v;
    dl1r = dl1(r, dr)+dl3(r, dr);
    dl2r = dl2(r, dr)+dl3(r, dr);
    dl1z = dl1(z, dz)+dl3(z, dz);
    dl2z = dl2(z, dz)+dl3(z, dz);
    /* */
    v.v[0] = dl1r*dl1z;
    v.v[1] = dl2r*dl1z;
    v.v[2] = dl2r*dl2z;
    v.v[3] = dl1r*dl2z;
    return v;
}
W fd2mdz2(D r, D z, D dr, D dz)
{
    D l1r, l2r, d211z, d212z;
    W v;
    l1r = l1(r, dr)+l3(r, dr);
    l2r = l2(r, dr)+l3(r, dr);
    d211z = d211(z, dz)+d213(z, dz);
    d212z = d212(z, dz)+d213(z, dz);
    /* */
    v.v[0] = l1r*d211z;
    v.v[1] = l2r*d211z;
    v.v[2] = l2r*d212z;
    v.v[3] = l1r*d212z;
    return v;
}
W fd3mdr2dz(D r, D z, D dr, D dz)
{
    D d211r, d212r, dl1z, dl2z;
    W v;
    d211r = d211(r, dr)+d213(r, dr);
    d212r = d212(r, dr)+d213(r, dr);
    dl1z = dl1(z, dz)+dl3(z, dz);
    dl2z = dl2(z, dz)+dl3(z, dz);
    /* */
    v.v[0] = d211r*dl1z;
    v.v[1] = d212r*dl1z;
    v.v[2] = d212r*dl2z;
    v.v[3] = d211r*dl2z;
    return v;
}
W fd3mdrdz2(D r, D z, D dr, D dz)
{
    D dl1r, dl2r, d211z, d212z;
    W v;
    dl1r = dl1(r, dr)+dl3(r, dr);
    dl2r = dl2(r, dr)+dl3(r, dr);
    d211z = d211(z, dz)+d213(z, dz);
    d212z = d212(z, dz)+d213(z, dz);
    /* */
    v.v[0] = dl1r*d211z;
    v.v[1] = dl2r*d211z;
    v.v[2] = dl2r*d212z;
    v.v[3] = dl1r*d212z;
    return v;
}
D gp(I n, I i)
{
    D z=0.0;
    switch (n) {
        case 2 : z = gp2(i);break;
        case 3 : z = gp3(i);break;
        case 4 : z = gp4(i);break;
        case 6 : z = gp6(i);break;
        case 8 : z = gp8(i);break;
        case 16 : z = gp16(i);break; }
    return z;
}
D gw(I n, I i)
{
    D w=0.0;
    switch (n) {
        case 2 : w = gw2(i);break;

```

```

        case 3 : w = gw3(i);break;
        case 4 : w = gw4(i);break;
        case 6 : w = gw6(i);break;
        case 8 : w = gw8(i);break;
        case 16 : w = gw16(i);break; }
    return w;
}
/*
    TWO POINT GAUSS-LEGENDRE FORMULA
*/
D gp2(I i)
{
    D z=0.0;
    switch (i) {
        case 0 : z = 0.577350269189626;break;
        case 1 : z = -0.577350269189626;break; }
    return z;
}
/*
    TWO POINT GAUSS-LEGENDRE FORMULA
*/
D gw2(I i)
{
    D w=0.0;
    switch (i) {
        case 0 : w = 1.000000000000000;break;
        case 1 : w = 1.000000000000000;break; }
    return w;
}
/*
    THREE POINT GAUSS-LEGENDRE FORMULA
*/
D gp3(I i)
{
    D z=0.0;
    switch (i) {
        case 0 : z = 0.000000000000000;break;
        case 1 : z = 0.774596669241483;break;
        case 2 : z = -0.774596669241483;break; }
    return z;
}
/*
    THREE POINT GAUSS-LEGENDRE FORMULA
*/
D gw3(I i)
{
    D w=0.0;
    switch (i) {
        case 0 : w = 0.888888888888889;break;
        case 1 : w = 0.555555555555556;break;
        case 2 : w = 0.555555555555556;break; }
    return w;
}
/*
    FOUR POINT GAUSS-LEGENDRE FORMULA
*/
D gp4(I i)
{
    D z=0.0;
    switch (i) {
        case 0 : z = 0.339981043584856;break;
        case 1 : z = -0.339981043584856;break;
        case 2 : z = 0.861136311594053;break;
        case 3 : z = -0.861136311594053;break; }
    return z;
}
/*
    FOUR POINT GAUSS-LEGENDRE FORMULA
*/
D gw4(I i)
{
    D w=0.0;
    switch (i) {
        case 0 : w = 0.652145154862546;break;
        case 1 : w = 0.652145154862546;break;
        case 2 : w = 0.347854845137454;break;
        case 3 : w = 0.347854845137454;break; }
    return w;
}
/*
    SIX POINT GAUSS-LEGENDRE FORMULA

```

```

*/
D gp6(I 1)
{
    D z=0.0;
    switch (i) {
        case 0 : z = 0.932469514203152;break;
        case 1 : z = -0.932469514203152;break;
        case 2 : z = 0.661209386466265;break;
        case 3 : z = -0.661209386466265;break;
        case 4 : z = 0.238619186083197;break;
        case 5 : z = -0.238619186083197;break; }
    return z;
}
/*
SIX POINT GAUSS-LEGENDRE FORMULA
*/
D gw6(I 1)
{
    D w=0.0;
    switch (i) {
        case 0 : w = 0.171324492379170;break;
        case 1 : w = 0.171324492379170;break;
        case 2 : w = 0.360761573048139;break;
        case 3 : w = 0.360761573048139;break;
        case 4 : w = 0.467913934572691;break;
        case 5 : w = 0.467913934572691;break; }
    return w;
}
/*
EIGHT POINT GAUSS-LEGENDRE FORMULA
*/
D gp8(I 1)
{
    D z=0.0;
    switch (i) {
        case 0 : z = 0.960289856497536;break;
        case 1 : z = -0.960289856497536;break;
        case 2 : z = 0.796666477413627;break;
        case 3 : z = -0.796666477413627;break;
        case 4 : z = 0.525532409916329;break;
        case 5 : z = -0.525532409916329;break;
        case 6 : z = 0.183434642495650;break;
        case 7 : z = -0.183434642495650;break; }
    return z;
}
/*
EIGHT POINT GAUSS-LEGENDRE FORMULA
*/
D gw8(I 1)
{
    D w=0.0;
    switch (i) {
        case 0 : w = 0.101228536290376;break;
        case 1 : w = 0.101228536290376;break;
        case 2 : w = 0.222381034453374;break;
        case 3 : w = 0.222381034453374;break;
        case 4 : w = 0.313706645877887;break;
        case 5 : w = 0.313706645877887;break;
        case 6 : w = 0.362683783378362;break;
        case 7 : w = 0.362683783378362;break; }
    return w;
}
/*
SIXTEEN POINT GAUSS-LEGENDRE FORMULA
*/
D gp16(I 1)
{
    D z=0.0;
    switch (i) {
        case 0 : z = 0.095012509837637440185;break;
        case 1 : z = -0.095012509837637440185;break;
        case 2 : z = 0.281603550779258913230;break;
        case 3 : z = -0.281603550779258913230;break;
        case 4 : z = 0.458016777657227386342;break;
        case 5 : z = -0.458016777657227386342;break;
        case 6 : z = 0.617876244402643748447;break;
        case 7 : z = -0.617876244402643748447;break;
        case 8 : z = 0.755404408355003033895;break;
        case 9 : z = -0.755404408355003033895;break;
        case 10 : z = 0.865631202387831743880;break;
        case 11 : z = -0.865631202387831743880;break;

```

```

        case 12 : z = 0.944575023073232576078; break;
        case 13 : z = -0.944575023073232576078; break;
        case 14 : z = 0.989400934991649932596; break;
        case 15 : z = -0.989400934991649932596; break; }
    return z;
}
/*
    SIXTEEN POINT GAUSS-LEGENDRE FORMULA
*/
D gw16(I i)
{
    D w=0.0;
    switch (i) {
        case 0 : w = 0.189450610455068496285; break;
        case 1 : w = 0.189450610455068496285; break;
        case 2 : w = 0.182603415044923588867; break;
        case 3 : w = 0.182603415044923588867; break;
        case 4 : w = 0.169156519395002538189; break;
        case 5 : w = 0.169156519395002538189; break;
        case 6 : w = 0.149595988816576732081; break;
        case 7 : w = 0.149595988816576732081; break;
        case 8 : w = 0.124628971255533872052; break;
        case 9 : w = 0.124628971255533872052; break;
        case 10 : w = 0.095158511682492784810; break;
        case 11 : w = 0.095158511682492784810; break;
        case 12 : w = 0.062253523938647892863; break;
        case 13 : w = 0.062253523938647892863; break;
        case 14 : w = 0.027152459411754094852; break;
        case 15 : w = 0.027152459411754094852; break; }
    return w;
}
V outdata(I pc, I ss, I n, I nrout, I nzout, I *pi, I *pe, F *rp, F *zp,
    D *pr, D *pz, D *dr, D *dz, I ihof, D t, C *title, D *data, FILE *out)
{
    I i, j, k, l, el;
    I iout[RW*ZW], eldef[EM][6];
    F rot[IM], zot[IM];
    D rr, zz, sum, edr[EM], edz[EM], r[NM], z[NM], f[NM];
    W nrzt;
    /* */
    for (i=0; i<NM; i++) {
        r[i] = *pr++;
        z[i] = *pz++;
        f[i] = *data++; }
    for (i=0; i<IM; i++) {
        rot[i] = *rp++;
        zot[i] = *zp++; }
    for (i=0; i<EM; i++) {
        edr[i] = *dr++;
        edz[i] = *dz++;
        for (j=0; j<6; j++)
            { eldef[i][j] = *pe++; } }
    for (i=0; i<RW*ZW; i++)
        { iout[i] = *pi++; }
    if (ss == 3)
        { ss = 0; }
    /* */
    fprintf(out, "%d %d %d %d\n", pc, nrout, nzout, n);
    /*
    TITLE 1 AND 2
    */
    fputs(title, out);
    switch (pc) {
        case 0: /* CONC */
            fprintf(out, "Concentration of Solute");
            break;
        case 1: /* PRES */
            fprintf(out, "Pressure Distribution");
            break;
        case 2: /* PECL */
            fprintf(out, "Peclet Distribution");
            break;
        case 3: /* POTL */
            fprintf(out, "(P-#sp&)/Pref");
            break; }
    switch (ss) {
        case 0 :
            fprintf(out, " at Steady-State.$\n");
            break;
        default :
            fprintf(out, " at t = %10.6f$\n", t);
    }
}

```

```

        break; }
/*
TITLE X, Y, AND Z AXES
*/
fputs("Distance into Tissue, dimensionless$\n", out);
fputs("Distance down Capillary, dimensionless$\n", out);
switch (pc) {
  case 0: /* CONC */
    fputs("Concentration, dimensionless$\n", out);
    break;
  case 1: /* PRES */
    fputs("Pressure, dimensionless$\n", out);
    break;
  case 2: /* PECL */
    fputs("Peclet Number$\n", out);
    break;
  case 3: /* POTL */
    fputs("(P-#sp&)/Pref$\n", out);
    break; }
for (i=0;i<nzout;i++) {
  for (j=0;j<nrout;j++) {
    k = i*nrout+j;
    el = iout[k];
    rr = rot[j]-r[eldef[el][0]];
    zz = zot[i]-z[eldef[el][0]];
    if (ihof == 1)
      { nrzt = fmrzt(rr, zz, edr[el], edz[el]); }
    else
      { nrzt = fnrzt(rr, zz, edr[el], edz[el]); }
    sum = 0.0;
    for (l=0;l<4;l++)
      { sum += nrzt.v[l]*f[eldef[el][l]]; }
    fprintf(out, " %10.6f %10.6f %15.12f\n",
            rot[j], zot[i], sum); }
  switch (pc) {
    case 0: printf(" CONC");break;
    case 1: printf(" PRES");break;
    case 2: printf(" PECL");break;
    case 3: printf(" POTL");break; }
}
V outuv2d(I wtf, I ss, I n, I nrout, I nzout, I *pi, I *pe, F *rp, F *zp,
D *pr, D *pz, D *dr, D *dz, I ihof, D t, C *title, D *ur, D *uz, FILE *out)
{
  I i, j, k, l, el;
  I iout[RW*ZW], eldef[EM][6];
  F rot[IM], zot[IM];
  D rr, zz, sr, sz, edr[EM], edz[EM], r[NM], z[NM], vr[NM], vz[NM];
  W nrzt;
  /* */
  for (i=0;i<NM;i++) {
    r[i] = *pr++;
    z[i] = *pz++;
    vr[i] = *ur++;
    vz[i] = *uz++; }
  for (i=0;i<IM;i++) {
    rot[i] = *rp++;
    zot[i] = *zp++; }
  for (i=0;i<EM;i++) {
    edr[i] = *dr++;
    edz[i] = *dz++;
    for (j=0;j<6;j++)
      { eldef[i][j] = *pe++; } }
  for (i=0;i<RW*ZW;i++)
    { iout[i] = *pi++; }
  if (ss == 3)
    { ss = 0; }
  /* */
  fprintf(out, "%d %d %d %d\n", 4, nrout, nzout, n);
  /*
TITLE 1 AND 2
*/
  fputs(title, out);
  fprintf(out, "Velocity Field");
  switch (ss) {
    case 0 :
      fprintf(out, " at Steady-State.$\n");
      break;
    default :
      fprintf(out, " at t = %10.6f$\n", t);
      break; }
  /*

```

```

TITLE X, Y, AND Z AXES
*/
fputs("Distance into Tissue, dimensionless$\n", out);
fputs("Distance down Capillary, dimensionless$\n", out);
fputs(" $\n", out);
switch (wtf) {
  case 0 :
    for (i=0;i<nzout;i++) {
      for (j=0;j<nrout;j++) {
        k = i*nrout+j;
        el = iout[k];
        rr = rot[j]-r[eldef[el][0]];
        zz = zot[i]-z[eldef[el][0]];
        if (ihof == 1)
          { nrzt = fmrzt(rr, zz, edr[el], edz[el]); }
        else
          { nrzt = fnrzt(rr, zz, edr[el], edz[el]); }
        sr = sz = 0.0;
        for (l=0;l<4;l++) {
          sr += nrzt.v[l]*vr[eldef[el][l]];
          sz += nrzt.v[l]*vz[eldef[el][l]]; }
        fprintf(out, " %10.6f %10.6f %10.6e %10.6e\n",
          rot[j], zot[i], sr, sz); }
      break;
    case 1 :
      for (i=0;i<n;i++)
        { fprintf(out, " %10.6f %10.6f %10.6e %10.6e\n",
          r[i], z[i], vr[i], vz[i]); }
      break; }
  printf(" VEL");
}
V outcoll(I pc, I ss, I n, D t, D *px, D *py, D *pf, C *title, FILE *out)
{
  I i;
  if (ss == 3)
    { ss = 0; }
  fputs(title, out);
  switch (pc) {
    case 0: /* CONC */
      fprintf(out, "Concentration of Solute");
      break;
    case 1: /* PRES */
      fprintf(out, "Pressure Distribution");
      break;
    case 2: /* PECL */
      fprintf(out, "Peclet Distribution");
      break;
    case 3: /* POTL */
      fprintf(out, "Potential Distribution");
      break; }
  switch (ss) {
    case 0 :
      fprintf(out, " at Steady-State.$\n");
      break;
    default :
      fprintf(out, " at t = %10.6f$\n", t);
      break; }
  fputs("Distance into Tissue, dimensionless$\n", out);
  fputs("Distance down Capillary, dimensionless$\n", out);
  switch (pc) {
    case 0: /* CONC */
      fputs("Concentration, dimensionless$", out);
      break;
    case 1: /* PRES */
      fputs("Pressure, dimensionless$", out);
      break;
    case 2: /* PECL */
      fputs("Peclet Number$", out);
      break;
    case 3: /* POTL */
      fputs("(P-#sp&)/Pref$", out);
      break; }
  fprintf(out, "\n %d\n", n);
  for (i=0;i<n;i++)
    { fprintf(out, " %10.6f %10.6f %15.12f\n", *px++, *py++, *pf++); }
  switch (pc) {
    case 0: printf(" CONC");break;
    case 1: printf(" PRES");break;
    case 2: printf(" PECL");break;
    case 3: printf(" POTL");break; }
}

```

```

V outcapp(I n, I ss, D t, D *pz, D *pc, D *qc, D *vm, D *cc, D *pe, D *vs, C *title, FILE
*out)
{
    I i;
    if (ss == 3)
        { ss = 0; }
    fputs(title, out);
    fprintf(out, "Capillary Variables");
    switch (ss) {
        case 0 :
            fprintf(out, " at Steady-State.\n");
            break;
        default :
            fprintf(out, " at t = %10.6f\n", t);
            break; }
    fprintf(out, " %d\n", n);
    fputs(" z          Pcap          Qcap          Vmem          Ccap          mPe          Vsol\n", out);
    for (i=0;i<n;i++)
        { fprintf(out, "%6.4f %8.6f %8.6e %8.6e %8.6e %8.6e %8.6e\n",
          *pz++, *pc++, *qc++, *vm++, *cc++, *pe++, *vs++); }
    printf(" CAPP");
}
V contour(I pc, I ss, I n, I nr, I nz, D *pz, D t, C *title, FILE *out)
{
    I i, j, k;
    D z[NM];
    /* */
    for (i=0;i<NM;i++)
        { z[i] = *pz++; }
    if (ss == 3)
        { ss = 0; }
    /* */
    fputs(title, out);
    switch (pc) {
        case 0: /* CONC */
            fprintf(out, "Concentration of Solute");
            break;
        case 1: /* PRES */
            fprintf(out, "Pressure Distribution");
            break;
        case 2: /* PECL */
            fprintf(out, "Peclet Distribution");
            break;
        case 3: /* POTL */
            fprintf(out, "Potential Distribution");
            break; }
    switch (ss) {
        case 0 :
            fprintf(out, " at Steady-State.\n");
            break;
        default :
            fprintf(out, " at t = %10.6f\n", t);
            break; }
    /* */
    for (i=nz;i>0;i--) {
        fprintf(out, "| ");
        for (j=0;j<nr;j++) {
            k = (i-1)*nr+j;
            fprintf(out, "%5.4f ", z[k]); }
        fprintf(out, "|\n"); }
}
V header(D rg, D zg, D knn, membr mem, media pp, FILE *out)
{
    fprintf(out, "AR = %3.1f:%d\n", (zg/rg), 1);
    fprintf(out, "Rf = %4.2f\n", pp.hind);
    fprintf(out, "#s& = %4.2f\n", mem.sigma);
    fprintf(out, "#s&g = %4.2f\n", pp.sigmag);
    fprintf(out, "PS = %4.2E m/s\n", mem.ps);
    fprintf(out, "D = %4.2E m2/s\n", pp.diff);
    fprintf(out, "Lp = %4.2E m/Pa.s\n", mem.lp0);
    fprintf(out, "K = %4.2E m2/Pa.s\n", knn);
    fprintf(out, "LS = %4.2E m3/m3.Pa.s\n", pp.ls);
}
I safechk(I ndnm, I elnm, I nr, I nz, I nrout, I nzout)
{
    I err=0;
    C *m1, *m2, *m3, *m4, *m5, *m6, *m7, *m8;
    m1 = " E: safechk()-> NM too small. Set > %d.\n";
    m2 = " E: safechk()-> EM too small. Set > %d.\n";
    m3 = " E: safechk()-> IM too small. Set > %d.\n";
}

```

```

m4 = " E: safechk()-> MM too small. Set > %d.\n";
m5 = " E: safechk()-> RW too small. Set > %d.\n";
m6 = " E: safechk()-> ZW too small. Set > %d.\n";
m7 = " E: safechk()-> nr > nz.      Set nr < nz.\n";
m8 = " E: safechk()-> NJ < IM.      Set NJ > IM.\n";
/*      */
if (ndnm+2 > NM) {
    printf(m1, ndnm);
    err = 1; }
if (elnm+2 > EM) {
    printf(m2, elnm);
    err = 1; }
if (nz+2 > IM) {
    printf(m3, nz);
    err = 1; }
if ((2*nr+2*nz) > MM) {
    printf(m4, 2*nr+2*nz);
    err = 1; }
if (nrout+2 > RW) {
    printf(m5, nrout);
    err = 1; }
if (nzout+2 > ZW) {
    printf(m6, nzout);
    err = 1; }
if (nr > nz) {
    printf(m7);
    err = 1; }
if (NJ < IM) {
    printf(m8);
    err = 1; }
/*      */
return err;
}
I datachk(I *pe)
{
    I i, err=0, nerr=0, chk[50];
    C *mssgl, *item="";
    mssgl = " E: datachk()-> %s card missing.\n";
    for (i=0;i<50;i++)
        { chk[i] = *pe++; }
    for (i=0;i<50;i++) {
        switch(i) {
            case 0 : if (chk[i] == 0) {
                err = 1;
                item = "$end input"; }
                break;
            case 1 : if (chk[i] == 0) {
                err = 1;
                item = "$beg input"; }
                break;
            case 2 : if (chk[i] == 0) {
                err = 1;
                item = "$prob size"; }
                break;
            case 3 : if (chk[i] == 0) {
                err = 1;
                item = "$tis refl coef"; }
                break;
            case 4 : if (chk[i] == 0) {
                err = 1;
                item = "$transient"; }
                break;
            case 5 : if (chk[i] == 0) {
                err = 1;
                item = "$max iterations"; }
                break;
            case 6 : if (chk[i] == 0) {
                err = 1;
                item = "$dispersivity"; }
                break;
            case 7 : if (chk[i] == 0) {
                err = 1;
                item = "$fluid sink LS"; }
                break;
            case 8 : if (chk[i] == 0) {
                err = 1;
                item = "$porosity"; }
                break;
            case 9 : if (chk[i] == 0) {
                err = 1;
                item = "$fluid viscosity"; }

```

```
break;
case 10: if (chk[i] == 0) {
    err = 1;
    item = "$relaxation"; }
break;
case 11: if (chk[i] == 0) {
    err = 1;
    item = "$hydraulic cond"; }
break;
case 12: if (chk[i] == 0) {
    err = 1;
    item = "$conc node sink"; }
break;
case 13: if (chk[i] == 0) {
    err = 1;
    item = "$mem refl coef"; }
break;
case 14: if (chk[i] == 0) {
    err = 1;
    item = "$fluid density"; }
break;
case 15: if (chk[i] == 0) {
    err = 1;
    item = "$diff mem PS"; }
break;
case 16: if (chk[i] == 0) {
    err = 1;
    item = "$geometry"; }
break;
case 17: if (chk[i] == 0) {
    err = 1;
    item = "$cap osm pr"; }
break;
case 18: if (chk[i] == 0) {
    err = 1;
    item = "$node definitions"; }
break;
case 19: if (chk[i] == 0) {
    err = 1;
    item = "$elem definitions"; }
break;
case 20: if (chk[i] == 0) {
    err = 1;
    item = "$conc node bc"; }
break;
case 21: if (chk[i] == 0) {
    err = 1;
    item = "$conc elem bc"; }
break;
case 22: if (chk[i] == 0) {
    err = 1;
    item = "$conc node ic"; }
break;
case 23: if (chk[i] == 0) {
    err = 1;
    item = "$pres node bc"; }
break;
case 24: if (chk[i] == 0) {
    err = 1;
    item = "$pres elem bc"; }
break;
case 25: if (chk[i] == 0) {
    err = 1;
    item = "$write results"; }
break;
case 26: if (chk[i] == 0) {
    err = 1;
    item = "$contour"; }
break;
case 27: if (chk[i] == 0) {
    err = 1;
    item = "$ref values"; }
break;
case 28: if (chk[i] == 0) {
    err = 1;
    item = "$tolerance"; }
break;
case 29: if (chk[i] == 0) {
    err = 1;
    item = "$frac volumes"; }
break;
```

```
case 30: if (chk[i] == 0) {
    err = 1;
    item = "$conv hindrance"; }
    break;
case 31: if (chk[i] == 0) {
    err = 1;
    item = "$gauss points"; }
    break;
case 32: if (chk[i] == 0) {
    err = 1;
    item = "$asq"; }
    break;
case 33: if (chk[i] == 0) {
    err = 1;
    item = "$cap conditions"; }
    break;
case 34: if (chk[i] == 0) {
    err = 1;
    item = "$hof"; }
    break;
case 35: if (chk[i] == 0) {
    err = 1;
    item = "$node results"; }
    break;
case 36: if (chk[i] == 0) {
    err = 1;
    item = "$osm pres"; }
    break;
case 37: if (chk[i] == 0) {
    err = 1;
    item = "$dgamma"; }
    break;
case 38: if (chk[i] == 0) {
    err = 1;
    item = "$lymph cond"; }
    break;
case 39: if (chk[i] == 0) {
    err = 1;
    item = "$cap wall Lp"; }
    break;
case 40: if (chk[i] == 0) {
    err = 1;
    item = "$wall th"; }
    break;
case 41: if (chk[i] == 0) {
    err = 1;
    item = "$perturbation"; }
    break; }
if (err != 0) {
    nerr++;
    printf(mssg1, item); }
err = 0; }
return nerr;
}
```